2-15-2015

Fermentative Production Of 1,3-Propanediol From Industrial Glycerol And Its Pervaporative Enrichment From Aqueous Mixture

Baishali Kanjilal
University of Connecticut - Storrs, Baishali.Kanjilal@gmail.com

Fermentative Production Of 1,3-Propanediol From Industrial Glycerol And Its Pervaporative Enrichment From Aqueous Mixtures

Baishali Kanjilal, PhD

University of Connecticut, [2015]

Abstract

A paradigm shift towards renewable feedstocks has given rise to a fast growing global market for biorenewable chemicals, of which, glycerin is a major platform chemical. Industrial glycerol production as a byproduct of the biodiesel and other industries has led to an over capacity with issues related to its disposal. Fermentation of this crude glycerol to 1,3-propanediol as a value added product may provide a recourse to capitalizing on the current over capacity. This thesis explores the fermentative production of 1,3-propanediol from industrial glycerol using a soil based bacterial inoculum and the development of several families of polymers as pervaporation membranes for enriching 1,3-propanediol from dilute aqueous broths.

The first part of the thesis studies and optimizes the yield of 1,3-propanediol from industrial glycerol using an organic soil based inoculum with various process parameters. The optimized parameters are used to run CSTR experiments wherein the specific 1,3-propanediol productivity is shown to increase with dilution rate.

In addition to substrate, the real process bottleneck in fermentative 1,3-propanediol production lies in high energy costs of concentration enrichment. While pervaporation is energetically advantageous, the proximity of the solubility parameters of 1,3-propanediol with those of water preclude the usage of conventional membrane materials for enrichment from dilute aqueous broths. The second part of the thesis concerns development of three polymer families– cyclohexylamine functionalized siloxanes, cyclohexylamine based methacrylates and imidazolium dibutylphosphate ionic liquid based methacrylates - with progressively increasing separation factors and good price–performance trade off. The final part of the thesis explores their performance with batch and continuous pervaporation to enrich 1,3-propanediol from simulated broths of compositions replicated from the CSTR fermentations. The imidazolium ionic liquid based methacrylates not only enrich 1,3-propanediol from water with highest efficiency, but also from other broth components while striking the best possible cost – performance balance. The development and fine tuning of such materials present themselves as steps towards possible membrane module fabrication for continuous pervaporation and hence establishment of commercially viable and energy efficient alternatives to conventional purification processes.

Fermentative Production Of 1,3-Propanediol From Industrial Glycerol And Its Pervaporative Enrichment From Aqueous Mixtures

Baishali Kanjilal

B.Sc., University of Calcutta, **[1998]**

B.Tech., University of Cacutta, **[2001]**

A Dissertation

Submitted in Partial Fulfillment of the

Requirements for the Degree of

Doctor of Philosophy

at the

University of Connecticut

[2015]

APPROVAL PAGE

Doctor of Philosophy Dissertation

Fermentative Production Of 1,3-Propanediol From Industrial Glycerol And Its Pervaporative Enrichment From Aqueous Mixtures

Presented by:

Baishali Kanjilal, B.Sc., B.Tech.

Major Advisor _____
Richard Parnas

Associate Advisor _____
Alexandru Asandei

Associate Advisor _____
Ranjan Srivastava

Associate Advisor _____
Jeffrey McCutcheon

Associate Advisor _____
Douglas Adamson

University of Connecticut
[2015]

Acknowledgements

I thank my advisory committee – Major Advisor, Prof. Richard Parnas, Associate Advisors Prof. Alex Asandei, Prof. Ranjan Srivastava, Prof. Jeff McCutcheon and Prof. Douglas Adamson for their valuable advice and support throughout the course of graduate studies. Special thanks are due to my associate advisors for their generosity in providing lab space and facilities for a large part of my experimental work.

I am very to grateful Prof. James Stuart, Emeritus Professor, Dept. of Chemistry for his support throughout my PhD in chromatography and to Prof. Monty Shaw, Emeritus Professor, Polymer Program, IMS, for great insights into the thermodynamic aspects of my computations. An enormous value and understanding has been added to me by virtue of discussions and experimental sessions with these stalwarts.

I am grateful to Prof. Steven Suib for moral and fiscal support. Mrs. Young Hee Chudy deserves special mention for her moral support and I shall always remember her with utmost love and respect. I am also thankful to Dr. Laura Pinatti, Dr. Marcus Giotto, Dr. Mark Dudley, Dr. Roger Ristau, Dr. Lichun Zhang and Dr. Jeff Roth for their support and mentorship.

I developed a wonderful working camaraderie with my colleagues, especially Dr. Iman Noshadi and Dr. Eddy Bautista to whom I owe gratitude for their help and scientific insights. I am thankful to Cheng, Dipendra, Dr. Sudsiri Hemsri and Dr. Si Yu Li for their support. I am very grateful to Prof. Asandei's group - Joon Sung, Olu, Chris and Vignesh – and to Tahereh of Prof. Suib's group for their support of my research activities. I have made wonderful friends especially Hyun-sook, Zhenhua, Aindrila, Debanjan, Bhargab, Anamica, amongst others. My roommates, Swarnali, Koyel and later, Reza made my life cheerful with their wonderful company, friendship and unadulterated fun.

Special thanks are due to Prof. Nitis & Mrs. Mahua Mukhopadhyay, Prof. Ashish and Mrs. Ruma Basu, Prof. Chandra and Mrs. Minati Roychoudhury, Dr. Sanjay & Mrs.Krishna Banerjee, Drs. Saumitra and Seema Banerjee and Prof. Nitya and Mrs. Soma Chakraborty for providing an extended family away from home. I am very grateful to Prof. Mukhopadhyay and Mahua Mashi for being like parents in a foreign country, their love and encouragement in cultural activities.

I am truly indebted to my father's friends Dr. Apurba & Mrs. Krishna Roy and to Dr. Sumanta Sanyal and his family for their moral support and love. I owe my gratitude to Prof. Haimanti Chakraborty and Prof. Priyabrata Sarkar and their students at University of Calcutta, Prof. Ajit Banthia of IIT Kharagpur, Dr. Swapan Dhara, Advanced Petrochemicals and Raj Datta, Haldia Petrochemicals for their mentorship. I am grateful to my alma mater, University of Calcutta for their travel endowment scholarship, which funded my travel to USA to join the PhD program. I am grateful to my uncle Mr. Subhamay Kanjilal for his advice, support and love.

I owe all that I have achieved to my parents and their enormous respect for the quest of knowledge. My parents Dr. Chinmay and Mrs. Subhadra Kanjilal and my brother Jishnu are my greatest inspiration and role models. I am very proud of them and to merely be grateful for their love and faith in me, under all circumstances, would be inadequate. I dedicate my thesis to my family.

TABLE OF CONTENTS

List of Tables

List of Tables

Chapter1. Introduction and Thesis Organization

Given the imminent depletion of fossil fuels, the impact that current petroleum based processes have on the environment and driven by the idea of sustainability, the chemical industry has begun to envision a paradigm shift to renewable feedstock's and a carbohydrate rather than a hydrocarbon economy[1]. This has led to an estimated $2.4 billion global market for biorenewable chemicals with a projected compounded average growth rate (CAGR) of 14.8%. The bio renewable chemicals industry is expected to reach $6.8Bn by 2016 and a CAGR of 22.8% as it awaits the advent of bioethylene. Currently, glycerin and lactic acid account for the bulk (79%) of the biorenewables as the platform chemicals. Among biorenewable chemicals, the market for intermediates such as 1,3-propanediol (1,3-PD) is still nascent and accounts for $575 million worldwide [2]. The ever increasing demand for fuel has made the biodiesel industry an attractive alternative energy source. The current world Biodiesel production is led by EU at ~12 MT and with rapid expansion in capacity and usage being declared in developing countries, the Global market is estimated to touch 37 Billion gallons by 2016 with a growth rate of 42% [3]. However this leads, simultaneously, to a huge production of glycerol, which though not hazardous per se, has been described as the wastebasket of the biodiesel process. Crude glycerol, with many impurities and little value has caused market disruptions due to the problems associated in its disposal [3]. The production of 5 – 10 gallons of crude glycerol for every 100 gallons of biodiesel has led to a current glycerol production of ~2Bn pounds by the US biodiesel industry, in addition to ~560 MT pounds of glycerol emanating annually from non biodiesel sources [4]. The bio-fermentation of crude glycerol to 1,3-PD as a value added product gives a recourse to capitalizing on the current over capacity of glycerol. The

differential in the price between glycerol and 1,3-PD makes this an attractive economic production proposition for 1,3 propanediol as it does to improve the economic viability of biodiesel production.

1,3-PD is a large volume commodity chemical with a world market of over 100 million pounds per year spanning a plethora of applications. It is used as a valuable monomer in poly (trimethylene terephthalate), commercialized by Shell as Corterra [5]. Additionally it is applied in the production of polyethers, and polyurethanes. DuPont manufactures a polymer named Sorona, based on bio 1,3 PD, manufactured from corn sugar in their Decatur, Illinois plant. 1,3 PD is used to make transparent ballistic polymers, used as impact resistant eyeglasses. Additionally, 1,3 PD also finds applications as a minor tranquilizer of the family of Merprobamate, as a low cost biocide (PCT 3015), its derivatives have been applied as an antifouling agent in water cooling towers, air conditioners etc. It is also used as an anti freeze thawing agent and can improve properties for solvents, adhesives, laminates, resins, detergents and cosmetics [6]. It is also used in the preservation of consumer, household and institutional products [6]. Though the fermentative production of 1,3-PD has been known for long, petroleum based processes have dominated the production of 1,3-PD. It is produced primarily from acrolein (Degussa – DuPont) and Ethylene Oxide (Shell) [7,8]. The yields for the two processes are around 40% and 80% respectively. The hydroformylation and hydrogenation steps use high temperature and expensive catalysts and release toxic intermediates. Given these constraints and the impetus towards environment protection, precedence has been given to its microbial production [8 – 14] . DuPont along with Genencor have undertaken an extensive effort to develop a biocatalyst for the fermentative production of 1,3-PD. DuPont

and Tate-Lyle have been jointly developing the commercial manufacturing process for fermentation-based 1,3-PD drawing on their respective expertise in biocatalyst engineering commercial fermentation and carbohydrate processing (Genencor International and DuPont Expand R&D collaboration, 2001).

A lifecycle analysis of 1,3-PD based on Fossils Vs Biomass was carried out by Urban et al. for understanding the broader implications of technological alternatives and the results indicated that bio-based 1,3-PD is more attractive than fossil-based 1,3-PD because of less nonrenewable resource consumption and greenhouse gas emissions [15]. However, it was also stated that producing 1,3-PD alone from corn may have a negligible impact in terms of emissions and resource use [15]. Developing an economically feasible integrated process based on fermentative production and purification of 1,3-PD using industrial waste glycerol as the feedstock is thus a sustainable and holistic method in terms of resource utilization. A number of fermentative pathways to make glycerol based on sugars [9]are known but the same microorganisms cannot ferment glycerol to 1,3-PD [16]. New metabolic pathways to ferment sugar to glycerol and the glycerol subsequently to 1,3-PD have been studied [17]. The natural producers of 1,3-PD from glycerol are of genera *Klebsiella*, *Clostridia*, *Citrobacter*, *Enterobacter* and *Lactobacilli* [18 – 22]. Although facultative anaerobes such as the *Klebsiella Pneumoniae* and *Citrobacter freundii* are suitable, their classification as opportunistic pathogens complicates their usage with strict bio safety legislations. The use of Genetically modified *E.Coli* which is employed in the current production of Bio 1,3-PD by DuPont is also substantially mired in legislation besides being an expensive organism to obtain. Non pathogenic *Clostridium butyricum* and *C. pasteurianum* have been noted to grow on glycerol and form 1,3-PD [23 - 25] .

Besides the cost of the substrate, the separation of 1,3-PD amounts to almost 50 – 70% of the total production cost. 1,3-PD can be easily separated from the other by products of bacterial metabolism. However, that said, the concentration of 1,3-PD in the broth amounts to ~1.5%. The hydrophilicity of 1,3-PD compounds the complexity of purification. So far all the separation techniques tried out: evaporation, distillation, membrane filtration, pervaporation, ion exchange chromatography, liquid–liquid extraction, and reactive extraction have had their limitations in terms of cost and energy consumption and hence applicability. The process of evaporation and distillation suffer from the major issue of large energy consumption, given that the 1,3-PD needs to be concentrated from a very dilute starting solution, the process turns out to be rather economically unattractive. Additionally, desalination and deproteinization need to be carried out prior to distillation [26, 27]. Electrodialysis, used for desalination suffers from low product yield due to loss of 1,3-PD and serious membrane fouling and has been applied as an upstream method to evaporation [28,29]. Pervaporation using Na-ZSM-5 and X-type zeolite have been used on aqueous mixtures and model fermentation broths. Their performance has not been verified on real time fermentation broths in addition to the disadvantage of the usage of expensive materials [30, 31]. Although chromatographic separation of 1,3-PD resulted in high purity product, the final solution obtained was extremely dilute consequentially leading to energy consumptions as high as evaporation [32]. Similar results were observed with the adsorption of 1,3-PD on hydrophobic zeolites or active charcoal. The chromatographic matrix had to be regenerated frequently. A preparative silica gel liquid has also been reported by groups as recently as 2011[33]. The high hydrophilicity of 1,3-PD has been the major impediment in using a method as simple as solvent extraction. It is only partly

partitioned into a hydrophobic solvent phase and the method only works when a large amount of solvent is added to a rather concentrated solution of 1,3-PD making it unfeasible [34]. An alternative to solvent extraction would be to convert 1,3-PD into a hydrophobic compound, extract it and then convert it back to 1,3-PD. The complications of a number of unit operations in reactive extraction notwithstanding the process suffers from side reacting with other broth components and loss at each stage [35].

This thesis explores the production and purification of 1,3-PD from waste industrial glycerol and its concentration enrichment from dilute aqueous binary mixtures and model fermentation broths. The thesis is organized into two parts – the first explores the fermentative production of 1,3-PD from waste industrial glycerol using a soil based bacterial inoculum, while the second part focuses on the development of polymeric materials for pervaporative enrichment of 1,3-PD from dilute aqueous mixtures. In the first part, which explores fermentative production, 1,3-PD was produced with a robust fermentation process using waste glycerol feedstock from biodiesel production and a soil based bacterial inoculum developed using an iterative inoculation method. Advantages of mixed inocula include lower expenses in inocula generation and maintenance, more robustness against phage infections which may obliterate the entire population in a single species culture, the ability to metabolize a wider range of carbon sources, providing a cheaper and safer alternative to genetically engineered strains, and possible optimization of 1,3-PD with simultaneous conversion of alternative metabolites to biohydrogen [36, 37] The selectivity and yield in batch fermentations was optimized by appropriate nutrient compositions. 16S rDNA sequencing results were used to show a systematic selective enrichment of 1,3-PD producing bacteria with subsequent process control. A statistical

design of experiments was carried out on industrial glycerol batches to optimize conditions, which were used to run 2 CSTR experiments over a period of >500 hours each. 1,3-PD productivity, specific productivity and yields obtained at a dilution rate of 0.1 hr^{-1} are bettered only by pure strains in pure glycerin feeds.

The second part of the thesis focuses on the development of three polymer families to address the process bottleneck of 1,3-PD enrichment from dilute aqueous mixtures [6, 7, 14]. The complexity of separation is compounded by its high water affinity [38]. Although pervaporation is an energetically advantageous process. However, 1,3-PD cannot be enriched by materials conventionally used for pervaporation, such as siloxane polymers [39].High separation factors have been reported with an ionic liquid based supported liquid membrane (SLM), but the ionic liquid is extremely extensive [40]. However, a highly functional material needs to be designed into a system for industrial application to get adequate financial return on process investment. This portion of the thesis illustrates the development and application of three novel polymer systems – (i) functionalized siloxane, (ii) Allylcyclohexylamine based methacrylate polymers and (iii) Vinylimidazolium alkylphosphate ionic liquid based methacrylate polymers. The synthesis, characterization and pervaporative application of these materials is explored in part 2 of the thesis with binary as well as simulated fermentation broth compositions that closely mimic the compositions obtained with the CSTR run in the first part of this thesis. The polymer membrane were shown to exhibit a balance of cost and performance. The development of novel materials with a good cost performance balance forms a crux to the establishment of industrial separation procedures for 1,3-PD enrichment from fermentation broths. The removal of this main process bottleneck may underscore the advantages of using waste

industrial glycerol as a sustainable resource for biotechnologically producing 1,3-PD as a biorenewable alternative to chemicals from a petroleum platform.

References:

1. Ragauskas AJ, Williams CK, Davison BH, Britovsek G, Cairney J, Eckert CA, et al. The path forward for biofuels and biomaterial. Science 2006;311:484–9.
2. Biorenewable Chemicals World Market – Review, December 1, 2010, 162 Pages - Pub ID: SB2747396
3. Zhang, X, et al, Fermentation of Glycerol to Succinate by Metabolically Engineered Strains of *Escherichia coli* , Applied and Environmental Microbiology, April 2010, p. 2397-2401, Vol. 76, No. 8
4. Papanikolou, S., Aggelis, G., Biotechnological valorization of biodiesel derived glycerol waste through production of single cell oil and citric acid by *Yarrowia lipolytica, Lipid Technology, Volume 21, 4, 83 – 87, 2009*
5. *Dangseeyun, N., et al,* Thermal, crystallization, and rheological characteristics of poly(trimethylene terephthalate)/poly(butylene terephthalate) blends, Polymer Testing 23 (2004) 187–194
6. Zeng AP, Biebl H. Bulk chemicals from biotechnology: the case of 1,3-propanediol production and the new trends. Advances in biochemical engineering and biotechnology, vol. 74. Heidelberg: Springer Berlin; 2002. p. 239–59
7. Saxena, R., et al, Microbial production of 1,3-propanediol: Recent developments and emerging opportunities Biotechnology Advances 27 (2009) 895–913
8. Deckwer WD. Microbial conversion of glycerol to 1,3-propanediol. FEMS

Microbiol Rev, 1995;16:143–9.

9. Biebl H, Menzel K, Zeng AP, Deckwer WD. Microbial production of 1,3-propanediol, Appl Microbiol Biotechnol 1999;52:289–97.
10. Hartlep M, Hussman W, Prayitno N, Meynial-Salles I, Zeng AP. Study of two-stage processes for the microbial production of 1,3-propanediol from glycerol. Appl Microbiol Biotechnol 2002;60:60–6
11. Nakamura CE, Whited GM. Metabolic engineering for the microbial production of 1,3-propanediol. Curr Opin Biotechnol 2003;14:454–9
12. Mu Y, Teng H, Zhang D-J, Wang W, Xiu Z-L. Microbial production of 1,3-propanediol by Klebsiella pneumoniae using crude glycerol from biodiesel preparation. Biotechnol Lett 2006;28:1755–9
13. Cheng KK, Zhang JA, Liu DH, Sun Y, Liu HJ, Yang MD, et al. Pilot-scale production of 1,3-propanediol using Klebsiella neumoniae. Process Biochem 2007;42:740–4.
14. Xiu ZL, Chen X, Sun YQ, Zhang DJ. Stoichiometric analysis and experimental investigation of glycerol–glucose cofermentation in Klebsiella pneumoniae under microaerobic conditions. Biochem Eng J 2007;33:42–52.
15. Urban, R., Bakshi, B., 1,3-Propanediol from Fossils versus Biomass: A Life Cycle Evaluation of Emissions and Ecological Resources, *Ind. Eng. Chem. Res.* 2009, *48*, 8068–8082
16. Cameron DC, Altaras NE, Hoffman ML, Straw AJ. Metabolic engineering of propanediol pathways. Biotechnol Prog 1998;14:116–25.
17. Tong LT, Cameron DC. Enhancement of 1,3-propanediol production by co-

fermentation in Escherichia coli expressing genes from Klebsiella pneumoniae dha regulon genes, Appl Biochem Biotechnol 1992;34\35:149–59.

18. Yang G, Tian J, Li J. Fermentation of 1,3-propanediol by a lactate deficient mutant of Klebsiella oxytoca under microaerobic conditions. Appl Microbiol Biotechnol 2007;73:1017–24.
19. Raynaud C, Sarcabal P, Meynial-Salles I, Croux C, Soucaille P. Molecular characterization of the 1,3-propanediol production of Clostridium butyricum. Proc Natl Acad Sci, USA, 2003;100:5010–5.
20. Seifert C, Bowien S, Gottschalk G, Daniel R. Identification and expression of the genes and purification and characterization of the genes products involved in reactivation of coenzyme B12-dependent glycerol dehydratase of Citrobacter freundii. Eur J Biochem 2001;268:2369–78.
21. Zhu MM, Lawman PD, Cameron DC. Improving 1, 3-propanediol production from glycerol in a metabolically engineered Escherichia coli by reducing accumulation of sn-glycerol-3-phosphate. Biotechnol Prog 2002;18:694–9.
22. Schutz H, Radler F. Anaerobic reduction of glycerol to 1,3-propanediol by Lactobacillus brevis and Lactobacillus buchneri. Syst Appl Microbiol 1984;5:169–78.
23. Papanikolaou S, Fick M, Aggelis G. The effect of raw glycerol concentration on the production of 1,3-propanediol by Clostridium butyricum. J Chem Technol Biotechnol, 2004;79:1189–96.
24. Biebl H. Fermentation of glycerol by Clostridium pasteurianum—batch and continuous culture studies. J Ind Microbiol Biotechnol 2001;27:18–26

25. Saint-Amans, S. et al, Regulation of Carbon and Electron Flow in *Clostridium butyricum* VPI 3266 Grown on Glucose-Glycerol Mixtures JOURNAL OF BACTERIOLOGY,Mar. 2001, p. 1748–1754 Vol. 183, No. 5
26. Ames TT (2002) Process for the isolation of 1,3-propanediol from fermentation broth. US Patent 6. 361. 983 B1
27. Sanz MT, Blanco B, Beltran S, Cabezas JI (2001) Vapor liquid equilibria of binary and ternary systems with water, 1,3-propanediol, and glycerol. J Chem Eng Data 46:635–639
28. Gong Y, Tong Y, Wang XL, Liu DH (2004) The possibility of the desalination of actual 1,3-propanediol fermentation broth by electrodialysis. Desalination 161:169–178
29. Hao J, Liu DH (2005) Desalination of fermented broth containing 1,3- propanediol by electrodialysis. Chinese J Proc Eng 5:36–39
30. Li S, Tuan VA, Falconer JL, Noble RD (2001a) Separation of 1,3- propanediol from glycerol and glucose using a ZSM-5 zeolite membrane. J Membr Sci 191:53–59
31. Li S, Tuan VA, Falconer JL, Noble RD (2001b) Separation of 1,3- propanediol from aqueous solutions using pervaporation through an X-type zeolite membrane. Ind Eng Chem Res 40(8):1952– 1959
32. Cho M-H, Joen SI, Pyo S-H, Mun S, Kim J-H (2006) A novel separation and purification process for 1,3-propanediol. Process Biochem 41(3):739–744
33. Anand, P. et al, A novel downstream process for 1,3-propanediol from glycerol-based fermentation, Appl. Microbiol. Biotechnol, 2011, 90(4), 1267 – 76

34. Malinowski JJ (1999) Evaluation of liquid extraction potentials for downstream separation of 1,3-propanediol. Biotechnol Tech 13:127–130
35. Hao J, Xu F, Liu H, Liu D (2006) Downstream processing of 1,3- propanediol fermentation broth. J Chem Technol Biotechnol 81:102–108
36. F. M. Driessen, 1981. Protocooperation of yogurt bacteria in continuous culture. Pp. 99-120 in: Mixed Culture Fermentations.
37. M. E. Bushell and J. H. Slater, Eds. London: Academic Press, Harrison, D. E. F.1978. Mixed cultures in industrial fermentation processes. Advances in Applied Microbiology 24:129-164).
38. Triguero, R. Blanco, H. Machado, M. Rodríguez, Evaluation of liquid extraction potentials for downstream separation of 1,3-propanediol, Biotechnology Techniques. 13 (1999) 127–130.
39. P. Shao, R.Y.M. Huang, Polymeric membrane pervaporation, Journal of Membrane Science. 287 (2007) 162-179.
40. P.Izák, M. Köckerling, U. Kragl, Stability and selectivity of a multiphase membrane, consisting of dimethylpolysiloxane on an ionic liquid, used in the separation of solutes from aqueous mixtures by pervaporation, Green Chem. 8 (2006) 947–948.

Chapter 2. Batch, Design Optimization and DNA Sequencing Study for Continuous 1,3-propanediol Production from Waste Glycerol by a Soil Based Inoculum*

Abstract

1,3-propanediol (1,3-PD) was produced with a robust fermentation process using waste glycerol feedstock from biodiesel production and a soil based bacterial inoculum. An iterative inoculation method was developed to achieve independence from soil and selectively breed bacterial populations capable of glycerol metabolism to 1,3-PD. The inoculum showed high resistance to impurities in the feedstock. 1,3-PD selectivity and yield in batch fermentations was optimized by appropriate nutrient compositions and pH control. The batch yield of 1,3-PD was maximized to ~0.7 mol/mol for industrial glycerol which was higher than with pure glycerin. 16S rDNA sequencing results show a systematic selective enrichment of 1,3-PD producing bacteria with iterative inoculation and subsequent process control. A statistical design of experiments was carried out on industrial glycerol batches to optimize conditions, which were used to run 2 CSTR experiments over a period of >500 hours each. A detailed analysis of steady states at three dilution rates is presented. Enhanced specific 1,3-PD productivity was observed with faster dilution rates due to lower levels of solvent degeneration. 1,3-PD productivity, specific productivity and yield of 1.1g/l.hr, 1.5 g/g.hr and 0.6 mol/mol of glycerol were obtained at a dilution rate of 0.1 hr^{-1}which is bettered only by pure strains in pure glycerin feeds.

Keywords: 1,3-propanediol, mixed bacterial inoculum, CSTR, batch fermentation, Design of experiment, 16S sequencing

***Published as: Batch, Design Optimization and DNA Sequencing Study for Continuous 1,3-propanediol Production from Waste Glycerol by a Soil Based Inoculum**

B. Kanjilal, I. Noshadi, E. J. Bautista, R. Srivastava, R. S. Parnas, Applied Microbiology and Biotechnology, 2014 (In Press)

Introduction

A paradigm shift in fuels and chemicals towards renewables has led to a growing market for bio-renewable chemicals such as 1,3-propanediol (1,3-PD) with a plethora of applications (Ragauskas et al 2006; Nikolau et al 2008). The production of biodiesel, an attractive renewable fuel, (Noshadi et al 2012; Jaliliannosrati et al 2013), albeit, leads to excess glycerol byproduct (Haas et al 2006). Fermentation of crude glycerol to 1,3-PD provides a sustainable and value added recourse to waste utilization (Cheng et al 2007).

Naturally occurring glycerol to 1,3-PD convertors of genera *Klebsiella*, *Clostridia*, *Citrobacter*, *Enterobacter* and *Lactobacilli* were studied by Urban and Bakshi (2009), Yang et al (2007), Pakanikolau (2004) and Biebl (2001). Bio 1,3-PD from sugars is being commercialized by DuPont, Genencor and Tate and Lyle using a genetically modified E. coli with a 51 wt% yield (Saxena et al 2009). However, with the current glut and decreasing value, glycerol will likely gain preference as a sustainable feedstock platform for biorenewables (Johnson and Taconi 2007). Recent works utilize mixed bacterial consortia for fermenting industrial glycerol. These directly use heat shocked and pretreated soil or sludge and report 1,3-PD yields from 0.41 to 0.65 mol/ mol of glycerol (Selembo et al 2009, Rossi et al 2012, Misturini et al 2012, Liu et al 2013). While Liu et al (2013) do not use pH control in batch fermentation, Dietz and Zheng (2013) do so for fed batch fermentation using activated sludge. A caveat is offered by the latter on the high yield by assuming presence of additional unknown carbon sources in the sludge contributing to metabolite production.

The present work established an iterative reinoculation procedure for preparing the starting culture. The selectivity and productivity were optimized by media and process variations. 16S rDNA sequencing was used to study bacterial population statistics in batches. A statistical Design of Experiment (DOE) was used to optimize batch production of 1,3-PD. The DOE results were used to run CSTR fermentations for over 500 hours.

The iterative reinoculation eliminated soil particles from the culture to minimize variations due to changes in soil quality over storage and allowed easy optical density measurement. For future intended industrial application, soil elimination may reduce maintenance and ease pipeline flow. The effect of two nutrient compositions on selectivity is presented in this paper. The performance of pure glycerin (PG) and industrial glycerol (IG) feeds was compared. pH control resulted in a 0.7 mol/mol conversion with IG which is one of the highest reported in literature so far with mixed inocula. 16S rDNA sequencing results, a powerful tool for eliciting phylogenetic relationships, are reported on the starting inoculum and several batches. The DNA sequencing was carried out to obtain preliminary information about the composition of the inoculum and to briefly look at the effect of certain experimental parameters on the relative populations of species present. Sequencing on several fermentation batches are reported to underscore the fermentation results. This work also reports results of a statistical DOE with IG feed and concludes with analysis of two CSTR runs. The DOE, carried out with three variables, optimized conditions for 1,3-PD production in an attempt to integrate and reconcile the stochasticity inherent in two non-standard inputs - the inoculum and the industrial glycerol - with their spread of species and impurities, respectively. Response Surface Methodology (RSM) was utilized to model and optimize conditions for maximum 1,3-PD output, which was used to run two CSTR

experiments for 500 hours each. Steady states were analyzed for productivities and molar yields. This appears to be the first systematic study of a mixed bacterial inoculum for fermenting industrial waste glycerol to 1,3-PD.

Mixed inocula offer advantages with cheaper inocula generation and maintenance, robustness against phage infections and the ability to metabolize a wider range of carbon sources. They provide a cheaper and safer alternative to genetically engineered strains (Driessen 1981; Harrison 1978). Additionally, mixed cultures offer more flexibility for optimization of multiple product yields such as 1,3-PD and biohydrogen (Liu et al 2013).

While Papanikolau et al (2004) and Chatzifragkou et al (2011) continuously ferment IG to 1,3-PD using pure *C. Butyricum* strains, this work used a mixed bacterial inoculum with more than 100 species. The molar 1,3-PD yield ~0.66 at dilution rate of $0.04h^{-1}$ equaled Chatzifragkou's results. This is the first time, in a well-controlled CSTR fermentation with mixed inocula, that yields of 1,3-PD have been obtained comparable to those with pure cultures.

Materials and Methods

Stock culture preparation

Bacterial cultures were grown from a University of Connecticut organic farm soil. 5 g of the soil were soaked in 10 ml of freshly prepared and autoclaved Difco™ Reinforced Clostridial Medium (RCM) from Beckton Dickinson, Maryland, USA (38 g/l) and glycerol from Sigma Aldrich, USA (10 g/l), and purged with high purity nitrogen for 10 minutes. The method to check for the absence of dissolved oxygen is as per Li et al (2011). The test

tubes containing the soil in the growth medium were anaerobically heat shocked at 80C for 10 minutes, cooled for 2 minutes and incubated at 37C and 100 RPM (Li et al 2011) for 7 days. The resultant supernatant medium was used for reinoculation under similar conditions. This procedure was iterated 4 times resulting in a thick inoculum as a seed culture for further bacterial inoculations and fermentation.

Feed media composition: Batch, DOE and CSTR

Feed compositions F1 and F2 with 3 g/l of pure glycerol (PG) were used to illustrate the effect of nutrient composition on selectivity. Compositions F2 and F3, with 20 g/l of PG and IG respectively, were used to compare their respective performances, with and without pH control. The IG was obtained as a byproduct from converting waste cooking oil to biodiesel (Pomykala et al 2013). Glycerol, yeast extract, potassium phosphates and ammonium sulfate solutions were autoclaved separately at 121C. Other nutrients and micronutrient solutions were sterile filtered by 0.22 μm syringe filter and stabilized under refrigeration at acidic pH.

F1,Composition per liter – Pure Glycerol-3g, $(NH4)_2CO_3$ 2g, KH_2PO_4 1g, $MgSO_4.7H_2O$ 0.1g, NaCl 0.01g, $MnSO_4.7H_2O$ 0.015g, $CaCl_2.2H_2O$ 0.01g, $Na_2MoO_4.2H_2O$ 0.01g, $FeCl_2.4H_2O$ 2.75 mg, Feed buffered with 0.05 M 2-N morpholino ethane sulfonic acid monohydrate. Initial pH ~ 5.5 – 5.7 (Liu et al 2013)

F2, Composition per liter - Pure Glycerol (PG) 3g or 20 g, Yeast Extract 1g, $(NH4)_2SO_4$ 2g, KH_2PO_4 0.5g, K_2HPO_4 1g, $MgSO_4.7H_2O$ 0.2g, $CaCl_2.2H_2O$ 15 mg, $FeSO_4$ 5mg, Micronutrients : $Na_2MoO_4.2H_2O$ 0.0072 mg, $FeCl_2.4H_2O$ 0.3 mg, $CoCl_2$. $4H_2O$ 0.38 mg,

$MnCl_2.4H_2O$ 0.2 mg, $ZnCl_2$ 0.014 mg, H_3BO_3 0.012mg, $NiCl_2.6H_2O$ 0.0048 mg, $CuCl_2.2H_2O$ 0.0034mg

F3, Composition per liter – Industrial Glycerol (IG) 20g, Yeast Extract 1g, (NH4)2SO4 2g, Micronutrient composition same as F2.

All commercially available salts and chemicals were obtained from Sigma Aldrich, USA and used without any further purification.

For the DOE, the concentrations of IG and yeast extract were varied over selected ranges. The CSTR experiments used the optimized concentrations of IG and yeast extract from the DOE. The $(NH4)_2SO_4$ and micronutrient composition was kept the identical to F3 for both DOE and CSTR.

Batches without pH control

Anaerobic, 150ml batch fermentations were carried out in serum bottles. The pH was adjusted to 6.8 – 6.9 prior to inoculum injection. The media were purged with nitrogen and the serum bottles incubated at 37C and 100 rpm. The absence of dissolved oxygen was checked as per Li et al (2011). The inoculum transferred to the batches was either ~3% or 7% of the batch volume. All batches were repeated in triplicate and the results averaged.

Batches with pH control

Fermentations were carried out in a BioFlo 3000 Bioreactor from New Brunswick Scientific. The pH was maintained by 2N NaOH and 1N HCl and the batch volume was 300 ± 10 ml. The temperature and agitator were kept at 37C and 100 rpm respectively and

nitrogen was purged through the headspace. The initial nitrogen flow rate of 250 mL/min, for 1.5 hours, was decreased to 120 mL/min for rest of the experiment (Li et al 2011). Inoculum transferred was 7% of batch volume and each batch was repeated in triplicate.

16s rDNA sequencing for identification and characterization of consortia

The genomic DNA was isolated, amplified, sequenced and analyzed. Sequences of the V4 hypervariable region of the DNA were analyzed to identify bacterial classification and relative abundances. An average of 68490 gene sequences were analyzed per sample. The experimental details are delineated in Nelson et al (2014). Sequencing was done on the stock culture (initial inoculum) and final samples of several batch fermentations. Average of triplicate results are presented for 6 samples: Feed F1 (3g/l PG)-no pH control, F2 (3 g/l PG)-no pH control, F2 (20g/l PG)-pH 5.5, F2(20g/l PG)-pH 6.5, F3(20g/l IG)-pH 5.5, F3(20g/l IG)-pH 6.5. The results of the 16s rDNA sequencing were submitted to the NCBI SRA database with an accession number of SRP047483.

Design of Experiment batches

A statistical DOE was performed on anaerobic batches with three process variables – pH, IG concentration, and yeast extract concentration. RSM was utilized to model and optimize the final 1,3-PD concentration as a response variable. The mineral nutrient compositions were identical to composition F3. The pH, IG and yeast extract concentrations were varied from 4.8 to 7.2, 15 to 35 g/l and 0.5 to 4g/l, respectively. Experimental details are as per section 2.4.

CSTR Fermentations

Two CSTR runs were carried out, based on conditions computed from the RSM optimization, in a BioFlo 3000 Bioreactor. The anaerobic fermentation was run in the batch mode until an exponential growth was initiated, at which point fresh medium was fed into the fermentor. The CSTR medium was a replica of the RSM optimized composition. The pH was maintained at the optimized value. The other experimental details are mentioned in section 2.4. The fermentation volume was kept constant while being run at various dilution rates. The dilution rate (D) is defined as the reciprocal of feed and cellular residence time in the absence of cell retention (Li et al 2011).

Analytical methods

The IG feedstock was analyzed by Thermogravimetric analysis (TGA) on a TA Instruments TG Analyzer, using 50ml/min nitrogen flow and 10C/min temperature ramp to 800C. Cell density was measured at 540 nm using a BioMate™ spectrophotometer (Thermo Spectronic, USA). Aliquot samples of known volume were centrifuged and the biomass weight measured after washing with PBS media and drying to constant weight. The estimated biomass in g/l was numerically correlated to corresponding optical density. The glycerol and metabolite concentrations were analyzed on 0.22μm syringe filtered samples by gas chromatography (GC) using a DB-FFAP capillary column with an MS detector and a 1μL injection volume. GC injector and detector temperatures were kept at 240C and 270C respectively. For the analysis of the 16S rDNA sequencing data, QIIME versions 1.6 and 1.7 were used (Nelson et al 2014) – a software package for statistically processing and analyzing sequencing data of microbial communities (Caporaso et al 2010).

Results

Analysis and Treatment of Industrial Glycerol

The industrial glycerol from the biodiesel run contained KOH transesterification catalyst, miscellaneous impurities and remnant methanol. Prior to methanol distillation, KOH was partly precipitated as KH_2PO_4 and K_2HPO_4 using H_3PO_4. The resultant IG had ~ 75 mass% glycerin, ~ 20 mass% methanol, and ~5 mass% inorganic residue after the TGA reached 800C which was likely remnant phosphates.

Batch Fermentation

Effect of feed nutrient composition on 1,3-PD selectivity

The effect of media composition is illustrated by comparing feed F1 and F2 (Figure 2.1A, Bars 1 and 2) in batches without pH control using a PG concentration of 3 g/l. The inoculum was 3% of batch volume. The major metabolite in F1 was acetate (0.718 mol/mol gly) and with F2, the major metabolite was 1,3-PD (0.197 mol/mol gly). F2 yielded a better molar conversion to 1,3-PD. 1,3-PD:Acid molar ratios were 0.19 with F1 and 1.01 with F2, which made F2 much more selective towards 1,3-PD. Although the 16S r-DNA sequencing results, in a later section, show little difference between bacterial populations, feed F2 encouraged metabolism in favor of 1,3-PD.

Comparison of pure and industrial glycerol without pH control

The performances of PG and IG were compared with feeds F2 and F3, respectively. The product yields are shown in Figure 2.1A (Bars 3 and 6). Total molar liquid metabolite

yields of 27% and 22% were obtained with PG and IG, respectively. 1,3-PD yields of 0.247 and 0.204 mol/mol of glycerol were achieved with PG and IG feeds, respectively. During the experiment, the pH dropped from ~ 6.9 to ~4.5 with a concomitant decrease in bacterial growth resulting in limited glycerol utilization. The acid production was higher with PG while the solvent production was similar with both feeds (Fig2.1A). The 1,3-PD:Total acids molar ratio was at 8.2 and 12.0 for PG and IG respectively. Comparing bars 2 and 3, the selectivity in favor of 1,3-PD was enhanced when the glycerol feed concentration was increased from 3 to 20 g/l and the inocculum volume was increased from 3 to 7% of the batch volume. Semi-log biomass profiles are shown in Figures 2.1B and 2.1C. The liquid metabolite production was delayed with IG feed. The semi-log Biomass-time plots for IG batch had a biphasic behavior (Fig.2.1C) but those with PG (Fig.2.1B) were not as clearly delineated. The IG feedstock with ~ 5 mass% phosphates and other impurities may have suppressed metabolic processes with the resultant initial lag. The metabolite profiles indicated the probable existence of *C. butyricum* as the most dominant species.

The effect of pH control on product yield

Batches with PG and IG feeds (F2 and F3, 20 g/l glycerol) were carried out at pH 5.5 and 6.5. Figure 2.1A (Bars 4,5 and 7,8) summarizes the yields. At pH 5.5 (Bars 4 and 7), the total metabolite molar yield of 77% was nearly identical for the two feeds. At pH 6.5 the total metabolite molar yields were ~83% and ~ 85.7%, with PG and IG respectively, which are indistinguishable. For both feeds the acid production increased marginally with pH, and the acetate production was slightly higher with PG than with IG. With PG, pH had little effect on the 1,3-PD molar yield. At pH 5.5 the molar 1,3-PD yield for PG and IG

respectively, was 56 and 63%. The same changed to 52 and 71% at pH 6.5. The molar 1,3-PD yield was higher with IG and increased with pH. This increased yield was at the expense of selectivity as the 1,3PD:Acids ratio dropped to ~2.5 and ~4.9 for PG and IG respectively. The limit of glycerol utilization here had much to do with toxic intermediate buildup.

At pH 5.5, exponential growth is seen with both feeds with no identifiable lag phase (Figs. 2.1D and 2.1E). The growth was faster in PG. At pH 6.5, both feeds exhibited a poor fit to an exponential pattern unless a lag phase was included (Figs. 2.1D and 2.1E). Fits to biphasic growth patterns at pH 6.5 (Fig 2.1D and 2.1E) indicate a ~10hour lag phase for both PG and IG feeds.

Batch results at pH 6.5 with PG and IG feeds of 30 g/l showed a drop in 1,3-PD yield by 8% for PG and ~19% for IG compared to batches with 20g/l glycerol concentration. The initial lag time increased from ~10 hours to ~15 hours but maximum biomass levels were unchanged. With even higher IG concentration of 42 g/l initial growth lag times increased from ~15 to ~24 hours, and a stunted biomass growth, inefficient glycerol utilization and even lower 1,3-PD yields were observed (0.27mol/mol). With 58g/l IG, the biomass did not reach an exponential growth stage.

16s r-DNA sequencing

The DNA sequencing yielded information on the relative populations of species and genera comprising the inoculum. A total of 160 bacterial species were identified in the initial inoculum, which decreased to 133 and 146 respectively with fermentation in feeds F1 and

F2 (with 3g/l glycerol, 3% inoculum) without pH control. pH control with a PG feed caused further reduction, especially at pH 6.5. The reduction in the number of species or the effect of pH was less evident with IG feeds. The results are shown in Figure 2.2(a). Figure 2.2(b) shows Shannon Index and Simpson's index of diversity. The Shannon index (SI) increases with richness and evenness of the community. The Simpson's index of diversity (SID), a measure of dominance also increases with diversity (Tumisto 2012). The reduction in SI and SID in F1 and F2 from the starting inoculum reflected reduced diversity, rise of the dominance of specific genera and the obliteration of some classes. The indices further dropped with pH control underscoring population unevenness and dominance by the *Clostridia* genus. In the initial inoculum *Clostridia* and *Enterobacter* were the most populous genera comprising 45% and 30% of the population followed by unidentifiable genera from *Clostridiaceae* and *Enterobacteriaceae* families at 15 and 9% respectively. 35 identified minor members and a host of unidentified classes were grouped together and these comprised rest of the population in the initial inoculum. The results are presented in Figure 2.2C. The average populations of *Clostridia* and *Enterobacter* genera were preserved in F1 and F2 batches without pH control.

Design of Experiments and Analysis of Variance

Response Surface methodology (RSM) was employed to optimize IG fermentation with 17 batch fermentations and final 1,3-PD concentration as the response variable. Three experimental factors, pH (A), feed IG concentration (B) and yeast extract concentration (C) as independent variables, were put in a box-behnken design and used at 3 levels between minima and maxima (Montgomery 1996). The ranges of the pH, IG concentration

and yeast extract concentration were 4.8 – 7.2, 15 – 35 g/l, 0.5 – 4 g/l, respectively. The design center experiment was repeated 5 times to estimate the error. The regression and test factor coding is detailed in Noshadi et al (2012). Table 1 provides the 1,3-PD concentration at the end of each batch. Biomass and metabolite profiles were noted for each experiment as a quality control check, but those details are not necessary for this discussion. The lag time for initial bacterial growth increased with glycerol feed concentration. The final metabolite concentrations were estimated by GC from samples taken once the inoculum had entered a stationary phase. The experimental response was related to independent variables by an optimization model (Eqn. 1).

$$\eta = \beta_0 + \sum_{j=1}^{k} \beta_j x_j + \sum_{j=1}^{k} \beta_{jj} x_j^2 + \sum_i \sum_{<j=2}^{k} \beta_{ij} x_i x_j + e_i \qquad (1)$$

η is the final 1,3PD concentration, x_i and x_j the independent factors of pH, glycerol concentration and yeast concentration, β_0 the constant coefficient, β_j, β_{jj} and β_{ij} the coefficients for linear, quadratic and interaction effects, and e_i is the error. Coefficients of determination R^2 and R_{adj}^2 were used to indicate the quality of fit. Statistical significance was checked with F-value, p-value and estimates detailed in Myers and Montgomery (2000) and Noshadi et al (2012). Experimental response and independent variables were correlated by Eq.(2). Least squares regression was used to obtain a best fit model.

$$\eta = +8.35426 + 2.70258*A - 1.30514*B + 0.15521*A*B + 0.013780*B^2 + 0.61289*C^2 \qquad (2)$$

Table 2 shows the ANOVA evaluations of this model. Appropriateness of fit was measured by F-value, R^2, p-value, and lack of fit (Myers and Montgomery 2000). Large F-values and

low p values indicate significance of linear terms for pH (A) and IG concentration (B) and underscores strong correlations of the quadratic terms for the glycerol concentration (B) and yeast concentration (C) with the response. Coefficient of term AB indicates significant coupling effect of pH with IG concentration on 1,3-PD concentration. Low p-values <0.0001 indicate that the chance of the model F value arising due to experimental noise is negligible. The lack of fit F-value of 3.29 indicated its insignificance relative to pure error. The regression equation and coefficient of determination were evaluated to test the fit of model. Randomly scattered studentized residuals vs responses (Figure 2.3A) indicate that variation in original observations is not related to response value. The experimental vs computed 1,3-PD concentration, from Eq. 2, are plotted in Figure 2.3B. A high adjusted determination coefficient underscores significance of the model (Myers and Montgomery 2000, Noshadi et al 2012). Numerical optimization was used to find the experimental factors expected to give the highest 1,3-PD concentration. Optimum conditions of 34.9 g/l glycerol, pH 7.2 and yeast extract 3.4 g/l were determined.

Continuous production of 1,3-propanediol

Continuous fermentation (CSTR) of IG to 1,3-PD was conducted with RSM optimized conditions at progressively increasing dilution rates, and steady states were identified. The fermentation was switched to CSTR once an exponential bacterial growth initiated. This corresponded with acidogenesis as the PID control system responded by switching on the base supply to maintain the pH. Two individual runs, each lasting > 500 hours, were carried out. The biomass, feed and remnant glycerol, and metabolite concentration profiles are presented in Figures 2.4A, 2.4B and 2.4C, for the first run. Three steady states at dilution

rates (D) of 0.04hr^{-1}, 0.11 hr^{-1} and 0.19 hr^{-1} were achieved for the first CSTR run. The details of the second CSTR run and the steady states of the first run at D = 0.11 hr^{-1} and D = 0.19 hr^{-1} are presented in Figures 2.7 – 2.10. Figures 2.4D, 4E, 4F and 4G show CSTR profiles on expanded time scales at D = 0.04 hr^{-1} for the first CSTR run. After 480 hours, when the system returned to D 0.04hr^{-1}, the metabolite profiles did not recover to earlier levels, even though the biomass recovered. This indicated solvent degeneration, typical in *Clostridial* fermentations (Li et al 2011).

The steady state volumetric and specific glycerol consumption rates, molar yields and productivities were computed. The 1,3-PD productivity (Figure 2.5 A) went through a maximum of 1.2 g/l.hr and yield of 0.6 mol/mol of glycerol at D = 0.11hr^{-1}. This trend was replicated by all metabolites. The volumetric glycerol consumption rate (Figure 2.5B) increases with dilution rate. 1,3-PD molar yield decreased from 0.65 to 0.50 mol/mol gly with increase in dilution from 0.04 to 0.19 hr^{-1} (Figure 2.5C). A similar trend in molar yields of other metabolites was observed. The solvent to acid ratio increased sharply at D = 0.19 hr^{-1} for both runs, plausibly due to a protracted or late acidogenesis of a species in the consortium. Despite increased specific glycerol consumption, molar yield decreased with dilution rate (Fig 2.5C) as the time allowed for residence and fermentative conversion decreased.

The specific metabolite productivity of 1,3-PD, specific glycerol consumption rates (Figures 2.6A and 2.6B) increased with dilution rate with the former reaching a maximum of 1.5g/g of biomss.hr. The specific ethanol, acetate and butyrate productivities went through a maximum at D =0.11 hr^{-1} (Fig 2.6A). The 1,3-PD productivities and specific

productivities were comparable to CSTR results of *C. Butyricum* VPI 3266 on raw and pure glycerol at D=0.11 hr^{-1} (Gonzalez et al 2004). Productivities and yields higher than those reported here were found in studies based on pure strains using pure glycerin feed (Kaur et al 2012). Table 3 lists a comparison between select glycerol to 1,3-PD fermentations with a variety of cultures and feeds.

The volumetric productivity and specific productivity follow dissimilar trends with increasing dilution rate, and this apparent contradiction is discussed below.

Discussion

Batch fermentations

The 1,3-PD production appeared growth rate dependent in pH controlled batch experiments. Solventogenesis slowed bacterial growth and efficiency due to 3-hydroxypropionaldehyde build up - a toxic intermediate (Beibl 2001). Although pH is not a solventogenesis trigger, it is a key factor in clostridial fermentations, such as ABE processes, where low pH is conducive to solventogenesis and detrimental to growth (Jones and Woods 1986). However, in the experiments reported here, a higher pH enhanced bacterial growth and 1,3-PD yield. Although, the course of growth and metabolism is dynamically influenced by acid concentrations in clostridial fermentation (Colin et al 2001), in these experiments, acids and 1,3-PD were produced simultaneously. 1,3-PD was the dominant product in all batches followed by butyrate, acetate and ethanol. Remarkably, 1,3-PD molar yield at pH 6.5 was enhanced with IG feed, relative to PG, despite slower biomass growth. At pH 5.5, 1,3-PD production was delayed with IG. Clearly, both pH and

nutrient conditions play a strong role in determining performance but conditions were found that were very favorable for 1,3-PD production.

Inhibition was observed at glycerol feed concentrations of 30 g/l and higher. While the reduction of 1,3-PD yield was only 8% with PG, it was 19% with IG at feed concentration of 30 g/l. This may indicate glycerin inhibition in the case of PG (Biebl 1991), and glycerin and phosphate inhibition in the case of IG. The inhibition becomes greater as IG feed concentration increases until biomass growth is completely inhibited at 58 g/l. Phosphates may enhance metabolic performance of bacterial cultures, but may be toxic at higher concentrations (Stewart 1975; Qureshi et al 2001). Each strain in the 160 species of the mixed inoculum used in this work may have individual phosphate responses. It is most probable that the phosphates in our IG feed improved fermentation performance at lower IG feed concentrations, compared to PG, but became toxic beyond a limit.

16S rDNA sequencing

The DNA sequencing results underscored the presence of 1,3-PD producing genera in the initial inoculum. With fermentations, even without pH control, the diversity of the bacterial population decreased. While the feed composition had little effect on the relative species' populations, feed F2 made it conducive for the production of 1,3-PD for the predominant species even without pH control. For batches without pH control, a drop in pH during the first 20 hours of the experiments (exponential growth) and concomitant stunted biomass growth allowed little time for disparities between the populations of different species to develop. However, the 16S rDNA sequencing of bacterial population at the end of the batches revealed a significant effect of pH on growth and obliteration of specific genera.

Control of pH allowed a marked growth of *Clostridia* genus to 80-95% of the population while nearly obliterating the *Enterobacter* genus. With pH control, the bacterial population diversity dropped further with rising dominance of specific genera and the obliteration of some classes.

DNA sequencing results are consistent with the metabolite profiles from the fermentations. While *Clostridium* is anaerobic, *Enterobacter* is facultatively aerobic. The main byproducts with *Clostridial* glycerol fermentation are acetate and butyrate and that with *Enterobacter* are ethanol and acetate (Barbarito et al 1995). With *Enterobacter*, pyruvate is cleaved to acetyl-CoA or condensed to α-acetolactate with subsequent transformation to acetoin and 2,3-butanediol. Very little ethanol was produced in the fermentations while the major secondary products were acetate and butyrate, consistent with the dominance of *Clostridial* species.

Statistical DOE - Influence of experimental parameters on the final 1,3-PD concentration

The regression results in Eq. 2 indicate that pH had the strongest effect on the final 1,3-PD concentration (Figures 2.3B ad 2.3C). The 1,3-PD concentration was an increasing function of both pH and IG concentration, but went through a minimum at ~ 2.5 g/l of yeast extract concentration. High final metabolite concentrations are a natural outcome of enhanced concentration of carbon source in feed and hence underscoring the significance may seem redundant. However, it may be stressed that batch experiments with > 35 g/l glycerol failed to give appreciable bacterial growth even after > 24 hours of lag time and hence the feed

IG had to be limited to a maximum of 35 g/l for the DOE. As with earlier batches, growth suppression may be linked to remnant phosphates and impurities in IG.

CSTR

It may be recalled that in pH controlled batches, solventogenesis was apparently independent of acid concentration and 1,3-PD was concomitantly produced with the acids. Increased dilution rates in CSTR, counterintuitively, enhanced the Solvent to Acid ratios (Figure 2.5C). This is in contrast to biphasic (eg; ABE glucose) fermentations, where solventogenesis is subsequent to acidogenesis, high dilution rates keep the inoculum in acidogenesis and low dilution rates allow time for solventogenesis and molecular reassimilation (Jones and Woods 1986). In ABE fermentation, butanol and butyrate are formed via butyryl CoA whose conversion to either metabolite allows for molecular reassimilation. Here 16S sequencing results prove *Clostridial* domination at controlled pH. In *Clostridial* glycerol fermentation, butyric acid and 1,3-PD are on competitive, not complimentary routes. The acids and 1,3-PD form via respective intermediates - dihydroxyacetone (DHA) and 3-hydroxypropionaldehyde (3HPA) (Ragauskas et al 2006). Simple molecular reassimilation pathway between acids and 1,3-PD is absent. The butyrate competes with 1,3-PD for re-generating NADH2 equivalents. The oxidative branch converts glycerol to DHA by NAD+ dependent glycerol dehydrogenase and phosphorylates it to enter glycolysis, resulting in acids. The remaining glycerol is dehydrated to 3HPA by a dehydratase and reduced to 1,3-PD by an NAD+-dependent oxidoreductase. The reductive branch regenerates NAD+ via butyrate synthesis from

acetyl-CoA. This needs two NADH2-oxidizing steps per butyrate molecule and is antagonistic to 1,3-PD production (Papanikolaou, et al 2004).

At lower D, the average age of cells is higher with longer toxic intermediate exposure, which may increase the propensity for solvent degeneration. In a CSTR, cells are washed away and replaced via cellular multiplication. At steady state, the rate of biomass production by cellular multiplication is matched by the rate at which the cells are washed out of the fermenter. The rate of biomass production is therefore given by $[\dot{m}]_p = [m] \bullet D$, where [m] is the steady state biomass concentration and D is the dilution rate. The computed steady state values of $[\dot{m}]_p$, in (g.dry wt.)/l-hr, were 0.046, 0.117 and 0.174 at respective D = 0.04, 0.11 and 0.19 hr^{-1}. Thus, mass balance reveals that bacteria multiplied faster at higher dilution rates (Figure 2.4A). Younger cells, with lower toxic intermediate exposure, are more efficient 1,3-PD producers leading to increased specific 1,3-PD productivity.

Over the course of the CSTR experiment, the bacterial population and its distribution may have undergone a significant statistical evolution with the obliteration and preservation of specific species. In addition to this statistical population evolution, genetic or mutative evolutions may also be at play determining the CSTR profiles, a detailed study of which is beyond the scope of this work. Drawing from the fermentation results and the DNA sequencing experiments, both of these evolutionary changes can contribute to shifts in metabolic propensities. The CSTR study of a multispecies culture thus presents future opportunities for evaluation of a directed evolution phenomena of bacterial population

statistics – a combination of systematic screening and mutative evolutions over generations of bacterial growth.

Studies on batch, 16S rDNA sequencing, statistical DOE and CSTR production of 1,3-PD from waste glycerol with a soil based inoculum was presented. The iteratively inoculated starting culture, feed composition and pH control enhanced 1,3-PD selectivity, productivity and selectively bred 1,3-PD producing bacteria as shown by 16S rDNA sequencing. The DOE was used to optimize conditions for CSTR, in which 1,3-PD molar yield decreased but selectivity and specific productivity increased with dilution rate due to faster bacterial growth and reduced solvent degeneration. 13-PD productivity and molar yields obtained were comparable to studies with pure strains using pure glycerin feed.

Acknowledgements

The authors gratefully acknowledge Prof. Joerg Graf and Department of Molecular and Cell Biology, University of Connecticut, for their assistance in the 16S rDNA sequencing experiments. Portions of this work were supported by DOE Grant DE-EE0003116.

References

Barbarito F, Camarassia-Claret C, Grivet JP, Bories A (1995) Glycerol fermentation by a new 1,3-propanediol-producing microorganism: *Enterobacter Agglomerans*. Appl. Microbiol Biotechnol 43: 786-793.

Biebl H (1991) Glycerol fermentation of 1,3-propanediol by *Clostridium Butyricum*. Measurement of product inhibition by use of a pH-auxostat. Appl Micro Bio Biotechnol 35: 701–705.

Biebl H (2001) Fermentation of glycerol by *Clostridium pasteurianum*—batch and continuous culture studies. J Ind Microbiol Biotechnol 27:18–26.

Caporaso JG, Kuczynski J, Stombaugh J, Bittinger, Bushman FD, Costello EK, Fierer N, Gonzalez Peña A, Goodrich JK, Gordon JI, Huttley GA, Kelley ST, Knights D, Koenig, JE, Ley RE, LozuponeCA, Mcdonald D, Muegge BD, Pirrung M, Reeder J, Sevinsky JR, Turnbaugh, PJ, Walters WA, Widmann J, Yatsunenko T, Zaneveld J, Knight R (2010) QIIME allows analysis of high-throughput community sequencing data. Nature Methods 7(5):335-336.

Chatzifragkou A, Papanikolaou S, Dietz D, Doulgeraki AI, Nychas GE, Zeng AP (2011) Production of 1,3-propanediol by *Clostridium butyricum* growing on biodiesel-derived crude glycerol through a non-sterilized fermentation process. Appl Microbiol Biotechnol 91:101–112.

Cheng KK, Zhang JA, Liu DH, Sun Y, Liu HJ, Yang MD, Xu JM (2007) Pilot-scale production of 1, 3-propanediol using *Klebsiella pneumonia*. Process Biochem 42: 740–4.

Colin T, Bories A, Lavigne C, Moulin G (2001) Effects of acetate and butyrate during glycerol fermentation by *Clostridium butyricum*. Current Microbiology 43:238 – 243.

Dietz D, Zheng AP (2014) Efficient production of 1,3-propanediol from fermentation of crude glycerol with mixed cultures in a simple medium. Bioprocess Biosyst. Eng 37: 225 – 233.

Driessen FM (1981) Protocooperation of yogurt bacteria in continuous culture. In: Bushell, ME and Slater JH (ed) Mixed culture fermentation, Academic Press, London, pp. 99-120.

Gallarso R, Faria C, Rodrigues LR, Pereira MA, Alves MM (2014) Anaerobic granular sludge as a biocatalyst for 1,3-propanediol production from glycerol in continuous bioreactors. Bioresource Technology 155: 28 – 33.

Gonzalez-Pajuelo M, Andrade JC, Vasconcelos EI (2004) Production of 1,3-propanediol by *Clostridium butyricum* VPI 3266 using a synthetic medium and raw glycerol. J Ind Microbiol Biotechnol 31: 442–446.

Haas MJ (2006) A process model to estimate biodiesel production costs. Bioresource Technology 97: 671–678.

Harrison DEF (1978) Mixed cultures in industrial fermentation processes. Advances in Applied Microbiology. 24:129-164.

Jaliliannosrati H, Amin NAS, Talebian-Kiakalaieh A, Noshadi I (2013) Microwave assisted biodiesel production from Jatropha curcas L. seed by two-step in situ process: Optimization using response surface methodology. Bioresource Technology 136:565–573.

Johnson DT, Taconi, KA (2007) The Glycerin Glut: Options for the Value-Added Conversion of Crude Glycerol Resulting from Biodiesel Production. Environmental Progress 26: 338–348.

Jones DT, Woods D (1986) Acetone-Butanol Fermentation Revisited. Microbiological Reviews 50:4:484-524.

Kaur G, Srivastava AK, Chand S (2012) Advances in biotechnological production of 1,3-propanediol. Biochemical Engineering Journal 64:106 – 118.

Li SY, Srivastava R, Suib SL, Li Y, Parnas RS (2011) Performance of batch, fed-batch, and continuous A–B–E fermentation with pH-control. Bioresource Technology 102: 4241–4250.

Liu B, Christiansen K, Parnas RS, Xu Z, Li B (2013) Optimizing the production of hydrogen and 1, 3-propanediol in anaerobic fermentation of biodiesel glycerol. Int. J. of Hydrogen Energy 38: 3196 – 3205.

Menzel K, Zeng AP, Deckwer WD (1997) High concentration and productivity of 1,3-propanediol from continuous fermentation of glycerol by *Klebsiella pneumonia*. Enzyme Microb. Technol 20(2):82–6.

Metsoviti M, Paraskeyajdi K, Koutinas A, Zeng AP, Papanikolaou S (2012) Production of 1,3-propanediol, 2,3-butanediol and ethanol by a newly isolated *Klebsiella oxytoca* strain growing on biodiesel-derived glycerol based media. Proc Biochem 47:1872–1882.

Montgomery DC (1996) Design and analysis of experiments. John Wiley & Sons, USA

Morandi A, Zhaxybayeva O, Gogarten JP, Graf J (2005) Evolutionary and Diagnostic Implications of Intragenomic Heterogeneity in the 16S rRNA gene in *Aeromonas* Strains. Journal of Bacteriology 187: 6561-6564.

Myers RH, Montgomery DC (2000) Response surface methodology: process and product optimization using designed experiments 2nd Edition. John Wiley & Sons, USA

Nelson MC, Morrison HG, Benjamino J, Grim SL, Graf J (2014) Analysis, Optimization and Verification of Illumina-Generated 16S rRNA Gene Amplicon Surveys. PLoS ONE 9(4): e94249.

Nikolau BJ, Perera MA, Brachova L, Shanks B (2014) Biorenewable Platform biochemicals for a biorenewable chemical industry. The Plant Journal 54: 536–545.

Noshadi I, Amin NAS, Parnas RS (2012) Continuous production of biodiesel from waste cooking oil in a reactive distillation column catalyzed by solid heteropolyacid: Optimization using response surface methodology (RSM). Fuel 94: 156-164.

Papanikolaou S, Fick M, Aggelis G (2004) The effect of raw glycerol concentration on the production of 1,3-propanediol by *Clostridium butyricum*. J Chem Technol Biotechnol 79: 1189–96.

Pomykala M, Stuart JD, Noshadi I, Parnas RS (2013) The interplay of phase equilibria and chemical kinetics in a liquid/liquid multiphase biodiesel reactor. Fuel 107, 623–632.

Qureshi N, Lolas A, Blaschek HP (2001) Soy molasses as fermentation substrate for production of butanol using *Clostridium beijerinckii* BA101. Journal of Industrial Microbiology and Biotechnology 26: 290–295.

Ragauskas AJ, Williams CK, Davison BH, Britovsek G, Cairney J, Eckert CA, Frederick WJ, Hallett JP, Leak DJ, Liotta CL, Mielenz JR, Murphy R, Templer R, Tschaplinski T (2006) The path forward for biofuels and biomaterials. Science 311:484–9.

Rossi DA, Da Costa JB, De Souza EA, Ruaro Peralba MC, Ayub MAZ (2012) Bioconversion of residual glycerol from biodiesel synthesis into 1,3-propanediol and ethanol by isolated bacteria from environmental consortia. Renewable Energy 39 : 223 – 227.

Saint-Amans S, Perlot P, Goma G, Soucaille P (1994) High production of 1,3-propanediol from glycerol by *Clostridium butyricum* VPI 3266 in a simply controlled fed-batch system. Biotechnol Lett 16:832–6.

Saxena RK, Anand P, Saran S, Isar J (2009) Microbial production of 1,3-propanediol: recent developments and emerging opportunities. Biotechnology Advances 27: 895–913.

Selembo PA, Perez JM, Lloyd WA, Logan BE (2009) Enhanced Hydrogen and 1,3-Propanediol Production From Glycerol by Fermentation Using Mixed Cultures. Biotech and Bioengineering 104:1098 -1106.

Stewart CS (1975) Some Effects of Phosphate and Volatile Fatty Acid Salts on the Growth of Rumen Bacteria. Journal of General Microbiology 89: 319–326.

Tuomisto H (2012) An updated consumer's guide to evenness and related indices. Oikos 121:1203-1218.

Urban R, Bakshi B (2009) 1,3-Propanediol from fossils versus biomass: A life cycle evaluation of emissions and ecological resources. Ind. Eng. Chem. Res 48: 8068–8082.

Yang G, Tian J, Li J (2007) Fermentation of 1, 3-propanediol by a lactate deficient mutant of *Klebsiella oxytoca* under microaerobic conditions. Appl Microbiol Biotechnol 73:1017–24.

Zheng ZM, Xu YZ, Liu HJ, Guo NN, Cai ZZ, Liu DH (2008) Physiological mechanism of sequential products synthesis in 1,3-propanediol fed-batch fermentation by *Klebsiella pneumoniae*. Biotechnol Bioeng 100(5):923–32.

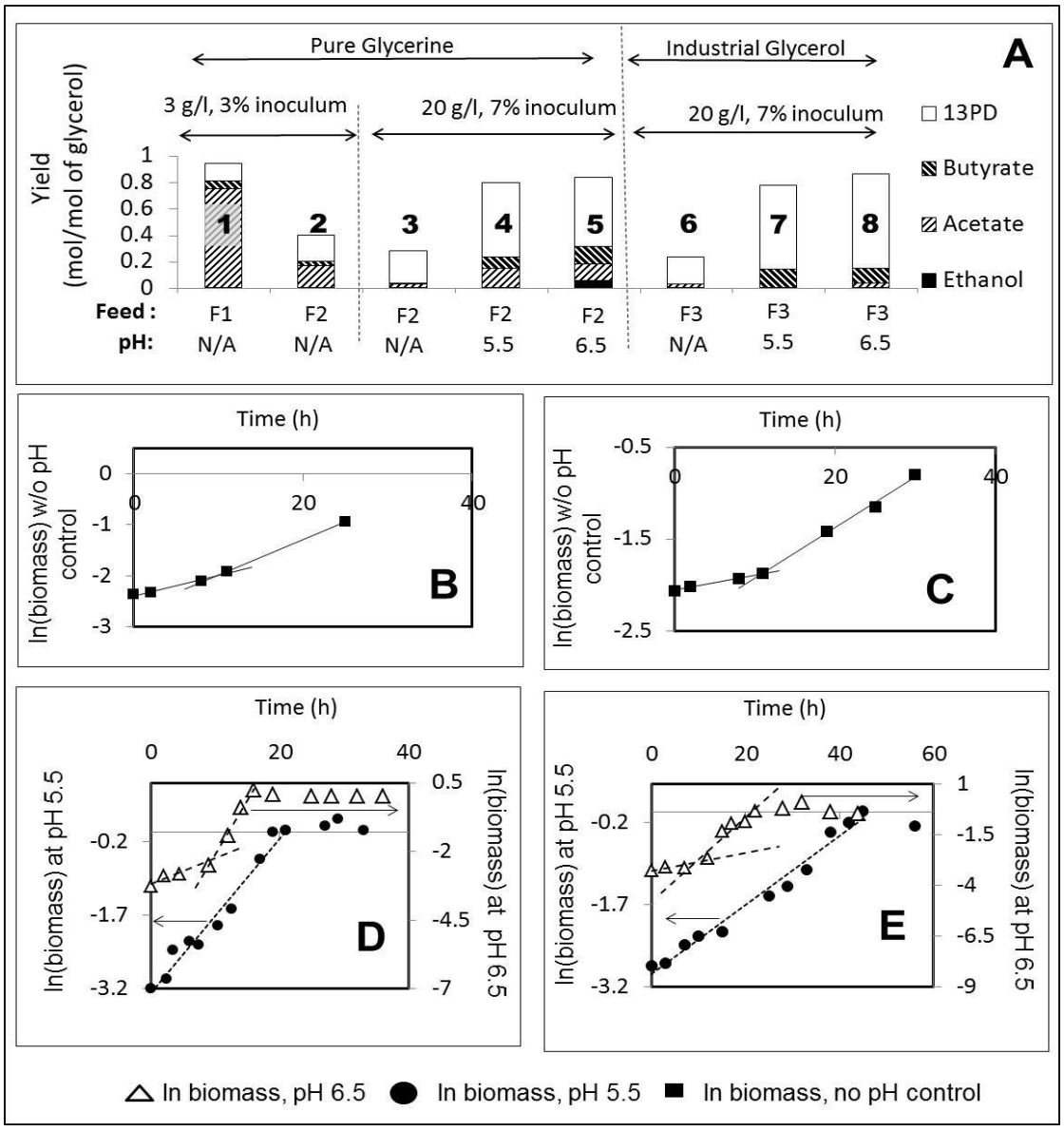

Figure 2.1: Summary of Batch fermentations, A: Metabolite molar yield comparing batches at various conditions, 1B – E : Semi log plots ln(biomass in g dry wt./l) Vs time (h) for batches with 20g/l glycerol and 7% inculum. (B): Feed F2, no pH control, (C): Feed F3, no pH control, (D): Feed F2, with pH control, (E): Feed F3, with pH control

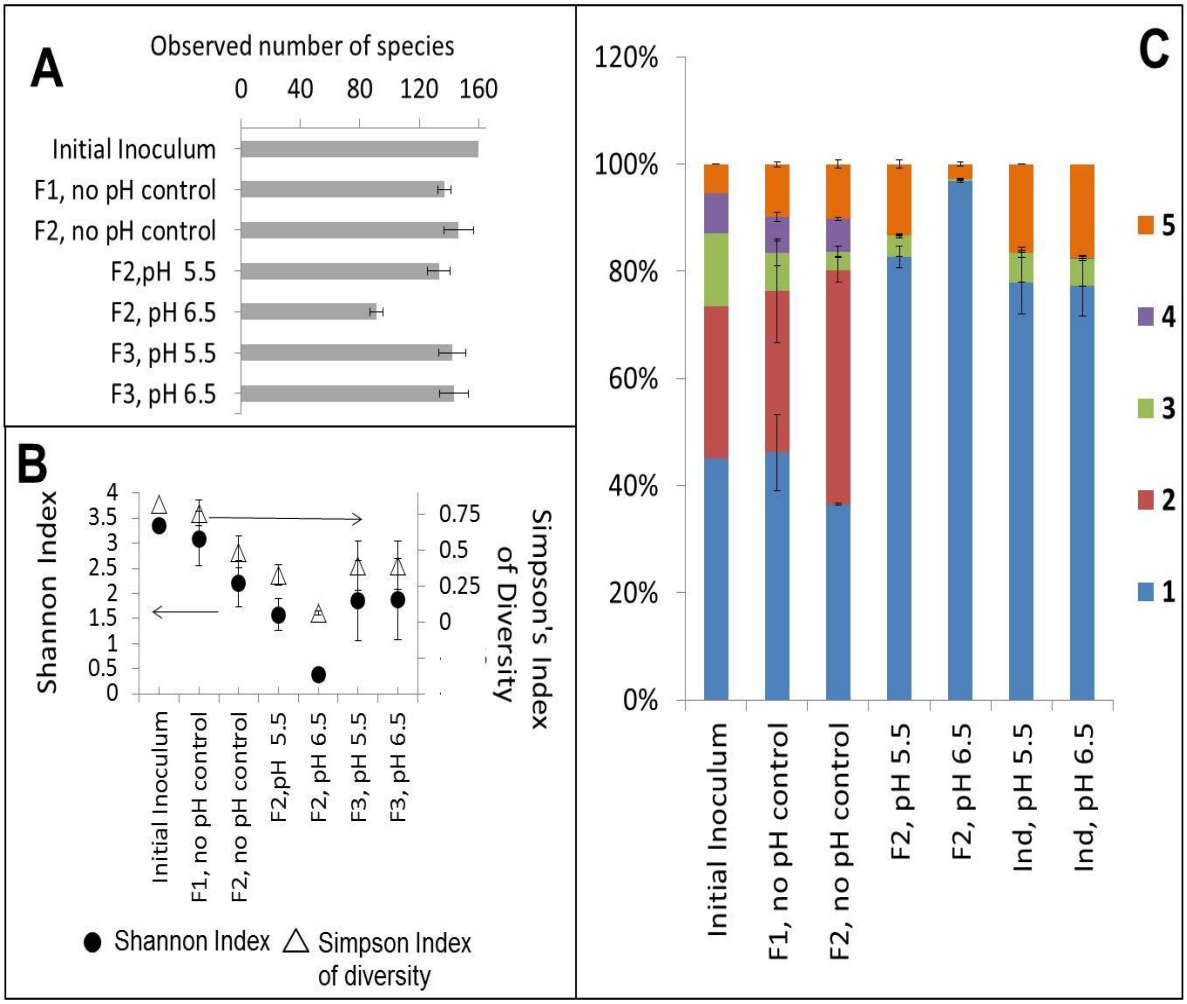

Figure 2.2: Summary of 16S r-DNA sequencing results, A: Average observed number of species, B: Shannon Index and Simpson's index of diversity, C: Population Distribution:1- phylum_ *Firmicutes*; class_*Clostridia*; order_*Clostridiales*; family_*Clostridiaceae*; genus_*Clostridium*,

2 - p_*Proteobacteria*; c_*Gammaproteobacteria*; o_*Enterobacteriales*; f_*Enterobacteriaceae*; g_*Enterobacter*,

3 - p_*Firmicutes*; c_*Clostridia*; o_*Closridiales*; f_*Clostridiaceae*; Other ,

4 - p_*Proteobacteria*; c_*Gammaproteobacteria*; o_*Enterobacteriales*; f_*Enterobacteriaceae*; Other,

5 - Miscellaneous Strains

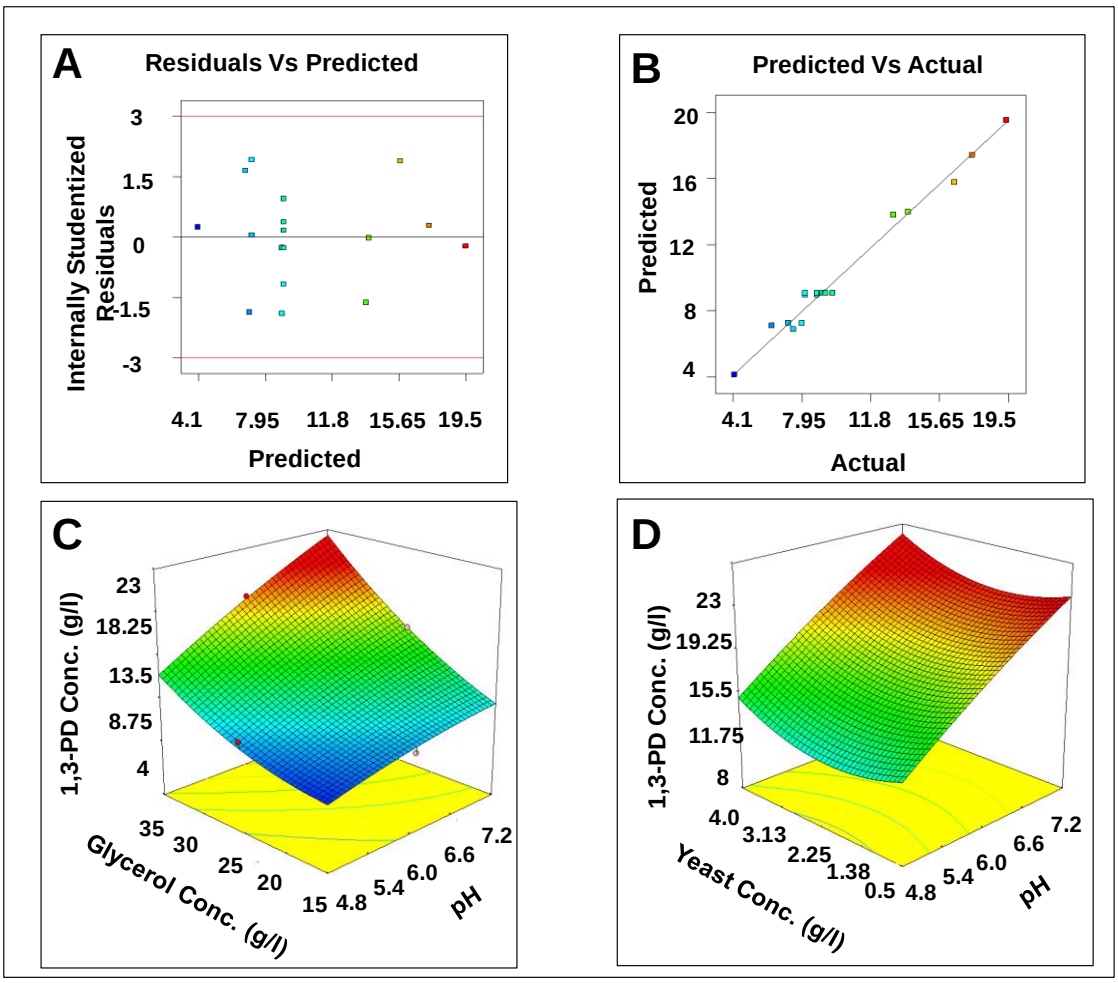

Figure 2.3: Summary of Design of Experiments, A: Studentized residuals and predicted response plot, B: Predicted response vs Actual response plot, C: Surface graph of final 1,3 propanediol concentration at different glycerol concentration and pH, D: Surface graph of final 1,3 propanediol concentration at different Yeast extract concentration and pH.

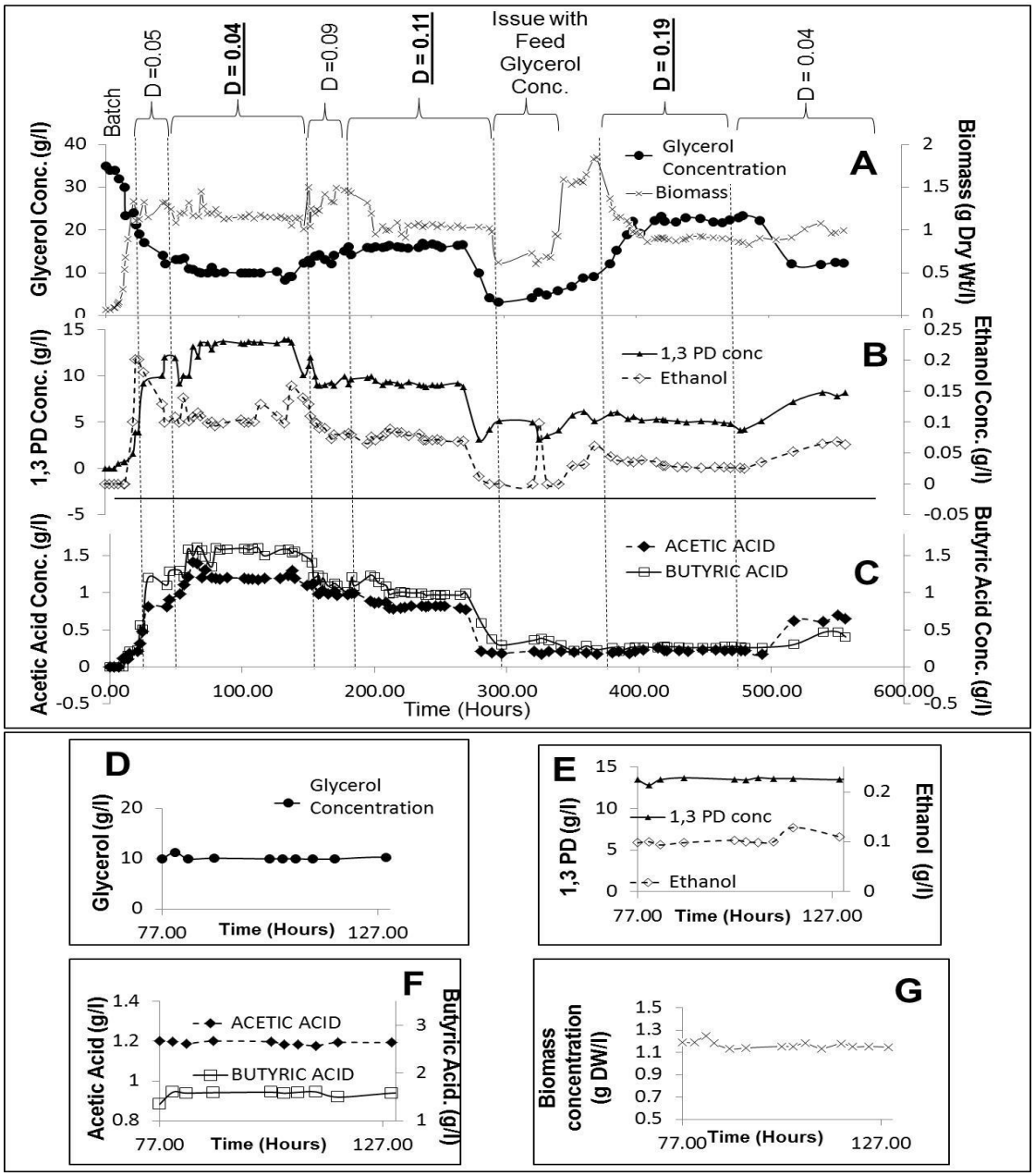

Figure 2.4: Continuous fermentation profiles, Run #1 (A) Biomass and glycerol concentrations (B) Solvent concentrations; (C) Acid concentrations, Dilution rates are indicated between vertical dotted lines and bold dilution rates are those for which well developed steady states were attained. (D–G): Steady state profiles on expanded time scale between 77 – 127 h, D = 0.04h^{-1}. (D) Glycerol concentration, (E): Solvent concentration, (F): Acid concentration, (G): Biomass concentration.

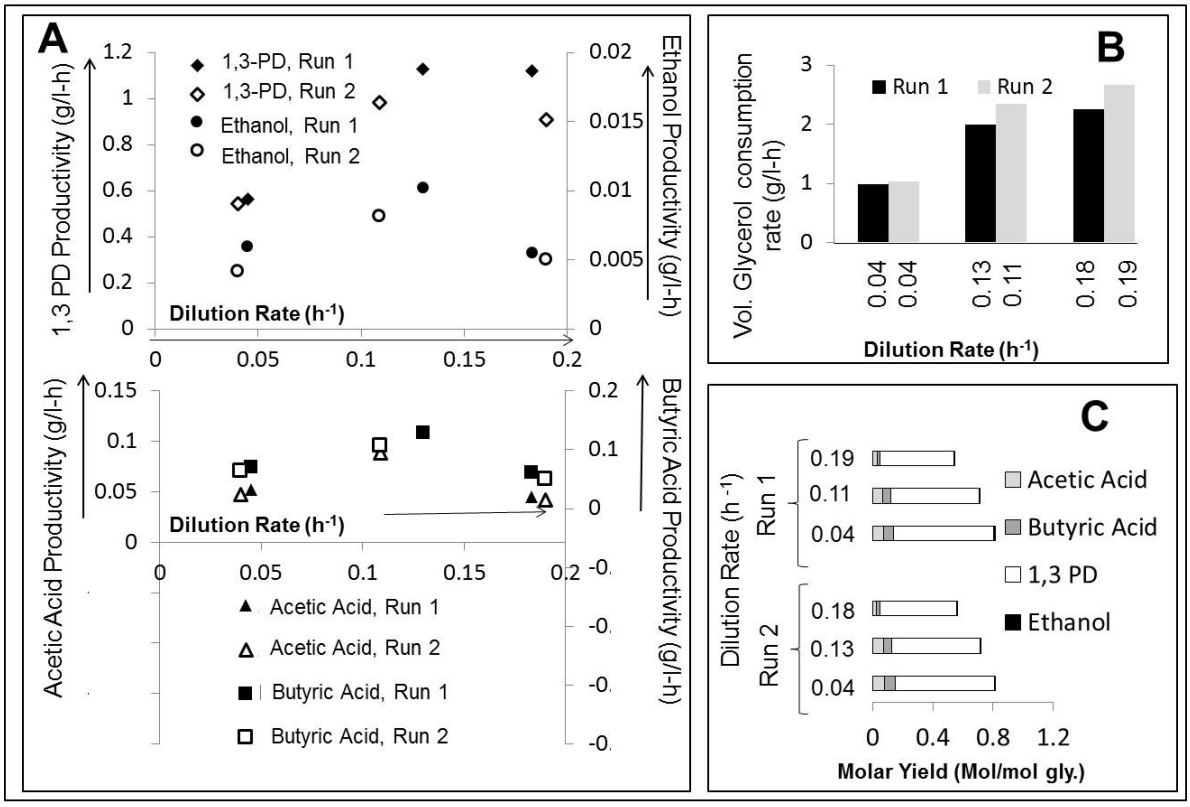

Figure 2.5. Productivities, Glycerol Consumption and Molar yield (A): Metabolite Productivities (g/l-h) vs Dilution rate (h^{-1}), (B): Volumetric Glycerol consumption rate (g/l-h) Vs Dilution rate (h^{-1}), (C): Molar yields of liquid metabolites (mol/mol of glycerol)

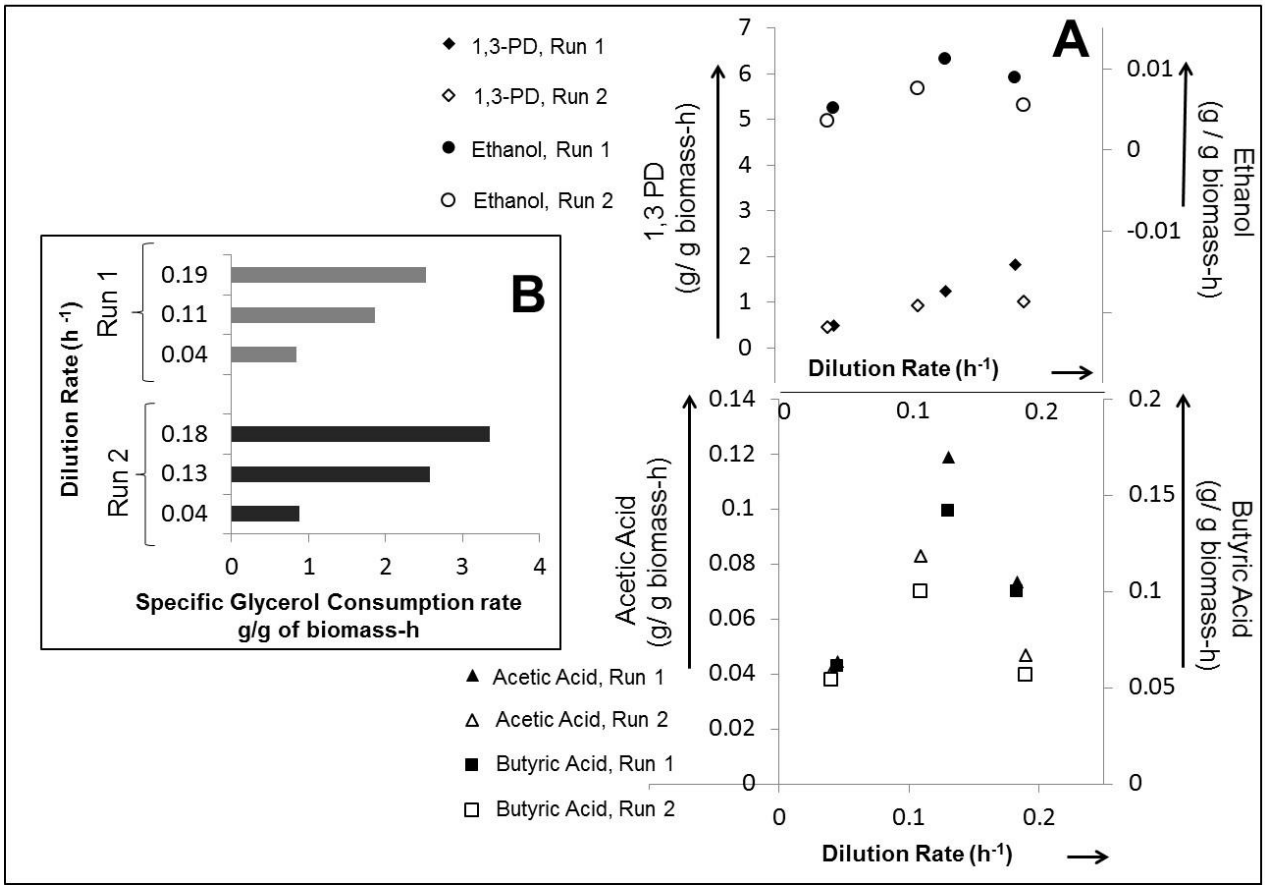

Figure 2.6. Specific Productivity and Specific Glycerol Consumption (A): Steady State Specific Metabolite productivity (g/g of biomass-h) , (B): Specific Glycerol Consumption rate (g/g of biomass-h).

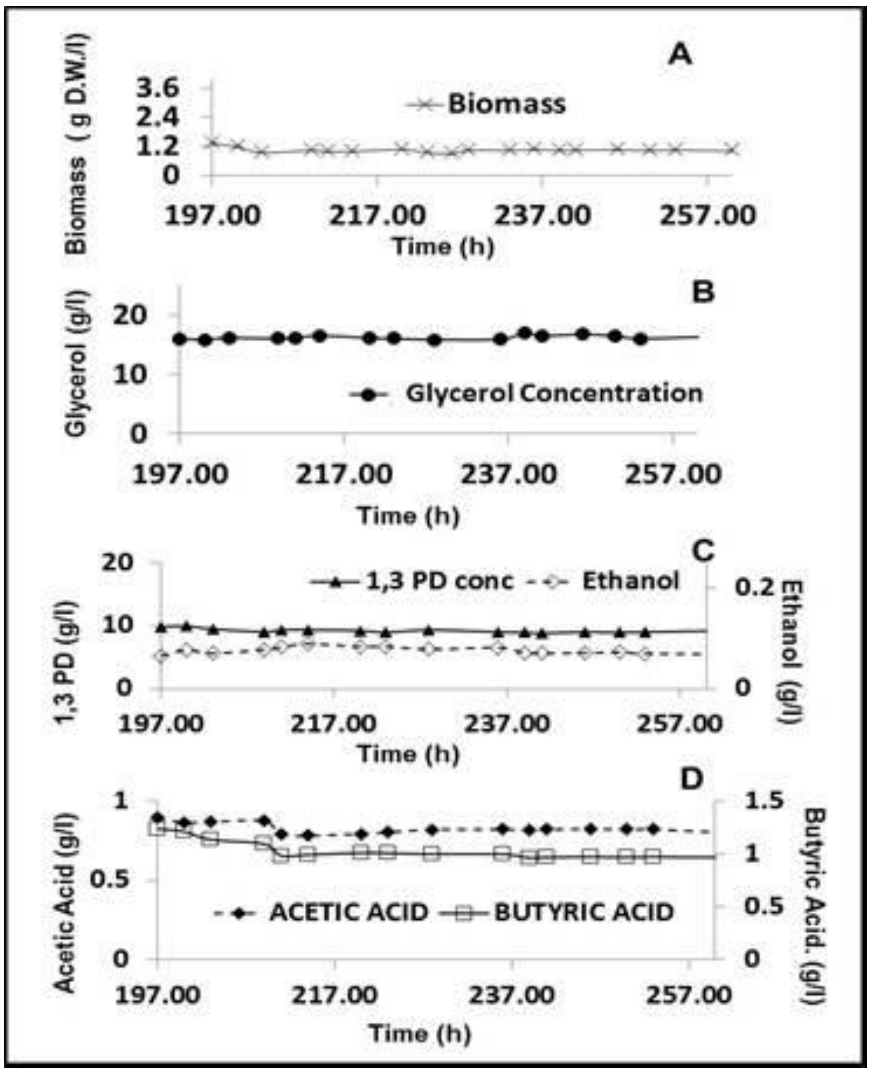

Figure 2.7: Steady state profiles on expanded time scale for CSTR run #1 D = 0.11h^{-1}. (A): Biomass concentration (g dry wt./l), (B) Glycerol concentration, (C): Solvent concentration, (D): Acid concentration

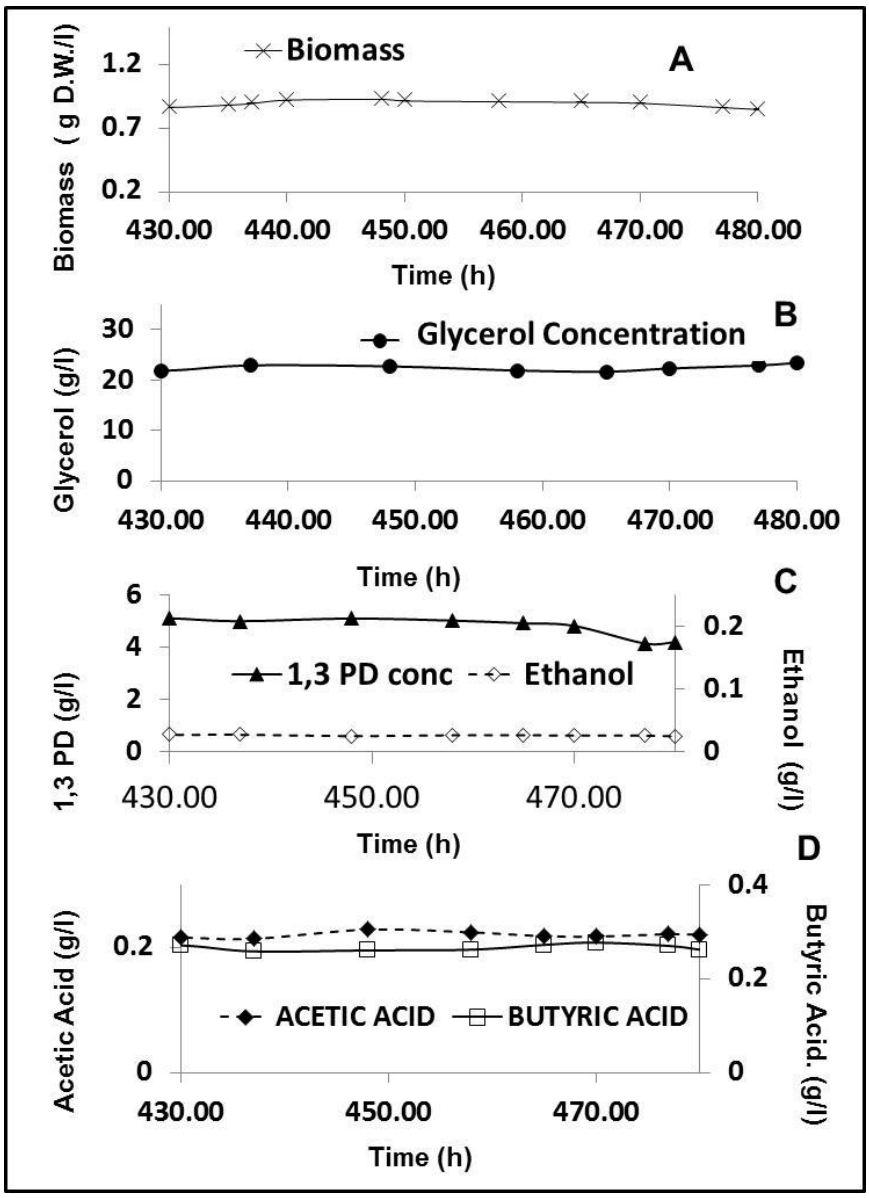

Figure 2.8: Steady state profiles on expanded time scale for CSTR run #1 D = 0.19h^{-1}. (A): Biomass concentration (g dry wt./l), (B) Glycerol concentration, (C): Solvent concentration, (D): Acid concentration

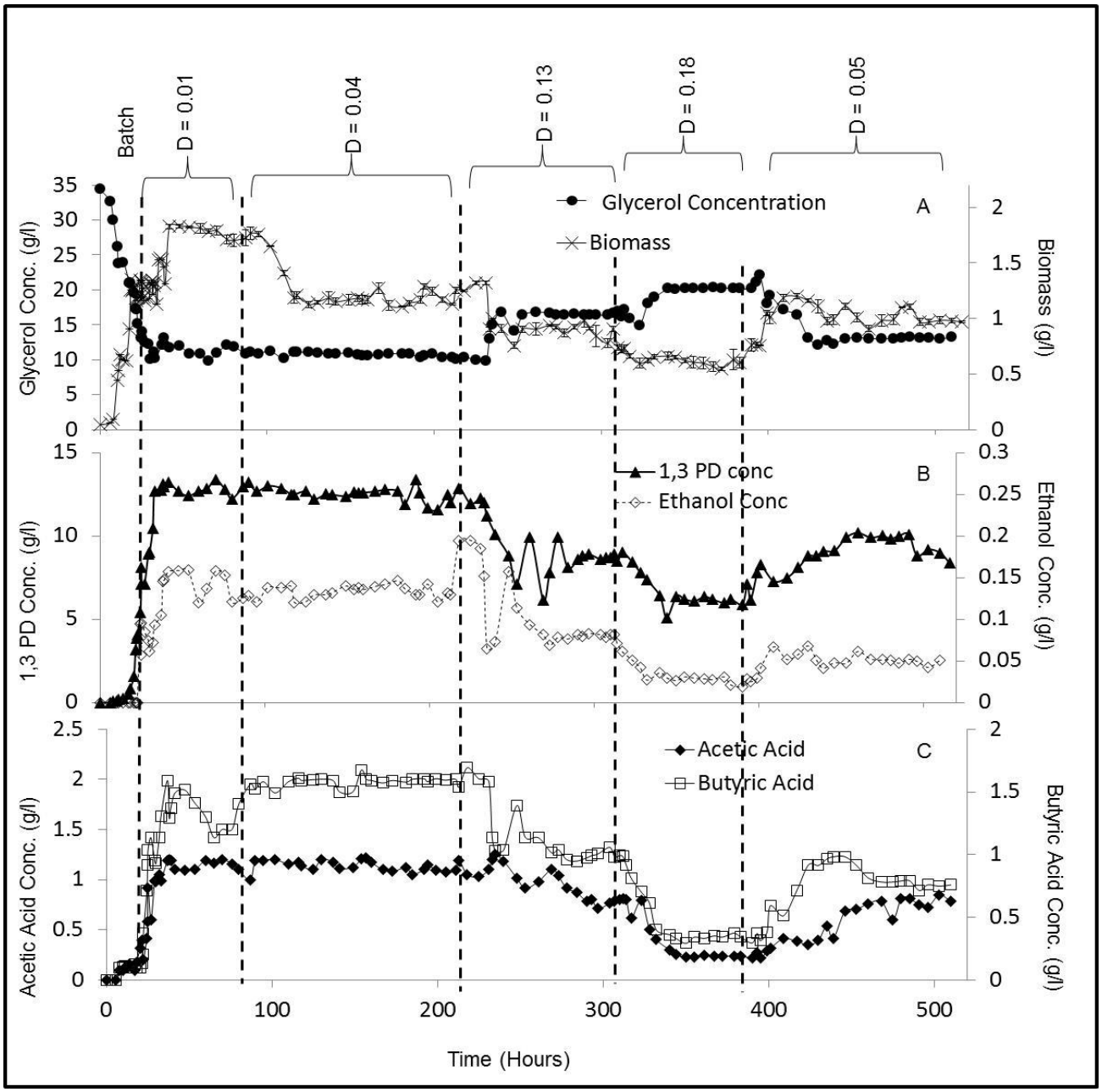

Figure 2.9: Continuous fermentation profiles, Run #2 (A) Biomass (g dry wt./l), Glycerol concentration, (B) Solvent concentrations; (C) Acid concentrations, Dilution rates are indicated between vertical dotted lines

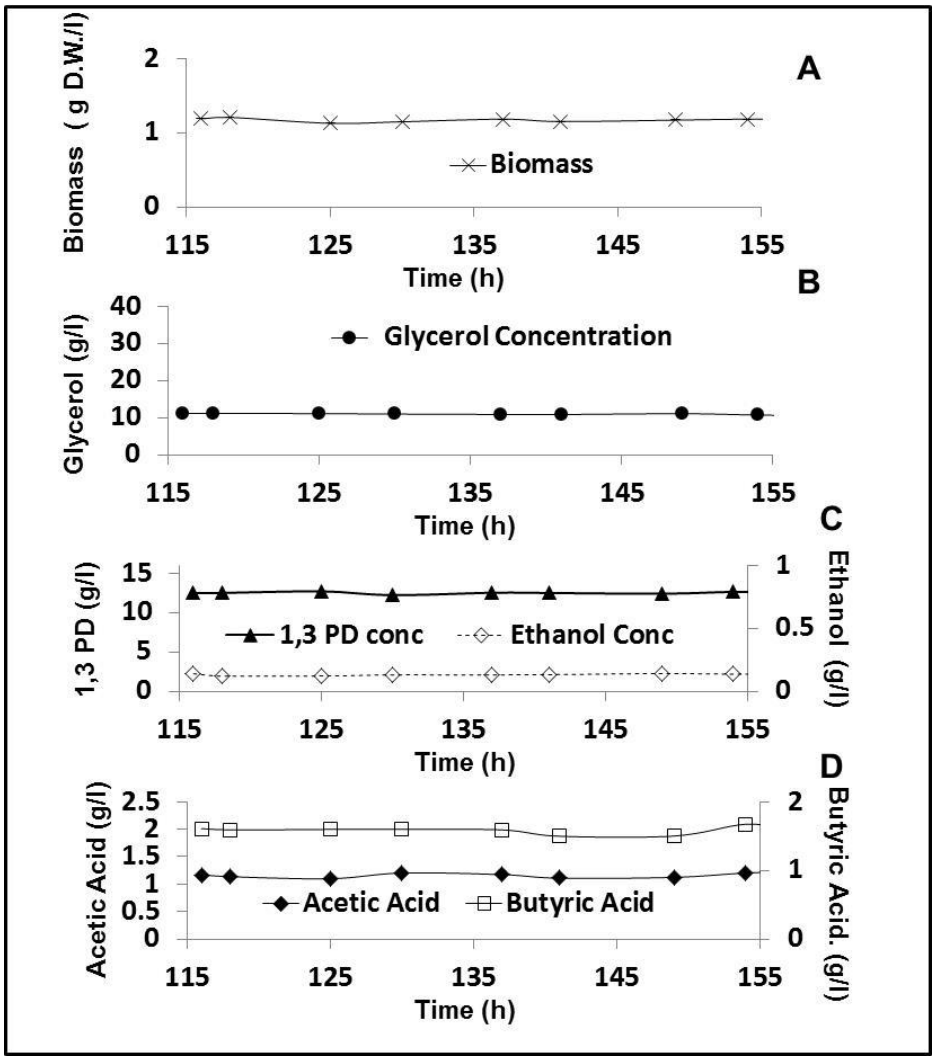

Figure 2.10: Steady state profiles on expanded time scale for CSTR run #2 D = 0.04h^{-1}. (A): Biomass concentration (g dry wt./l), (B) Glycerol concentration, (C): Solvent concentration, (D): Acid concentration

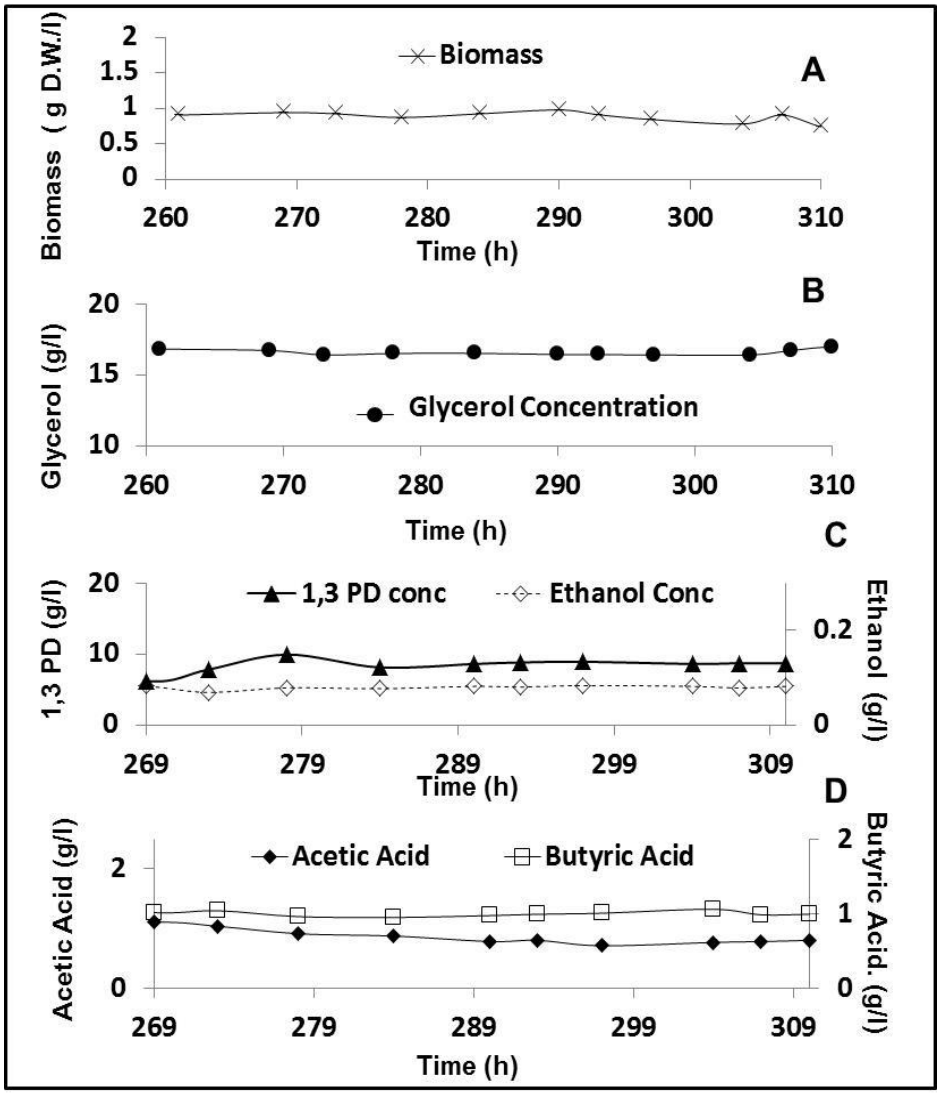

Figure 2.11: Steady state profiles on expanded time scale for CSTR run #2 D = 0.13h^{-1}. (A): Biomass concentration (g dry wt./l), (B) Glycerol concentration, (C): Solvent concentration, (D): Acid concentration

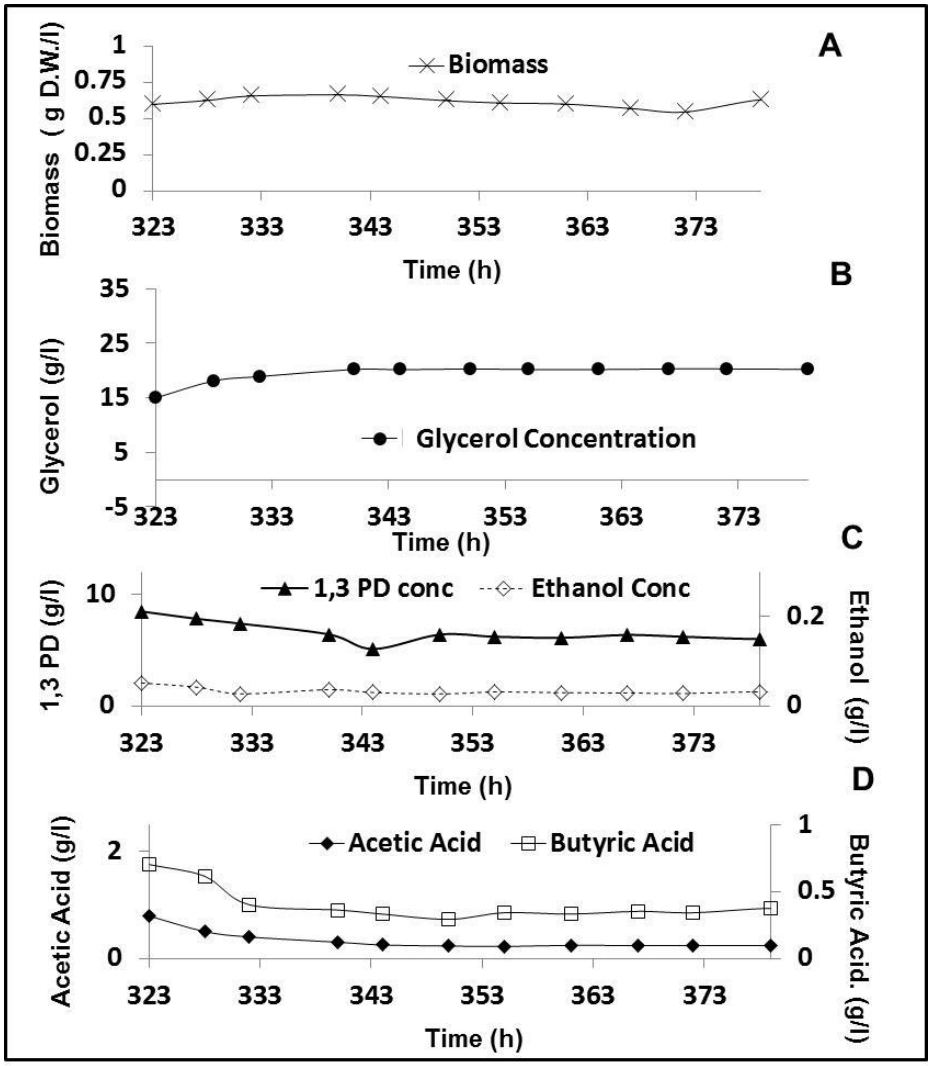

Figure 2.12: Steady state profiles on expanded time scale for CSTR run #2 D = 0.18h^{-1}. (A): Biomass concentration (g dry wt./l), (B) Glycerol concentration, (C): Solvent concentration, (D): Acid concentration

Table 2.1: Experimental design results

Expt. No.	pH	Glycerol Feed Conc. (g/l)	Yeast extract Conc. (g/l)	1,3-PD Conc. (g/l)
1	7.2	15	2.25	7.98
2	6	25	2.25	9.14
3	6	35	4	17.50
4	4.8	25	0.5	7.22
5	4.8	25	4	7.50
6	4.8	15	2.25	4.20
7	6	25	2.25	9.71
8	6	25	2.25	9.29
9	6	15	0.5	8.82
10	4.8	35	2.25	8.16
11	6	35	0.5	16.50
12	6	15	4	6.30
13	7.2	35	2.25	19.40
14	7.2	25	4	13.92
15	6	25	2.25	8.16
16	6	25	2.25	8.82
17	7.2	25	0.5	13.10

Table 2.2: ANOVA for the regression model and respective model terms.

Source	Sum of Squares	df	Mean Square	F Value	p-value Prob > F	
Model	281.507	9	31.27856	47.01922	< 0.0001	significant
A	93.34042	1	93.34042	140.3132	< 0.0001	
B	146.7137	1	146.7137	220.5461	< 0.0001	
C	0.022184	1	0.022184	0.033348	0.8603	
AB	13.876	1	13.876	20.85897	0.0026	
AC	0.072387	1	0.072387	0.108816	0.7511	
BC	3.097019	1	3.097019	4.655568	0.0678	
A^2	0.913004	1	0.913004	1.372466	0.2797	
B^2	7.995	1	7.995	12.01841	0.0105	
C^2	14.83379	1	14.83379	22.29876	0.0022	
Residual	4.656604	7	0.665229			
Lack of Fit	3.315028	3	1.105009	3.294661	0.1398	not significant
Pure Error	1.341576	4	0.335394			
Cor Total	286.1636	16				

Table 2.3: Comparison of selected studies on fermentative production of 1,3-propanediol from Pure and Raw Glycerol.

Inoculum	Process	Yield (mol/mol gly.)	Reference
Feed: *Pure Glycerol*			
C.Butyricum (VPI 3266)	Batch Fed Batch	0.65 0.69	Saint-Amans et al (1994)
K. Pneumonae M5al *K. Pneumonae* AC15 *K. Pneumonae* DSM 2016	Batch Fed Batch Continuous	0.53 0.64 0.61	Cheng et al 2007 Zheng et al 2008 Menzel et al (1997)
Enetrobacter Agglomerans	Batch	0.51-0.61	Barbarito et al (1995)
Organic Soil: Iterative re-inoculation	Batch	0.56	This Work
Feed: *Raw Glycerol*			
C.Butyricum (VP 1718)*	Batch Fed Batch Continuous	0.63 0.66 0.63 ($0.02hr^{-1}$), 0.64 ($0.04hr^{-1}$), 0.60 ($0.06hr^{-1}$), 0.62 ($0.08hr^{-1}$), 0.64 ($0.1hr^{-1}$),	Chatzifragkou et al (2011)
K. Oxytoca FMCC-197`*	Batch Fed Batch	0.56 0.24	Metsoviti et al (2012)
Sludge bacterial culture	Batch Fed Batch	0.51 – 0.76 0.52 – 0.56	Dietz & Zheng, 2014
Organic soil, heat treated	Batch	0.65	Liu et al, 2013
Tomato Soil, heat treated	Batch	0.69	Selembo at el, 2009
Treated Granular Sludge*	Continuous (EGSB reactors)	0.52 ($0.08hr^{-1}$)	Gallardo et al, 2014
Organic Soil: Inoculum prepared by Iterative re-inoculation procedure	Batch, DOE, RSM optimization CSTR	0.71 (Batch) 0.658- 0.664 (0.04-$0.045hr^{-1}$) 0.586-0.583 (0.11-$0.13hr^{-1}$) 0.506-0.517 (0.183-$0.19hr^{-1}$)	This Work

* Mass yields reported were converted to molar yields

Chapter 3. Introduction: Development of Materials for Pervaporation enrichment of 1,3-propanediol from dilute aqueous mixtures

While 1,3 PD can be easily separated from the other by products of bacterial metabolism, the real challenge lies in enriching it from dilute concentrations in aqueous mixtures which amounts to almost 50 – 70% of the total production cost in fermentative 1,3-PD production. The hydrophilic character of 1,3 PD compounds the difficulty of purification. Conventional and reported separation techniques have had their limitations in due cost and energy consumption and hence applicability [1-9]

Membrane separation processes offer a cheap and energy efficient method of upgrading the value of specific components typically produced in dilute mixtures. Although pervaporation is an energetically advantageous process [10]. 1,3-PD cannot be enriched by materials conventionally used for pervaporation. The development of novel materials with a good cost performance balance is essential for the establishment of industrial separation procedures for 1,3-PD enrichment from dilute broths.

Separation processes involving phase changes are typically energy intensive, but pervaporation can be energy efficient as it removes only the minor components [10]. The membrane chemistry and structure should be chosen in such a way so as to effect selective enrichment of the minor components [10]. Zeolite membranes have been used for pervaporative separation of 1,3-PD from other minor fermentation products but the membranes were also selective towards water[11, 12]. Supported liquid membrane based on cyanoborate ionic liquid has been reported with high separation factors and moderate 1,3-PD fluxes [13] but supported liquid membranes suffer from stability issues and are

difficult to scale-up. This is in addition to high material costs associated with hydrolytically stable ionic liquids [14].

For separation processes, the development of materials needs to be done with a view towards possible engineering retrofitting into a system for sustainable industrial application with a cost – performance balance. Additionally, process design considerations are important to get adequate financial return on investment.

Pervaporation is driven by a chemical potential difference across the membrane in which the feed remains in the liquid phase while the permeate is in vapor phase. The Membrane Performance is calculated based on the selectivity and flux. The selectivity or enrichment factor is an indication of the purity of the product obtained which, in this research shall be on the permeate side. The primary crux of pervaporation lies in a combination of the solubility and diffusivity of the respective components in the membrane. The higher the affinity of a component for a membrane, the more likely it will be absorbed into the polymer matrix. The higher the mobility the higher would be its diffusivity. However the overall efficacy of separation and the relative fluxes depend as much on the diffusivity as they do on the solubility. The overall permeation, a product of diffusivity and solubility in effect determines the relative fluxes and the effective separation of components.

The development of materials for this part of the thesis started off in 2011 with proposed flat sheet membrane structures based on Poly (hydroxyethyl methacrylate) and its blends with Poly (Styrene-co-Allyl alcohol). A preliminary study carried out on the 1,3 PD and water mass uptake by sheets cast from Poly(Hydroxyethylmethacrylate) {Poly(HEMA)}, Cross linked Poly(HEMA) and its blends with Poly(Styrene Allyl alcohol) [PSAA],

Poly(Methyl methacrylate) [PMMA] and Poly(Butyl Methacrylate) [PBMA]. A radical initiator was used for the polymerization of HEMA monomer and Gluteraldehyde was employed as the cross linker. The blending was carried out with a view to reducing the hydrophilicity of Poly(HEMA) without adversely affecting its affinity towards 1,3 PD. The blends were made by polymerising HEMA monomer in a solution of the respective polymers (PSAA, PMMA and PBMA) in THF and casting this mixture as sheets. The polymer sheets were immersed in water & 1,3 PD and the increase in weight, over time, was measured. The equilibrium uptake of 1,3 PD by both uncrosslinked & cross linked Poly(HEMA) was seen to be at least 3 – 4 times greater than that of water. Crosslinking slowed down the initial rate of 1,3 PD uptake while having no significant impact of the equilibrium uptake. A major disadvantage with the uncrosslinked membrane was the lack of mechanical integrity when exposed for a prolonged period to pure 1,3 PD. This was mitigated by crosslinking with the membrane retaining structural integrity even at equilibrium swelling levels in 1,3 P.D. Similar results were obtained with the blends containing 90% and 80% by weight of Poly(HEMA). The results were not as encouraging with the PMMA and PBMA blends as those with Poly(HEMA), crosslinked Poly(HEMA) and the Poly(HEMA)-PSAA blend. The results assimilated in Table 1 and Table 2.

The swelling data on Poly(HEMA), Crosslinked Poly(HEMA) and its blends, for all compositions, led to the inference that the equilibrium uptake of 1,3 PD by the polymer is higher than that of water but the "initial rate" of water uptake is higher.

Based on Crank's seminal work[15], a classical Fickian diffusion model links the diffusant mass with time and membrane thickness from where the diffusion coefficient can be

essentially approximated from the initial slope of M_t / M_∞ Vs $t^{1/2}/L$ based on the following equation :

$$\frac{M_t}{M_\infty} = \frac{4}{\pi}\sqrt{\frac{D.t}{L^2}} \text{ ----------(1)}$$

The equation holds true for short time spans. The symbols, respectively, in their order of appearance represent: Mass at time t, Mass at equilibrium swelling, Diffusion Coeff, time, Avg initial thickness of the sample. However, given the complex nature of sorption kinetics, the permeation of an analyte through a polymer matrix may be non Fickian in nature. Additionally a concentration dependence of diffusion coefficients has been empirically postulated and described Frisch [16].

From the preliminary data on mass uptake, the graphs of M_t / M_∞ Vs $t^{1/2}/L$ were seen to deviate substantially after sometime from Fickian behavior. Once the membranes are swollen, the permeation and absorption changes may be thought to change. The value of Diffusion coefficient of water, estimated from the initial slope of the mass uptake graphs, is greater than that of 1,3 PD. A measure of permeation is calculated from the following equation [10].

$$P = D.S\text{--------(2)}$$

Where P is the permeability, D is the diffusivity and S is the equilibrium swelling is taken as a measure of solubility. The computed results for some polymers are summarized in Table 2. It was hypothesized that the ratio of the permeability computed from the mass

uptake results would roughly indicate the separation factor of 1,3-PD over water for that given membrane.

Based on the significant difference in the mass uptake of 1,3 PD vis-à-vis water, the permeability of 1,3 PD was expected to be higher than that of water. This hypothesis was assimilated in Table 3. This hypothesis was verified by actual permeation experiments on flat sheet membranes made from Poly(HEMA) – PSAA blends. A sample picture of the membrane is shown in Figure 1. The pervaporation set up has been detailed in an earlier work by Li et al 2011 [17]. The pervaporation results for the 2 membranes are shown in Table 4.

While the flux of both 1,3-PD and water is fairly high, the separation factor fall short of expectations from the mass uptake experiments. A hydrophilic membrane as the ones evaluated, would suffer from the twin disadvantage of allowing a lot of water through in the first place owing to significant water uptake. Additionally, the very high uptake of 1,3-PD would mean that the membranes may swell and lead to further diffusion of water as well as 1,3-PD causing a reduction in selectivity. Thus, in a hydrophilic membrane, the advantage proffered by the very high mass uptake of 1,3-PD is countered by the diffusional advantage of water which has a lower kinetic diameter compared to 1,3-PD and this called for the need to develop materials from a hydrophobic platform which would conclusively reject water while maintaining allowing 1,3-PD. The affinity in favor of 1,3-PD would still be measured by the sorption or mass uptake of 1,3-PD. But the material needs to reject water while being inclined towards 1,3-PD which is again a challenge since the solubility parameters of 1,3-PD are very close to those of water.

This section of the thesis, in the ensuing chapters, explores the development of three families of hydrophobic yet "1,3-PD philic" polymeric materials with progressively increasing separation efficacy and their application in separating 1,3-PD from binary aqueous mixtures and model broth compositions.

References:

1. Ames TT (2002) Process for the isolation of 1,3-propanediol from fermentation broth. US Patent 6. 361. 983 B1
2. Sanz MT, Blanco B, Beltran S, Cabezas JI (2001) Vapor liquid equilibria of binary and ternary systems with water, 1,3-propanediol, and glycerol. J Chem Eng Data 46:635–639
3. Gong Y, Tong Y, Wang XL, Liu DH (2004) The possibility of the desalination of actual 1,3-propanediol fermentation broth by electrodialysis. Desalination 161:169–178
4. Hao J, Liu DH (2005) Desalination of fermented broth containing 1,3- propanediol by electrodialysis. Chinese J Proc Eng 5:36–39
5. Cho M-H, Joen SI, Pyo S-H, Mun S, Kim J-H (2006) A novel separation and purification process for 1,3-propanediol. Process Biochem 41(3):739–744
6. Anad, P. et al, A novel downstream process for 1,3-propanediol from glycerol-based fermentation, Appl. Microbiol. Biotechnol, 2011, 90(4), 1267 – 76
7. Malinowski JJ (1999) Evaluation of liquid extraction potentials for downstream separation of 1,3-propanediol. Biotechnol Tech 13:127–130

8. Hao J, Xu F, Liu H, Liu D (2006) Downstream processing of 1,3- propanediol fermentation broth. J Chem Technol Biotechnol 81:102–108
9. Quereshi, N., et al, Acetone butanol ethanol (ABE) recovery by pervaporation using silicalite–silicone composite membrane from fed-batch reactor of *Clostridium acetobutylicum*, *Journal of Membrane Science, 1-2, 2001, 93 – 102*
10. P. Shao, R.Y.M. Huang, Polymeric membrane pervaporation, Journal of Membrane Science. 287 (2007) 162-179.
11. S. Li, V.A. Tuan, J.L. Falconer, R.D, Noble, Separation of 1,3- propanediol from glycerol and glucose using a ZSM-5 zeolite membrane, J. Membr Sci. 191 (2001a) 53–59.
12. S. Li, V.A. Tuan, J.L. Falconer, R.D. Noble, Separation of 1,3- propanediol from aqueous solutions using pervaporation through an X-type zeolite membrane, Ind Eng Chem Res 40 (2001b) 1952– 1959.
13. P.Izák, M. Köckerling, U. Kragl, Stability and selectivity of a multiphase membrane, consisting of dimethylpolysiloxane on an ionic liquid, used in the separation of solutes from aqueous mixtures by pervaporation, Green Chem. 8 (2006) 947–948.
14. N.M. Kocherginsky, Q. Yang, L. Seelam, Recent advances in supported liquid membrane technology. Separation and Purification Technology, Separation and Purification Technology 53 (2007) 171–177.
15. Crank, J.; Park, G. S. Methods of measurement. In The Mathematics of Diffusion; Oxford University Press: London, 1975; pp 1-39.
16. Frisch, H. L. The time lag in diffusion. *J. Phys. Chem.* 1957, *61*, 93-95.

17. Li, S.Y., Srivastava, R., Panas, R.S., Separation of 1-butanol by pervaporation using a novel tri-layer PDMS composite membrane, Journal of Membrane Science, 363, 1-2, 2010, Pg 287 – 294

Table 3.1: Mass Uptakes : Poly (HEMA), Crosslinked Poly(HEMA) & Poly(HEMA) – PSAA blends

System	**Poly (HEMA)**	**Xlinked Poly (HEMA)**	**Poly(HEMA): PSAA (blend90:10)**	**Poly(HEMA): PSAA (blend80:20)**
Equilbrium Water uptake (%)	**52**	**50**	**46**	**73**
Equilibrium 1,3Propanediol uptake (%)	**174**	**169**	**259**	**235**

Table 3.2: Mass Uptakes : Poly(HEMA)-PBMA blends, Poly(HEMA)-PMMA Blends

System	**Poly(HEMA): PBMA (blend90:10)**	**Poly(HEMA): PBMA(blend 80:20)**	**Poly(HEMA): PMMA (blend90:10)**	**Poly(HEMA): PMMA (blend80:20)**
Equilbrium Water uptake (%)	**49**	**41**	**49**	**45**
Equilibrium 1,3Propanediol uptake (%)	**162**	**98**	**124**	**85**

.

Table 3.3. Estimated Diffusivities, Solubility and Permeation

System	Diffusion Coefficient (mm^2/hr)		Solubility α Equilibrium swelling (%)		P' = D X S	
	D_{water}	$D_{1,3PD}$	S_{water}	$S_{1,3PD}$	P_{water}	$P_{1,3PD}$
Poly(HEMA)	0.4084	0.2107	52	174	21.64	36.65
X LinkedPoly(HEMA)	0.4037	0.1859	50	169	20.18	31.43
PHEMA:PSAA(90:10)	0.34068	0.1237	46	235	15.62	32.03
PHEMA:PSAA(80:20)	0.3309	0.2579	73	235	24.15	60.62

Table 3.4. Pervaporation Results

Membrane	Feed 1,3-PD concentration 30 g/l, Temperature 30 ^{0}C, Cross Flow Rate 32 l/h		
	Water Flux (kg/m^{2}h)	**1,3-PD Flux (kg/m^{2}h)**	**Separation factor**
PHEMA-PSAA(90:10)	0.69±0.05	0.033±0.003	1.43±0.02
PHEMA-PSAA(80:20))	0.37±0.04	0.021±0.005	1.64±0.16
	Temperature 30 ^{0}C, Cross Flow Rate 32 l/h		
PHEMA-PSAA(90:10), Feed 1,3-PD conc. 20 g/l	0.89±0.04	0.037±0.004	2.04±0.26
PHEMA-PSAA(90:10), Feed 1,3-PD conc. 50 g/l	0.25±0.06	0.017±0.003	1.42±0.09

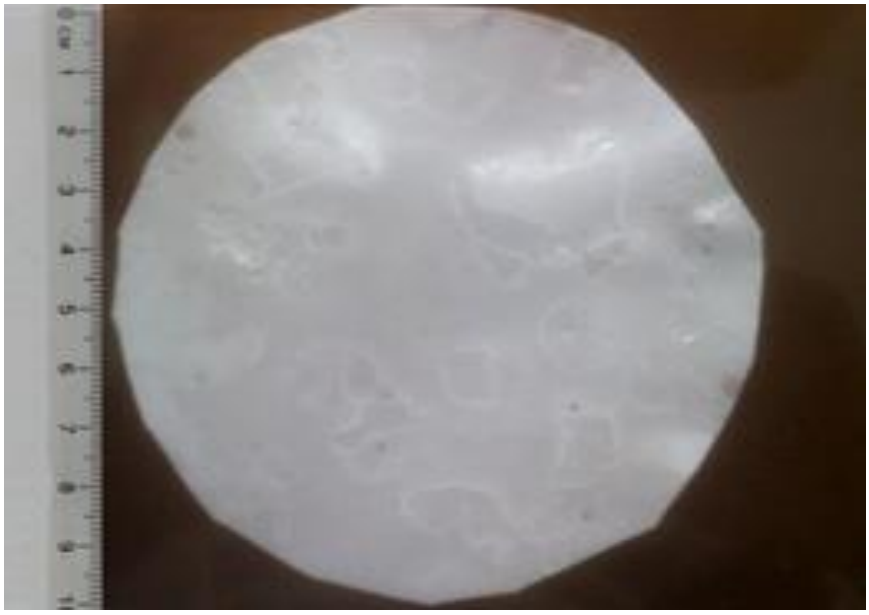

Figure 3.1: Picture of a 500μm PHEMA-PSAA 90:10 blend membrane

Chapter 4. Allylcycohexylamine functionalized siloxane polymer and its phase separated blend as pervaporation membranes for 1,3-propanediol enrichment from binary aqueous mixtures*

Abstract

This work reports the synthesis of a novel allylcyclohexylamine functionalized siloxane and its phase separated blend with styrene-butyl acrylate copolymer and their application for pervaporative enrichment of 1,3-propanediol from dilute aqueous solutions. The phase separated blend allowed for the recovery of mechanical strength lost due to functionalization without loss in separation performance. Separation factors of 9 – 15 were achieved with functionalization levels of 50-90%, while 1,3-propanediol flux was 5.5 - 5.8g/m^2h. Separation efficiency increased with functionalization and decreased with increasing temperature and feed concentration. Solution diffusion model was used to compute the overall mass transfer coefficients, concentration polarization and intrinsic material mass transport properties. The overall mass transfer coefficient for 1,3-propanediol was between $1.0 \cdot 10^{-7}$ – $3.0 \cdot 10^{-7}$ m/s while the boundary layer mass transfer coefficient ranged from $12.9 \cdot 10^{-7}$ m/s to $40 \cdot 10^{-7}$ m/s indicating the dominance of the membrane on the transport resistance. A computation of Hansens solubility parameters by a group contribution method was carried out to underscore the results. The membrane, with its good cost/performance tradeoff and excellent mechanical integrity, offers the possibility of fabrication into modules and scale up.

Keywords: Allylcyclohexylamine Siloxanes, Pervaporation, 1,3-propanediol, Solution-Diffusion

*Allylcycohexylamine functionalized siloxane polymer and its phase separated blend as pervaporation membranes for 1,3-propanediol enrichment from binary aqueous mixtures, B. Kanjilal, I. Noshadi, J. R. McCutcheon, A. D. Asande, R.S. Parnas, Journal of Membrane Science (Submitted)

1. Introduction

The fermentation of crude glycerol to 1,3-propanediol (1,3-PD) provides value to the current over capacity of waste industrial glycerol [1]. The separation of 1,3-PD accounts for a major portion of the total production cost and is a process bottleneck [2]. The separation bottleneck is the enrichment of 1,3-PD concentration from dilute starting concentration in the aqueous mixture [2 – 4]. The complexity of separation is compounded by its high water affinity [2, 5]. Several separation techniques have been reported which attempted to enrich 1,3-PD concentrations from aqueous mixtures and broths with concomitant energy, cost and applicability limitations [5 – 18]. For instance, high separation factors have been reported with an ionic liquid based supported liquid membrane (SLM), but the ionic liquid is extremely extensive [18]. However, a highly functional material needs to be designed into a system for industrial application to get adequate financial return on process investment. This paper illustrates the development and application of a novel siloxane based polymer membrane with a balance of cost and performance. Additionally, siloxane based polymers are relatively fouling resistant and appropriate for use with fermentative processes [19, 20]

Amongst separation processes explored for 1,3-PD enrichment from dilute aqueous mixtures and broths, distillation consumes large amounts of energy given the large excess of water [6–8]. Solvent extraction with sequential steps using simple solvents to complex methanol-phosphate blends has been investigated [5,9,10]. However, 1,3-PD is only partly partitioned into a hydrophobic solvent phase rendering the methods unfeasible [5].

Chromatography, while achieving excellent separation from other metabolites, results in an extremely dilute final concentration [11–13]. Reactive extraction converts 1,3-PD to a less water soluble compound which is first extracted and then converted back but suffers from complications of multiple unit operations, side reactions and yield losses [14, 15]. Studies of pervaporative enrichment of 1,3-PD have been less numerous than other techniques [16–18]. Works with Na-ZSM-5 and X-type zeolite membrane pervaporations have only reported selectivity over broth components other than water [16,17]. A supported ionic liquid membrane has been used in a ceramic nanofiltration module coated with a PDMS layer exhibiting high 1,3-PD selectivity with aqueous mixtures in batch pervaporation [18]. While pervaporation, like distillation, involves a liquid to vapor phase change, it deals with the minor component using selective membranes. These features reduce energy consumption and make pervaporation the most efficient 1,3-PD separating technology [21]. To the best of our knowledge no reports exist on synthesized polymeric structures with continuous pervaporative enrichment of 1,3-PD and with a potential for scale up.

Poly(Dimethylsiloxane) (PDMS) is an appropriate material for membrane pervaporation due to its hydrophobic character, good thermal, chemical and mechanical stability, low base material cost and ease of fabrication [22] . However, PDMS has very little affinity for 1,3-PD and hence needs to be modified or functionalized to improve selectivity. Studies on PDMS membranes functionalized with a variety of organofunctional side chains have been carried out for pervaporative separation of volatile organics such as phenol and cresol from water [23–25].

This paper reports a novel membrane structure for continuous pervaporative enrichment of 1,3-PD from binary aqueous feed solutions. The structure is based on Allylcylcohexylamine (ACA) functionalized Poly(hydromethylsiloxane) (PHMS). The hydrosilylated PHMS is fabricated into a membrane structure on a porous Polyethylene support using two methods. In one, it is cross-linked with a high molecular weight hydroxyl terminated PDMS while the other method entails the formation of a microphase separated semi interpenetrating polymeric network (SIPN) blend with a high molecular weight Styrene-Butyl acrylate copolymer. The properties of functionalized PHMS and the membrane forming materials are characterized. The membranes are applied for the continuous pervaporative enrichment of 1,3-PD from dilute binary aqueous mixtures. The performance of the system is analyzed with respect to levels of functionalization, membrane fabrication method and various process parameters. The overall mass transfer coefficients, concentration polarization and other transport properties were analyzed using the solution diffusion model. In the absence of significant concentration polarization, the intrinsic mass transfer coefficients of the membrane materials were computed. Reasonable fluxes and separation factors were achieved for the membranes in addition to good mechanical stability. These structures may be viable alternatives to conventional purification processes as well as to supported liquid membranes offering a balance between separation performance and material cost in addition to mechanical integrity. The mechanical integrity also makes it possible to fabricate pervaporation modules, including its application in multilayer membranes, for use in continuous processes with concomitant reduction of the energy cost bottleneck pertaining to 1,3-PD concentration enrichment.

2. Experimental

2.1 Materials:

2.1.1 PHMS Functionalization by Hydrosilylation:

For the hydrosilylation reactions on PHMS, Poly(methylhydrosiloxane) (PHMS) of degree of polymerization ~ 35 to 40 , Allylcyclohexyl amine (ACA) and Bone dry toluene (<30 ppm water) were purchased from Sigma Aldrich and dried prior to use. The chloroplatinic acid and Dibutyl Tin dilaurate catalysts were purchased from Sigma Aldrich and used without modification.

Hydroxyterminated Poly Dimethylsiloxane (HPDMS) and Tetraethyl orthosilicate (TEOS) were purchased from Sigma Aldrich. These components were passed through a drying column prior to use.

2.1.2 Styrene Butyl Acrylate Emulsion Polymerization:

For the Styrene Butyl Acrylate Emulsion Polymerization, Styrene and Butyl Acrylate were purchased from SigmaAldrich and passed through a column of inhibitor remover prior to emulsion polymerization. Potassium persulphate, tert-Butyl perbenzoate, Sodium bicarbonate and Sodium dodecylbenzenesulfonate were purchased from Sigma Aldrich and used without modification.

2.2 Membrane Fabrication and Pervaporation Feed:

Porous polyethylene sheets were obtained from Interstate Specialty Products for use as the support sheet for membrane fabrication. The nominal thickness reported was 500 microns with pore diameters of 75 -110 microns and a porosity of 48%.

1,3 propanediol (1,3-PD), 98% purity was purchased from Sigma Aldrich and used for the partition coefficient measurements and for preparation of binary mixtures with distilled water as feed solutions for pervaporation experiments.

2.3 Analytical Methods:

^{1}H NMR was carried out to monitor the extent of functionalization of PHMS in the hydrosilylation reaction and to characterize the emulsion polymerized Styrene – Butyl acrylate copolymer on a Brucker DMX-500 MHz spectrometer. IR spectra were taken on samples with a Nicolet Magna-IR 560 spectrometer, with KBr powder being used as background. The molecular weight of the functionalized PHMS was determined by GPC with an Agilent 1260 Infinity system using toluene as eluent and narrow molecular weight PDMS from Sigma Aldrich as calibration standards. The molecular weight of the Styrene-Butyl acrylate copolymer was determined by GPC using toluene as the eluent and PMMA calibration standards. Thermo-gravimetric analysis was carried out on all the polymers in a TA Instruments Hi-Res 2950 TGA instrument at a ramp of 20^{0}C/min in nitrogen up to a temperature of 800^{0}C. The thermal transitions of the polymer were determined in TA Instruments Q100 and DSC 2920 instruments under liquid nitrogen cooling. Contact angle measurements were carried out on an Olympus TGHM goniometer. Tensile testing was carried out on rectangular samples of width 10mm and thickness 200µ on an Instron Universal Testing Machine (UTM). A gage length of 25.4 mm and a cross head speed of

50mm/min was employed to obtain break stress and strain values. Field Emission scanning electron microscopy (FESEM) images of the porous PE and composite membrane structures were obtained with a JEOL 6335F field emission scanning electron microscope. The feed and permeate compositions from the pervaporation experiments were analyzed using 0.22μm syringe filtered fermentation samples by gas chromatography (GC) using a DB-FFAP capillary column and an MS detector and a 1μL injection volume. GC injector, detector and initial over temperatures were kept at 240^0C, 270^0C, and 40^0C for 2 minutes respectively.

2.4 Partition Coefficient Measurement:

The partition coefficient of 1,3-PD between water and ACA was determined at 30^0C. 1 ml of a 10 g/l 1,3-PD solution was shaken in a vortex mixer with 1ml of ACA for 15 minutes and left for separation between the water and ACA phases. The 1,3-PD partitioned between the two phases and its concentration in the two phases was computed from GC results of the aqueous phase before and after partitioning. The partition coefficient was calculated based on equation 1:

$$K_p = \frac{C_{ACA}}{C_{water}} \quad \text{----------(1)}$$

2.5 Synthesis, purification and characterization of ACA functionalized PHMS:

The PHMS was functionalized with ACA by hydrosilylation using the Chloroplatinic acid catalyst solution [23–25]. The reaction was carried out in a clean and dry glass pressure tube flushed with high purity argon on a schlenk line. A 25mg/ml chloroplatinic acid catalyst solution in isopropanol was prepared. A typical run consisted of 1.5 g PHMS with

varying quantities of ACA, depending upon the targeted extents of substitution, and 1 ml of toluene as solvent. The catalyst solution was added to the extent of 5 µl/ml of reaction volume. The reaction temperature was controlled at 70 $\pm 2^0$C. Given the sensitivity of the reaction to moisture and temperature, with hydride elimination occurring at high temperatures and in the presence of moisture, all reagents were thoroughly dried prior to use [23–25]. The reaction was monitored by ^{1}H NMR in $CDCl_3$ and FTIR. The polymer solution was cooled by immersing the pressure tube in a dry ice and acetone mixture, with a small amount of liquid nitrogen, to facilitate the separation of the functionalized polymer from the solvent and remaining catalyst and unreacted volatiles. The functionalized PHMS was re-dissolved in toluene, the procedure repeated thrice and the remnant toluene solvent removed by rotary evaporation. The polymer was finally washed with ethanol and vacuum dried again. The functionalized polymer was characterized for glass transition temperature and molecular weight by DSC and GPC, respectively. The reaction scheme is depicted in Figure 4.1(a). The NMR and FTIR are depicted in Figure 4.1(b) and 4.1(c). The glass transition temperatures and molecular weights are shown in Figures 4.1(d) and 1(e).

2.6 Synthesis, purification and characterization of Styrene-Butylacrylate copolymer:

A high molecular weight Styrene-Butyl acrylate copolymer (SBA) was synthesized by emulsion polymerization modified from an earlier patented process on pressure sensitive adhesive latex production [26]. The reaction was carried out at 80^0C in a 250 ml two necked round bottom flask fitted with a reflux condenser with the system being constantly purged with nitrogen. A typical batch consisted of 50 g deionized water, 0.5g Potassium Persulphate, 0.25g Sodium Bicarbonate, 1g Sodium dodecylbenzenesulfonate 0.25g tert-

Butyl perbenzoate, 50g Butyl acrylate and 50g Styrene. While Sodium Bicarbonate and Sodium dodecylbenzenesulfonate were added beforehand, the monomer mixture was added dropwise over a period of 15 minutes through the second neck. After the monomer addition, the temperature was reduced to 65^0C and the Potassium Persulphate and tert-Butyl perbenzoate added and the reaction was allowed to run for 2 hours. A silicone rubber tube fitted with a needle was used to blanket the surface of the reaction mixture with nitrogen throughout the 2h course of the reaction. At the end of the reaction, the emulsion was flocculated by Sodium Chloride, the flocculated polymer washed thoroughly and repeatedly, centrifuged and dried at room temperature. The purified polymer was analyzed for composition, thermal transitions and molecular weight by NMR, DSC and GPC respectively.

2.7 Membrane fabrication and characterization:

2.7.1 Scheme 1:

The ACA functionalized PHMS (AP) was blended with the high molecular weight silanol terminated PDMS (HPDMS) and TEOS [23, 24]. The HPDMS and TEOS were kept at 10% and 2% of the total weight of the mixture respectively. Undiluted Dibutyl Tin Dilaurate catalyst was added to this mixture at 0.1% by weight of the mixture. A small amount of toluene was added to this mixture to lower its viscosity. A piece of porous Polyethylene sheet was soaked in measured quantities of this mixture and the solvent was allowed to evaporate at room temperature over a period of ~ 24 hours. The membrane was then allowed to cure at 60^0C for 4 days to ensure completion of crosslinking and cut to the required shape. Membranes were fabricated using 50%, 70% and 90% ACA functionalized

PHMS and were given the nomenclature PDMS_50ACA, PDMS_70ACA and PDMS_90ACA respectively.

2.7.2 Scheme 2:

In a separate scheme the ACA functionalized PHMS (AP) was blended with the emulsion polymerized Styrene-Butylacrylae polymer (SBA) and TEOS. The SBA and TEOS were kept at 10% and 2% of the total weight while the Dibutyl Tin Dilaurate catalyst was kept at 0.1% by weight of the mixture. The methods of membrane fabrication and evaluation are the same as above. The nomenclature used membrane fabricated with this scheme, employing 90%ACA functionalized PHMS was SBA_90ACA.

All membranes were evaluated for thickness, viewed under FESEM and used for pervaporation experiments. The membrane forming recipes were separately cast, without the porous support, on a Kapton sheet into 100 micron thick sheets for tensile tests. Pieces of these sheets were used for mass uptake experiments [22] and DSC measurements. The recipes were also cast as a thin layer on clean glass slides for evaluation of water contact angle.

2.8 Pervaporation experiments:

Pervaporation was carried out in a custom made membrane holder providing a pervaporation area of 43 cm^2. It was fabricated at the Technical Services Facility at University of Connecticut. The feed solutions consisting of 1,3-PD-water binary mixtures were maintained at various temperatures. The feed solutions were recirculated over the membrane on a perforated brass support in the membrane holder by a peristaltic pump,

providing varying cross flow rates. The permeate was collected in two parallel cold traps, cooled in a dry ice – acetone bath. A vacuum pump was employed to maintain the permeate side pressure at less than 1 mm Hg. Permeate samples were collected at regular time intervals until steady state was reached. The permeate compositions were analyzed by Gas Chromatography. The pervaporation equipment used and its schematic are detailed in an earlier work by Li et al 2010 [22]. As in a typical pervaporation runs, the slope of the total accumulated permeate mass vs time increased and reached a plateau after steady state was reached by that particular run. Pervaporation experiments were carried out with varying membrane recipes, different temperatures, cross flow rates and feed compositions. The average bulk concentration is essential to determine the overall mass transfer coefficient. The pervaporation experiments entailed a broth volume of 1000 ml, ~ 0.4-0.5 ml of the collected permeate was used for chromatographic analysis. The remaining permeate collected was weighed and returned to the system to maintain the feed concentration at as constant a level as possible. The feed composition was also evaluated from time to time to verify the concentrations of the components. The feed composition was taken to be the average of the initial and final feed compositions as the feed composition changed by less than 2% of the initial composition for each component. The key performance indicators of the pervaporation experiment were defined by the component fluxes and the separation factor defined as:

$$\alpha = \frac{Jp}{Jw} . \frac{xw}{xp} \text{ ------(2)}$$

Where J_p and J_w represent the 1,3-PD and water fluxes and x_p and x_w represent the feed mass fractions of 1,3-PD and water, respectively.

3. Results and Discussions:

3.1 Partition Coefficient in Amine:

The partition coefficient of 1,3-PD in ACA over water was estimated at 0.5±0.03. Allylcyclohexylamine is a hydrophobic solvent, with a Log P_{ow} (octanol – water redistribution coefficient) ~ 2.2 – 2.4, in which 1,3 propanediol is miscible in all proportions.

3.2 Functionalization of PHMS by hydrosilylation – Monitoring of reaction and Polymer characterization:

Linear, organofunctional Polysiloxanes were prepared by the platinum catalyzed reaction of ACA with PHMS as depicted in the reaction scheme in Figure 4.1(a) [23]. The sensitivity of the reaction to moisture warranted that all components be dried thoroughly prior to reaction [23]. Water reacts with the hydride groups of PHMS producing silanol groups which upon heating crosslink the chains. It was also essential to achieve high levels of functional substitution of the PHMS in order to have the required amount of ACA in the final membrane structure. The degree of substitution is defined as the percentage of Si-H bonds substituted with ACA. It was possible to quantitatively substitute the targeted number of Si-H bonds in PHMS. The degree of substitution was monitored by the reduction in ^{1}H NMR peak and FTIR peak areas pertaining to the Si-H bond and C=C bond. The NMR and FTIR figures (Fig. 4.1(b) and 4.1(c)) are for a reaction system attempting to substitute 100% of the Si-H bonds in PHMS. The level of ACA functionalization achieved was monitored by comparison of the integrated areas under the peak at δ= 4.8ppm (Si-H

bond) with that at δ= 0.2ppm (-Si-CH-). As the reaction progressed, the latter increased at the expense of the former. With higher levels of substitution, the reaction became sluggish with time. This can be attributed to steric hindrances with larger degrees of substitution. The purified polymer was characterized for thermal transitions and molecular weight by DSC and GPC as shown in Figures 4.1(d) & 4.1(e). The increase in molecular weight numerically corroborates the quantitative substitution of Si-H bonds as seen with NMR. The ACA functionalized polymers retained flow even at high levels of substitution, underscoring the fact that there had been no hydride elimination and hence no undue crosslinking during the reaction. The glass transition increases with increasing functionalization. Beyond 50% substitution, the rate of increase in Tg becomes slower. The functionalized polymers were amber colored highly viscous liquids.

3.3 Styrene Butyl acrylate copolymer characterization

Emulsion polymerization allowed the attainment of a high molecular weight Styrene – Butyl acrylate copolymer. The weight average molecular weight from GPC measurements was 344,365 and Mz of 909,459, with a PDI of 2.95. The glass transition temperature of the polymer obtained was 4.4 (±0.3) ^{0}C. The average copolymer composition was ascertained from the ratios of the area under the peak at δ= 7 – 7.5ppm (aromatic proton from styrene) and δ = 3.8-4ppm (–O–CH_2 – from butylacrylate). The average molar copolymer composition was ~43% Butyl acrylate and 57% styrene.

3.4 Membrane characterization

The reaction mechanisms of membrane formation for both scheme 1 and scheme 2 are depicted in Figure 4.2(a) and 4.2(b). All membranes were evaluated for thickness, viewed under FESEM and used for pervaporation experiments. A representative FESEM, along with an FESEM of the porous PE support sheet, as the inset, is shown in Figure 4.2(c). The membrane forming recipes, as described in the sections above, wet and fill the pores of the 500micron porous polyethylene support sheet while forming a dense 100 micron top layer.

The Tg of the membrane forming recipes (Fig 4.2d.), as per scheme 1, with hydroxyl terminated PDMS reflected the Tg trends obtained with increasing ACA functionalization of the PHMS as shown in an earlier figure (Fig 4.1d.). In scheme 2, which blended the ACA functionalized PHMS with the high molecular weight styrene butyl acrylate polymer followed by crosslinking the former with TEOS, the existence of a microphase segregation between the Siloxane and SBA domains was underscored by the presence of two distinct Tg inflexion regions. The membranes formed using scheme 2 were opaque in appearance versus the translucent appearance of those formed using scheme 1. The membrane material formed as per scheme 2, at the molecular level can be thought of as a semi interpenetrating polymeric network, wherein the TEOS mediated crosslinked ACA functionalized PHMS is interspersed and networked in between the thermoplastic chains of the SBA copolymer. At the same time, the microphase separation means that there exist segregated domains of the two major components in the matrix. This is schematically represented in Fig. 4.2e.

The membrane forming recipes were cast as a thin layer on clean glass slides for water contact angle measurements. All membranes were fairly hydrophobic, with water contact angles varying between 99.5^0 and 106^0 (Fig. 4.3a.). There appeared to be no correlation to

the level of ACA functionalization of the PHMS and the ensuing water contact angle in the membrane recipe. However, the membrane recipe SBA_90ACA, formed with 90% ACA substituted PHMS blended with styrene-butyl acrylate emulsion polymer exhibited a higher water contact angle than other recipes. Super-hydrophobic electrospun non-woven fibrous mats from Block copolymers of poly (styrene-b-dimethylsiloxane) have been shown to exhibit water contact angles up to 163°, wherein the superhydrophobicity was attributed to a microphase separation resulting in differential surface enrichment by the siloxanes [27]. Additionally, superhydrophobic surfaces mimicking lotus leaf properties have been reported on cotton fibers treated with poly (butylacrylate)-modified CNT [28].

The results of water and 1,3-PD mass uptake experiments are shown in Figure 4.3b. While there is a slight decrease in water uptake with increasing ACA functionalization of PHMS, the 1,3-PD uptake increases rapidly with increasing ACA loading.

The results of tensile testing are shown in Figure 4.3c. For the materials made per scheme 1, ACA functionalization adversely affected the break stress and strain. The poor mechanical integrity of these materials precluded their prolonged application in pervaporation studies with varying process conditions. A marked enhancement in tensile strength is obtained by blending the functionalized PHMS with the High Molecular weight SBA copolymer (Scheme 2) and allowed for its prolonged usage in pervaporation under varying experimental conditions. The scheme 1 membrane material using unfunctionalized PHMS is an elastomer with a tensile break stress and a tensile break strain of 0.54 MPa and ~640 % respectively. With the inclusion of ACA functionalized PHMS, the stress and strain at break reduced significantly. The break stresses and strains reduce to

0.13MPa, 0.098MPa and 0.051MPa and 413%, 128% and 43% with 50%, 70% and 90% functionalization of PHMS. By blending the 90% ACA substituted PHMS with SBA, the break stress levels recovered to earlier levels at 0.68MPa and break strain increased to 760%. The stress in the phase separated SIPN material is shared by the two networks. Even as the substituted PHMS network fails, the high molecular weight SBA matrix with its entanglements allows the system further plastic deformation and possible stress induced orientation to re-attain better break stress and strain levels [29].

3.5 Pervaporation results on 1,3-propanediol – water binary feed mixtures

3.5.1 The effect of amine loading in membrane

Figure 4.4 illustrates the variation of steady state component fluxes and separation factors with increasing ACA functionalization. A decrease in steady state water flux, due to decreasing water affinity, was seen with increasing ACA functionalization in the membrane. The steep initial rise in the affinity of the membrane towards 1,3 PD plateaued with increasing ACA functionalization. A slight decrease in 1,3 PD flux with greater ACA loading may be attributed to increase of Tg and hence loss of chain flexibility impeding the diffusion of 1,3-PD molecules.

3.5.2 Effect of process parameters: Feed Temperature, Feed Composition, Cross Flow Velocity

The effect of process parameters was studied on the membrane structure SBA_90ACA, which allowed for long-term experiments on account of its better mechanical integrity. Figure 4.5a illustrates the effect of temperature on pervaporation performance. A slight

increase in water and 1,3-PD flux is seen with temperature. The membrane selectivity reduces with temperature as seen from the separation factor. Increase in temperature enhances the diffusion of both components and to some extent offsets the predominance of the solubility of 1,3-PD over water controlling the overall permeability.

Figure 4.5a also illustrates the effect of 1,3-PD feed concentration at constant temperature and cross flow rate. While the water flux decreased and the 1,3-PD flux increased, the separation factor decreases with increase in the feed 1,3-PD concentration. The reduced selectivity may be attributed to plasticization and swelling of the membrane with increasing1,3-PD concentration in the feed which allowed for a greater amount of both components to diffuse through and resulted in lower selectivity.

Figures 4.5b and 4.5c examine the effect of cross flow rate at three temperatures on the flux and separation factors. The feed 1,3-PD concentration was 10g/l. Increase in the cross flow rate increased the components fluxes as well as the separation factors. The effect on selectivity enhancement with cross flow rate was more significant at 30 ^{0}C than it was at 50 ^{0}C. Cross flow velocity is associated with concentration polarization. For permeating components that are enriched, the concentration polarization assumes values <1 and for components with high levels of enrichment it becomes the deciding factor in pervaporation performance. In these experiments, the enrichment achieved was fair and hence the concentration polarization and the transport coefficients of the static layer were not decisive in determining selectivity and component fluxes.

3.6 Mass transport analysis:

3.6.1 Overall Mass Transfer Coefficient and Permeability:

Pervaporation mass transport in nonporous dense membranes is often described by the solution diffusion mechanism where the diffusion is typically described by Fick's first law [30,31]. The driving force is the difference in activity or fugacity of the i^{th} species given by Equation 3.

$$f_i = x_i^* \gamma_i P_i^{sat} \text{-------(3)}$$

where f is the fugacity, x_i^* is the mole fraction of the i^{th} component in the feed at the interface, γ_i is the activity coefficient, P_i^{sat} is the saturation pressure. The flux of the solute (i^{th} species) across the pervaporation membrane may be expressed as follows (Equation 4):

$$Ji = \frac{P_i}{l}(x_i^* \ \gamma_i \ P_i^{sat} - y_i^* P_p) \text{-------(4)}$$

Where J_i and P_i are the flux and membrane permeability of the i^{th} species, l is membrane thickness, y is mole fraction of the vapor and P_p is the total pressure at the permeate side. The steady state flux can be expressed alternatively, as per Equation 5, in terms of concentration in bulk solution [22, 25].

$$J_i = \frac{p_{i,ov}}{l} (x_i \gamma_i \ p_i^{sat} - \ y_i P_p) \text{ --------(5)}$$

where $P_{i,ov}$ is the overall permeability. The partial pressure on the permeate side, $y_i P_p$, upon application of vacuum, is neglected and thus the equation above becomes:

$$J_i = \frac{p_{i,ov}}{l} x_i \gamma_i p_i^{sat} = K_{i,ov} C_i \text{ ------(6)}$$

where $K_{i,ov}$ is the overall mass coefficient of solute *i and* C_i is the molar concentration in kg mole/m^3. $K_{i,ov}$ can be expressed as $P_{i,ov} \cdot \gamma_i \cdot \frac{P_i^{sat}}{l \cdot C^T}$ where C^T is the total molar concentration of the feed solution, and $C_i = x_i \cdot C^T$ relates the species flux to the concentration of the respective species in the feed. Thus the component flux could be used to compute the overall mass transfer coefficient and overall permeability of 1,3-PD. Activity coefficients of the feed concentrations were computed by the Wilson equation and saturation vapor pressure by the Antoine equation [30]. The 1,3-PD mass transfer coefficients and permeability are shown in Table 1. All computed data shown is based on experiments with a feed 1,3-PD concentration of 10 g/l. The data for the membranes shown are those for the SBA_90ACA membrane. Data for other membranes was also generated at a volumetric cross flow rate of 31.9L/h. The variations with temperature follow the same pattern as reported for SBA_90CA in Table 1.

3.6.2 Boundary Layer Mass Transfer Coefficient:

Concentration polarization adversely affects the separation performance due to the build up a liquid side boundary layer whose resistance adds to the intrinsic membrane resistance. In severe cases, measured separation factors can be as low as 10% of the intrinsic separation factors [32]. The mass transfer coefficient of 1,3-PD through the liquid boundary layer in a circular cell membrane channel with two parallel plates can be obtained by the semi-empirical correlation [33,34]

$Sh = 0.3Re^{\frac{1}{2}}Sc^{\frac{1}{3}}$------- (7)

Where *Sh* is the Sherwood number. It is equal to $K_{1,3-PD,l}\frac{d_H}{D}$. This correlation is used to compute $K_{1,3-PD,l}$, the mass transfer coefficient of 1,3-PD through the liquid layer in m/s. The diffusivity, *D* (m^2/s), of 1,3-PD in water was computed from the Wilke – Chang equation [34] *Re* is the Reynolds number and is equal to $d_h\frac{v}{\upsilon}$, where d_h(m) is the characteristic length of the membrane channel given by $\frac{2Wh}{(W+h)}$, *W* and *h* being the width and height of the channel, v is the mean linear velocity on m/s and υ, the kinematic viscosity in m^2/s at the respective temperature [32, 35,36]. *Sc* is the Schmidt number and is equal to $\frac{\upsilon}{D}$. The mass transfer resistance on the downstream vapor side boundary layer is negligible and is ignored. The overall mass transfer coefficients and boundary layer mass transfer coefficient are shown in Table 2.

3.6.3 Concentration Polarization Modulus:

Pervaporation membranes are much more permeable to dissolved organics than water and so the edge of the boundary layer adjacent to the membrane surface becomes depleted in the organic concentration [32]. Convective mixing is absent in this layer. Mass transfer can be described as a combination of diffusion across concentration gradients formed in the boundary layer and convective flow of fluid through the membrane. Assuming that no mixing occurs in the boundary layer adjacent to the membrane, the convective flux is given by $J_v c_i^{'}$, where J_v is the convective velocity towards the membrane and $c_i^{'}$, the concentration of solute in the well mixed bulk. The convective flow is counterbalanced by diffusive flow perpendicular to the membrane surface given by the x coordinate. At steady state the two, balancing each other out, may be expressed as

$$J_v c_i^{'} - D\frac{dc_i^{'}}{dx} = J_v c_i^{''} \text{ ---------(8)}$$

D is the diffusion coefficient in the boundary layer and $c_i^{''}$ is the permeate solute concentration which can be linked to the bulk solute concentration by the enrichment factor $E_i = \frac{c_i^{''}}{c_i^{l}}$. The equation above can integrated and rewritten in terms of the enrichment factor as:

$$-\ln\left(1-\frac{1}{E}\right) = -\ln\left(1-\frac{1}{E_0}\right) + J_v\frac{\delta}{D} \text{ ----------(9)}$$

δ is the thickness of the boundary layer, D/δ is the boundary layer mass transfer coefficient computed in the section above and E_0 is the intrinsic enrichment factor. The ratio $\frac{E}{E_0}$ or $\frac{c_{i0}^{'}}{c_i^{'}}$ is known as the concentration polarization modulus and is <1 for systems getting enriched. A linear regression on experimental results required D/δ to be substituted by $k_0 u^n$, where u is the superficial linear feed velocity in the channel, k_0 and n are constants. Linear regression with best fit values for n yielded the concentration polarization modulus which was computed based on experimental results shown in Figure 4.5b. The concentration polarization modulus for the SBA_90ACA membrane with varying cross flow velocity and a feed 1,3-PD concentration of 10g/l is shown in Figure 4.6a. The major resistance to mass transfer lies in the membrane itself and not in the boundary layer, even though the Reynolds numbers are in the laminar flow regime range of 72 – 460. The concentration polarization modulus deviates from unity with increasing peclet number [32] approaching the limiting value of $\frac{1}{E_0}$ when the boundary layer negates the separation power of the membrane. Also compounds that are enriched by the membrane, with intrinsic enrichment, $E_0 > 1$ are more

affected by this phenomenon than those that are rejected. Concentration Polarization plays a non trivial role in cases when the intrinsic enrichments are > 100. In these experiments the computed intrinsic enrichment factors lay between 12 and 14. This, and the limited mass uptake of 1,3-PD in the membrane are the reason for the trivial role of the boundary layer resistance and the predominance of the membrane in separation performance.

3.6.4 Computation of the material mass transport property of the membrane material:

The membrane structure as shown in the FESEM image (Fig.4.2c) is schematically represented in Figure 4.6b. The figure also shows the permeation pathway for the diffusing components. The membrane dominates the resistance offered to the mass transport and the concentration polarization is trivial (Fig 4.6a.). The intrinsic mass transport coefficient of the material may be derived from the overall mass transfer coefficients. For practical purposes, ignoring the effects of boundary layer, the total mass flux, J and the individual mass fluxes though the top dense layer and bottom porous PE supported layer, J_1 and J_2 may be respectively represented by, $J = k_{ov}(\frac{dp}{dz})$, $J_1 = k_{m,1}(\frac{dp}{dz})_1$ and $J_2 = k_{m,2}(\frac{dp}{dz})_2$.

Where k_{mi} and $(\frac{dp}{dz})_i$ represent the mass transfer coefficients and the potential drop across the i^{th} layer represented by the partial pressure drop over the membrane thickness. Mass flow rates through the respective layers are given by $F_1 = J_1 A_1$ and $F_2 = J_2 A_2 = J_2 A_1 \xi$, where A_1 is the pervaporative area proffered by the dense top layer and A_2 the total area allowed for pervaporation in the second layer and ξ is the % porosity of the porous PE layer. A fundamental assumption made here is that the polyethylene material completely disallows any permeation of either 1,3-PD or water and that the permeating components

travel only through the siloxane based material that fills in the pores. Thus, $k_{m1} = k_{m2}$. At steady state, the flow rates through the two layers equal each other. $F_1=F_2$ and hence $J_1 = J_2\xi$ and $(\frac{dp}{dz})_1 = (\frac{dp}{dz})_2\xi$. The partial pressures at the interface of layer 1 and layer 2 and at the layer 2 – downstream vapor interface can be expressed as:

$$P_1 = P_0 + z_1(\frac{dp}{dz})_1 \text{ ----------(10)}$$

$$P_2 = P_1 + (z_2 - z_1)(\frac{dp}{dz})_2 = P_0 + [z_1 + \frac{1}{\xi}(z_2 - z_1)](\frac{dp}{dz})_1\text{.----------(11)}$$

Where z_1 and z_2 are the thicknesses of the top and bottom layers respectively and P_0, P_1 and P_2 represent the partial pressures of 1,3-PD at the feed side of the membrane, at the layer1-layer2 interface and at the vapor permeate side. . These expressions can be used to yield an expression in terms of the intrinsic mass transfer coefficient for the membrane material, sans the porous support. Drawing from section on overall mass transfer coefficient, the partial pressures were substituted by the experimentally determined concentrations of 1,3-PD on the feed and permeate sides and the equation rewritten :

$$k_m^{'} = \frac{F}{A_1[\frac{C_{permeate}-C_{feed}}{z_1+\frac{1}{\xi}(z_2-z_1)}]} \text{ ----------(12)}$$

Where $k_m^{'}$ is the representative mass transfer coefficient of the membrane material and represents a material property. The computed material mass transfer coefficients at various temperatures for the membrane SBA_90ACA based on experiments with a feed 1,3-PD concentration of 10 g/l were : 1.07 X 10^{-11} m^2/s (30 ^{0}C), 1.22 X 10^{-11} m^2/s (40 ^{0}C) and 1.43 X 10^{-11} m^2/s (50 ^{0}C).

3.7 Solubility Parameters

Permeation may be defined as $P = D.S$ where D is the diffusion coefficient and S is the solubility for components into the membrane from the feed. The relative enrichment of components in a pervaporation feed occurs by virtue of their higher affinity for the membrane material or greater diffusivity or both [37]. The membrane- component affinity is described by the Hansen solubility parameter comprising hydrogen bonding interaction (δ_H), polar interaction (δ_P) and dispersion interaction (δ_D) [21,37]. For a binary system, the Hansen's solubility parameter distance Ra is a measure of the dissimilarity between two components [38].

$$R_a = \sqrt{4(\delta_{d1} - \delta_{d2})^2 + (\delta_{p1} - \delta_{p2})^2 + (\delta_{H1} - \delta_{H2})^2} \text{ ----------(13)}$$

The chemistry of the membrane and its interaction with permeating components affects Ra and the separation performance [39, 40]. Water has the highest δ_P, closely followed by glycols, such as 1,3-PD [21]. Water also possesses the highest δ_H also closely followed by glycols [21]. Large differences between δ_H for water and organic solvents makes their pervaporative dehydration feasible and efficient [21, 40]. Additionally, the diffusive efficacy of components through a membrane depends upon their kinetic diameter (d_k) which considers the molecular size and shape [21, 39]. Given that the d_k of water is significantly lower than that of 1,3-PD, it diffuses faster. Hence the onus of pervaporative enrichment in favor of 1,3-PD lies on preferential sorption of 1,3-PD into the membrane and the concomitant rejection of water [21]. The proximity of the solubility parameters of water and 1,3-PD compounds the difficulty of separation using conventional membrane

materials such as PDMS and hence calls for its functionalization. The chemistry of functionalization, while enhancing the affinity for 1,3-PD must also make the membrane more hydrophobic and this is reflected in the partial solubility parameters.

The partial solubility parameters of water and 1,3-PD were obtained from literature [40–42]. The δ_H for PDMS were obtained from literature while δ_P and δ_D computed from the refractive index and dipole moments respectively [41–43]. Those of ACA were computed using a group contribution method [44], employing two kinds of characteristic groups: first-order groups that describe the basic molecular structure of compounds and second-order groups based on the conjugation theory to improve the accuracy of predictions. The contribution towards δ_H, δ_P and δ_D were computed from literature values provided for the participating groups and identifiable conjugates in ACA [44]. In the absence of the availability of reliable δ_H, δ_P and δ_D group contribution for Si-O, Si-H and Si-CH_3 the partial solubility parameters for the ACA modified siloxane materials could not be computed. TEAS parameters or fractional parameters, were computed from the partial interaction parameters and indicate a fractional contribution of each partial parameter to the whole solubility parameters. They are defined as

$$f_D = \frac{\delta D}{\delta D + \delta H + \delta P} \quad \text{.....(14)}$$

$$f_H = \frac{\delta H}{\delta D + \delta H + \delta P} \quad \text{.....(15)}$$

$$f_P = \frac{\delta P}{\delta D + \delta H + \delta P} \quad \text{.....(16)}$$

The TEAS parameters are illustrated Fig 4.6 (c). The distance of separation between 1,3-PD and water is similar to that between 1,3-PD and ACA. Thus 1,3-PD can be only partly partitioned into ACA, while the hydrophobic character of ACA is underscored by its large separation distance from water, due primarily to the disparities in δ_H and δ_P. While two materials may end up with the same solubility parameters, computed arithmetically, the individual contributions that make up this value may be different with ramifications on their mutual affinity [45]. The behavior of unfunctionalized siloxane PDMS is dominated by dispersion forces with very little polar and hydrogen bonding based affinity for 1,3-PD as well as water [21]. The distances of separation from water for both ACA and siloxanes are comparable. When the siloxane is functionalized with ACA, which is the major component in the membrane matrix fabricated by either scheme, the affinity for 1,3-PD increases while that for water remains practically unchanged.

Permeant transport through membranes with strong membrane-species interactions has been visualized to occur either by random walk or by jumps from one interactive site to another [46]. Unfunctionalized PDMS has very little affinity for either water or 1,3-PD. When functionalized, all its interaction parameters with 1,3-PD are superior to those with water. In light of the transport theory, the movement of 1,3-PD through the membrane may be thought of as a random walk supported by a balance between polar interactions and dispersion interactions with functional groups on ACA and siloxane chains. In an alternative theory, the permeants are thought to cluster around given functional groups [32, 37]. With a binary feed, when one permeant molecule jumps from one cluster, the vacancy left behind may be filled up by a permeant molecule of either species [46]. In this system,

the filling of this vacancy may be selective, pertinent to the interaction parameters allowing for a greater absorption and permeation of 1,3-PD than water.

The classical solution diffusion model used here is valid only for non-swollen membranes. In cases where appreciable swelling occurs, the partition and diffusion coefficients become concentration dependent and the theory must be modified to adapt to these changes and also to define the effect of coupled transport in multicomponent pervaporations with model fermentation broths [37].

3.8 Comparative Performance Analysis

Table 3 provides an overview of the comparative performance of systems that have been employed to enrich 1,3-PD from aqueous mixtures and broth compositions. This includes earlier pervaporation experiments on zeolite membranes, which were successful in separating 1,3-PD from broth components other than water. While the pervaporative zeolite membranes achieved separation of 1,3-PD from other broth components, the membranes were not selective for 1,3-PD over water [16, 17]. The ionic liquid SLM reported separation factors greater than 100 for 1,3-PD in batch pervaporation in a nano-porous module of ~1000 μ thickness. While a stability of 9 months was claimed in this particular work [18], SLM s typically suffer from intrinsic long term stability issues on account of leaching. Additional limitations include fabrication of membrane modules and scale up.

Hydrolytic instability of many ionic liquids limit their applications to anhydrous conditions [47]. The requirement for hydrolytically stable ionic liquids has resulted in several developments, yet their technical applications are limited by the high price of the anions

[47]. A brief comparison of the price of materials developed in this work versus that used for the cyanoborate ionic liquid based membrane [18] was carried out with current retail price data from Sigma Alridch (www.signmaaldrich.com), Oakwood Chemicals Inc. (http://www.oakwoodchemical.com) and Fluorochem Ltd. (http://www.fluorochem.co.uk). A simple stoichiometric computation based on the molecular weights and the prices of the individual moieties making up the compound reveals that the cyanoborate ionic liquid costs $36,004/mole, while the ACA functionalized PHMS materials cost $1133/mol, $892/mol and $655/mol for the 90%, 70% and 50% functionalized materials, respectively. The cost per unit weight of the ionic liquid is $120/g, while those of the ACA functionalized siloxanes are $6/g, $5.6/g and $4.9/g for 90%, 70% and 50%, respectively. Price/performance trade off estimates can be generated using either the molar prices or the mass prices in terms of the separation factors. The 1,3-PD flux obtained in this work is also 1.5 times higher than that reported with the cyanoborate ionic liquid.

A preliminary estimation was made of the total volume of membrane material required to enrich a flow of 100g/h of feed with 1 mass% 1,3-PD to a final 1,3-PD concentration of >90%. The separation factor and flux of 1,3-PD was assumed constant in each enrichment stage. This assumption is an oversimplification but quite adequate for a rough comparison. The average separation factor for the SBA_90ACA membrane was taken as 14 at an average 1,3-PD flux of 5.89 g/m^2h. The computation indicated that 3 enrichment steps with a total membrane area of 4650cm^2 are required. The membrane volume was estimated by taking into consideration that the 550μm thick porous polyethylene support has a porosity

of 48% and the dense layer thickness is 100 μm. Thus, the required volume is 169cm^3. Also assuming an approximate density of 1g/cm^3, the cost of the material required to achieve the aforementioned enrichment level is ~$1015.

The same computation was carried out for the cyanoborate ionic liquid membrane stabilized in a nanoporous ceramic module. The flux of 1,3-PD (3.86 g/m^2h) and separation factor (177) reported [18] were assumed constant for the computation. The same enrichment levels from a starting composition of 1% 1,3-PD was calculated to require 2 enrichment steps with a total area of 4660cm^2. The thickness of the module reported in their work [48] is 3 mm (with a 7mm inner diameter and 10 mm outer diameter). The nanoporous module reported in their work has a porosity of 30% [18, 48]. Thus, the total cyanoborate ionic liquid requirement is 419 cm^3. Assuming a density of 1g/cm^3, the cost of material required to achieve the same enrichment level is ~$50,328.

The work reported here reacts a 1,3-PD solvent, ACA, into a Siloxane backbone. The membrane, with its mechanical integrity, allows the flexibility of fabrication into structures and modules. While fair separation was achieved for the structure reported in this paper, the structure provides a pathway for scale up with design flexibility to optimize the cost/performance tradeoff. Membrane structures can be envisioned wherein a thin surface layer of highly ACA functionalized membrane is followed by support layers with enhanced flux while making no adverse contribution towards the separation efficacy.

4. Conclusions

The paper reports an ACA functionalized siloxane membrane for the pervaporative enrichment of 1,3-PD concentration from binary aqueous. The functionalized siloxane materials were crosslinked by two mechanisms with superior mechanical stability being obtained with the phase separated blend. The separation factors increased with increasing functionalization. The feed concentration and temperature also played an important role in determining separation efficacy. A minimal amount of concentration polarization was observed as is the norm for such systems with fair separation factors, with the resistance to permeation being dominated by the membrane. The solution diffusion model was used to compute the overall mass transfer coefficient of the membrane and the intrinsic mass transfer of the functionalized material. An analysis of the Hansen's solubility parameters was carried out to explain the results obtained.

5. Acknowledgements

The authors acknowledge the advice of Prof. M.T. Shaw, (Professor Emeritus, University of Connecticut) in thermodynamic computations. Portions of this work were supported by DOE Grant DE-EE0003116.

6. References

1. A.J. Ragauskas, C.K. Williams, B.H. Davison, G. Britovsek, J. Cairney, C.A. Eckert, W.J. Frederick Jr., J.P. Hallett, D.J. Leak, C.L. Liotta, J.R. Mielenz, R. Murphy, R. Templer, T. Tschaplinski, The path forward for biofuels and biomaterial, Science. 311 (2010) 484–489.

2. Z.L. Xiu, A.P.Zeng, Present state and perspective of downstream processing of biologically produced 1,3-propanediol and 2,3-butanediol, Appl Microbiol Biotechnol. 78 (2008) 917–926.
3. R.K. Saxena, P. Anand, S. Saran, J. Isar, Microbial production of 1,3-propanediol: Recent developments and emerging opportunities, Biotechnology Advances. 27 (2009) 895–913.
4. A.P. Zeng, H. Biebl, Bulk chemicals from biotechnology: the case of 1,3-propanediol production and the new trends, in: T. Scheper, K. Schugerl, A.P. Zeng (Eds.), Advances in biochemical engineering and biotechnology, Vol. 74, Springer-Verlag, Berlin, Heidelberg, New York, 2002, pp239–59.
5. A. Triguero, R. Blanco, H. Machado, M. Rodríguez, Evaluation of liquid extraction potentials for downstream separation of 1,3-propanediol, Biotechnology Techniques. 13 (1999) 127–130.
6. T.T. Ames, Process for the isolation of 1,3-propanediol from fermentation broth. US Patent 6361983 B1 (2002).
7. Y. Gong, Y. Tong, X.L. Wang, D.H. Liu, The possibility of the desalination of actual 1,3-propanediol fermentation broth by electrodialysis, Desalination. 161 (2004) 169–178.
8. J. Hao, D.H. Liu, Desalination of fermented broth containing 1,3-propanediol by electrodialysis, Chinese J Proc Eng. 5 (2005) 36–39.
9. Z. Li, B. Jiang, D. Zhang, Z. Xiu, Aqueous two-phase extraction of 1,3-propanediol from glycerol-based fermentation broths, Separation and Purification Technology. 66 (2009) 472–478.

10. A. Baiada, A. Vitner, R.P. Jansen, A.M. Baniel, Process for producing 1, 3-propanediol. US Patent 7056439 B2 (2006).
11. A.K. Hilaly, T.P. Binder, Method of recovering 1,3-propanediol from fermentation broth. US Patent 6479716 B2 (2002)
12. M.H. Cho, S.I. Joen, S.H. Pyo, S. Mun, J.H. Kim, A novel separation and purification process for 1,3-propanediol, Process Biochem. 41 (2006) 739–744.
13. P. Anand, R.K. Saxena, R.G. Marwah, A novel downstream process for 1,3-propanediol from glycerol-based fermentation, Appl. Microbiol. Biotechnol. 90 (2011) 1267–1276.
14. J. Hao, F. Xu, H. Liu, D. Liu, Downstream processing of 1,3-propanediol fermentation broth, Journal of Chemical Technology and Biotechnology.81(2006) 102–108.
15. J.J. Malinowski, Reactive Extraction for Downstream Separation of 1,3-Propanediol, Biotechnology Progress. 16 (2000) 76–79.
16. S. Li, V.A. Tuan, J.L. Falconer, R.D, Noble, Separation of 1,3- propanediol from glycerol and glucose using a ZSM-5 zeolite membrane, J. Membr Sci. 191 (2001a) 53–59.
17. S. Li, V.A. Tuan, J.L. Falconer, R.D. Noble, Separation of 1,3- propanediol from aqueous solutions using pervaporation through an X-type zeolite membrane, Ind Eng Chem Res 40 (2001b) 1952– 1959.
18. P.Izák, M. Köckerling, U. Kragl, Stability and selectivity of a multiphase membrane, consisting of dimethylpolysiloxane on an ionic liquid, used in the separation of solutes from aqueous mixtures by pervaporation, Green Chem. 8 (2006) 947–948.

19. S.Y. Li, R. Srivastava, R.S. Parnas, Study of in situ 1-Butanol Pervaporation from A-B-E Fermentation Using a PDMS Composite Membrane: Validity of Solution-Diffusion Model for Pervaporative A-B-E Fermentation, Biotechnol. Prog. 27 (2011) 111–120.
20. S. Krishnan, C.J. Weinman, C.K. Ober, Advances in polymers for anti-fouling surfaces, J. Mater.Chem. 18 (2008) 3405 – 3413.
21. P. Shao, R.Y.M. Huang, Polymeric membrane pervaporation, Journal of Membrane Science. 287 (2007) 162-179.
22. S. Li, R. Srivastava, R.S. Parnas, Separation of 1-butanol by pervaporation using a novel tri-layer PDMS composite membrane, J. Membr. Sci. 363 (2010) 287–294.
23. P.Wu, R.W.Field, R.England, B.J.Brisdon, Performance of PDMS and organofunctionalised PDMS membranes for the pervaporative recovery of organics from aqueous streams, J. Membr. Sci. 137 (1997) 63–88.
24. P.Wu, R.W.Field, R.Englanda, B.J. Brisdon, A fundamental study of organofunctionalised PDMS membranes for the pervaporative recovery of phenolic compounds from aqueous streams, J. Membr. Sci. 190 (2001) 147–157.
25. P. Wu, B.J. Brisdon, R. England, R.W. Field, Preparation of modified difunctional PDMS membranes and a comparative evaluation of their performance for the pervaporative recovery of p-cresol from aqueous solution, J. Membr. Sci. 206 (2002) 265–275.
26. C.B. Mallon, B.Mead, Surfactant free process for production of pressure sensitive adhesive latexes. US Patent 4316830 (1982).

27. M. Ma, R.M. Hill, J.L. Lowery, S.V. Fridrikh, G.C. Rutledge, Electrospun Poly(Styrene-block-dimethylsiloxane) Block Copolymer Fibers Exhibiting Superhydrophobicity, Langmuir. 21 (2005) 5549–5554.
28. P. Roach, N.J. Shirtcliffe, M.I. Newton, Progress in superhydrophobic surface development, Soft Matter. 4 (2008) 224–240.
29. J. Sun, X. Zhao, W. R. K. Illeperuma, O. Chaudhuri, K.H.Oh, D.J. Mooney, J.J. Vlassak, Z. Suo, Highly stretchable and tough hydrogels, Nature. 489 (2012) 133–136.
30. J.G. Wijmans, R.W.Baker, The solution Diffusion model: a review, J. Membr.Sci. 107 (1995) 1–21.
31. S.J. Lue, W.W. Chen, S.Y. Wu, L.D. Wang, Vapor permeation modeling of multicomponent systems using a poly(dimethylsiloxane) membrane, J. Membr. Sci. 311 (2008) 380–389.
32. R.W. Baker, J.G. Wijmans, A.L. Athayde, R. Daniels, J.H. Ly. M. Le, The effect of concentration polarization on the separation of volatile organic compounds from water by pervaporation, J. Membr. Sci. 137 (1997) 159–172.
33. C. Lipski, P. Côté, The use of pervaporation for the removal of organic contaminants from water, Environmental Progress. 9 (1990) 254–261.
34. C.R. Wilke, P. Chang, Correlation of diffusion coefficients in dilute solutions AICHE Journal. 1, (1955) 264–270.
35. M.T. Sanz, B. Blanco, S. Beltran, J.I. Cabezas, Vapor liquid equilibria of binary and ternary systems with water, 1,3-propanediol and glycerol, J Chem Eng Data. 46 (2001) 635–639.

36. D.M. Bajić, G.R. I.Zoran, P. Visak, E.M. Živković, S.P. Šerbanović, M.L. Kijevčanin. Densities, viscosities, and refractive indices of the binary systems (PEG200 + 1,2-propanediol, +1,3-propanediol) and (PEG400 + 1,2-propanediol, +1,3-propanediol) at (288.15 to 333.15) K and atmospheric pressure: Measurements and modeling, J. Chem Thermodynamics. 57 (2013) 510–529.
37. M. Mulder, T. Franken, C.A. Smolders, Preferential sorption versus preferential permeability in pervaporation, J. Membr. Sci. 22 (1985) 155–173.
38. D.J. Benedict, S.J. Parulekar, S.P. Tsai, Pervaporation assisted esterification of lactic and succinic acids with downstream ester recovery, J. Membr. Sci. 281 (2006) 435–445.
39. W.J.Koros, Membranes: Learning a lesson from nature, Chem Eng. Prog. 91 (1995) 68–81.
40. C.M. Hansen, Hansen solubility parameter: A users handbook, second ed., CRC press Taylor and Francis group, Boca Raton, London, New York, 2007.
41. M. Alizadeh, F. Abbassi, M. Farahi, K. Jalili, Silicone based hydrogels prepared by interpenetrating polymeric network synthesis: Swelling properties and confinements effects on the formation kinetics, J appl Poly Sci. 124 (2012) 985–992.
42. J.N. Lee, C. Park, G.M. Whitesides, Solvent Compatibility of Poly(dimethylsiloxane)-Based Microfluidic Devices, Anal Chem. 75 (2003) 6544–6554.
43. N.A.Diachun, A.H. Marcus, D.M. Hussey, M.D.Fayer, Dynamics in Polydimethylsiloxane: The Effect of Solute Polarity, JACS. 116 (1994) 1027–1032.

44. E. Stefanis. C. Panayiotou, Prediction of Hansen Solubility Parameters with a New Group-Contribution Method, Int J. Thermophys. 29 (2008) 568–585.
45. M. Oshikawa, N. Ogata, T. Shimidzu, Polymer membrane as a reaction field. III: Effect of membranes polarity on selective separation of water-ethanol binary mixtures through synthetic polymer membranes, J. Membr. Sci. 26 (1986) 107–113.
46. R.Y.M. Huang, P. Shao, X. Feng, C.M. Burns, Pervaporation separation of water / isopropanol mixture using sulfonated poly(ether ether ketone) (SPEEK) membranes: transport mechanism and separation performance, J. Membr. Sci. 192 (2001) 115–127.
47. E. Kuhlman, S. Himmler, H. Giebelhaus, P. Wasserscheid, Imidazolium dialkylphosphates – a class of versatile, halogen-free and hydrolytically stable ionic liquids, Green Chem. 9 (2007) 233 – 242.
48. P. Izak, M. Köckerling, U. Kragl, Mehrphasen–Membran. German Patent DE102006024397 B3 (2007).

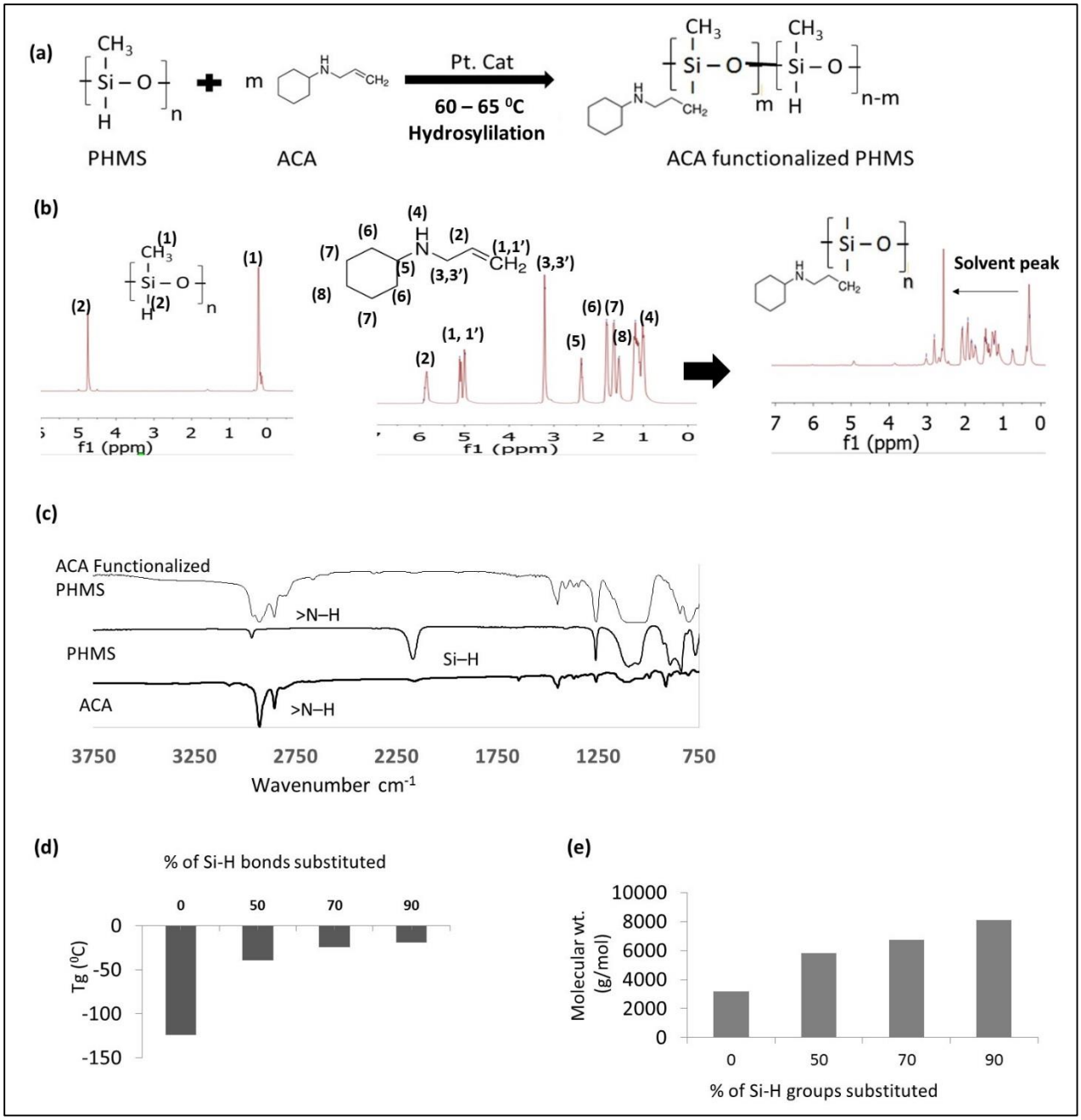

Figure 4.1: (a) Hydrosilylation Reaction Scheme (b) Representative H1 NMR for hydrosilylation (c) Representative FTIR for hydrosilylation (d) Glass transition temperature at various levels of functionalization (e) Molecular weight at various levels of functionalization

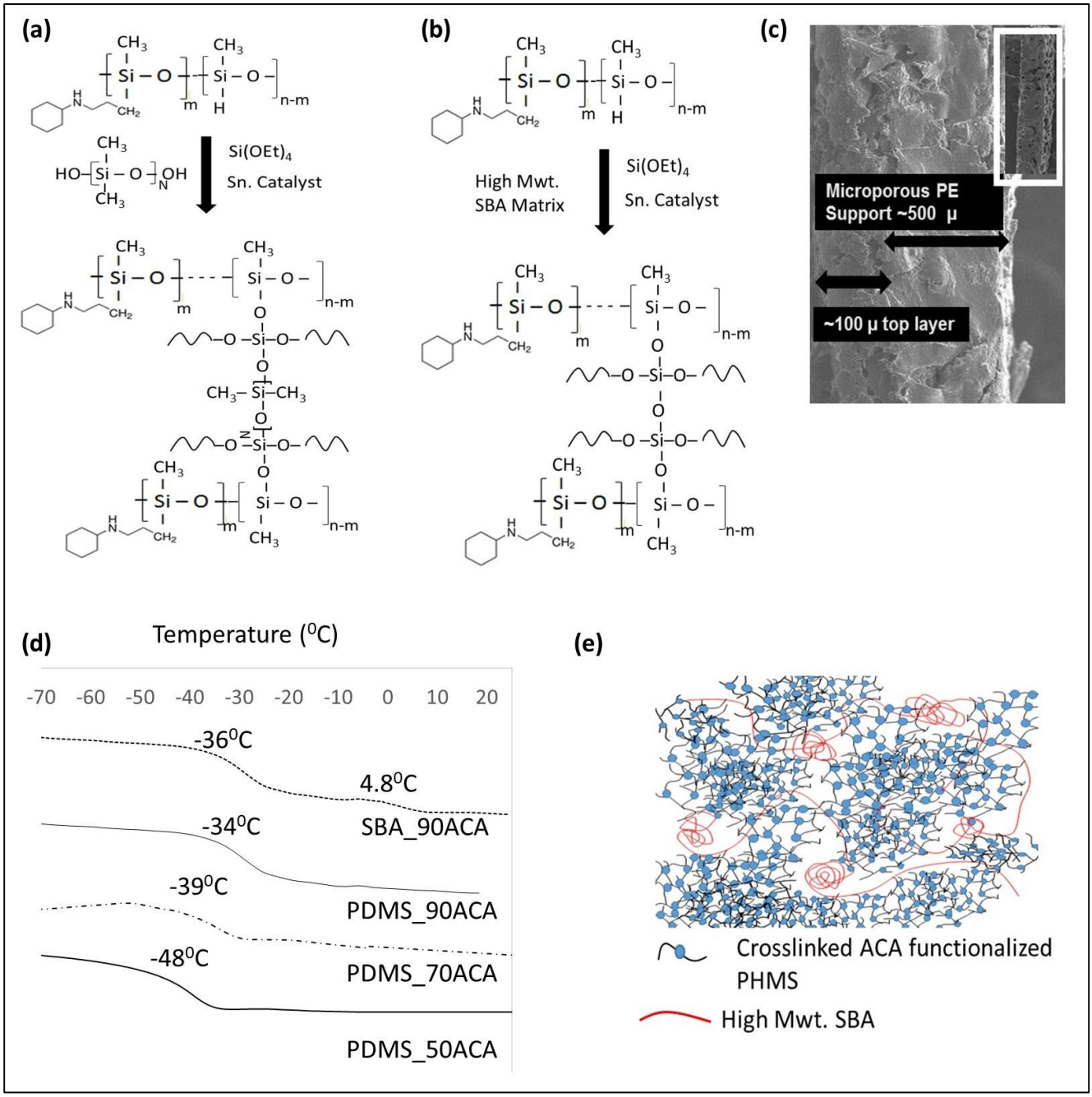

Figure 4.2: (a) Crosslinking reaction Scheme-1 (b) Crosslinking reaction Scheme-2 (c) FESEM of composite membrane structure with FESEM of porous PE sheet as inset (d) Glass transition temperature of membrane forming recipes (e) Schematic representation of microphase segregated blend formed by scheme 2

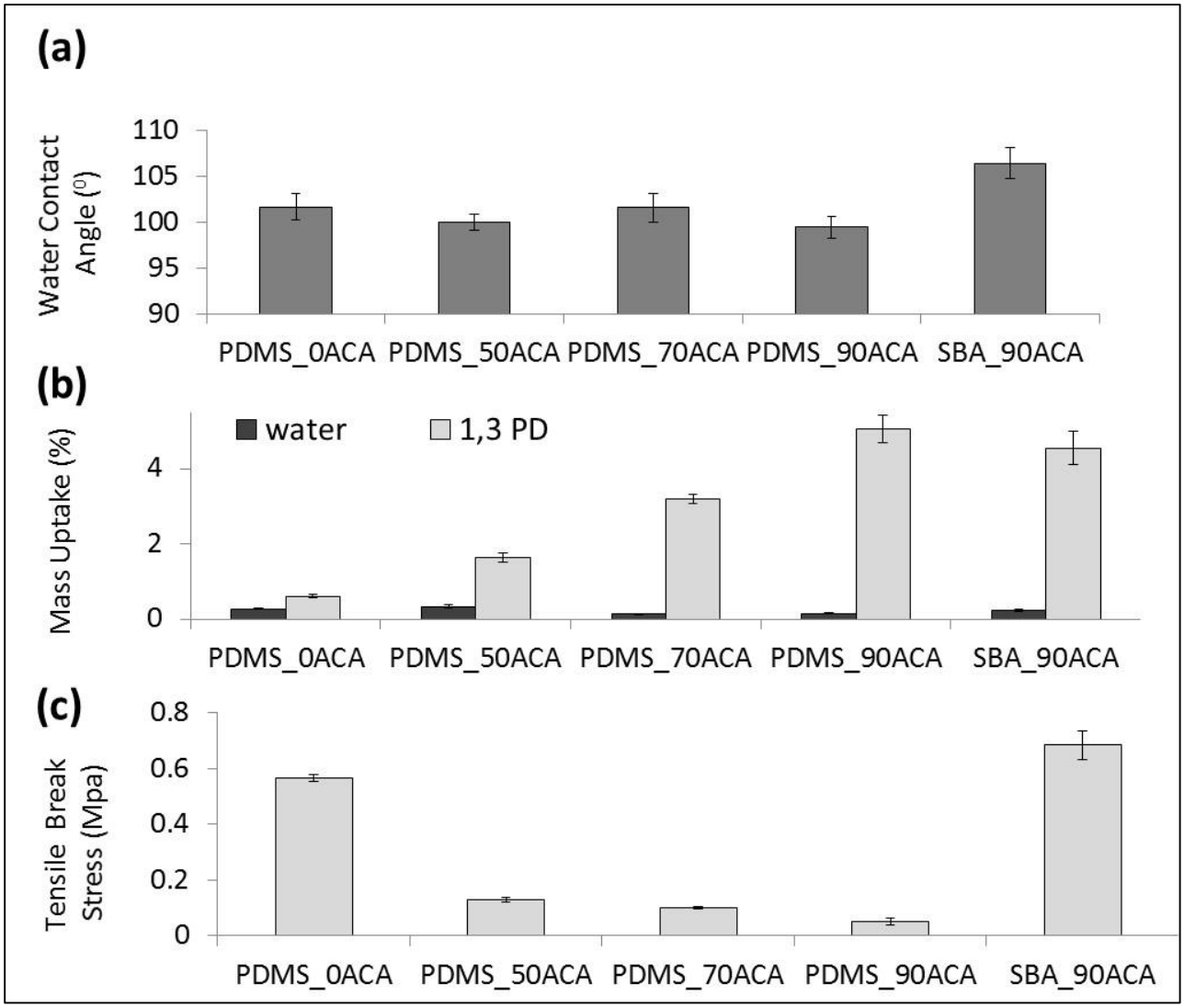

Figure 4.3: (a) Water contact angle on membrane forming recipes (b) Mass uptake results of membrane forming recipes (c) Tensile break stresses of membrane forming recipes.

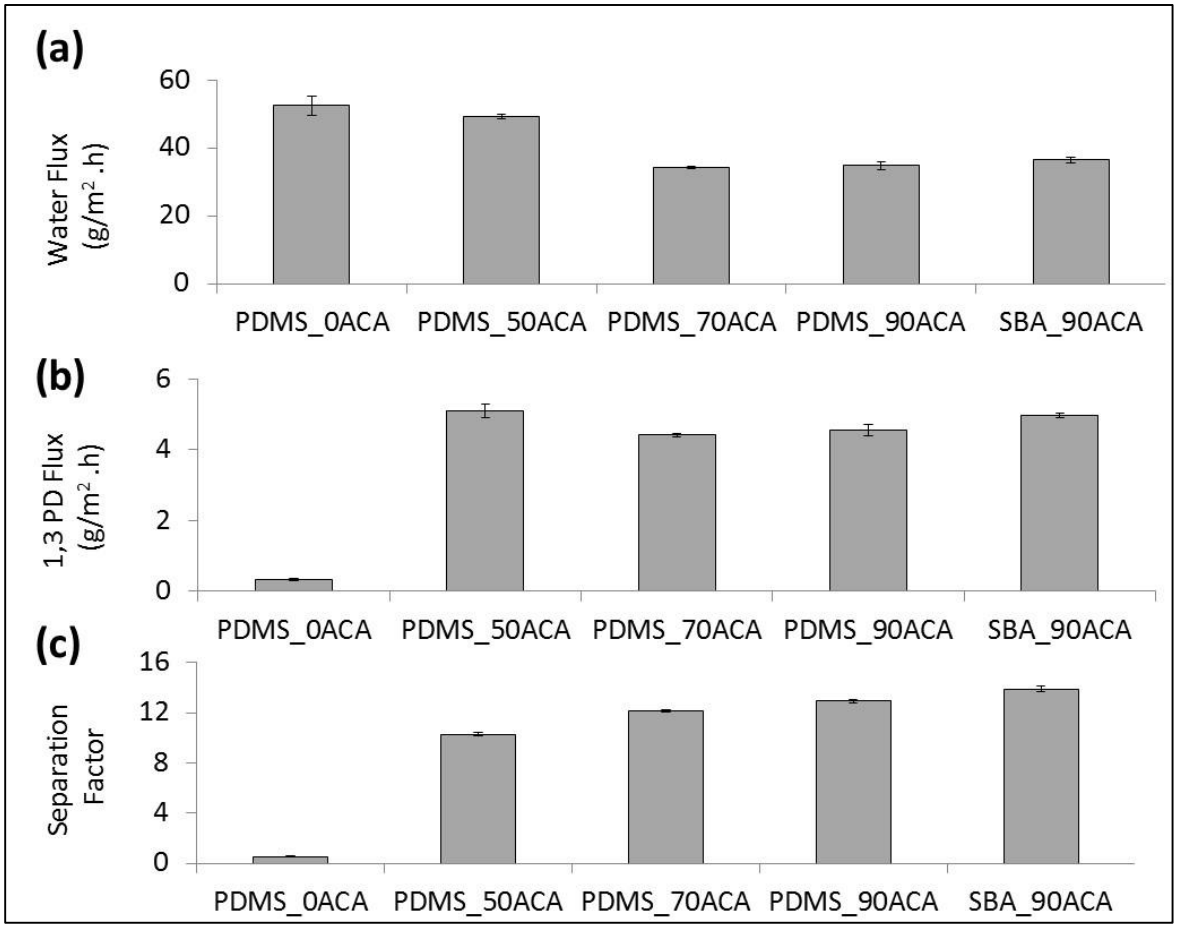

Figure 4.4: Variation of steady state component flux and separation factors with increasing ACA functionalization (a) Water Flux (b) 1,3-PD flux (c) Separation Factor

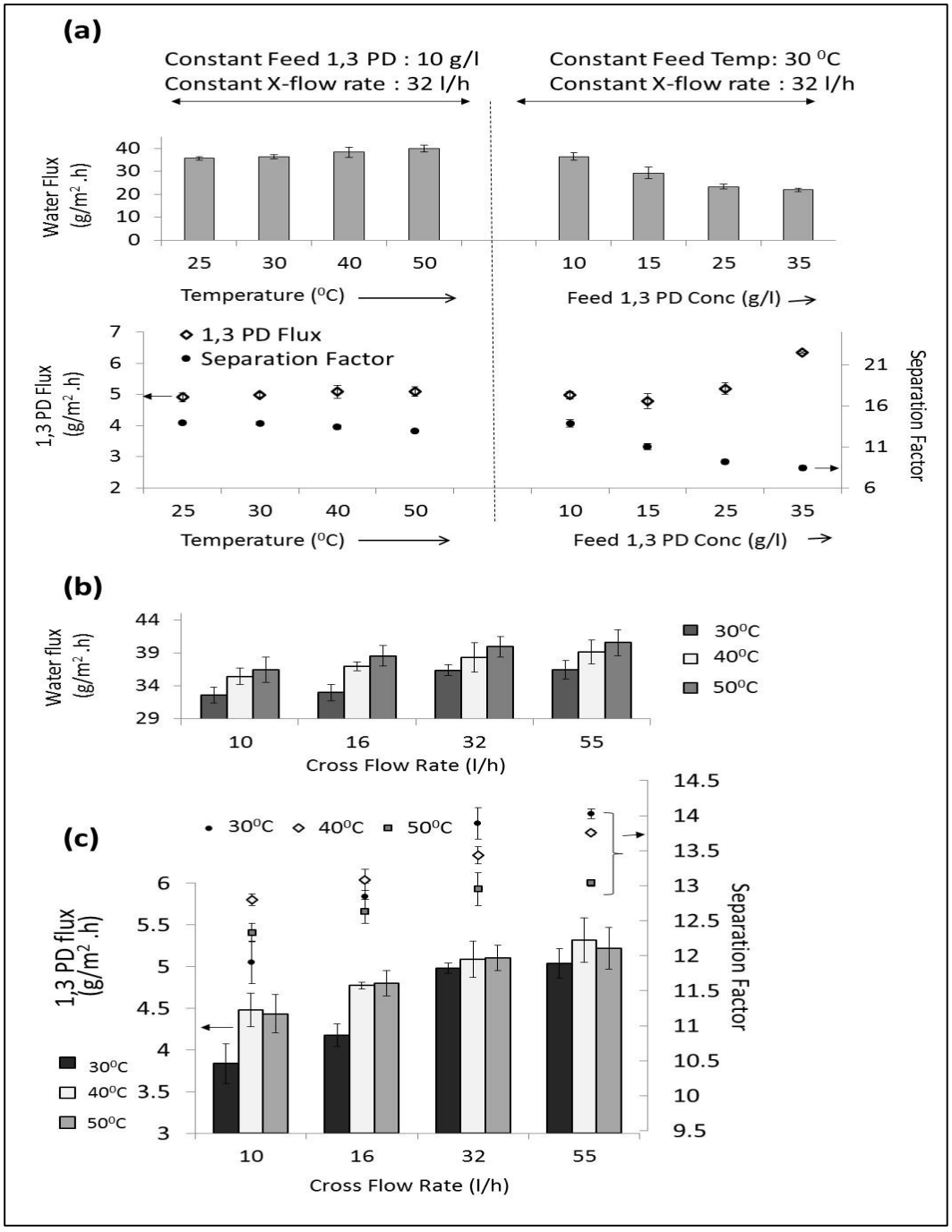

Figure 4.5: (a) Effect of feed 1,3-PD concentration and Feed Temperature (b) Effect of cross flow rate on water flux (c) Effect of cross flow rate on 1,3-PD flux and separation factors.

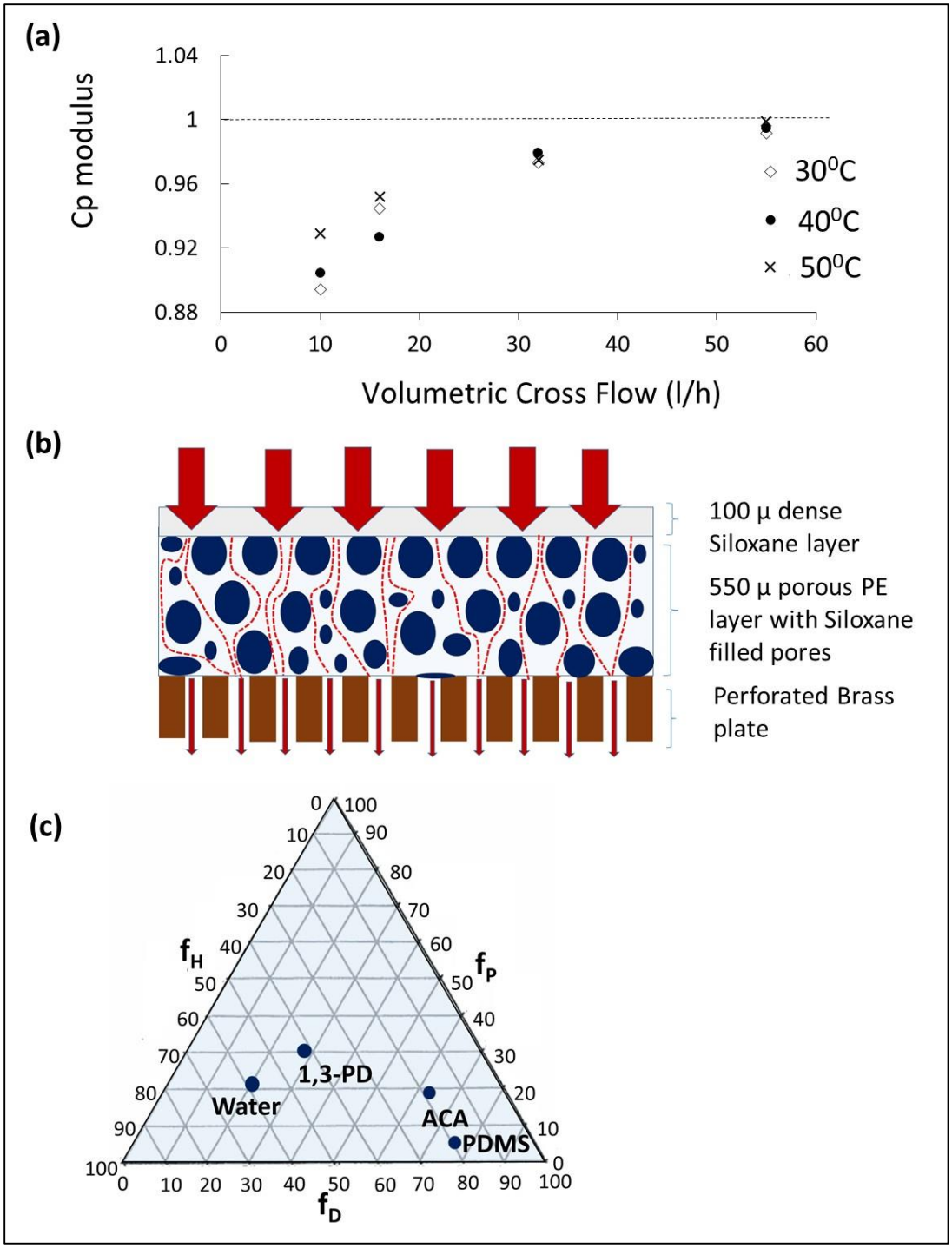

Figure 4.6: (a) Variation of Concentration Polarization modulus with cross flow rate and temperature at feed 1,3-PD concentration of 10g/l (b) Schematic of composite membrane structure showing the three layers. Permeation pathway is shown with red arrows and red dotted line (c) TEAS graph of the percentage contribution by the partial solubility parameters for each component.

Table 4.1: 1,3 propanediol Mass Transfer Coefficient and Permeability at various temperatures for SBA_90ACA membrane

Cross Flow, L/h	10		16.3		31.9		54.5	
Reynolds number	72		121		273		460	
Temperature (C)	K_{ov} $X10^{-7}$, m/s	P_{ov} $X10^{-14}$, kmol/m/Pa/s	K_{ov} $X10^{-7}$, m/s	P_{ov} $X10^{-14}$, kmol/m/Pa/s	K_{ov} $X10^{-7}$, m/s	P_{ov} $X10^{-14}$, kmol/m/Pa/s	K_{ov} $X10^{-7}$, m/s	P_{ov} $X10^{-14}$, kmol/m/Pa/s
30	1.01	2.19	1.1	2.38	1.29	2.82	1.32	2.87
40	1.18	2.55	1.25	2.72	1.31	2.9	1.4	3.03
50	1.16	2.53	1.26	2.74	1.34	2.91	1.37	2.97

Table 4.2: Boundary layer Mass Transfer Coefficient, $K_{bl,\ 1,3PD}$ (m/s)

Cross Flow, L/h	10	16.3	31.9	54.5
Reynolds Number	72	121	273	460
Temperature (C)	$K_{bl,\ 1,3PD}$ (m/s)			
30	$15.9X10^{-7}$	$20.7X10^{-7}$	$31.1X10^{-7}$	$40.4X10^{-7}$
40	$14.3X10^{-7}$	$18.0X10^{-7}$	$27.9X10^{-7}$	$36.2X10^{-7}$
50	$12.9X10^{-7}$	$16.7X10^{-7}$	$25.1X10^{-7}$	$32.7X10^{-7}$

Table 4.3: Comparison of works on 1,3 propanediol separation and enrichment from dilute aqueous mixtures

Process	Remarks	References
Distillation, Electrodialysis	High Energy Consumption Low Yield	6 - 8
Chromatography	High Purity final product free from other fermentation products and broth components except water Very dilute 1,3-PD concentration in final product	11 – 13
Solvent Extraction	Limited partitioning due to highly hydrophilic character of 1,3-PD	5, 9, 10
Reactive Extraction	Complicated process, multiple unit operations required Possible side reactions Low Yield	14, 15
Pervaporation-Zeolite membranes	Membrane non selective towards 1,3-PD w.r.t water	16, 17
Pervaporation – Supported ionic liquid membrane	High separation factor in batch pervaporation Limitation of scale up and continuous operation Ionic liquid is expensive Possible membrane instability over long term	18
Pervaporation – ACA Functionalized Polysiloxane	Fair separation factors and flux with Continuous pervaporation Scale up possible Membrane offers flexibility for tailoring intrinsic membrane properties and membrane module design Mechanical Integrity Superior cost – performance trade off	This work

Chapter 5. Poly(3-((3-(cyclohexylamino)propyl)thio)propyl methacrylate Based Membranes for Improved Pervaporative 1,3-Propanediol Enrichment From Aqueous Mixtures*

Abstract

Towards improving the pervaporation performance of 1,3-propanediol-water mixtures and providing inexpensive polymeric membrane materials, and taking advantage of the affinity of cyclohexyl amine towards 1,3-PD, a novel methacrylate monomer was synthesized by the thiol-ene coupling of allylcyclohexyl amine with mercaptoethanol followed by the esterification with methacryloyl chloride. Plug membranes based on such homo and random copolymers with butyl acrylate and divinyl benzene exhibited high separation factors (65 - 80) and fair (2.3 and 3.4 g/m^2h) 1,3-PD fluxes. The butyl acrylate copolymers gave the highest separation factors with a slight reduction in component fluxes. Increase in temperature and 1,3-propanediol feed concentrations caused a reduction in separation factors. Hansens solubility parameters were computed based on group contribution method to underscore the balance between water and 1,3-propanediol affinity. The integration of a hydrophobic solvent into a polymeric structure with good cost – performance trade off makes this an attractive candidate for possible industrial applications in multilayer modules.

Keywords: Allylcyclohexylamine, thiol-ene click, pervaporation, 1,3-propanediol

* Poly(3-((3-(cyclohexylamino)propyl)thio)propyl methacrylate Based Membranes for Improved Pervaporative 1,3-Propanediol Enrichment From Aqueous Mixtures, B. Kanjilal, I.Noshadi, J. R. McCutcheon, A.D. Asandei, R. S. Parnas, Polymer (Submitted)

1. Introduction

The primary process bottleneck for the production of hydrophilic organic molecules by fermentation is the downstream concentration enrichment of the product [1]. For highly hydrophilic molecules such as 1,3-propanediol (1,3-PD), the difficulty lies not so much in its separation from other fermentation products as it does in separating it from water [2]. The main factors are thermodynamic, and lie in the proximity of the 1,3-PD solubility parameter with that of water [3]. Additionally, given the smaller molar volume and kinetic diameter of water, the diffusivity of 1,3-PD is sluggish under comparable conditions [3,4]. The highly hydrophilic character of 1,3-PD also limits the applicability and efficacy of solvent extraction [2]. Other processes employed for separation include evaporation, chromatography and reactive extraction with concomitant high-energy usage and process complications [5-17]. Pervaporation is an energetically advantageous process [3]. However, 1,3-PD cannot be enriched by materials conventionally used for pervaporation, such as siloxane polymers. Thus, the development of novel materials with a good cost/performance balance is central to the establishment of industrial separation procedures for 1,3-PD enrichment from fermentation broths. The removal of this process bottleneck may increase the feasibility of using waste industrial glycerol as a sustainable resource for producing 1,3-PD as a biorenewable alternative to a petroleum platform.

Although separation processes that include phase changes are typically energy intensive, pervaporation can be energy efficient as it removes only the minor components [3]. Additionally, the membrane chemistry and structure may be tailored for affinity towards and selective enrichment of the minor components [3]. Zeolite membranes have

been used for pervaporative separation of 1,3-PD from other minor fermentation products, but the membranes were also selective towards water [15, 16]. A supported liquid membrane based on cyanoborate ionic liquid has been reported with high separation factors and moderate 1,3-PD flux [17]. However, supported liquid membranes suffer from stability issues and difficulty in scale-up, in addition to high cost associated with hydrolytically stable ionic liquids [18]. For membrane processes, the development of new polymers is constrained by the necessity of using them in an engineered module suitable for sustainable industrial application with adequate cost/ performance balance.

This paper presents the synthesis of a novel acrylate monomer (3-((3-(cyclohexylamine)propyl)thio)propyl methacrylate) containing a cyclohexylamine fragment, derived from allylcyclohexylamine (ACA), The membrane prepared from the resulting polymer is used in the pervaporative separation of 1,3-PD from water. The choice of ACA was prompted by its balance of hydrophobic character and its high affinity for 1,3-PD. While the partitioning of 1,3-PD into ACA is not high enough for solvent extraction [2], its incorporation into a polymerized structure was shown to successfully separate 1,3-PD from water with high selectivity. Conversely, while the allyl functionality allows for a wide variety of reactions, radical homopolymerization of the allyl group does not occur [19].

The conversion of ACA into an acrylate monomer *via* a thiol-ene click chemistry route was explored to enable simple radical chemistry and copolymerization with conventional vinyl and acrylate monomers. A straightforward and economical route to a polymer with high separation factor for 1,3-PD enrichment from dilute aqueous solutions was developed. The ACA-based acrylate monomer was homopolymerized and

copolymerized with butyl acrylate and divinyl benzene. The monomer and polymers were synthesized and characterized. The polymers were fabricated into supported plug membranes and used for batch pervaporation and enrichment of 1,3-propanediol from binary aqueous mixtures at various temperatures and feed 1,3-PD concentrations. The polymers demonstrate separation factors in the range 65 to 80. The 1,3-PD fluxes vary between 1.9 g/m^{2}h to 3.4 g/m^{2}h, while the water fluxes range between 3.5 g/m^{2}h to 5g/m^{2}h. While cyanoborate based ionic liquid membranes in a TiO_2 ceramic nanofiltration module reported high separation factors [17], ionic liquids are quite expensive. The polymers developed in this work achieved good cost/performance trade-off, in addition to the ability to be fabricated into modules for commercial scale-up. As a comparison, tetrapropyl ammonium cyanoborate ionic liquid [17] costs $36,004/mole, while the methacrylate monomer developed in this work costs $1,326/mol. Additional details about cost comparison for 1,3-PD separation are provided in the discussion.

2. Experimental

2.1 Materials

For the synthetic scheme involving monomer preparation and polymerization, all chemicals were purchased from Sigma Aldrich. Allylcyclohexyl amine (ACA) was dried prior to use. Mercaptoethanol and Triethyl amine were used without modification. The solvents Toluene, Chloroform, Dioxane and Hexane were dried prior to use. Methacryloyl chloride, Divinyl benzene (DVB) and Butyl acrylate monomer (BuA) were dried prior to use. Azobisisobutyronitrile (AIBN) radical initiator was used without modification.

For the fabrication of the plug membranes, 0.65 cm inner diameter glass pipettes from Fischer were used. Cotton wool was used to act as the porous support base and was purchased from the local market.

1,3 propanediol (1,3-PD), 98% purity was purchased from Sigma Aldrich and used for the partition coefficient and preparation of binary mixtures with distilled water as feed solutions for pervaporation experiments.

2.2 Analytical Methods

NMR spectroscopy was carried out on a Brucker DMX-500 MHz and Brucker Ascend 400 WB spectrometers. IR spectra were taken on samples with a Nicolet Magna-IR 560 spectrometer, with KBr powder being used as background. The molecular weight of the polymer samples were determined by GPC in an Agilent 1260 Infinity system using N,N-Dimethylacetamide as eluent and narrow molecular weight PMMA from Sigma Aldrich as calibration standard. For Thermo-gravimetric analysis (TGA), a TA Instruments Hi-Res 2950 TGA instrument was used. A temperature ramp of 20C/min in nitrogen up to a temperature of 800C was employed. Differential Scanning Calorimetry was carried out in TA Instruments Q100. Contact angle was measured on an Olympus TGHM goniometer. Field Emission scanning electron microscopy (FESEM) images of the membrane structure were obtained with a JEOL 6335F field emission scanning electron microscope. The feed and permeate compositions from the pervaporation experiments were analyzed using 0.22μm syringe filtered samples by gas chromatography (GC) using a DB-FFAP capillary

column and an MS detector and a 1μL injection volume. GC injector, detector and initial oven temperatures were 240C, 270C, and 40C, respectively.

2.3 Partition Coefficient Measurement

The partition coefficient of 1,3-PD between water and ACA was determined at 30°C. 1 ml of a 10 g/l 1,3-PD solution was mixed in a vortex mixer with 1ml of ACA for 15 minutes and the layers allowed to separate. The concentration of 1,3-PD, in the aqueous phase, determined by GC, before and after partition, was used to compute the partition coefficient based on equation 1:

$$K_p = \frac{C_{ACA}}{Cwater} \qquad (1)$$

2.4 Synthesis, purification and characterization of 3-((3-(cyclohexylamino)propyl)thio)propyl methacrylate (CHAPTPMA) monomer

The monomer synthesis scheme is depicted in Figure 5.1. The thiol-ene click chemistry adduct was synthesized by AIBN mediated addition of mercaptoethanol to the allyl double bond of the ACA [20]. The reaction was carried out in a pressure tube, in bulk, and in the presence of UV light at 60°C. The pressure tube was degassed with dry Ar in a Schlenk line and the reactants were kept under argon [20]. The reactants were weighed out in nearly stoichiometric amount, with the ACA being in slight excess. The progress of the reaction was checked after 24 hours by ^{1}H NMR. The product was purified by vacuum removal of the excess ACA, which is the lower boiling component. The purified click

adduct was characterized by FTIR and NMR, and its vaporization temperature was estimated by TGA.

The click adduct was esterified using methacryloyl chloride and triethyl amine as the catalyst to form the methacrylate monomer [21]. The click adduct was dissolved in dry toluene and a stoichiometric amount of methacryloyl chloride and triethylamine were added, and the mixture was refluxed at 70°C for 12 hours [21]. The toluene was evaporated off from the system at 40°C overnight. The resultant mixture of the methacrylate monomer and triethyamine hydrochloride was added to hexane. The triethyamine hydrochloride being hexane insoluble separated, and the supernatant fluid containing the methacrylate monomer was filtered and the hexane evaporated overnight in a vacuum oven at 40 °C. The final purified methacrylate monomer product was characterized by ^{1}H NMR and FTIR and TGA. The NMR spectra for the monomer synthesis are shown in Figure 5.2(a) – (c) . The FTIR and TGA results are shown in Figure 5.3 (a) and 3 (b).

2.5 Synthesis and characterization of polymers

The homopolymerization of CHAPTPMA and its copolymerizations with 5 mol% BuA or 5mol% DVB were initiated by AIBN in dioxane at 70 °C in a 250 ml two necked round bottom flask fitted with a reflux condenser with the system being constantly purged with nitrogen. The resultant polymers are referred to below as P(Acryl), P(Acryl)_BuA and P(Acryl)_DVB, respectively. Prior to polymerization, the dioxane solutions of the monomer(s) were passed through an inhibitor removal column For a typical run, a 25 mL dioxane batch contained ~5 g of the methacrylate monomer. The stoichiometric molar ratio

of the methacrylate monomer to AIBN was kept at 100:1 in all batches. A silicone rubber tube fitted with a needle was used to blanket the surface of the reaction mixture with nitrogen throughout the 4-hour course of each polymerization. At the end of each polymerization, a portion of the batch was dried by evaporation at 100 °C and then further dried to constant weight at 80 °C under vacuum. The thermal transitions of the solid polymers were estimated by DSC. The reaction mixtures were used to cast films of the polymers and copolymers on clean glass substrates for evaluation of the contact angle [22,23]. Films were similarly cast on a Kapton surface and peeled off for evaluation of solvent uptake [22, 23]. The NMR spectra of the polymers are shown in Figure 5.4(a)-(c). The results for water and 1,3-PD contact angles, mass uptake and DSC thermal transitions are shown in Figure 5.5 (a), (b) and (c). The non-crosslinked polymers (i.e. those not employing DVB in their composition) were evaluated by GPC.

2.6 Membrane fabrication

Plug membranes were fabricated inside 0.6 cm inner diameter glass pipettes. The glass pipettes were weighed and stuffed with a known weight of dry cotton wool. A small, but known weight of dry cotton wool was soaked with the polymer solution and the solvent allowed to evaporate slowly at 40 °C over a period of 3-4 days. When the solvent had nearly all evaporated, the polymer solution soaked cotton wool was lightly pressed with a flat surface to set the membrane on top of the cotton wool base inside the glass pipettes, and the weight of the plug noted. The solvent was allowed to further evaporate over a period of 1 week at room temperature till the plug attained a constant weight. The slow solvent evaporation was carried out to prevent the formation of pinholes and to allow the plug membrane to adhere to the inner wall of the glass pipettes. This process gave rise to a

fiber supported membrane structure. The volume inside the glass pipette above the membrane was used to hold ~1.5-1.7 ml of pervaporation feed solution. Plug membrane structures are schematically depicted in Figure 5.6(a) along with a picture of the actual membrane plug in Figure 5.6(b). Figure 5.6(c) is an FESEM image of the membrane.

2.7 Pervaporation experiments

Batch Pervaporation experiments were carried out on the fabricated plug membranes. The plug membrane structures were affixed in an upright position in a water bath maintained at 30 °C, 40 °C or 50 °C. The membranes were monitored for leakage by checking for abnormally high flux. The plug membranes had a pervaporation area of 4.91 mm^2. Each batch pervaporation experiment was allowed to run for a period of 20 hours. The permeate was collected in a cold trap, cooled in a dry ice – acetone bath. A vacuum pump was employed to maintain the permeate side pressure at less than 1 mm Hg. The permeate collected was weighed and analyzed for 1,3-PD concentration by GC [24]. The key performance indicators of the pervaporation experiment were defined by the component fluxes and the separation factor defined as:

$$\alpha = \frac{Jp}{Jw} . \frac{xw}{xp} \qquad (2)$$

Where J_p and J_w represent the 1,3-PD and water fluxes and x_p an x_w represent the initial feed mass fractions of 1,3-PD and water, respectively [24]. The respective fluxes of water and 1,3-PD and the separation factor of 1,3-PD over water were computed. Batch pervaporation experiments do not achieve a true steady state. In these experiments the total

permeation of water and 1,3-PD changed the feed composition by less than 5% over the course of the entire pervaporation experiment.

3. Results and discussion

3.1 Partition Coefficient in Amine

The partition coefficient of 1,3-PD between ACA and water was estimated at 0.5±0.03 from 3 independent experiments. Allylcyclohexylamine is a hydrophobic solvent, with a Log P_{ow} (Octanol – water redistribution coefficient) ~ 2.2 – 2.4, in which 1,3-PD is miscible in all proportions.

3.2 Synthesis, purification and characterization of monomer

The scheme for methacrylate monomer synthesis is shown in Figure 5.1. Thiol-ene click chemistry was employed to react ACA with mercaptoethanol [20]. Figure 5.2(a)-(c) shows NMR spectra to illustrate the monomer synthesis. The allyl protons labeled 1, 1' and 2 in the ACA NMR appear at roughly δ of 5 and 6 ppm as seen in Fig 5.2(a).

In the NMR of the thiol-ene click adduct there is a significant reduction of the allyl proton signal due to the reaction between ACA and mercaptoethanol (Fig 5.2(b)). In these experiments, a slight excess of ACA was used, which is the reason residual allyl proton signal is still seen in the thiol-ene click adduct NMR. The hydroxyl proton is labeled 'a' in the thio-ene click adduct NMR and appears at δ ~ 3.7 ppm.

A subsequent conversion of the thiol-ene click adduct to the methacrylate monomer was carried out [21]. The ^{1}H NMR of the methacrylate monomer is shown in Figure 5.2 (c). The reduction of the hydroxyl proton signal at δ ~ 3.7ppm is evident. The NMR of the

methacrylate monomer also shows the appearance of the protons of the double bond, labeled α, α', with signals at δ ~ 5.5 to 6.5 ppm. In the methacrylate monomer NMR, the O=C–O–CH_2– protons are labeled as β and they appear at δ~4.2 ppm.

Figure 5.3(a) shows the FTIR of the purified click adduct and the methacrylate monomer. The disappearance of the C-O stretch in primary alcohol and the appearance of the C–O and C=O stretch in the methacrylate ester monomer are delineated.

The vaporization temperatures of the thiol-ene click adduct and the subsequent methacrylate monomer were also estimated using TGA shown in Figure 5.3(b). Both the thiol-ene click adduct and the methacrylate monomer were viscous amber colored fluids with high boiling points. In an alcohol (thiol-ene adduct) some molecular association can be attributed to the presence of hydrogen bonding. Corresponding esters are usually lower boiling compared to alcohols. In this case, the loss of the hydrogen bonding due to conversion of the primary hydroxyl in the click adduct was offset by an increase of the molecular weight of the moiety leading to a modest increase in the boiling point by nearly 35^0C.

3.3 Characterization of polymers

The NMR traces of the final polymer solutions are shown in Fig 5.4 (a) – (c). The NMR traces were utilized to estimate copolymer composition by comparing the integrated peak areas of the N – H proton from the methacrylate monomer at δ ~ 2.4ppm, with those at δ= 7.8ppm (aromatic proton from DVB) or δ = 3.8 ppm (–O–CH_2– from BuA). Figure 5.4 (a) is the NMR of the homopolymer. Polymerization occurs with a reduction in the relative

abundance of acrylate double bonds. Figure 5.4(b) is the NMR of the copolymer with Butyl acrylate. An expanded view of the position of the –O–CH_2– protons is shown as an inset. Both the methacrylate monomer and the BuA co-monomer exhibit chemical shifts at δ ~ 3.8 ppm due to –O–CH_2– protons. The difference between the –O–CH_2– signals in the copolymer and the homopolymer, divided by the N-H signal at δ ~2.4 ppm, was used to estimate the BuA composition in the copolymer. Figure 5.4(c) is the NMR of the copolymer with DVB. The position of the aromatic protons is shown in an expanded view as an inset. The average molar copolymer composition was seen to nearly replicate the feed composition for the copolymerization batches.

It is worthwhile to note that the rather small presence of DVB (5 mol%) results in limited degree of crosslinking. Since the DVB copolymer is very lightly crosslinked it does not spontaneously separate out of the reaction mixture [22, 23]. However, unlike the two uncrosslinked polymer compositions, once dried it cannot be redissolved into any solvent. GPC molecular weight measurements were made for the homopolymer and the copolymer with butyl acrylate. The weight average molecular weight of the homopolymer and butyl acrylate copolymer were 74,320 and 61,262 with a PDI of 4.1 and 4.3, respectively.

All polymers were evaluated for thermal transition by DSC. The results are presented in Fig 5.5(a), where the homopolymer T_g is approximately 105 °C, the BuA copolymer T_g is approximately 98 °C, and the lightly crosslinked DVB copolymer T_g is approximately 107 °C. While the thermal transitions of acrylate polymers are also dependent on the molecular weight, they are known to follow a pattern of decreasing glass transition temperature with increasing length of the alkyl side chain [25]. This is particularly true for linear alkyl side

chains in acrylate polymers. Thus while poly(methyl methacrylate) has a Tg of 110 °C, poly(n-octyl methacrylate) exhibits a Tg of 10 °C. This is attributed to an internal plasticization effect by the increasing length of the side chain [25]. However, the large side chain of the methacrylate polymers reported here is more complicated, with a secondary amine and a bulky, stiff cyclohexyl ring. Additionally, a carbon-sulfur bond also exists, which along with the amine, may play a part in enhancing polar interactions, explaining the high glass transitions obtained with the polymers. The effect of cross linking with DVB is minimal. The effect of incorporation of ~ 5% BuA is as expected with a ~7C reduction in the glass transition temperature.

Thin films of the polymers cast on glass substrates were evaluated for water and 1,3-PD contact angle. The water contact angle is shown in Figure 5.5(b). The high water contact angles confirm polymer hydrophobicity. The acute 1,3-PD contact angles, on the other hand, indicate the wettability of the surfaces of all three polymers by 1,3-PD [26]. No significant differences between the contact angles were noted for the three polymers. Polymer films cast on Kapton, and then peeled off from the kapton surface, were used for estimating the water and 1,3-PD mass uptake, and the results are shown in Figure 5.5(c). The water mass uptake is lower than 1% for all the polymers, while that of 1,3-PD is between 15 – 18%. As with the contact angles, no significant differences between the mass uptakes were noted for the three polymers. The much larger mass uptake of 1,3-PD compared to water, combined with the differences in wettability, are evidence that these three polymers have much greater affinity for 1,3-PD compared to water [24].

3.4 Pervaporation results on 1,3-propanediol – water binary feed mixtures

The pervaporation set up and membrane fabrication have been described in earlier sections and depicted in Figures 5.6(a) to (c). Figure 5.7(a), 5.7(b), 5.8(a) and 5.8(b) illustrate the component flux and separation factors for the three polymers with varying membrane composition, feed temperature and 1,3-PD feed concentration. The polymers demonstrate separation factors in the range 65 to 80. The 1,3-PD fluxes vary between 1.9 g/m^2h and 3.4 g/m^2h, while the water fluxes range between 3.5 g/m^2h to 5g/m^2h.

3.4.1 Effect of Copolymer Composition

A comparison of the separation performance at 30 °C shows that the butyl acrylate copolymer exhibited the highest separation factor compared to the other two membranes. The findings are replicated at 40 °C and with varying 1,3-PD feed concentrations. At higher temperature or feed 1,3-PD concentrations, the disparity between the separation factors of the three membranes reduces. The incorporation of a small percentage of butyl acrylate into the polymer composition may have enhanced its hydrophobic character while making little difference to the 1,3-PD affinity. A comparable phenomenon is seen in the mass uptake, where the incorporation of butyl acrylate reduced the water uptake while keeping the 1,3-PD uptake at the same level (Fig 5.5c). While the incorporation of butyl acrylate depressed the glass transition temperature, the effect of an increase in free volume was negligible as the fluxes of both components decreased to some extent despite the apparent plasticization by the butyl acrylate fraction.

3.4.2 Effect of Temperature

The polymers were evaluated for pervaporative performance with binary 1,3-PD – water mixtures at three different temperatures and the results are shown in Figure 5.7(a) and 5.7(b). An increase in temperature, predictably reduced the separation efficacy by enhancing the flux of both permeating components. For the homopolymer, P(Acryl) and the lightly crosslinked DVBcopolymer, P(Acryl)_DVB, the effect of temperature on separation factor was less pronounced than it was on P(Acryl)_BuA. The BuA fraction causes some plasticization as evident in the reduction in glass transition. With increase in temperature, the chain mobility increases more in the BuA copolymer allowing a higher flux of both components causing a reduction in selectivity. The sensitivity of the P(Acryl)_BuA to increased temperature reduced the separation factor so that at 50 °C all three polymers had nearly identical separation factors.

3.4.3 Effect of Feed 1,3-propanediol concentration

The polymers were evaluated for pervaporative performance with varying 1,3-PD feed concentrations. The results are shown in Figure 5.8(a) and 5.8(b). With an increase in the feed 1,3-PD concentration, the separation factor reduces for all three polymers. The reduction in separation factor with increasing 1,3-PD feed concentration is the steepest for the BuA copolymer. The high affinity of the polymers towards 1,3-PD causes swelling and subsequently higher flux of both water and 1,3-PD, which may contribute to the observed reduction in the separation factor. In the lightly crosslinked DVB copolymer, these changes in flux and separation factor were less significant than in the homopolymer or the BuA

copolymer, perhaps due to the crosslinking. A contributing factor to the reduction in separation factor may be coupling between the transport of 1,3-PD and water. Higher concentrations of 1,3-PD in the membrane, at higher 1,3-PD feed concentrations, are expected to increase the concentration of water in the membrane as well due to swelling and the high miscibility of water in 1,3-PD.

3.5 Analysis of Hansen Solubility Parameters

Permeation may be defined as $P = D\ x\ S$, where D is the diffusion coefficient and S is the solubility of components of the feed in the membrane [3]. Thus, the components of the feed must dissolve into the membrane polymer and then diffuse downstream through the membrane. The membrane polymer can therefore be considered a solvent phase for the feed components.

The relative enrichment during pervaporation occurs by virtue of the higher solubility or greater diffusivity in the membrane material of one component compared to the other [3,4, 27]. The membrane-component affinity may be described by the Hansen solubility parameters, comprising hydrogen bonding interactions (δ_H), polar interactions (δ_P) and dispersion interactions (δ_D) [3]. The interactions of the membrane material with each permeating component can be expressed by a single number, R_a, which combines the Hansen solubility parameters and indicates the distance between the membrane and each component in Hansen space [3].

$$R_a = \sqrt{4(\delta_{d1} - \delta_{d2})^2 + (\delta_{p1} - \delta_{p2})^2 + (\delta_{H1} - \delta_{H2})^2} \qquad (3)$$

The Hansen parameters were computed for water, 1,3-PD and the methacrylate monomeric unit using a group contribution method [28] employing two kinds of characteristic groups: first-order groups that describe the basic molecular structure of compounds and second-order groups based on the conjugation theory to improve the accuracy of predictions. The contribution towards δ_H, δ_P and δ_D were computed from values provided for the participating groups and identifiable conjugates in the monomeric structure [29]. The free volume of the polymer was not accounted for in these calculations, and the contributions of the BuA and DVB co-monomers were also ignored. The Hansen parameters for water, 1,3-PD and the methacrylate monomer synthesized in this work are shown in Table 5.1, along with the computed R_a between all components. The computed values of Hansen parameters for water and 1,3-PD closely match literature values [29, 30], but there are no literature values for the polymeric membrane material for comparison purposes.

Table 5.1 indicates that the methacrylate monomeric unit has a much higher affinity for 1,3-PD than for water as R_a for the interaction of 1,3-PD and the monomeric unit is much smaller than R_a for the interaction of water and the monomeric unit. This difference is largely due to the differences in polar interactions. The higher affinity of the monomeric unit for 1,3-PD over water is consistent with the results for contact angle and mass uptake from Figures 5.4b and 5.4c. Thus, the affinity calculations with the monomeric unit provide some guidance for the affinity of the membrane polymer towards the permeating components.

The diffusion rate of the feed components through the membrane depends upon their kinetic diameter (d_k), which considers the molecular size and shape [27]. Given that

the d_k of water is significantly lower than that of 1,3-PD, water diffuses faster. Hence the onus of pervaporative enrichment in favor of 1,3-PD lies on preferential sorption of 1,3-PD into the membrane and the concomitant rejection of water [3,27]. The proximity of the solubility parameters of water and 1,3-PD compounds the difficulty of separation using conventional membrane materials. If 1,3-PD and water were equally soluble in the membrane, the preferentially permeating component would be water since water diffuses faster. However, given the hydrophobic character of the membrane material and its affinity for 1,3-PD, the preferentially permeating component is 1,3-PD, as shown in Figure 5.6.

3.6 Comparative Analysis of Performance

This work can be directly compared to one investigation on pervaporative separation of 1,3-PD from water. Thus, Izak *et al* (2007) achieved a separation factor of 177 and flux of 3.86 g/m^{2}h at 22 °C for 1,3-PD in a binary mixture with water [17] and using a supported liquid membrane (SLM) based on cyanoborate ionic liquid, while claiming 9 month membrane stability. The work reported herein achieved separation factors of 60 - 80 with 1,3-PD fluxes between 2.3 and 3.4 g/m^{2}h. However, the polymers developed in this work can be produced as flat sheets that can be fabricated into modules and scaled-up for commercial separations.

Pervaporation of aqueous broths require that the membrane materials be hydrolytically stable. Ionic liquids have shown great promise in various applications but their technical applications are limited by either hydrolytic instability or high price of the anions for hydrolytically stable ionic liquids [18, 31]. A brief comparison of the material

price developed in this work versus that used for the cyanoborate SLM [17, 32] was carried out with retail price data from Sigma Alridch (http://www.sigmaaldrich.com), Oakwood Chemicals Inc (http://www.oakwoodchemical.com/) and Fluorochem Ltd. (http://www.fluorochem.co.uk). The computation was based on molecular structures and prices of the individual chemicals making up the compound. The tetrapropyl ammonium cyanoborate ionic liquid costs $36,004/mole, while the methacrylate monomer developed in this work costs $1326/mol. The cost per unit weight of the ionic liquid is $120/g, while that of the methacrylate monomer is $ 4.65/g.

A price/performance trade off estimate was generated using the experimental results detailed here and reported in the work on the cyanoborate SLM. A rough estimation was made of the total volume of membrane material required to reach a final 1,3-PD concentration of >90%, from a starting composition of 1% 1,3-PD for a feed flow of 100 g/h. The computation assumes that separation factor and flux of 1,3-PD remained constant after each enrichment stage. This assumption was made because separation factor and flux data for high 1,3-PD feed concentrations were not available. The average separation factor for the homopolymer, P(Acryl), membrane was taken as 72 with an average 1,3-PD flux of 3.1g/m^2h. The computation yielded a requirement of 3 enrichment steps requiring a total pervaporation area of 6000 cm^2. The volume required using a 400 micron thick membrane was computed as 240 cm^3. Assuming an approximate density of 1g/cm^3, the cost of the material required to achieve the aforementioned enrichment level is ~$1116.

The same computation was carried out for the cyanoborate ionic liquid membrane stabilized in a nanoporous ceramic module. The flux of 1,3-PD (3.86 g/m^2h) and the

separation factor (177) reported in their work [17, 32] were used as constants for the computation. The same enrichment level from a starting composition of 1% 1,3-PD was calculated to require 2 enrichment steps with a total area of 4660m^2. The thickness of the module reported [32] is 3 mm (with a 7mm inner diameter and 10 mm outer diameter). The nano porous module reported in their work has a porosity of 30% [17, 32]. Thus the total cyanoborate ionic liquid requirement is 419 cm^3. Assuming a rough density of 1g/cm^3, the cost of material required to achieve the same enrichment level is ~$50,328.

The high intrinsic enrichment factors may lead to concentration polarization with a concomitant reduction in separation efficacy. Membrane module designs and multilayer membrane structures may be used in the case of a polymer membrane to optimize separation performance and impart mechanical robustness to membrane structures.

This work used established routes of chemistry to covalently bond a 1,3-PD solvent functionality into a polymeric structure, which mitigates the stability issues faced by SLM, while enhancing affinity in favor of 1,3-PD. At the same time, the hydrophobic character of the membrane is significantly enhanced to achieve a large difference in preferential sorption, which is critical for separating 1,3-PD from water.

4. Conclusion

Towards improving the pervaporation performance of 1,3-propanediol-water mixtures and providing inexpensive polymeric membrane materials, and taking advantage of the affinity of cyclohexyl amine towards 1,3-PD, a novel methacrylate monomer was synthesized by the thiol-ene coupling of allylcyclohexyl amine with mercaptoethanol

followed by the esterification with methacryloyl chloride. Plug membranes based on such homo and random copolymers with butyl acrylate and divinyl benzene exhibited high separation factors (65 - 80) and fair (2.3 and 3.4 g/m^2h) 1,3-PD fluxes. A superior cost-performance balance was achieved with these membranes by comparison with other systems while providing a possible route to fabrication of membrane modules with multilayer compositions.

5. Acknowledgements

The authors acknowledge the advice of Prof. M.T. Shaw, (Professor Emeritus, University of Connecticut) in thermodynamic computations.

6. References

1. Z.L. Xiu, A.P.Zeng, Present state and perspective of downstream processing of biologically produced 1,3-propanediol and 2,3-butanediol, Appl Microbiol Biotechnol. 78 (2008) 917–926.
2. A. Triguero, R. Blanco, H. Machado, M. Rodríguez, Evaluation of liquid extraction potentials for downstream separation of 1,3-propanediol, Biotechnology Techniques. 13 (1999) 127–130.
3. P. Shao, R.Y.M. Huang, Polymeric membrane pervaporation, Journal of Membrane Science. 287 (2007) 162-179.
4. M. Mulder, T. Franken, C.A. Smolders, Preferential sorption versus preferential permeability in pervaporation, J. Membr. Sci. 22 (1985) 155–173.

5. T.T. Ames, Process for the isolation of 1,3-propanediol from fermentation broth. US Patent 6361983 B1 (2002).
6. Y. Gong, Y. Tong, X.L. Wang, D.H. Liu, The possibility of the desalination of actual 1,3-propanediol fermentation broth by electrodialysis, Desalination. 161 (2004) 169–178.
7. J. Hao, D.H. Liu, Desalination of fermented broth containing 1,3-propanediol by electrodialysis, Chinese J Proc Eng. 5 (2005) 36–39.
8. Z. Li, B. Jiang, D. Zhang, Z. Xiu, Aqueous two-phase extraction of 1,3-propanediol from glycerol-based fermentation broths, Separation and Purification Technology. 66 (2009) 472–478.
9. A. Baiada, A. Vitner, R.P. Jansen, A.M. Baniel, Process for producing 1, 3-propanediol. US Patent 7056439 B2 (2006).
10. A.K. Hilaly, T.P. Binder, Method of recovering 1,3-propanediol from fermentation broth. US Patent 6479716 B2 (2002)
11. J. Hao, F. Xu, H. Liu, D. Liu, Downstream processing of 1,3-propanediol fermentation broth, Journal of Chemical Technology and Biotechnology.81(2006) 102–108.
12. J.J. Malinowski, Reactive Extraction for Downstream Separation of 1,3-Propanediol, Biotechnology Progress. 16 (2000) 76–79.
13. M.H. Cho, S.I. Joen, S.H. Pyo, S. Mun, J.H. Kim, A novel separation and purification process for 1,3-propanediol, Process Biochem. 41 (2006) 739–744.
14. P. Anand, R.K. Saxena, R.G. Marwah, A novel downstream process for 1,3-propanediol from glycerol-based fermentation, Appl. Microbiol. Biotechnol. 90 (2011) 1267–1276.

15. S. Li, V.A. Tuan, J.L. Falconer, R.D, Noble, Separation of 1,3- propanediol from glycerol and glucose using a ZSM-5 zeolite membrane, J. Membr Sci. 191 (2001a) 53–59.
16. S. Li, V.A. Tuan, J.L. Falconer, R.D. Noble, Separation of 1,3- propanediol from aqueous solutions using pervaporation through an X-type zeolite membrane, Ind Eng Chem Res 40 (2001b) 1952– 1959.
17. P.Izák, M. Köckerling, U. Kragl, Stability and selectivity of a multiphase membrane, consisting of dimethylpolysiloxane on an ionic liquid, used in the separation of solutes from aqueous mixtures by pervaporation, Green Chem. 8 (2006) 947–948.
18. N.M. Kocherginsky, Q. Yang, L. Seelam, Recent advances in supported liquid membrane technology. Separation and Purification Technology, Separation and Purification Technology 53 (2007) 171–177.
19. G. Odian in Principles of Polymerization, fourth ed., John Wiley & Sons Inc., Hoboken, NJ, 2004.
20. U. Mansfeld, C.Pietsch, R.Hoogenboom, C.Remzi Becer, U.S. Schubert, Clickable initiators, monomers and polymers in controlled radical polymerizations – a prospective combination in polymer science, Polym. Chem. 1 (2010) 1560–1598.
21. Y. Xia, R.C.Larock, Castor oil-based thermosets with varied crosslink densities prepared by ring-opening metathesis polymerization (ROMP), Polymer 51 (2010) 2508-2514.
22. T. Boyle, A. Szopinski, A. Verrall, Method and apparatus for continuously preparing crosslinked, solution–cast polymer film. US Patent 20070085235 A1 (2007)

23. Q. Guo, P.N. Pintauro, H. Tang, S.O'Connor, Sulfonated and cosslinked polyphosphazene – based proton – exchange membranes, J. Membr. Sci. 154 (1999) 175 – 181.
24. S. Li, R. Srivastava, R.S. Parnas, Separation of 1-butanol by pervaporation using a novel tri-layer PDMS composite membrane, J. Membr. Sci. 363 (2010) 287–294.
25. S. Rogers, L.Mandelkern, Glass Transitions of the Poly-(n-Alkyl Methacrylates), *J. Phys. Chem. 61 (*1957) 985–991.
26. D. K. Owens, R. C. Wendt, Estimation of the surface free energy of polymer, Journal of Applied Polymer Science 13 (1969) 1741 – 1747.
27. W.J.Koros, Membranes: Learning a lesson from nature, Chem Eng. Prog. 91 (1995) 68–81.
28. E. Stefanis. C. Panayiotou, Prediction of Hansen Solubility Parameters with a New Group-Contribution Method, Int J. Thermophys. 29 (2008) 568–585.
29. C.M. Hansen, Hansen solubility parameter: A users handbook, second ed., CRC press Taylor and Francis group, Boca Raton, London, New York, 2007.
30. M. Alizadeh, F. Abbassi, M. Farahi, K. Jalili, Silicone based hydrogels prepared by interpenetrating polymeric network synthesis: Swelling properties and confinements effects on the formation kinetics, J appl Poly Sci. 124 (2012) 985–992.
31. E. Kuhlman, S. Himmler, H. Giebelhaus, P. Wasserscheid, Imidazolium dialkylphosphates – a class of versatile, halogen-free and hydrolytically stable ionic liquids, Green Chem. 9 (2007) 233 – 242.
32. P. Izak, M. Köckerling, U. Kragl, Mehrphasen–Membran. German Patent DE102006024397 B3 (2007).

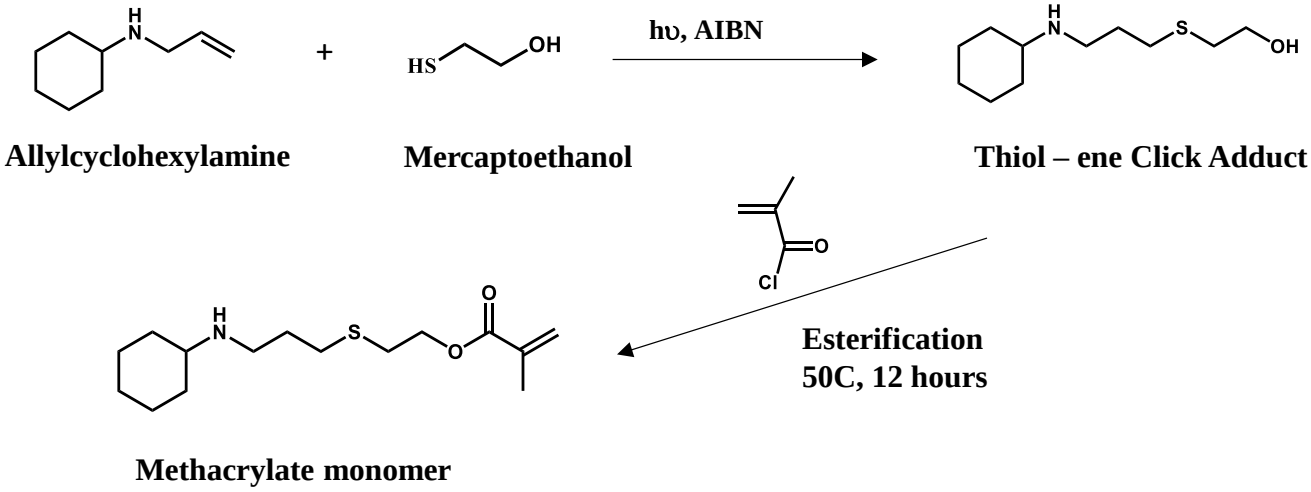

Figure 5.1: Monomer Synthesis Scheme

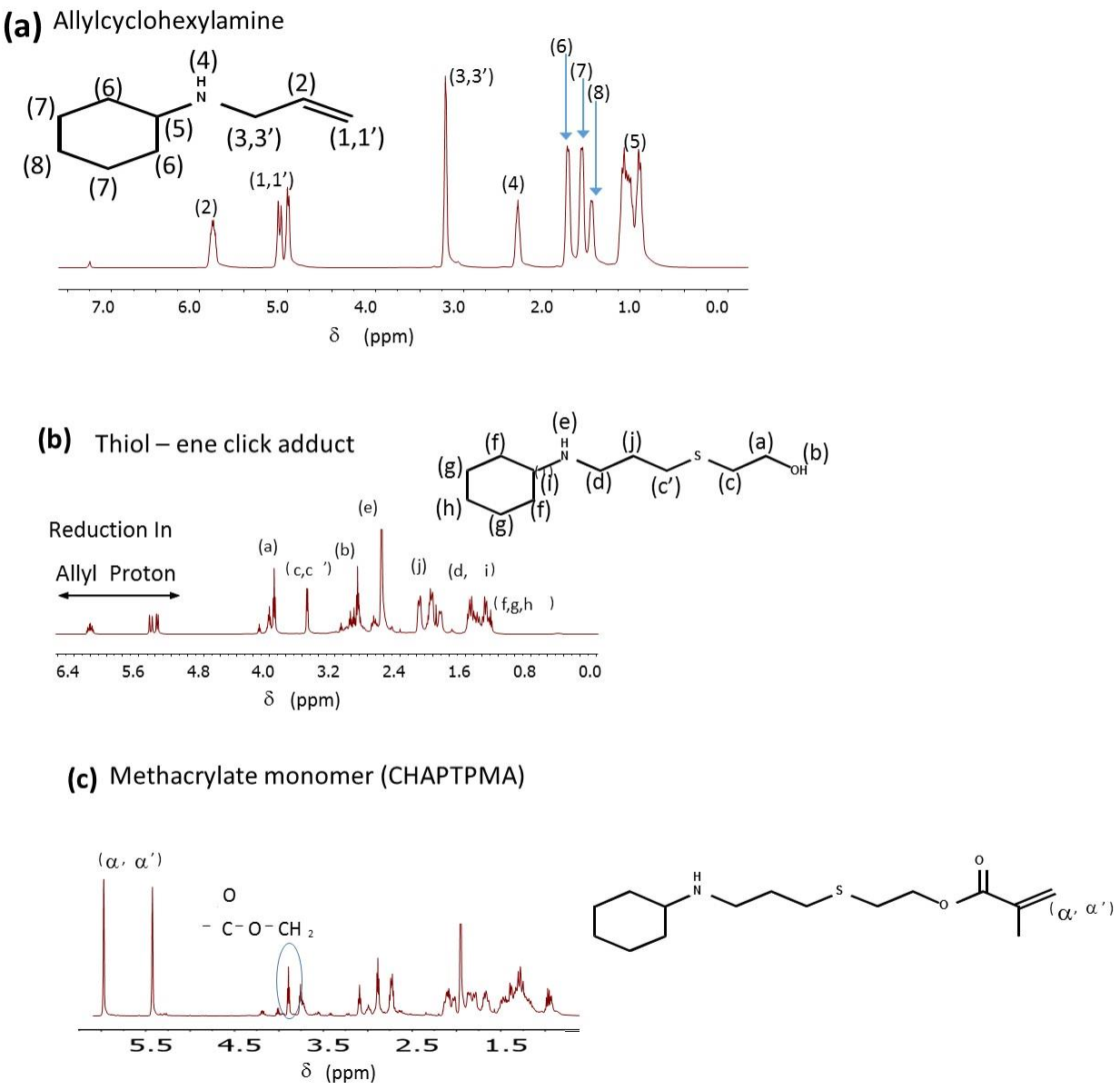

Figure 5.2: NMR (a) ACA (b) Click adduct (c) Methacrylate monomer CHAPTPMA

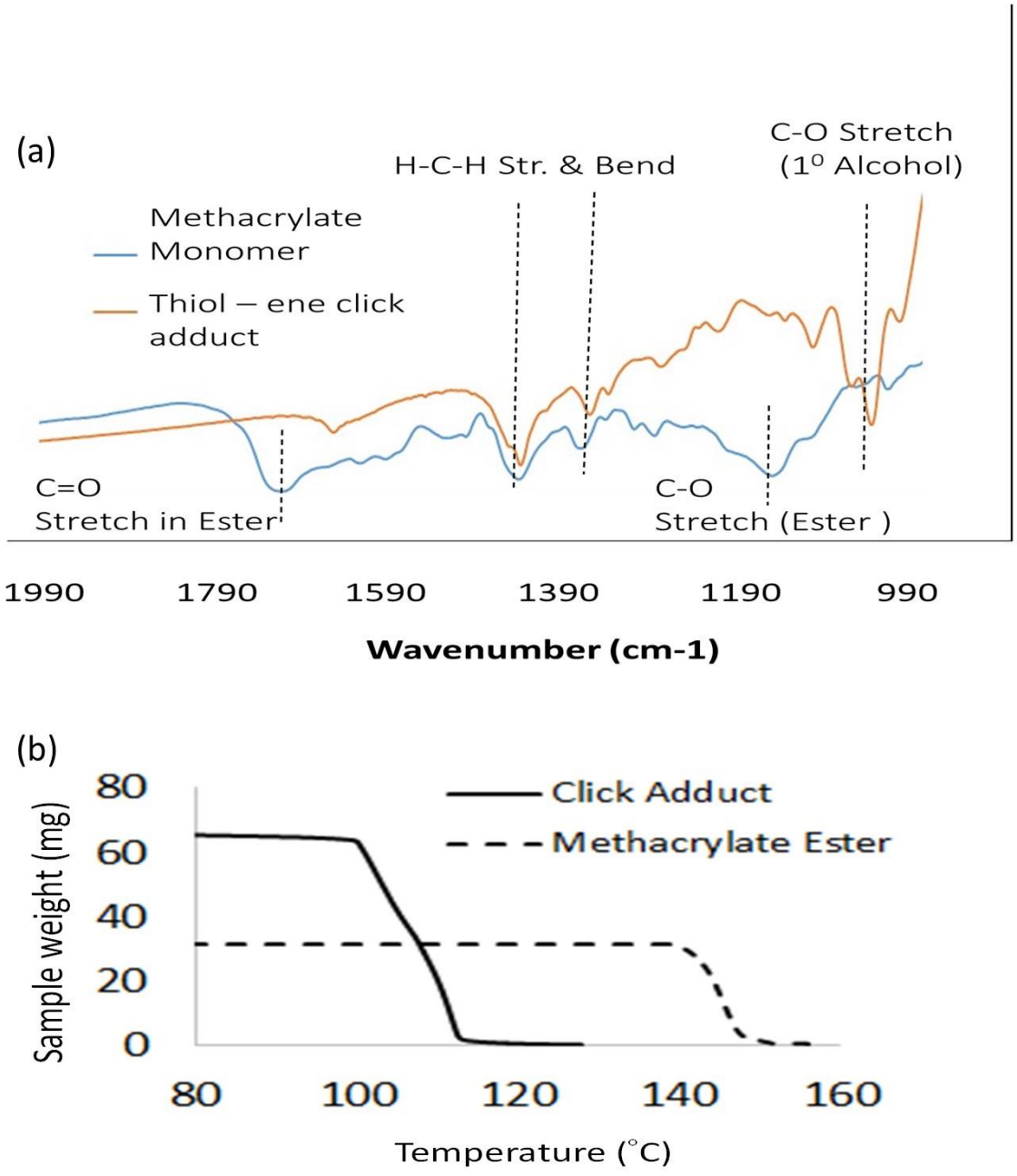

Figure 5.3: Characterization of Thiol-ene click adduct and methacrylate (a) FTIR, of click adduct and monomer (b) TGA

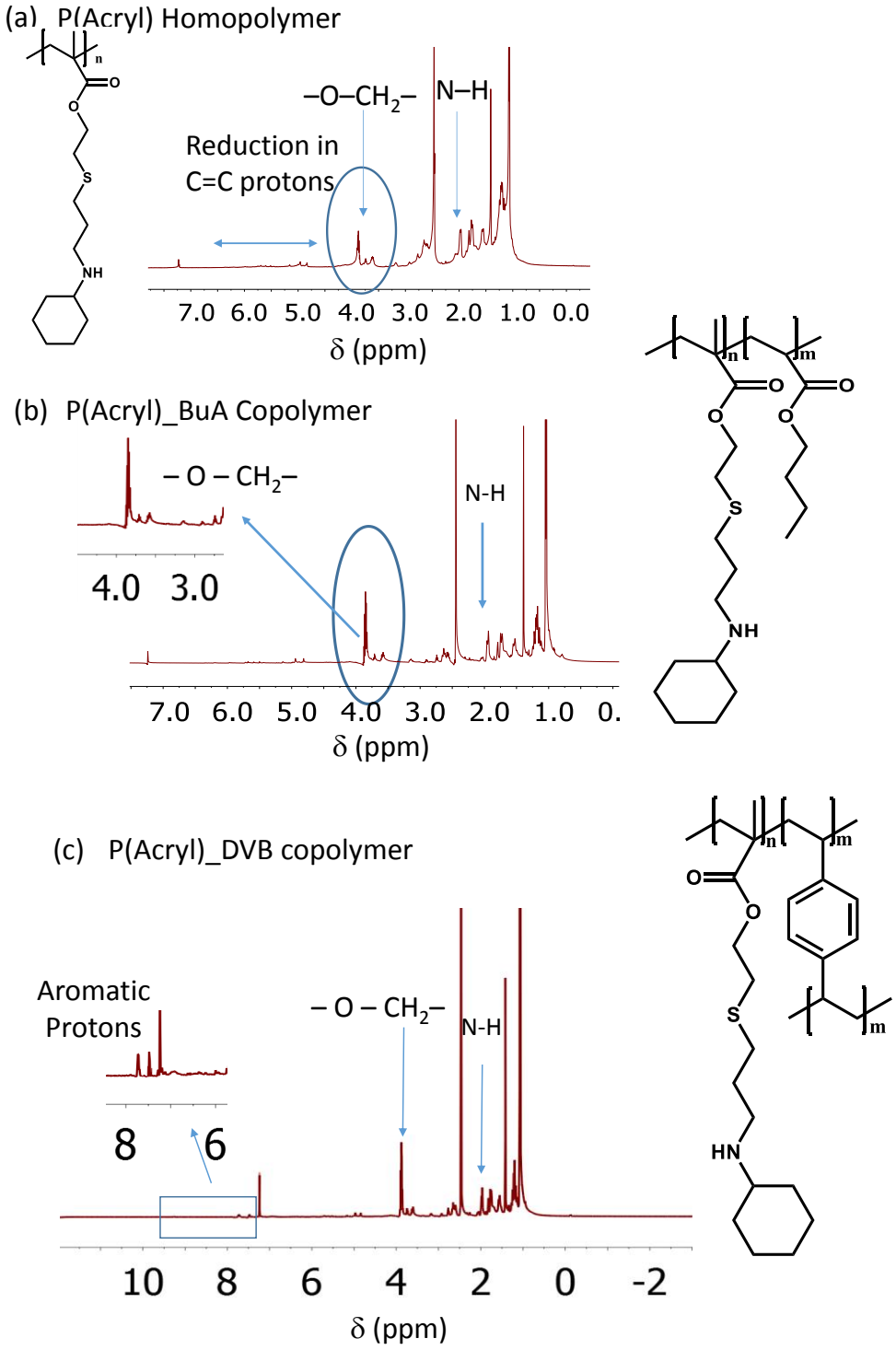
(a) P(Acryl) Homopolymer
–O–CH2–
N–H
Reduction in
C=C protons
7.0 6.0 5.0 4.0 3.0 2.0 1.0 0.0
δ (ppm)
(b) P(Acryl)_BuA Copolymer
– O – CH2–
N-H
4.0 3.0
7.0 6.0 5.0 4.0 3.0 2.0 1.0 0.
δ (ppm)
(c) P(Acryl)_DVB copolymer
Aromatic
Protons
– O – CH2–
N-H
8 6
10 8 6 4 2 0 -2
δ (ppm)

Figure 5.4: NMR Spectroscopic Characterization of polymers. a. P(Acryl), b. P(Acryl_BuA Copolymer, (c). P(Acryl_DVB copolymer)

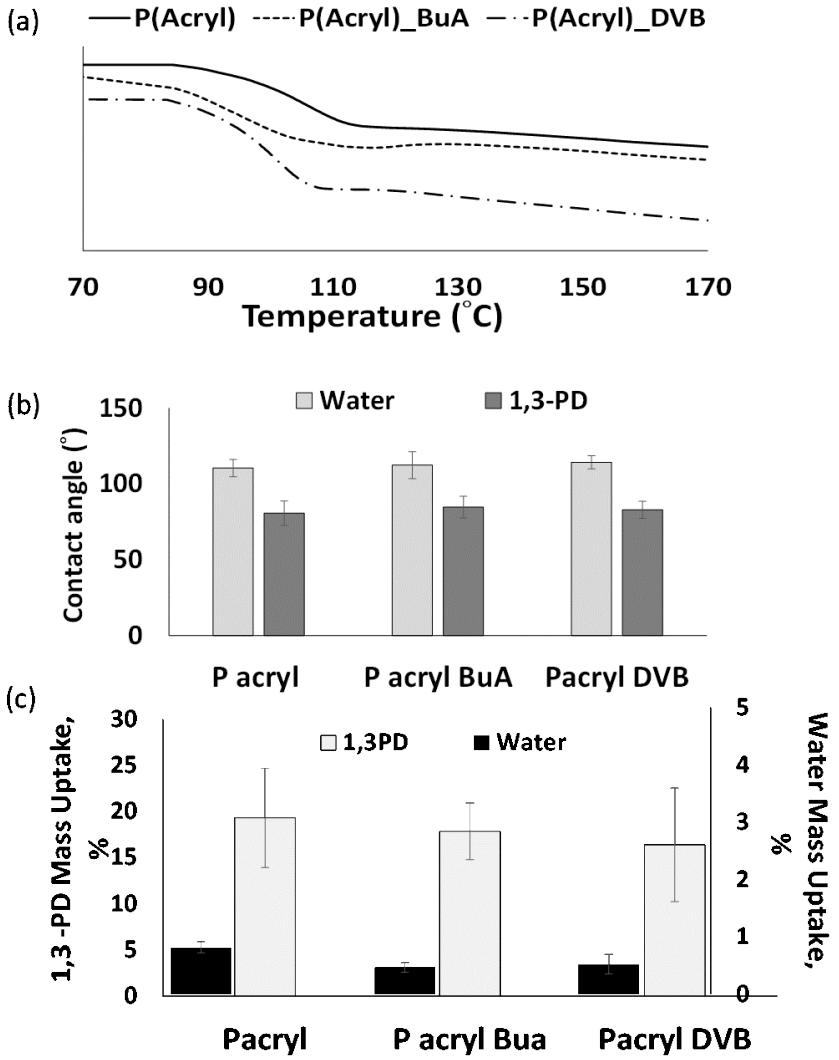

Figure 5.5: Polymer characterization (a) DSC overlay demonstrating the thermal transition temperatures (b)Water and 1,3-PD contact angle (c) Water and 1,3-PD mass uptake

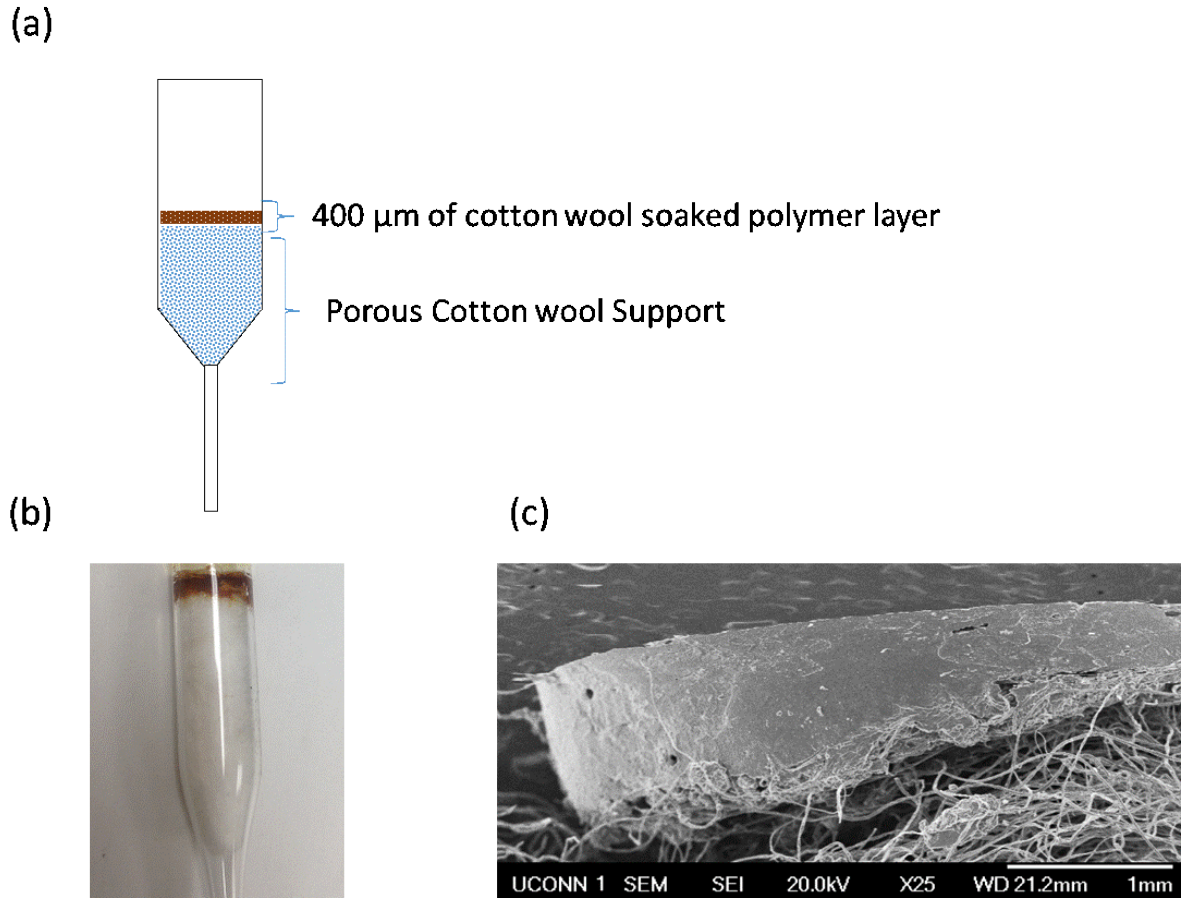

Figure 5.6: Plug Membrane (a) Schematic (b)Photograph (c) Section FESEM

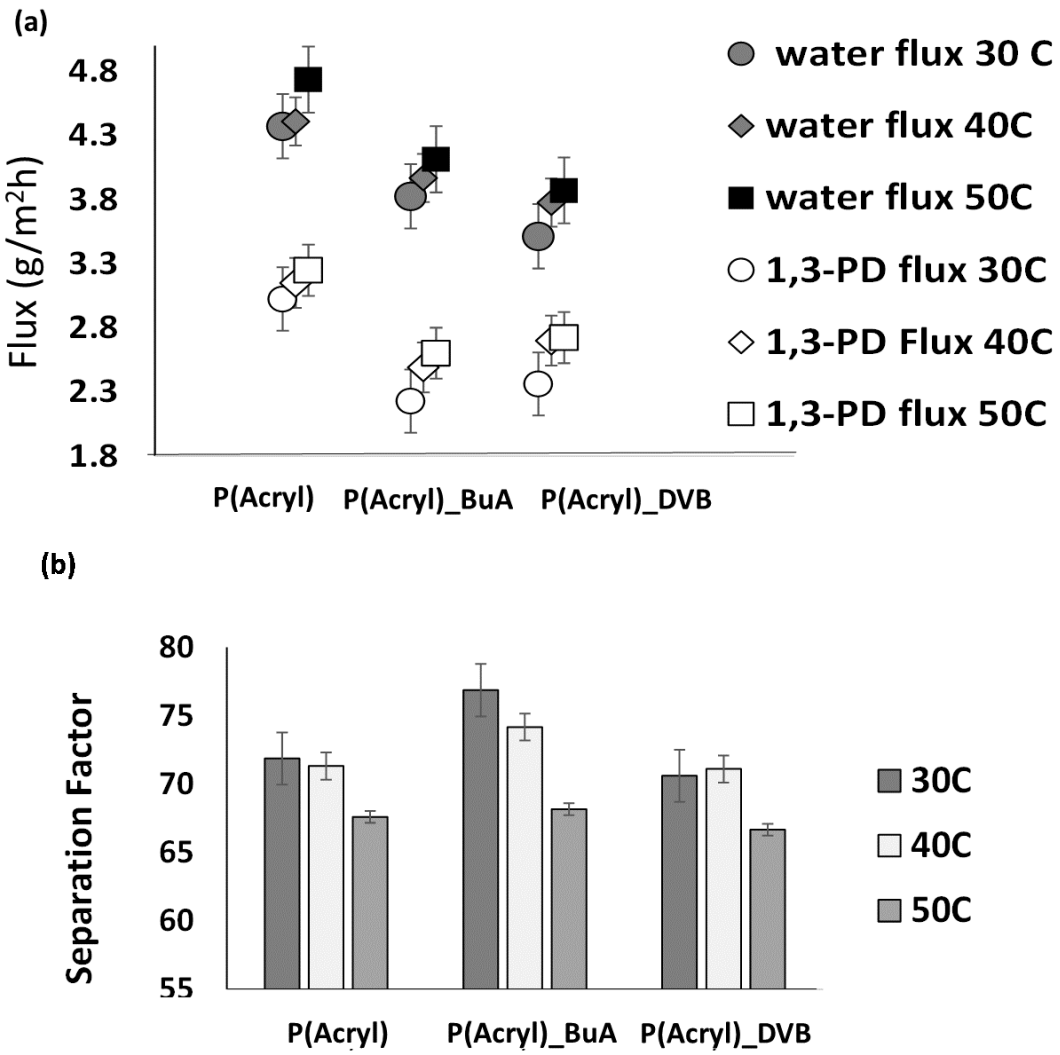

Figure 5.7 : Batch Pervaporation – Variation with temperature (a) Component Flux (b)1,3-PD separation factor

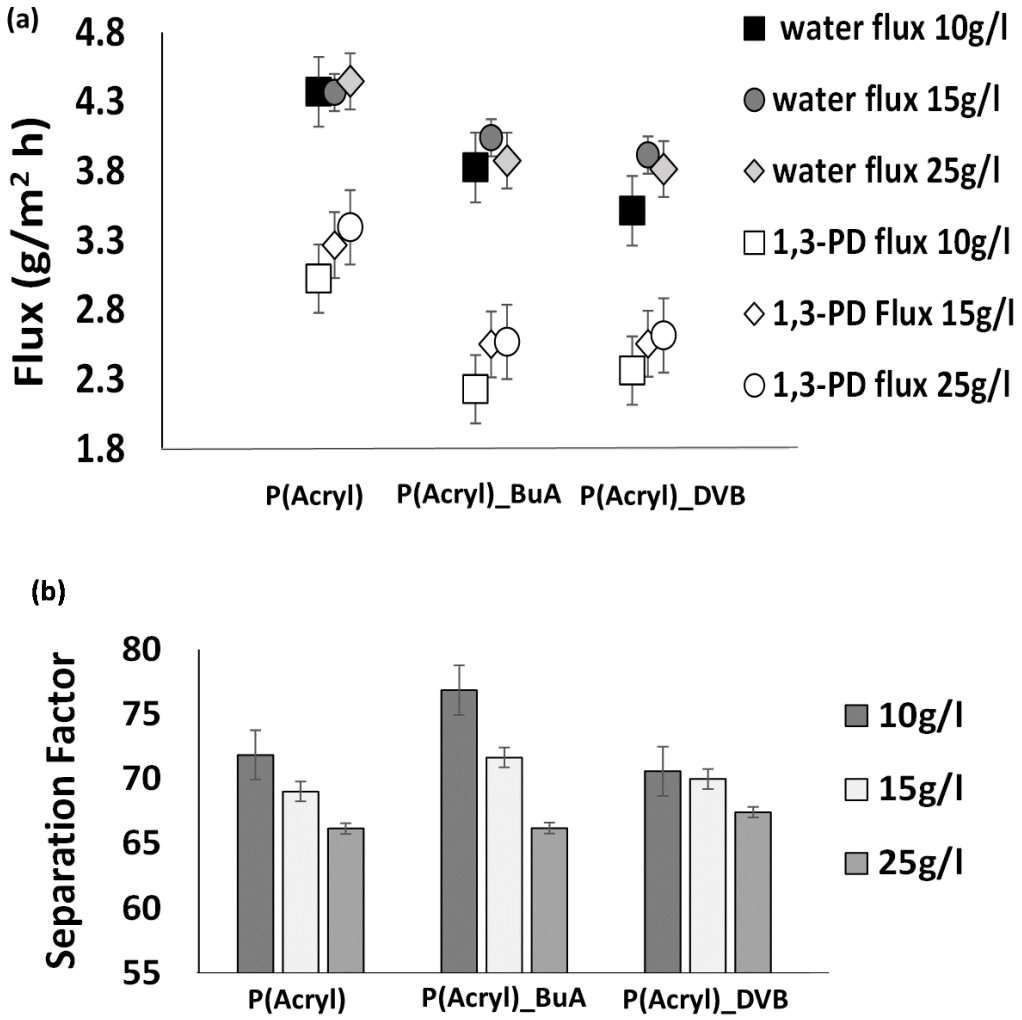

Figure 5.8 : Batch Pervaporation – Variation with 1,3-PD feed concentration (a) Component Flux (b)1,3-PD separation factor

Table 5.1 : Hansen Parameters and corresponding Ra computed using group contribution method

Parameter	**δ_D**	**δ_H**	**δ_P**	**Ra**
Methacrylate Monomer	19.52	3.97	5.01	water / monomer 40.01; 1,3-PD/monomer 21.25; 1,3PD/water 19.43
Water	15.50	16.00	42.31	
1,3-PD	16.80	13.51	23.20	

Chapter 6. Imidazolium Dibutylphosphate Ionic Liquid Based Methacrylate Polymer Membranes For Efficient Pervaporative Enrichment of 1,3-propanediol From Binary Aqueous Mixtures*

Abstract

The challenge of pervaporative enrichment of 1,3-propanediol (1,3-PD) from dilute aqueous mixtures was addressed by the synthesis of a novel hydrophobic imidazolium dibutylphosphate ionic liquid structure based methacrylate monomer. Vinylimidazole was "thiol-ene coupled" with mercaptoethanol followed by conversion into an imidazoliumdibutyl phosphate ionic liquid and finally to the methacrylate monomer by esterification with methacryloyl chloride. Plug membranes based on such homo and random copolymers with butyl acrylate and divinyl benzene exhibited high separation factors (88 - 115) and fair (2.8 and 3.6 g/m^2h) 1,3-PD fluxes. The membrane performance was robust against changes in temperature and feed 1,3-PD concentrations. The monomer provides a inexpensive recourse to high performing materials by balancing its 1,3-PD affinity with its hydrophobic nature. The excellent cost – performance trade off makes this an attractive candidate for possible industrial applications in multilayer modules.

Keywords: Imidazolium ionic liquids, 1,3-propanediol, pervaporation, Tributyl phosphate

*Imidazolium Dibutylphosphate Ionic Liquid Based Methacrylate Polymer Membranes For Efficient Pervaporative Enrichment of 1,3-propanediol From Binary Aqueous Mixtures, B. Kanjilal, I.Noshadi, J.R. McCutcheon, A.D. Asandei, R.S. Parnas, Green Chemistry (In Preparation)

Introduction

Glycerol, a platform chemical for the production intermediate biorenewable chemicals, can be obtained as a low value waste feed stock from a wide variety of industries. Its fermentative conversion to intermediate biorenewable chemicals such as 1,3-propanediol (1,3-PD is an environmentally and economically sustainable recourse to its utilization [1]. However, the principle impediment in fermentative conversion of glycerol to 1,3-PD lies in the downstream enrichment of 1,3-PD concentration given that it has to be enriched from very low starting concentrations [2 – 4]. Conventional processes, like evaporation, chromatography and reactive extraction amongst others have been used but are associated with either high energy usage or yield and process complication issues [5-17].

Pervaporation mitigates the challenge of high energy associated with processes involving phase change [18]. It deals with the minor component hence reducing the bulk energy usage. Additionally, pervaporation uses membranes with affinities tailored to be selective towards a given component. Pervaporation has been ranked as one of the better technologies for liquid separation and has found viable application in solvent dehydration, removal of volatile organic content, aroma recovery and some organic/organic separations [19].

The thermodynamic and kinetic factors that control permeation are manifested as the preferential solubility of one permeating component over the other and the diffusivity of the permeating components [18]. Since water, as a smaller molecule, has greater diffusivity than 1,3-PD, a high preferential sorption of 1,3-PD and low water solubility in

the membrane must be exploited to allow preferential permeation of 1,3-PD across a membrane [20]. Herein, the proximity of the thermodynamic solubility parameters of 1,3-PD and its highly hydrophilic character marks the limitation in the availability of appropriate materials.

Ionic Liquids have attracted attention due to their unique properties one of which is low vapor pressure at ambient temperatures [21]. They have been put to use in applications which require low solvent and their uses range from electrochemisty and catalysis to being used as engineering and process fluids, heat transfer agents, as liquid pistons in gas compressors and paint and coating additives [22 – 29]. They have been used in the field of extraction, extractive distillation and as supported liquid membranes [17]

For the separation of 1,3-PD from water and model aqueous fermentation broths, Zeolite membranes have been used for pervaporative separation of 1,3-PD from model fermentation broths where the membranes proved to be selective towards water [15,16]. Izak et al reported the application of a cyanoborate ionic liquid based based supported liquid membrane with high separation factors [17]. The low vapor pressure of Ionic liquids makes them particularly attractive for application in liquid membranes [17, 21, 30]. However, the leaching and loss of solvent cannot be completely alleviated [30]. Yet another major requirement for the use of IL in pervaporative applications such as separation of organic hydrophilic compounds from aqueous broths is the water stability at operating temperatures [21, 30]. The hydrolytic instability limits the application of hexaflurophosphate and tetrafluoroborate based ionic liquids to anhydrous processes [21]. Additionally, ionic liquids are usually expensive and their technical applications are limited by the price of their anions [21, 30].

A Dupont patent deals with solvent extraction of 1,3-PD with feed broths containing ~5% 1,3-PD and a wide variety of hydrophibic solvents of which one reported solvent is Tributyl Phosphate [5,9,10]. 1,3-PD is extracted into the hydrophobic solvent, preferentially over other fermentation products [5,9, 10]. The choice of TBP is prompted by its balance of hydrophobic character and its high affinity for 1,3-PD [10]. While solvent extraction for 1,3-PD in general has efficiency limitations owing to the high water affinity of 1,3-PD and limited partitioning [31], the incorporation of the TBP into a polymerized ionic liquid structure in this work was shown to successfully separate 1,3-PD from water with high selectivity.

Polymers of ionic liquids (PIL) have been used in select applications such as ion conduction, as polymer electrolytes and for the synthesis of phase transferrable graphene sheets [32]. However, the application of ionic liquids in separations has been largely limited to them being used in supported liquid membrane structures [21, 32].

This work reports the synthesis of an acrylate monomer based on an ionic liquid of tributyl phosphate (TBP), its polymerization, fabrication into a plug membrane and subsequent batch pervaporation on binary water-1,3-PD mixtures. A vinyl imidazole as first converted into an alcohol using a thiol-ene click chemistry step. This was followed by the formation of an imidazolium ionic liquid by high temperature reaction with TBP, in which the dibutylphosphate anion forms the counter ion for the 3-N-imidazolium cation. The remnant hydroxyl on the IL was esterified and converted to a methacrylate monomer which was then polymerized by simple radical polymerization. Membranes fabricated from the polymers were evaluated for 1,3-PD selectivity in batch pervaporation experiments. High separation factors and good 1,3-PD fluxes were achieved by creating a highly hydrophobic

membrane with high affinity for 1,3-PD. The wide difference in solubility of water and 1,3-PD is the major factor exploited in deciding the selective permeability of 1,3-PD over water and hence its enrichment. The development and fine tuning of such materials present themselves as steps towards establishment of commercially viable and energy efficient alternatives to conventional purification processes presenting a possibility of membrane module fabrication for continuous pervaporation.

Experimental

Materials:

For the synthetic scheme involving monomer preparation and polymerization, Vinylimidazole (VIM), Methacryloyl chloride, Divinyl benzene(DVB) and Butyl Acrylate(BuA) monomer was dried prior to use. Mercaptoethanol, Tri ethylamine (TEA) and AIBN radical initiator were used without modification. The solvents, Toluene, Chloroform, Dioxane and Hexane were dried prior to use. All chemicals were purchased from Sigma Aldrich.

For the fabrication of the plug membranes, 0.65 cm inner diameter glass pipettes from Fischer were used. Cotton wool was used to act as the porous support base and was purchased from the local market.

1,3 propanediol (1,3-PD), 98% purity was purchased from Sigma Aldrich and used for the partition coefficient and preparation of binary mixtures with distilled water as feed solutions for pervaporation experiments.

Analytical Methods:

Brucker DMX-500 MHz and Brucker Ascend 400 WB spectrometers were used for NMR spectroscopy, while IR spectra were taken on samples on a Nicolet Magna-IR 560 spectrometer using KBr powder as background. Molecular weight of the polymers were determined by GPC in an Agilent 1260 Infinity system using N,N-Dimethylacetamide as eluent. The system used narrow molecular weight PMMA from Sigma Aldrich calibration standards. Thermo-gravimetric analysis (TGA) was carried out in a TA Instruments Hi-Res 2950 TGA instrument in nitrogen. Thermal transitions were measured by Differential Scanning Calorimetry in TA Instruments Q100 DSC instrument. An Olympus TGHM goniometer was used to measure Contact angles on thin clean glass substrates and on polymer films cast on clean glass surface. Field Emission scanning electron microscopy (FESEM) was used to obtain images of the membrane structure with a JEOL 6335F field emission scanning electron microscope. The 1,3-PD concentrations in the initial feed solutions and permeate samples from the pervaporation experiments were analyzed using on 0.22μm syringe filtered aqueous samples by gas chromatography (GC) using a DB-FFAP capillary column and an MS detector and a 1μL injection volume. GC injector, detector and initial oven temperatures were kept at 240C, 270C, and 40C respectively.

Partition Coefficient Measurement:

The coefficient of partition of 1,3-PD between water and TBP was determined at 30C. 1 ml of a 10 g/l of 1,3-PD solution was vortexed with 1ml of TBP for 15 minutes and the layers allowed to separate. The concentration of 1,3-PD, in the aqueous phase, determined

by GC, before and after partition, was used to compute the coefficient of partition based on equation 1:

$$K_p = \frac{C_{TBP}}{C_{water}} \quad \text{----------(1)}$$

Synthesis, purification and characterization of methacrylate monomer:

The monomer synthesis scheme is depicted in Figure 6.1. The thiol-ene click chemistry adduct was synthesized by AIBN mediated addition of the vinyl double bond of the VIM to the thiol bond of mercaptoethanol [33]. The reaction was carried out in a pressure tube, degassed prior to reaction with dry argon in a schlenk line. The solventless reaction was carried out at 60^0C in the presence of UV and catalyzed by AIBN [33]. The reactants were weighed out in stoichiometric amount. The product was purified by vacuum drying off the excess VIM. The thiol-ene click adduct was spectroscopically characterized by ^{1}H NMR and FTIR, while its vaporization temperature was estimated by TGA. A typical run consisted of 0.94 g of Vinylimidazole, 0.78 g of Mercaptoethanol and 0.02 g of AIBN initiator.

The click adduct was subsequently reacted with TBP at 140^0C. The dibutyl phosphate anion serves as the counter ion for the imidazolium cation in this ionic liquid [21]. The ionic liquid product was spectroscopically characterized by ^{1}H NMR. A typical run consisted of 1.7 g of the thiol – ene click adduct and 2.7 g of TBP. The reaction was carried out for at least 72 hours.

The remnant hydroxyl group from the mercaptoethanol moiety on the ionic liquid was subsequently esterified using methacryloyl chloride and triethyl amine as the catalyst [34].

A typical run consisted of 4.3 g of the ionic liquid, 1 g of triethyl amine and 1 g of methcryloyl chloride in ~ 10 ml of solvent. The ionic liquid was dissolved in dry toluene and a stoichiometric amount of methacryloyl chloride and triethylamine were added and refluxed at 75^0C for 12 hours. The solvent was evaporated off by stirring in an open beaker at 40^0C overnight. The resultant mixture of the methacrylate monomer, which still contained triethyammonium hydrochloride, was dissolved in hexane. The triethyamine hydrochloride separated out, the supernatant hexane layer containing the hydrophobic methacrylate ester of the ionic liquid was filtered off. The hexane was subsequently evaporated overnight in a vacuum oven at 40^0C. The purified methacrylate monomer was characterized by ^{1}H NMR, ^{13}C NMR, FTIR and TGA. The absolute density of the methacrylate monomer was measured by weighing a fixed volume of the monomer. The NMR results are epicted in Figures 6.2(a) – (c) and in Figures 6.3 (a) and 6.3(b). The FTIR and TGA results for the monomer are shown in Figure 6.4 (a) and (b). Figure 6.5 (a) and (b) illustrate the solubility of the methacrylate monomer in water and 1,3-PD.

Synthesis, purification and characterization of polymers:

The methacrylate monomer was homopolymerized and copolymerized separately with 5 mol% of BuA and 5mol% of DVB using AIBN initiator. The polymerizations were carried out at 70^0C in a 250 ml two necked round bottom flask fitted with a reflux condenser with the system being constantly purged with nitrogen. The dioxane solutions of the monomer(s) were passed through an inhibitor remover column to remove the inhibitor contained in the methacryoylchloride prior to polymerization. A 25ml dioxane batch typically consisted of contained ~5g of the methacrylate monomer with AIBN in a stoichiometric monomer:

initiator ratio of 100:1. The polymerizations were blanketed by a stream of nitrogen. At the end of each batch, the reaction mixtures were characterized by ^{1}H NMR. The polymer was stripped off the remnant volatiles and solvent by evaporation and dried to constant weight at $80^{0}C$ under vacuum. The solid polymers were spectroscopically evaluated for thermal transitions by DSC.

The reaction mixtures were used to cast films on clean glass and kapton substrates. The former were used to evaluate the water and 1,3-PD contact angles, while the latter were peeled off from the kapton substrate and evaluated for water and 1,3-PD mass uptake. The NMR of the polymers are shown in Figures 6.6 (a) – (c).

The DSC results are shown in Figure 6.7(a), while Figure 6.7(b) shows the results for water and 1,3-PD contact angle measurement. The mass uptake results are shown in Figure 6.8(a). The non crosslinked polymers (i.e. those not employing DVB in their composition) were evaluated by GPC for molecular weight.

The acronyms used for the homopolymer, butylacrylate copolymer and divinyl benzene copolymer are PVIM, PVIM_BuA and PVIM_DVB respectively

Membrane Fabrication and Pervaporation experiments:

Plug membranes were fabricated inside 0.65 cm inner diameter glass pipettes. A known weight of dry cotton wool was stuffed inside a glass pipette to form a base. A small and known weight of dry cotton wool was soaked in a known volume of with the polymer solution and allowed to dry slowly at $40^{0}C$ over 3-4 days. Once nearly dry, the polymer solution soaked cotton wool was lightly pressed with a flat screw head to set it as a

membrane on top of the cotton wool base inside the glass pipette. The solvent was evaporated slowly over nearly a week at room temperature till the plug attained a constant weight. The slow solvent evaporation prevented pinhole formation and allowed the plug membrane to adhere to the inner wall of the glass pipettes. Figure 6.8 (b) is an FESEM image of a section of a typical membrane plug. The volume inside the glass pipette above the membrane was used for ~1.5-1.7 ml of pervaporation feed solution.

The materials were evaluated in a batch pervaporation set up using the fabricated plug membranes. The structures were affixed in an upright position in a water bath at 30C. The plug membrane proffered a pervaporation area of 4.91 mm^2. Each batch pervaporation experiment was allowed to run for a period of 20 - 30 hours and the permeate collected in two dry –ice cooled traps. A vacuum pump was employed to pull a vacuum of 1 – 3mmHg on the downstream side. The permeate collected was thawed, weighed, diluted and analyzed for 1,3-PD concentration by GC.

Pervaporation is monitored by key performance indicators of permeate flux and separation factor given by equation 2 [35].

$$\alpha = \frac{Jp}{Jw} . \frac{xw}{xp} \text{ ------(2)}$$

J_p and J_w represent the 1,3-PD and water fluxes and x_p an x_w represent the feed mass fractions of 1,3-PD and water respectively.

Results and Discussions:

Partition Coefficient in Amine:

The partition coefficient of 1,3-PD in Tributyl Phosphate (TBP) over water was estimated at 0.62±0.12. TBP is a hydrophobic solvent, with a Log P_{ow} (Octanol – water redistribution coefficient) ~4 in which 1,3 propanediol is miscible in all proportions.

Synthesis, purification and characterization of methacrylate monomer

The scheme for synthesis of the methacrylate monomer is shown in Figure 6.1. Thiol-ene click chemistry was used to block the vinyl double bond on VIM (Step 1) and yield a Thiol-enelick adduct This was done to prevent any polymerization in the subsequent high temperature step which converted the imidazole based thiol-ene click adduct to an imidazolium hydrophobic ionic liquid (Step 2). The remnant hydroxyl proton on the imidazolium ionic liquid was esterified using methacryoyl chloride into the final methacrylated monomer (Step 3). The NMR for the monomer synthesis sequence is shown in Figure 6.2(a) – (c) and in Fig 6.3(a) and (b).

Vinyl protons of vinylimidazole appear at $\delta \sim 5 – 5.5$ in Figure 6.2a and are marked 1,1'. The conversion of vinylimidazole into the thiol-ene click adduct was confirmed by the disappearance of these vinyl upon conversion to the thiol – ene click adduct (Fig. 6.2b). Mercaptoethanol shows a thiol proton signal (SH) at $\delta \sim 1.38$ (figure not shown here). This thiol (SH) proton signal was also seen to disappear [33]. The ratio of the area integrals under $\delta_{5.5\ ppm}$ and $\delta_{7.7\ ppm}$ ($\delta_{5.5\ ppm}/\ \delta_{7.7\ ppm}$) for vinylimidazole were compared to those obtained for the thiol – ene click adduct to arrive at an approximate yield of 97%.

The click adduct was then converted to an imidazolium ionic liquid by high temperature reaction with TBP. The NMR of the imidazoliul ionic liquid is shown in Fig 6.2c. The signal at δ ~ 10.25 corresponds to the N–C*H*=N+ proton. The figure also shows the appearance of the protons from the dibutylphosphate counteranion at δ~ 3.71, 1.43, 1.22 and 0.74 with progressive distance from oxygen in the $[O=P(OCH_2CH_2CH_2CH_3)_2]^-$ counter anion structure. The $–OCH_2CH_2CH_2CH_3$ attached to the imidazolium ring Nitrogen shows NMR signals at δ~ 4.27, 1.77, 1.26 and 0.86 with progressive distance from the nitrogen atom [21]. The chemical shifts of these groups are individually delineated in Fig 6.2c as insets. The conversion is also marked by the disappearance of the N–CH=N proton at δ ~ 7.7. The ratio of the area for this proton to that at δ~7.4, marked as 5 in the vinylimidazole NMR, Figure 6.2 (a), ($\delta_{7.7\ ppm}$/ $\delta_{7.4\ ppm}$) is used to estimate the % conversion for the formation of the ionic liquid at ~ 89%.

The imidazolium ionic liquid is then subsequently converted to a methacrylate monomer by reacting the hydroxyl group with Methacryoyl chloride [34]. The NMR of the methacrylate ester monomer is shown in Fig 6.3(a). The appearance of the methacrylate protons ($-C=CH_2$) are shown in the figure at δ~ 5.4 and 6.1. The reaction is marked by the reduction in the C-OH proton NMR peak at δ ~3.5 ppm. The area of this peak to that at δ ~7.4 ppm ($\delta_{3.5\ ppm}$/ $\delta_{7.4\ ppm}$) before and after formation of the methacrylate ester was used to estimate the approximate % conversion for the formation of the methacrylate ester at ~ 78%.

Figure 6.3(b) represents the ^{13}C NMR spectrum of the methacrylate monomer. The positions of the carbons pertinent to the dibutylphosphate counteranion and the butyl chain attached to the quaternary nitrogen are shown as insets on the figure.

The FTIR spectra of the thiol – ene click adduct and the methacrylate monomer are shown in Figure 6.4 (a). The key bonds are shown on the figure. The conversion of the thiol – ene click adduct to the methacrylate via the imidazolium ionic liquid pathway is underscored by the disappearance of the C – O single stretch in primary alcohols and the disappearance of the C – Nsingle bond stretch and the C = N double bond stretch in the imidazole ring at wavenumbers 1080-1100cm^{-1}, 1230cm^{-1} and 1500 cm^{-1} respectively.

The TGA results on the thiol-ene click adduct, the imidazolium ionic liquid and the methacrylate monomer are shown in Figure 6.4(b). While the thiol-ene imidazole click adduct was amber colored viscous liquid, the color deepened and the viscosity increased significantly with the formation of the ionic liquid. In the thiol-ene adduct hydrogen bonding is responsible for some molecular associations leading to a vaporization temperature of ~ 315^0C.

The subsequent step of reaction with TBP leads to the formation of an ionic liquid. The ionic liquid shows weight loss in two steps. Imidazolium ionic liquids are known to undergo dissociation via competing mechanisms in this temperature range [38]. The cleavages are thought to occur via the breaking of the C-N bond cleavage at an alkyl group due to nucleophilic attack by the counter negative ion [38]. The exact mechanism of cleavage and the products formed can only be ascertained upon a GC MS analysis of the fragmented products. That study is however, beyond the scope of this work. The ionic

liquid formed has a fairly high boiling point. Ionic liquids are considered as “low melting salts” and hence are liquids with fairly high boiling points with niche applications[21, 38]. The conversion of the click-adduct-imidazolium ionic liquid to the methacrylated ester made an insignificant change in the vaporization temperature.

The presence of hydroxyl group in the imidazolium ionic liquid contributes to hydrogen bonding and hence a high vaporization temperature. Its conversion to the methacrylate group is expected to lower the vaporization temperature. The effect is balanced out by a slight increase in molecular weight resulting in nearly the same vaporization temperature for both the ionic liquid and the subsequent methacrylate. As in the ionic liquid, so also in the final methacrylate monomer, the imidazolium moiety, exhibits decomposition before the material reaches vaporization. It may be noted that decomposition also leads to eventual carbonization manifested as nearly 8-9% residue in the ionic liquid and subsequent methacrylate monomer.

The density of the methacrylate monomer at 30^0C was estimated at 1.047 ± 0.06 kgm^{-3}.

The solubility of the methacrylated monomer in water, 1,3-PD and a hydrophobic solvent such as chloroform was evaluated. This is shown in Figures 6.5(a) and 6.5(b) which are photographs of a drop of the methacrylated monomer dropped into ~2 ml of water and 2 ml 1,3-PD. While the monomer liquid droplet appears miscible with both chloroform and 1,3-PD, the immiscibility with water is apparent in the photograph.

Characterization of polymers:

The methacrylate monomer was solution polymerized to yield a homopolymer and copolymerized separately with 5 mol% BuA and 5 mol% DVB. The NMR traces of the homopolymer and copolymers are shown in Figure 6.6 (a) – (c).

An estimate of the percentage of butylacrylate incorporation into the copolymer was made from the NMR spectra. Figure 6.6 (a) is the NMR of the homopolymer. Polymerization occurs with a reduction in the relative abundance of acrylate double bonds. Figure 6.6(b) is the NMR of the copolymer with Butyl acrylate. The ^{1}H NMR traces were utilized to estimate the BuA content in the copolymer composition by comparing the integrated peak areas of the N – H proton from the methacrylate monomer at $\delta \sim 2.4$ppm, with those at $\delta =$ 3.8 ppm (–O–CH_2– from BuA). Both the methacrylate monomer and the BuA co-monomer exhibit chemical shifts at $\delta \sim 3.8$ ppm due to –O–CH_2– protons. The difference between the –O–CH_2– signals in the copolymer and the homopolymer, divided by the N-H signal at $\delta \sim 2.4$ ppm, was used to estimate the BuA composition in the copolymer. The estimated BuA incorporation was computed as ~6.8 mol%.

An estimate of the divinyl benzene incorporation in the polymer structure (Fig 6.6c) was made from the 13C NMR spectra of the DVB compolymer. The NMR traces were utilized to estimate copolymer composition by comparing the integrated peak areas of the C=O carbon from the methacrylate monomer at $\delta \sim 168$ppm with those at $\delta \sim 145$-155 ppm (aromatic ring carbons from DVB). The estimated DVB incorporation was computed as ~ 8.3 mol%. Due to the limited degree of crosslinking with ~5mol% of DVB, the polymer does not separate out of solution unless the solvent is evaporated off.

GPC molecular weight measurements were made only on the homopolymer and the copolymer with butyl acrylate. The weight average molecular weight of the homopolymer and butylacrylate copolymer were 45073 and 39850 with a PDI of 4.99 and 4.06 respectively.

The thermal transitions of the polymers were evaluated by DSC and the results are presented in Figure 6.7(a). Polymers of ionic liquids are generally characterized by high thermal transition temperatures. Glass transitions in the range of 176 -184^{0}C were noted. The presence of a small amount of BuA copolymer reduced the thermal transition by ~3^{0}C while crosslinking with DVB increased the glass transition by ~ 4^{0}C.

The polymerization reaction mixtures, at the end of the polymerization process were used to cast this films on clean glass substrates and evaluated for water and 1,3-PD contact angles and the results are shown in Figure 6.7(b). The polymer was found to be hydrophobic as the average water contact angles ranged between 117–121^0. Conversely, the wettability of the surfaces with 1,3-PD was confirmed by the acute contact angles ranging from 68–72^0. The overlapping error bars on the measurements indicated insignificance of the difference in behavior between the three polymers.

Figure 6.8(a) shows the water and 1,3-PD mass uptake results. The low water mass uptake (< 0.5%) and the high 1,3-PD mass uptake (18 – 23%) underscore the comparative preference of the polymers for 1,3-PD over water. The overlapping error bars meant that no significant difference between the mass uptakes were noted for the four polymers. The results are in corroboration with the solubility behavior of the methacrylate monomer in water versus 1,3-PD

A representative FESEM of the membrane is shown in Figure 6.8(b). The average thickness of the membranes, as obtained by Image J analysis software was ~400 – 450 μm.

Pervaporation results on 1,3-propanediol – water binary feed mixtures

The 1,3-PD and water flux and separation factors for batch pervaporation are illustrated in Figures 6.9(a) – (c) and 6.10 (a) – (c). Each data point was an average of experiments in triplicate. The polymers demonstrated high separation factors between 88 and 115. The highest data point obtained for separation factor was 125 with the homopolymer.1,3-PD flux between 2.8g/m^2h and 3.6g/m^2h were obtained. The water flux varied between 2.6g/m^2h and 3.8g/m^2h.

Effect of Copolymerization

While the separation factors appeared to follow a trend, the error bars obtained from averaging experimental results in triplicate overlapped indicating statistical insignificance of the variations. Nonetheless, the incorporation of Butyl acrylate as a comonomer was seen to reduce the average separation factor from 115 with the homopolymer to 106. It was accompanied by statistically insignificant changes in either water or 1,3-PD flux. Butyl acrylate on its own has affinity neither in favor of water nor 1,3-PD.

The incorporation of a small molar percentage of divinyl benzene changed the separation factor to 97.7. With the DVB copolymer, the flux 1,3-PD reduced. The incorporation of DVB decreased the affinity of the material towards 1,3-PD and water, since DVB is partial towards neither component. The extent of crosslinking may be seen as too low to cause

any statistically significant change in the flux of the components. However a slight decrease in 13-PD flux and a slight increase in water flux was noted.

Effect of Temperature

The separation factors for all polymers were seen to decrease very slightly with temperature. The water flux increased with temperature and this effect was more obvious with the DVB copolymer than with the other two structures. Similarly, the 1,3-PD flux increased with temperature with all membrane structures. An increase in temperature enhances diffusion of both water and 1,3-PD. This causes a concomitant reduction in selectivity. The results are presented in Figure 6.9 (a) – (c).

Effect of 1,3-PD feed concentration

The average separation factors for the homopolymer and the BuA copolymer decreased with an increase in the feed 1,3-PD concentration. An increased 1,3-PD in the feed possibly causes plasticization of the membrane allowing a greater amount of water to diffuse through. Additionally, 1,3-PD may possibly act as a "water carrier" an enhance the water transport leading to a decrease in selectivity. A slight anomaly was observed with the DVB copolymer where the separation factor decreased with an increase in the feed 1,3-PD concentration from 10g/l to 15 g/l but increased slightly with feed 1,3-PD of 25 g/l. The results are presented in Figure 6.10 (a) – (c).

Discussions:

In pervaporation, a component is preferentially removed by virtue of its high solubility in the membrane phase or its higher diffusivity or both [18]. Pervaporation has found

applications for removal of water in solvent dehydration, volatile organic removal from water or in aroma recovery [19]. Amongst all applications, the dehydration of solvents is the best developed due to the fact that the use of hydrophilic membranes ensures in a solubility – diffusivity synergistic effect in favor of water selectivity [18, 19]. Water, due to its smaller molecular size diffuses faster and the use of hydrophilic membranes also ensures a higher solubility [20]. However, for the separation of organic molecules from water, the solubility selectivity into the membrane material in favor of the organic molecule must be higher than that of water [19]. The membrane material must be significantly hydrophobic and must have substantial affinity for the organic permeant[18, 19]. This is the way a membrane may reject water and cause selective enrichment of the organic permeant.

The solubility is proportional to the affinity of a given component for the membrane material. The affinity is described by the Hansen solubility parameters comprising of hydrogen bonding interaction (δ_H), polar interaction (δ_P) and dispersion interaction (δ_D). The large differences in Hansen parameters, especially the hydrogen bonding interaction, δ_H determines the feasibility of organic solvent dehydration [18]. The proximity of 1,3-PD with water in terms of these parameters makes the pervaporative separation of 1,3-PD a difficult task.

While ionic liquids are liquids are room temperature, polymers of ionic liquids (PIL) are mostly solids [32]. The uses of PILs was targeted at mostly electrochemical applications [39 – 41]. Their low vapor pressure has also prompted their use in refrigeration and energy applications requiring fluids for heat transfer [42, 43]. PILs can be synthesized with direct

polymerization of the IL monomer [32]. Alternatively, chemical modification of existing monomeric structure is sought for subsequent polymerization. For example, in synthesizing a methacryoyl PIL monomer, the conventional route chosen is the conversion of methacryloyl cfhloride to an ester of an organic alcohol with a halide group at another end of the alcohol moiety. This is subsequently converted into an imidazolium halide IL and polymerised through the acrylic double bond [32]. The synthetic scheme explored in this paper is different and combines simple synthetic routes to derive a novel route (Figure 6.1). While ILs can be polymerized through almost all conventional routes of addition polymerization, such as AIBN initiated radical polymerization and controlled radical polymerzations such as ATRP and RAFT, the incorporation of a thiophene group is required for oxidative polymerizations [32].

The water solubility of an IL and PIL depends on both the cation as well as the counter anion. A small alkyl substituent such as ethyl or methyl on the 3-N atom for an imidazolium halide has been shown to be hydrophilic. However as the size of the alkyl substituent grows, the hydrophilic character reduces. Similarly the water affinity is defined by counter anion too [32, 44]. With small counter anions, such as halides NO3-, CF3CO2- etc, if the character of a given IL is hydrophilic, its water affinity reduces when the counter anion s substituted by eg; BF6- or CF3SO3-. When the counter anion is substituted by PF6- or [N(CF3SO2)2]-, the same IL becomes completely hydrophobic [32, 44]. In this case the counter anion (CH3CH2CH2CH2)2PO4-, derived from the hydrophobic TBP is sufficiently large and hydrophobic to effectively reject water but still have high affinity for 1,3-PD [21, 32]. This is underscored by the contact angle and water and 1,3-PD mass uptake results.

Hydrolytic instability of many anions such as hexafluorophosphate and tetrafluoroborate limits their use to anhydrous applications [21, 45]. The research on halogen free, hydrolytically stable ionic liquids is of current interest and dialkylphosphate anions provide an easy recourse to the same.

Anion exchange is yet another route in which IL monomers and polymers may be modified by changing the counter anion [32, 46]. Replacement of halide counter anions with ore hydrophobic anion have been shown to convert hydrophilic ILs to hydrophicic [46]. This paper showcases results on batch pervaporations. However, given the simplicity of the polymerization process and the ease of material availability, the method holds promise for scale up and use in continuous pervaporation modules. A possible problem that can be envisaged during continuous pervaporation using the material developed in this work is that of concentration polarization which is concomitant with high intrinsic enrichments. Membrane module designs and multilayer membrane structures may be used in the case of a polymer membrane to optimize separation performance and impart mechanical robustness to membrane structures.

According to the literature, 1,3-propanediol has been separated from water using pervaporation through an X-type zeolite membrane where the membrane is selective for water [15, 16]. Additionally, one report exists on the separation of 1,3-PD from binary mixtures using an ionic liquid based SLM stabilized in a nano porous module with a separation factor of 177 and flux of permeability 3.86 g m2 h-1 at 22C [17, 47]. However, despite the promising performance of this module, the low stability of SLM modules due

to leaching and the difficulty of their fabrication into stable and mechanically robust structures makes them difficult to scale up [30].

Yet another limitations associated with the usage of ionic liquids is the expense associated with the counter anion [21]. Pervaporation of aqueous broths require that the membrane materials be hydrolytically stable [45]. Ionic liquids have shown great promise in various applications but their technical applications are limited by either hydrolytic instability or high price of the anions for hydrolytically stable ionic liquids [21, 45]. The ionic liquid structure developed in this work is based on a rather inexpensive 1,3-PD solvent which has been proven as a hydrolytically stable counter ion in an earlier work.

This work can be directly compared to one investigation on pervaporative separation of 1,3-PD from water. Izak et al (2007) achieved a separation factor of 177 and flux of 3.86 g/m^2h at 22C for 1,3-PD in a binary mixture with water [17, 47]. Their work used a supported liquid membrane (SLM) based on cyanoborate ionic liquid and claimed 9 month membrane stability. The work reported herein achieved separation factors between 85 - 118 with 1,3-PD fluxes between 2.4 and 3.5 g/m^2h. The polymers developed in this work can be produced as flat sheets that may be fabricated into modules and scaled-up for commercial separations.

A brief comparison of the material price developed in this work versus that used for the cyanoborate SLM was carried out with retail price data from Sigma Alridch [48], Oakwood Chemicals Inc [49] and Fluorochem Ltd. [50]. The computation was based on molecular structures and prices of the individual chemicals making up the compound. The tetrapropyl ammonium cyanoborate ionic liquid costs $36,004/mole, while the methacrylate monomer

developed in this work costs $168.5/mol. The cost per unit weight of the ionic liquid is $120/g, while that of the methacrylate monomer developed in this work is $ 0.33/g.

A Price/performance trade off estimate was generated using the experimental results detailed here and reported in the work on the cyanoborate SLM. A rough estimation was made of the total volume of membrane material required to reach a final 1,3-PD concentration of >90%, from a starting composition of 1% 1,3-PD for a feed flow of 100 g/h. The computation assumes that separation factor and flux of 1,3-PD remained constant after each enrichment stage. This assumption was made because separation factor and flux data for high 1,3-PD feed concentrations were not available. The average separation factor for the homopolymer, PVIM, membrane was taken as 104 with an average 1,3-PD flux of 3.0g/m^2h. The computation yielded a requirement of 3 enrichment steps requiring a total pervaporation area of 6000 cm^2. The volume required using a 400 micron thick membrane was computed as 240 cm^3. Using the estimated density for the ionic liquid, the cost of the material required to achieve the aforementioned enrichment level is ~$86.

The same computation was carried out for the cyanoborate ionic liquid membrane stabilized in a nanoporous ceramic module. The flux of 1,3-PD (3.86 g/m^2h) and the separation factor (177) reported in their work [17,47] were used as constants for the computation. The same enrichment level from a starting composition of 1% 1,3-PD was calculated to require 2 enrichment steps with a total area of 4660m^2. The thickness of the module reported [47] is 3 mm (with a 7mm inner diameter and 10 mm outer diameter). The nano porous module reported in their work has a porosity of 30% [17, 47]. Thus the total

cyanoborate ionic liquid requirement is 419 cm^3. Assuming a rough density of 1g/cm^3, the cost of material required to achieve the same enrichment level is ~$50,328.

The price versus performance attractiveness, in addition the possibility of fabrication into variety of membrane module designs and scale up offers this novel polymer as a feasible route to the alleviating the downstream process bottleneck of 1,3-PD concentration enrichment in fermentation processes.

Conclusion:

This work developed a novel methacrylate monomer based on a vinylimidazolium-tributylphosphate IL. The IL based methcrylate monomer was polymerized and copolymerized with DVB and BuA by conventional AIBN initiated radical polymerization and fabricatedito plug membranes. Batch pervaporation with 1,3-PD – water binary mixtures showed high separation factors and moderate 1,3-PD fluxes and were studied at varying temperatures and 1,3-PD feed concentrations. The Hildebrand solubility arameters were used to underscore the performance which is determined by the high 1,3-PD solubility and hydrophobicity of the polymers. The polymers can be an easy to use and cheap alternatives to conventional processes and other reported developments.

References

1. A.J. Ragauskas, C.K. Williams, B.H. Davison, G. Britovsek, J. Cairney, C.A. Eckert, W.J. Frederick Jr., J.P. Hallett, D.J. Leak, C.L. Liotta, J.R. Mielenz, R.

Murphy, R. Templer, T. Tschaplinski, The path forward for biofuels and biomaterial, Science. 311 (2010) 484–489.

2. Z.L. Xiu, A.P.Zeng, Present state and perspective of downstream processing of biologically produced 1,3-propanediol and 2,3-butanediol, Appl Microbiol Biotechnol. 78 (2008) 917–926.
3. R.K. Saxena, P. Anand, S. Saran, J. Isar, Microbial production of 1,3-propanediol: Recent developments and emerging opportunities, Biotechnology Advances. 27 (2009) 895–913.
4. A.P. Zeng, H. Biebl, Bulk chemicals from biotechnology: the case of 1,3-propanediol production and the new trends, in: T. Scheper, K. Schugerl, A.P. Zeng (Eds.), Advances in biochemical engineering and biotechnology, Vol. 74, Springer-Verlag, Berlin, Heidelberg, New York, 2002, pp239–59.
5. T.T. Ames, Process for the isolation of 1,3-propanediol from fermentation broth. US Patent 6361983 B1 (2002).
6. Y. Gong, Y. Tong, X.L. Wang, D.H. Liu, The possibility of the desalination of actual 1,3-propanediol fermentation broth by electrodialysis, Desalination. 161 (2004) 169–178.
7. J. Hao, D.H. Liu, Desalination of fermented broth containing 1,3-propanediol by electrodialysis, Chinese J Proc Eng. 5 (2005) 36–39.
8. Z. Li, B. Jiang, D. Zhang, Z. Xiu, Aqueous two-phase extraction of 1,3-propanediol from glycerol-based fermentation broths, Separation and Purification Technology. 66 (2009) 472–478.

9. A. Baiada, A. Vitner, R.P. Jansen, A.M. Baniel, Process for producing 1, 3-propanediol. US Patent 7056439 B2 (2006).
10. A.K. Hilaly, T.P. Binder, Method of recovering 1,3-propanediol from fermentation broth. US Patent 6479716 B2 (2002)
11. J. Hao, F. Xu, H. Liu, D. Liu, Downstream processing of 1,3-propanediol fermentation broth, Journal of Chemical Technology and Biotechnology.81(2006) 102–108.
12. J.J. Malinowski, Reactive Extraction for Downstream Separation of 1,3-Propanediol, Biotechnology Progress. 16 (2000) 76–79.
13. M.H. Cho, S.I. Joen, S.H. Pyo, S. Mun, J.H. Kim, A novel separation and purification process for 1,3-propanediol, Process Biochem. 41 (2006) 739–744.
14. P. Anand, R.K. Saxena, R.G. Marwah, A novel downstream process for 1,3-propanediol from glycerol-based fermentation, Appl. Microbiol. Biotechnol. 90 (2011) 1267–1276.
15. S. Li, V.A. Tuan, J.L. Falconer, R.D, Noble, Separation of 1,3- propanediol from glycerol and glucose using a ZSM-5 zeolite membrane, J. Membr Sci. 191 (2001a) 53–59.
16. S. Li, V.A. Tuan, J.L. Falconer, R.D. Noble, Separation of 1,3- propanediol from aqueous solutions using pervaporation through an X-type zeolite membrane, Ind Eng Chem Res 40 (2001b) 1952– 1959.
17. P.Izák, M. Köckerling, U. Kragl, Stability and selectivity of a multiphase membrane, consisting of dimethylpolysiloxane on an ionic liquid, used in the separation of solutes from aqueous mixtures by pervaporation, Green Chem. 8 (2006) 947–948.

18. P. Shao, R.Y.M. Huang, Polymeric membrane pervaporation, Journal of Membrane Science. 287 (2007) 162-179.
19. M. Mulder, T. Franken, C.A. Smolders, Preferential sorption versus preferential permeability in pervaporation, J. Membr. Sci. 22 (1985) 155–173
20. W.J.Koros, Membranes: Learning a lesson from nature, Chem Eng. Prog. 91 (1995) 68–81
21. E. Kuhlman, S. Himmler, H. Giebelhaus, P. Wasserscheid, Imidazolium dialylphosphates – a class of versatile, alogen – free and hydrolutically stable ionic liquids, Green Chemistry, 2007, 9, 233-242
22. F. Endres and S. Z. El Abedin, *Phys. Chem. Chem. Phys.*, 2006, **8**, 2101–2116
23. R. Kawano, H. Matsui, C. Matsuyama, A. Sato, M. A. B. H. Susan, N. Tanabe and M. Watanabe, *J. Photochem. Photobiol., A*, 2004, **164**, 87
24. A. Bosmann and T. J. S. Schubert, GB 2005-10772 2414553, 2005
25. T. Brinz and U. Simon, Robert Bosch GmbH, DE 2002-10245337 10245337, 2004
26. K. Fukumoto, M. Yoshizawa and H. Ohno, *J. Am. Chem. Soc.*, 2005, **127**, 2398
27. M. Earle in *Ionic Liquids in Synthesis, 2003,* ed. P. Wasserscheid and T. Welton, Wiley-VCH, Weinheim, 2003, pp. 174–213
28. T. Welton and P. J. Smith, *Adv. Organomet. Chem.*, 2004, **51**, 251
29. R. A. Sheldon, R. M. Lau, M. J. Sorgedrager, F. van Rantwijk and K. R. Seddon, *Green Chem.*, 2002, **4**, 147
30. N.M. Kocherginsky, Q. Yang, L. Seelam, Recent advances in supported liquid membrane technology. Separation and Purification Technology, Separation and Purification Technology 53 (2007) 171–177.

31. J.J. Malinowski, Evaluation of liquid extraction potentials for downstream separation of1,3-propanediol, Biotechnology Techniques 13: 127–130, 1999.
32. J. Yuan, M. Antonietti, Poly(ionic liquid)s: Polymers expanding classical property profiles, Polymer 52 (2011) 1469 – 1482
33. U. Mansfeld, C.Pietsch, R.Hoogenboom, C.Remzi Becer, U.S. Schubert, Clickable initiators, monomers and polymers in controlled radical polymerizations – a prospective combination in polymer science, Polym. Chem. 1 (2010) 1560–1598.
34. Y. Xia, R.C.Larock, Castor oil-based thermosets with varied crosslink densities prepared by ring-opening metathesis polymerization (ROMP), Polymer 51 (2010) 2508-2514.
35. S. Li, R. Srivastava, R.S. Parnas, Separation of 1-butanol by pervaporation using a novel tri-layer PDMS composite membrane, J. Membr. Sci. 363 (2010) 287–294
36. T. Boyle, A. Szopinski, A. Verrall, Method and apparatus for continuously preparing crosslinked, solution–cast polymer film. US Patent 20070085235 A1 (2007)
37. Q. Guo, P.N. Pintauro, H. Tang, S.O'Connor, Sulfonated and cosslinked polyphosphazene – based proton – exchange membranes, J. Membr. Sci. 154 (1999) 175 – 181.
38. C. Maton, N. De Vos, C. V. Stevens, Ionic liquid thermal stabilities: decomposition mechanisms and analysis tools, **Chem. Soc. Rev.,** 2013,**42,** 5963-5977
39. H. Ohno, M. Yoshizawa, W. Ogihara, Electrichimica Acta 50(2004) 255-261
40. W. Ogihara, S. Washiro, H. Nakajima, H. Ohno, Electrochimica Acta 51 (2006) 2614-2619

41. H. Nakajima, H. Ohno, Polymer 46 (2005) 11499 – 11504
42. X. Wang, Y. Chi, T. Mu, Journal of Molecular Liquids 193 (2014) 262 – 216
43. D. Zheng, L. Dong, W. Huang, X. Wu, N. Nie, A review of imidazolium ionic liquids research and development towards working pair of absorption cycle, Renewable and Sustainable Energy Reviews, 37 (2014) 47 – 68
44. K. Vijayakrishna, S.K. Jewrajka, A. Ruiz, R. Marcilla, J.A. Pomposo, D. Mecerreyes, D. Taton, Y. Gnanou, Macromolecules, 41 (2008), pp. 6299–6308
45. R.P. Swatloski, J.D. Holbrey, R.D. Rogers, Green Chem , 2003 5, 361
46. R. Marcilla, J. Alberto Blazquez, J. Rodriguez, J.A. Pomposo, D. Mecerreyes, J Polym Sci Part A Polym Chem, 42 (2004), pp. 208–212
47. P. Izak, M. Köckerling, U. Kragl, Mehrphasen–Membran. German Patent DE102006024397 B3 (2007).
48. Sigma Alridch, www.sigmaaldrich.com, (accessed November 2013)
49. Oakwood Chemicals Inc, http://www.oakwoodchemical.com/ProductsList.aspx?CategoryID=-2&txtSearch=51553&ExtHyperLink=1, (accessed November 2013)
50. Fluorochem Ltd., http://www.fluorochem.co.uk/Products/Product?Code=062234, (accessed November 2013)

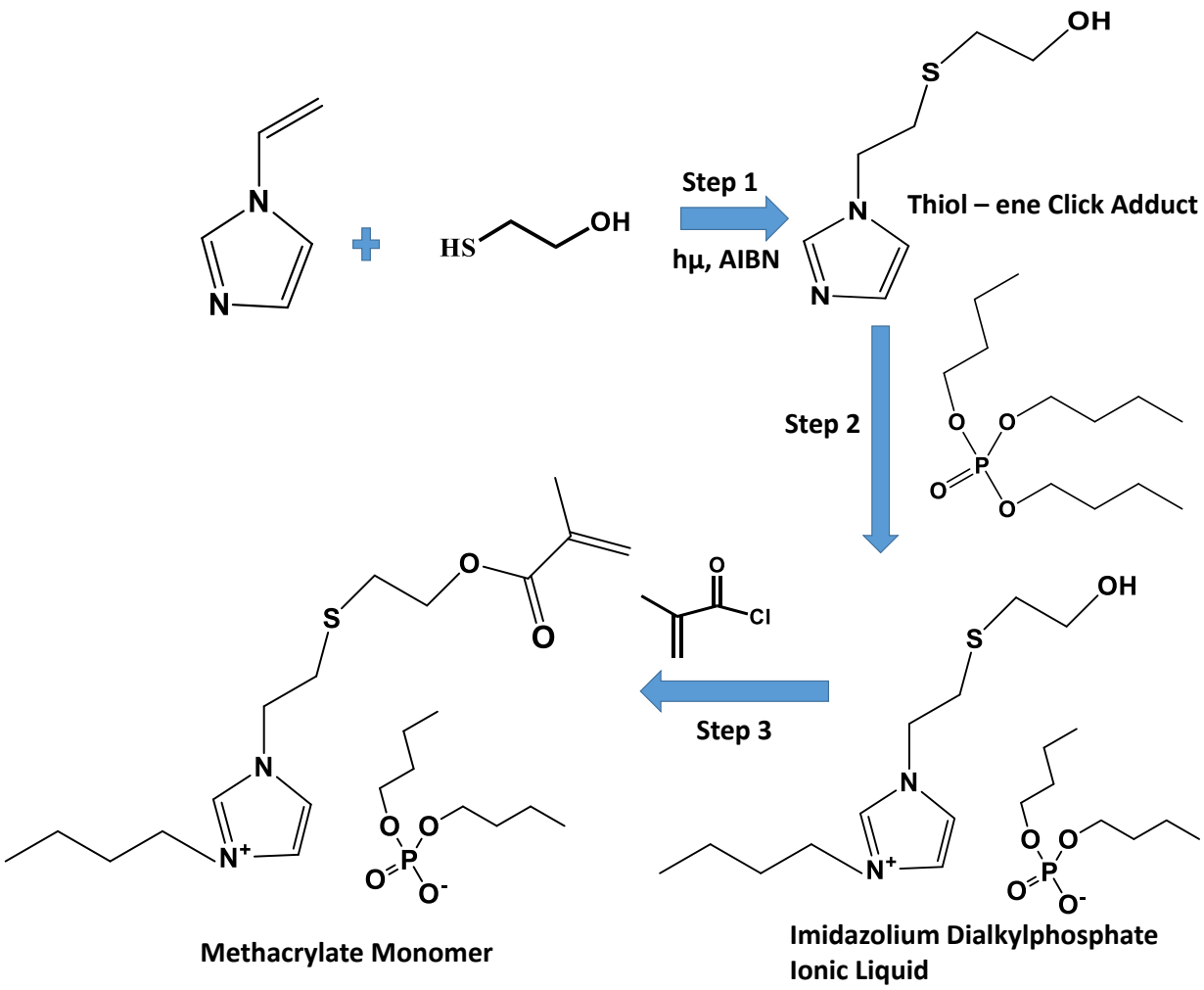

Figure 6.1: Monomer Synthesis Scheme

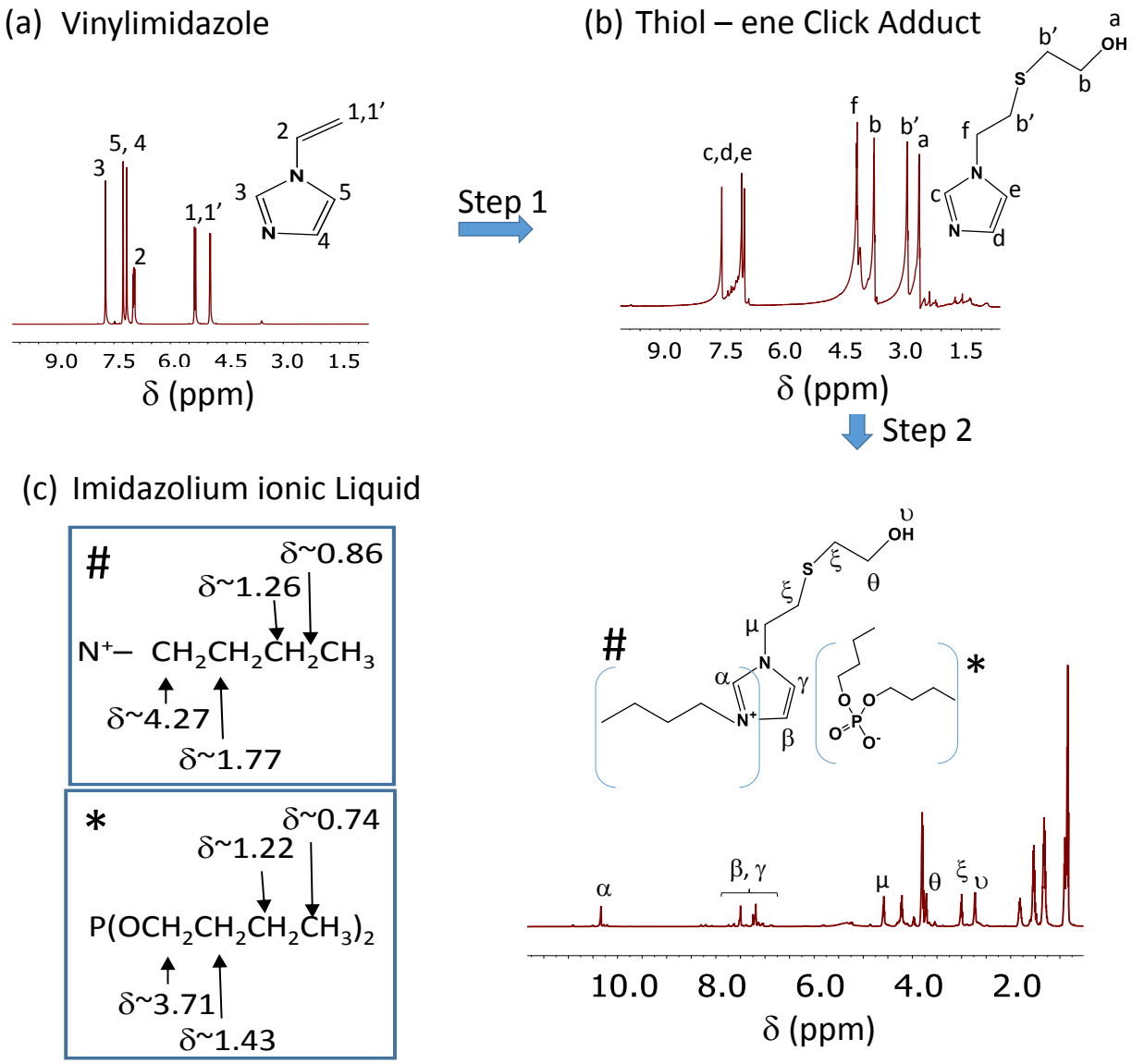

Figure 6.2: NMR of the monomer synthesis scheme (a) Vinylimidazole ^{1}H NMR, (b) Thiol – ene click adduct ^{1}H NMR, (c) Imidzolium ionic liquid ^{1}H NMR, Insets showing the proton shifts for the butyl group attached to Imidazolium nitrogen and the dibutyl phosphate counter anion

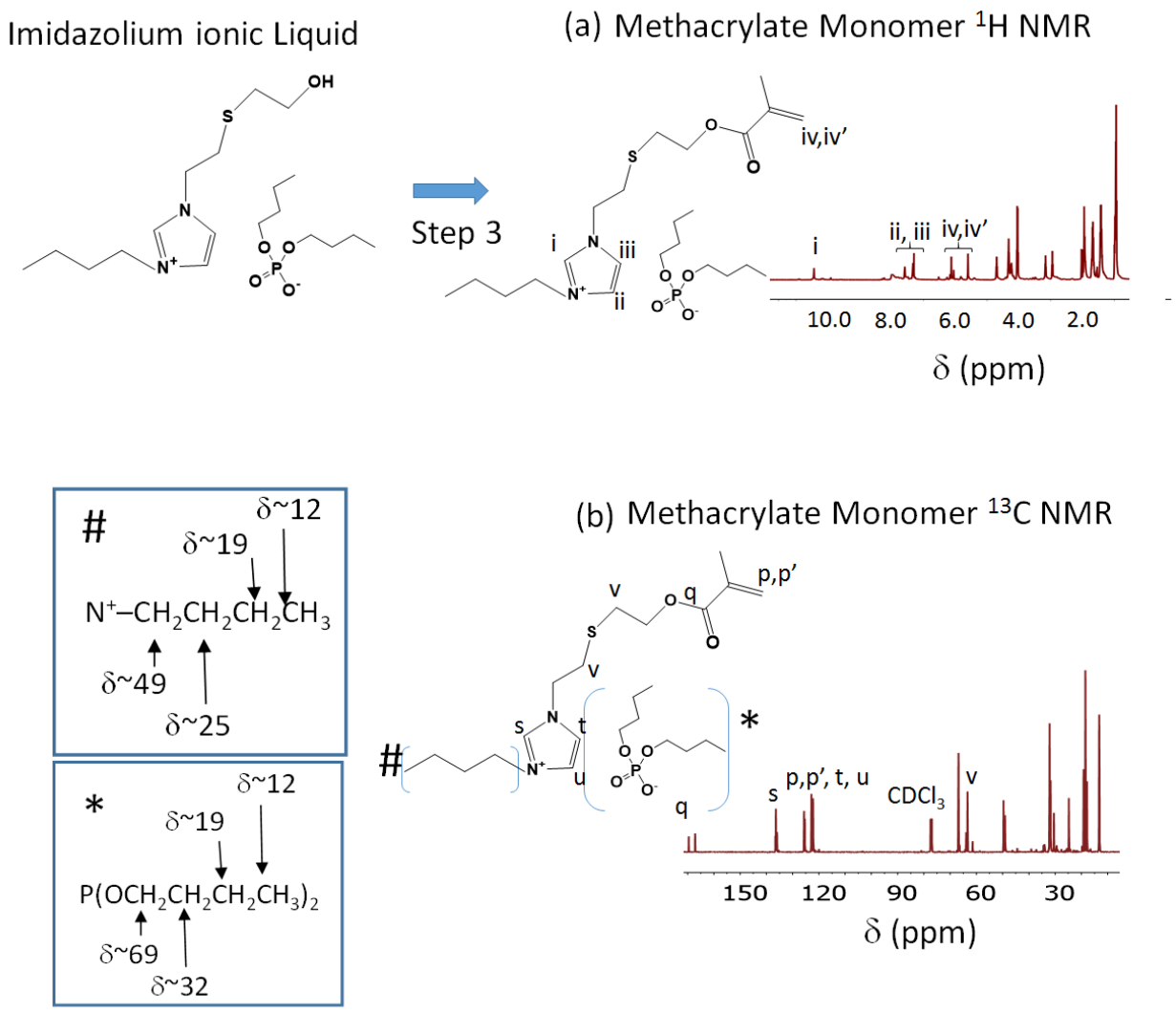

Figure 6.3: NMR of the monomer synthesis scheme (a) Methacrylate monomer ^{1}H NMR, (b) Methacrylate Monomer ^{13}C NMR, Insets showing the carbon shifts for the butyl group attached to Imidazolium nitrogen and the dibutyl phosphate counter anion

(a)

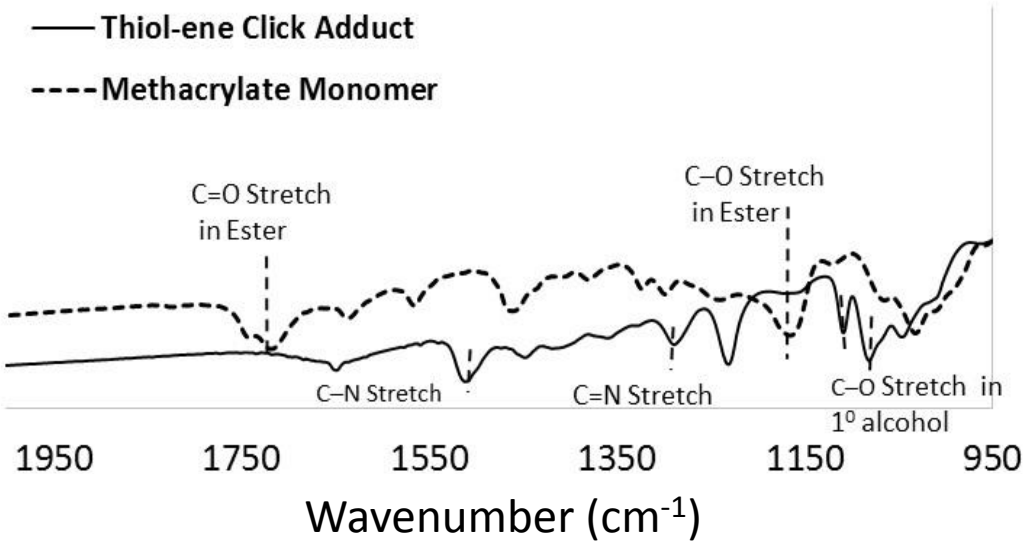

(b)

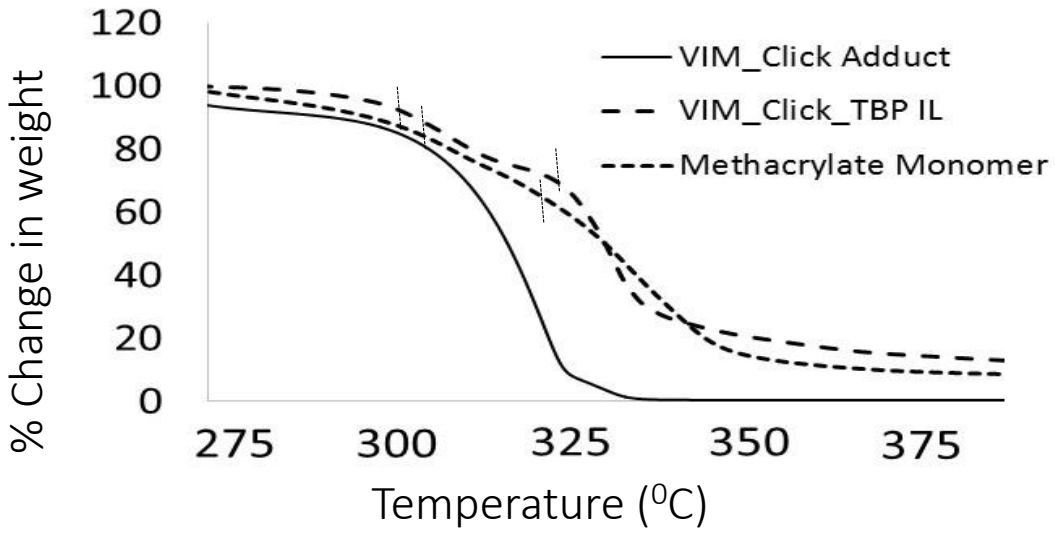

Figure 6.4: Monomer Characterization (a) FTIR, (b) TGA

(a)

Drop of methacrylate monomer in Water

(b)

Drop of methacrylate monomer in 1,3-PD

Figure 6.5: Photographs of monomer solubility (a) In water, arrow indicating the insoluble droplet of monomer in water (b) In 1,3-propanediol

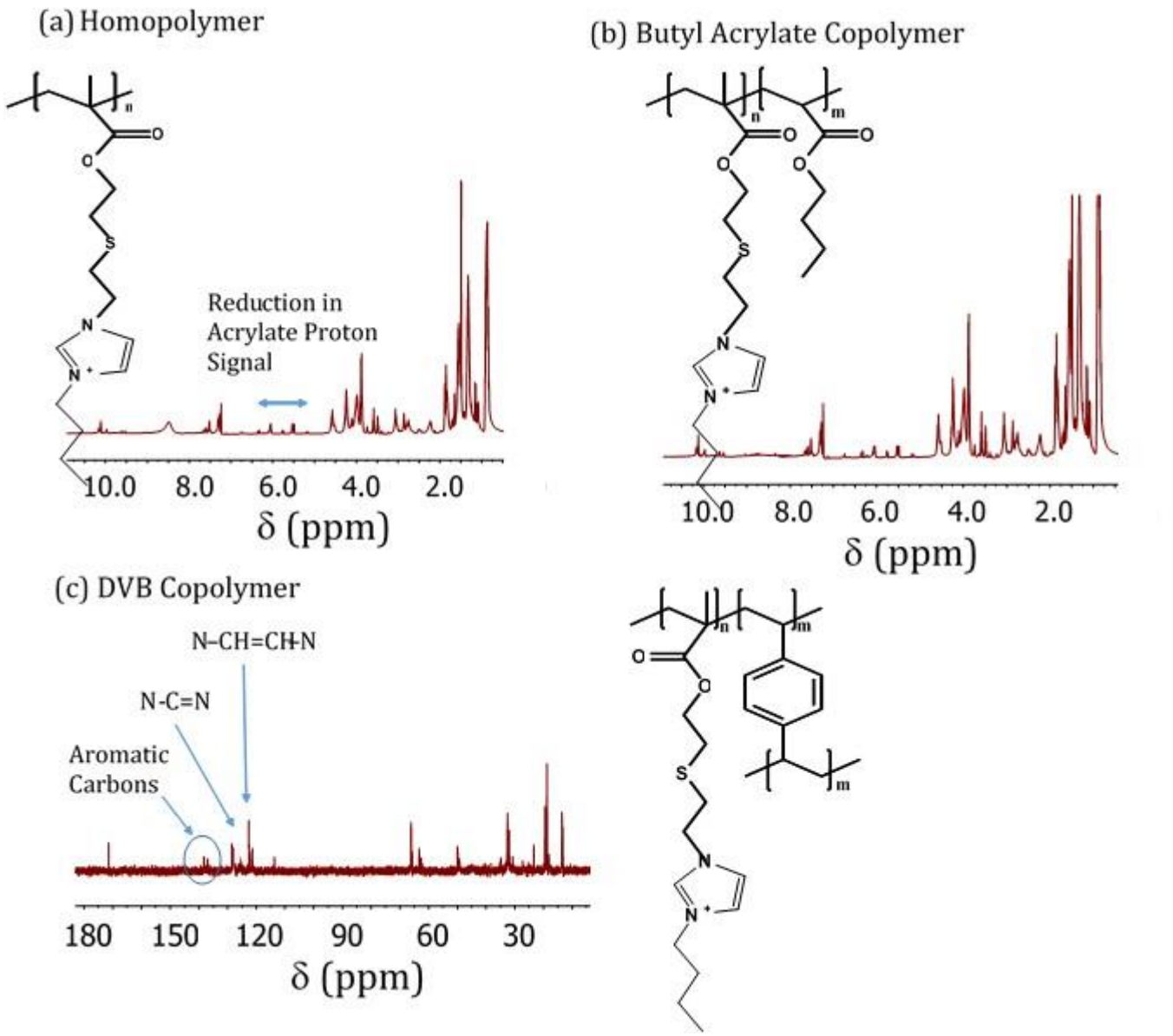

Figure 6.6: NMR of the polymers (a) PVIM - Homopolymer ^{1}H NMR , (b) PVIM_BuA Copolymer ^{1}H NMR, (c) PVIM_DVB Copolymer ^{13}C NMR

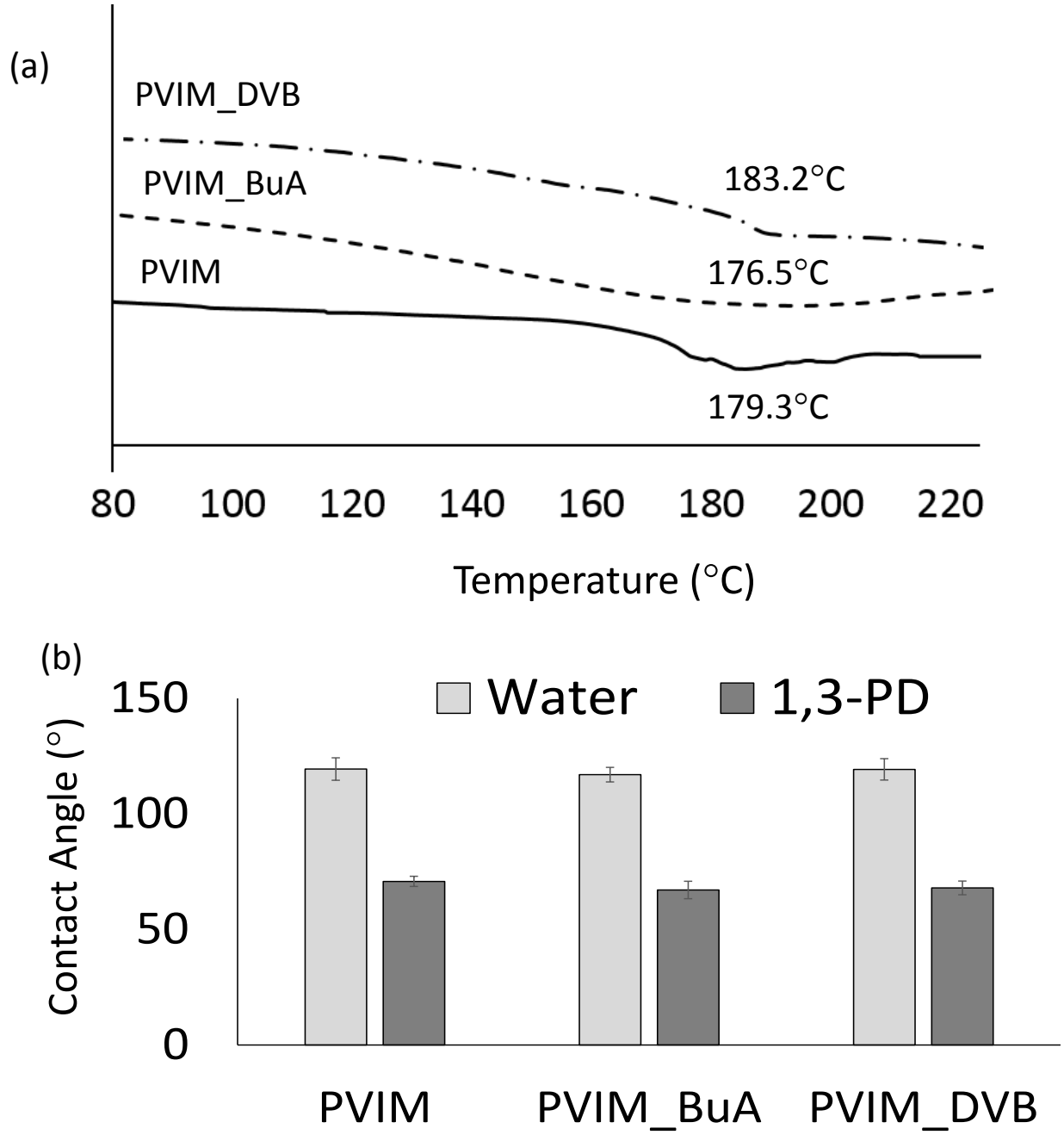

Figure 6.7: Polymer Characterization (a) DSC (b) Contact Angle

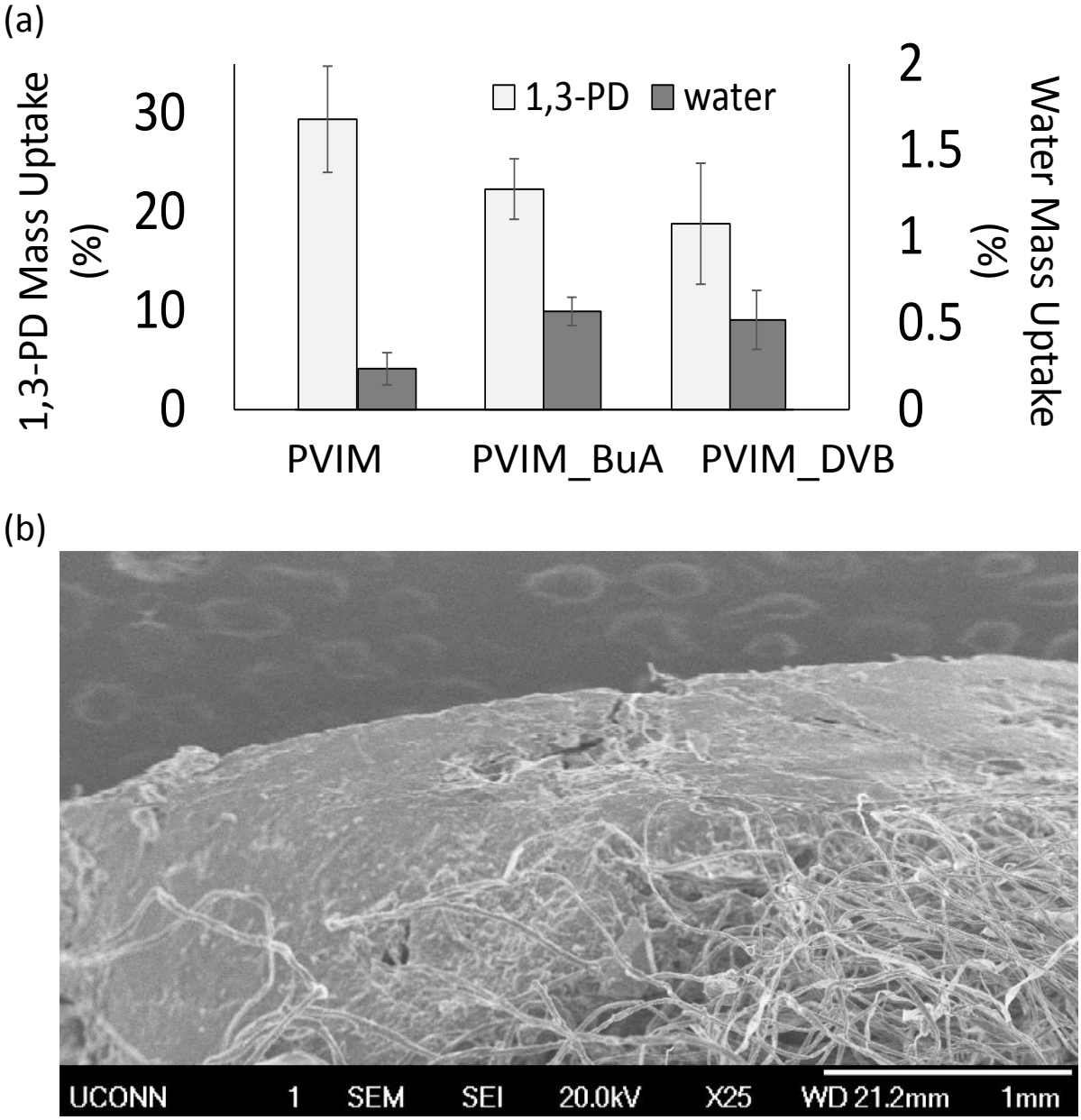

Figure 6.8: Polymer Characterization and Plug Membrane Fabrication (a) Mass Uptake, (b) FESEM of membrane plug section.

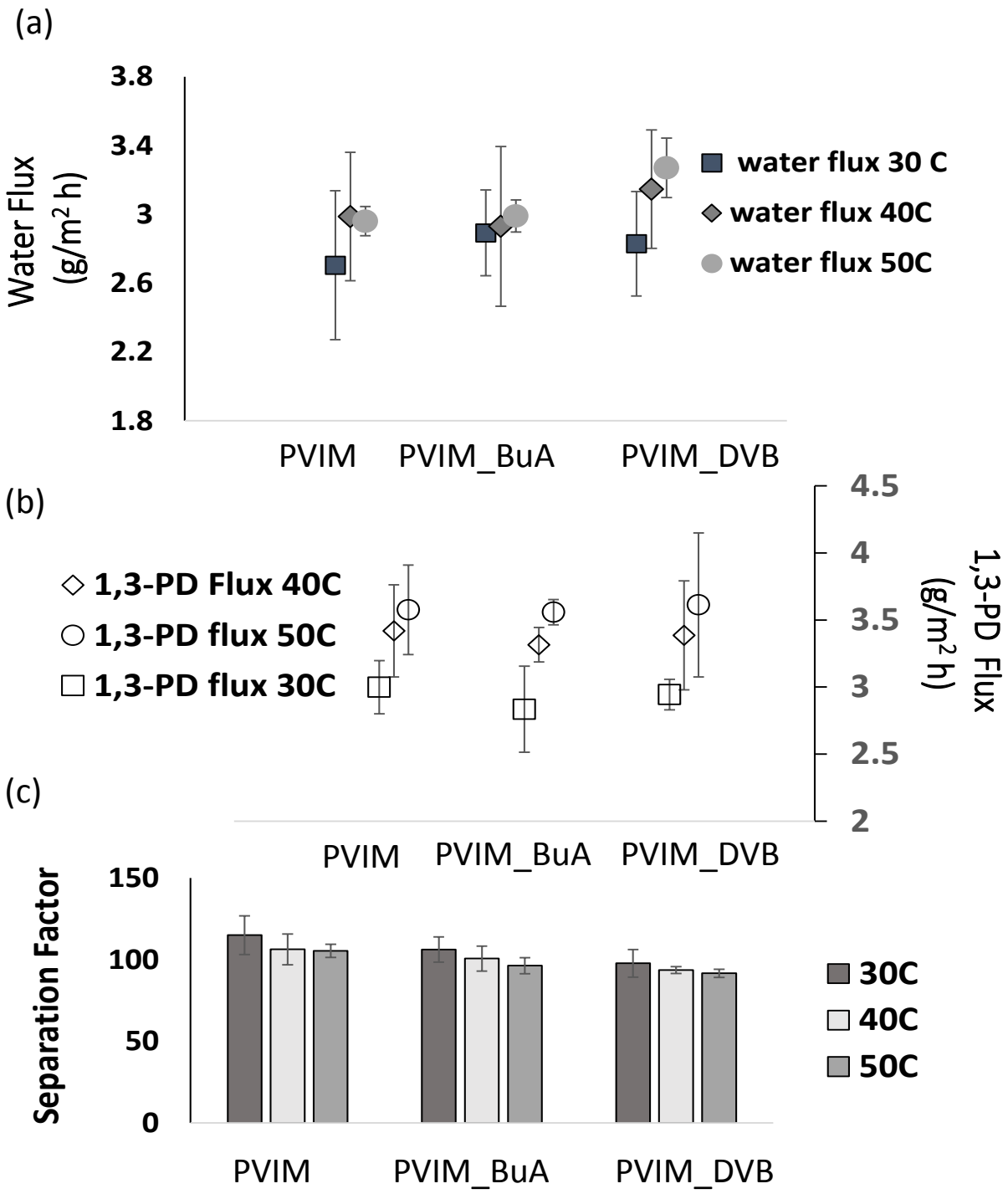

Figure 6.9: Component flux and separation factors with varying temperatures (a) Water Flux (b) 1,3-PD (c) Separation factors

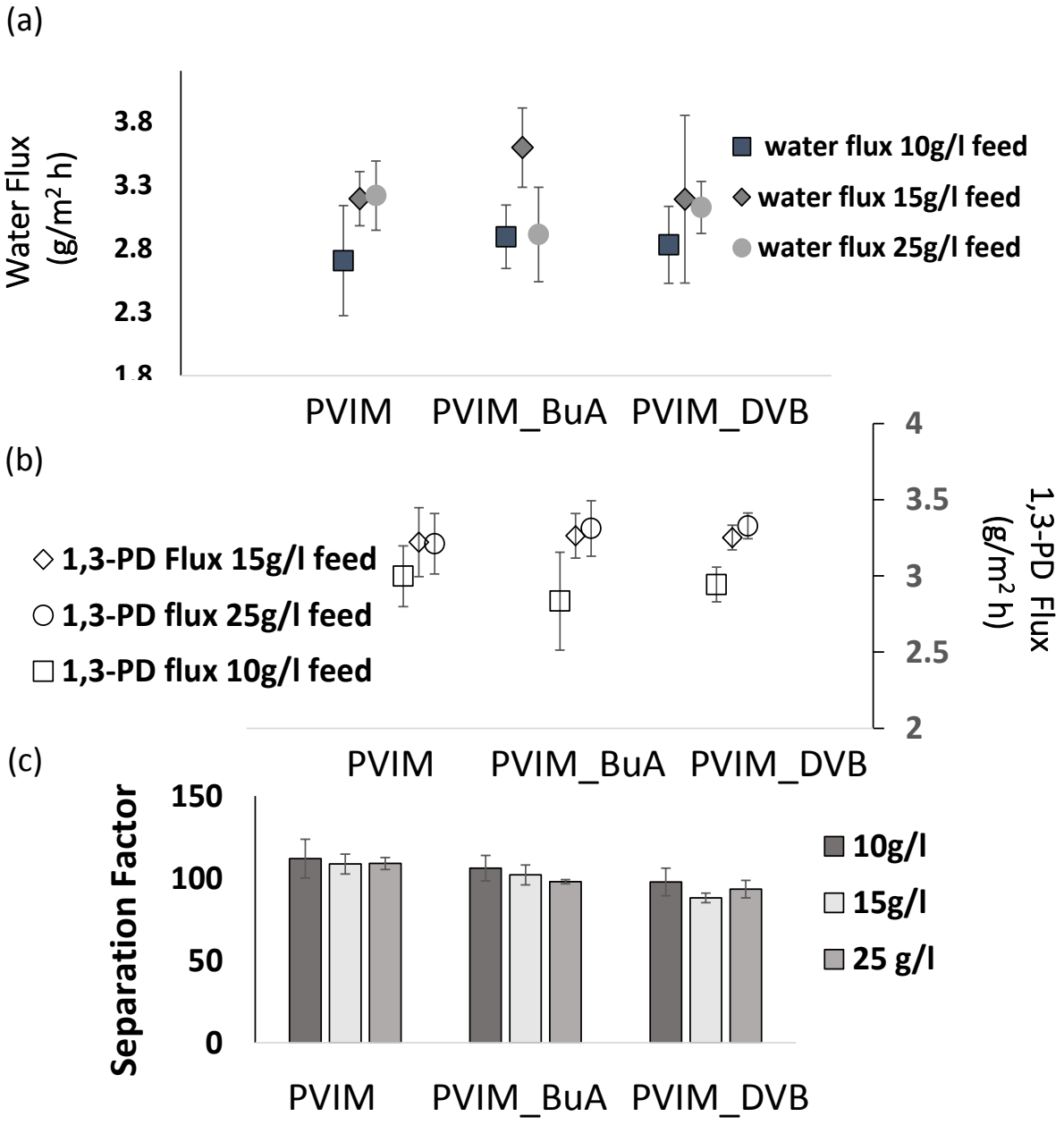

Figure 6.10: Component flux and separation factors with varying feed 1,3-PD concentrations (a) Water Flux (b) 1,3-PD (c) Separation factors

Chapter 7. Pervaporative enrichment of 1,3-propanediol from model fermentation broths by hydrophobic specialty polymers

Abstract

The present work describes a study on the pervaporation enrichment of 1,3-propanediol from model fermentation broths using three hydrophobic polymer families – functionalized siloxanes, cyclohexylamine base methacrylates and imidazolium ionic liquid based methacrylates with progressively increasing separation efficiency. While the highest 1,3-PD permeabilities were seen with the siloxane polymers, the imidazolium IL based methacrylates exhibited the best separation factors both with respect to water and glycerol. The effect of glycerol on transport coupling was evaluated. The permeability and separation factors from the pervaporation experiments with these polymers were siloxanes were collated to arrive at a Robeson's upper bound of pervaporation of 1,3-propanediol from aqueous solution by polymeric membranes.

Keywords: 1,3-propanediol, membranes, pervaporation

1. Introduction

The production of 5 – 10 gallons of crude glycerol for every 100 gallons of biodiesel, in addition to glycerol being produced as a byproduct from other industries, has led to a current glycerol overcapacity [1]. The bio-fermentation of crude glycerol to 1,3-propanediol as a value added product gives a recourse to capitalizing on the current over capacity of glycerol as it does to improve the economic viability of biodiesel production [1]. The principle process bottleneck in fermentative conversion of glycerol to 1,3-PD lies in the downstream enrichment of 1,3-PD concentration given that it has to be enriched from very low starting concentrations [2-4]. While the main difficulty lies in enriching 1,3-propanediol from water, it also needs to be separated from other products of fermentation [2, 5]. Conventional processes, like evaporation, chromatography and reactive extraction amongst others are associated with either high energy usage or yield and process complication issues [5-18]. Pervaporation mitigates the challenge of high energy associated with processes involving phase change as it deals with the minor component [19]. Additionally, pervaporation membranes are tailored to have affinities to favor the enrichment of a select component. Pervaporation has found viable application in solvent dehydration, removal of volatile organic content, aroma recovery and some organic/organic separations [19].

Water, as a smaller molecule, diffuses faster than 1,3-PD. Thus, membrane materials with a high preferential sorption of 1,3-PD and low water solubility allow preferential permeation of 1,3-PD across a membrane [19, 20]. A real time fermentation

system deals with separating 1,3-PD from other broth components in addition to water. The presence of glycerol in concentrations, at times, exceeding those of 1,3-PD makes it an important factor in affecting separation efficacy. The membrane affinity for each individual component and the ability of each individual component to effect a coupled transport phenomenon drives the eventual efficacy of the membrane, both in enriching 1,3-PD from water as well as separating it from other broth components [19].

The pervaporative separation of 1,3-PD from model aqueous fermentation broths has been studied in earlier work on zeolite membranes [16, 17]. However, since such membranes work by size exclusion processes, the systems proved to be selective towards water [16, 17]. Izak et al reported the application of a cyanoborate ionic liquid based supported liquid membrane in batch pervaporation with high separation factors for 1,3-PD enrichment from binary aqueous feed [18].

While the membranes examined in this work base their separation efficacy on the wide difference in solubility of water and 1,3-PD, a compromise on the 1,3-PD flux becomes unavoidable to achieve a high separation factor. A hydrophilic membrane with a 1,3-PD mass uptake several times that of water may prove to be inefficient in separating 1,3-PD from water. While, ideally, its sorption characteristics may tilt the balance in favor of 1,3-PD permeation, coupling of water transport with 1,3-PD along with swelling of the membrane allows for water permeation greater than expected reducing the separation efficacy despite showing higher flux. Preferred membrane chemistries are hence those that not only have large differences between mass uptakes of water and 1,3-PD but also

concomitantly reject water [21]. As a caveat, such structures also have a limitation in their affinity towards 1,3-PD, owing to the proximity of thermodynamic parameters of 1,3-PD and water, which contribute to the limitation in flux, resulting in the upper bound [22]. The development and fine tuning of such materials and membrane structures based on a combination of 1,3-PD enriching materials are steps towards establishment of commercially viable and energy efficient alternatives to conventional purification processes.

In this paper, three membrane material systems are examined for properties and pervaporation performance with simulated model broth compositions. The first system is an allylcyclohexylamine functionalized siloxane and its phase separated blend with styrene-butyl acrylate copolymer. The phase separated blend allowed for the recovery of mechanical strength lost due to functionalization without loss in separation performance. The second system is a conventional radical polymer based on an allylcyclohexylamine based methacrylate monomer which was synthesized using thiol-ene click chemistry. The third material is also a methacrylate polymer system based on an ionic liquid of tributyl phosphate (TBP). Its synthesis involved the conversion of vinyl imidazole into an alcohol using a thiol-ene click chemistry step. This was followed by the formation of an imidazolium ionic liquid by high temperature reaction with TBP, in which the dibutylphosphate anion formed the counter ion for the imidazolium cation. The remnant hydroxyl on the IL was subsequently esterified and converted to a methacrylate monomer which was then polymerized by simple radical polymerization. All three systems are hydrophobic materials with high affinity for 1,3-propanediol. The pervaporative performance is examined with continuous pervaporation in one material system, while the

other two are studied in a batch pervaporation set up with a small plug membrane. The separation factors of 1,3-PD over water as well as its preferential enrichment over other broth components is examined with respect to temperature and glycerol concentration. Coupling effects were examined by comparing results under similar process conditions with binary 1,3-PD feed mixtures. The effect of temperature on the coupling was also evaluated. The permeability and separation factors were collated from this work and compared with earlier works on binary mixtures, zeolite membranes and ionic liquid supported liquid membrane systems to estimate a Robeson's upper bound for pervaporative enrichment of 1,3-PD.

2.Experimental

2.1 Materials:

Poly(methylhydrosiloxane) (PHMS) of degree of polymerization ~ 35 to 40, Allylcyclohexyl amine (ACA), Vinylimidazole (VIM), Tributyl Phosphate (TBP), Methacryloyl chloride, Styrene, Divinyl benzene (DVB) and Butyl acrylate monomer (BuA) were dried prior to use. The Chloroplatinic acid, Dibutyl Tin dilaurate, Potassium persulphate, tert-Butyl perbenzoate, Sodium bicarbonate, Sodium dodecylbenzenesulfonate, AIBN radical initiator and Tetraethyl orthosilicate (TEOS) were used without modification. 1,3 propanediol (1,3-PD), 98% purity, Glycerol, Ethanol, Butyric Acid and Acetic Acid were used for the partition coefficient measurements and for preparation of binary mixtures with distilled water as feed solutions for pervaporation experiments. The solvents Toluene, Chloroform, Dioxane and Hexane were dried prior to use. All chemicals were purchased from Sigma Aldrich. Porous polyethylene sheets were

obtained from Interstate Specialty Products for use as the support sheet for membrane fabrication. The nominal thickness reported was 500 microns with pore diameters of 75 - 110 microns and a porosity of 48%. For the fabrication of the plug membranes, 0.65cm inner diameter glass pipettes from Fischer were used. Cotton wool was used to act as the porous support base and was purchased from the local market.

2.2 Polymer Synthesis and Membrane Fabrication

2.2.1Allylcyclohexylamine functionalized Siloxane polymer and phase-separated blend

The PHMS was functionalized with ACA by hydrosilylation using the Chloroplatinic acid catalyst solution. The reaction was carried out in a clean and dry glass pressure tube flushed with high purity argon on a schlenk line. A 25mg/ml chloroplatinic acid catalyst solution in isopropanol was prepared. A typical run consisted of 1.5 g PHMS with varying quantities of ACA, depending upon the targeted extents of substitution, and 1 ml of toluene as solvent. The catalyst solution was added to the extent of 5 μl/ml of reaction volume. The reaction temperature was controlled at 70 $\pm 2^0$C. All reagents were thoroughly dried prior to use.

A high molecular weight Styrene-Butyl acrylate copolymer (SBA) was synthesized by emulsion polymerization. The reaction was carried out at 80^0C in a 250 ml two necked round bottom flask fitted with a reflux condenser with the system being constantly purged with nitrogen. A typical batch consisted of 50 g deionized water, 0.5g Potassium Persulphate, 0.25g Sodium Bicarbonate, 1g Sodium dodecylbenzenesulfonate 0.25g tert-

Butyl perbenzoate, 50g Butyl acrylate and 50g Styrene. Sodium bicarbonate and Sodium dodecylbenzenesulfonate were added beforehand and the monomer mixture was added dropwise over a period of 15 minutes through the second neck. After the monomer addition, the temperature was reduced to 65^0C and the Potassium Persulphate and tert-Butyl perbenzoate added and the reaction was allowed to run for 2 hours. A silicone rubber tube fitted with a needle was used to blanket the surface of the reaction mixture with nitrogen throughout the 2h course of the reaction. At the end of the reaction, the emulsion was flocculated by Sodium Chloride, the flocculated polymer washed thoroughly and repeatedly, centrifuged and dried at room temperature. ACA functionalized PHMS polymers were blended with the emulsion polymerized Styrene-Butylacrylae polymer (SBA) and TEOS. The SBA and TEOS were kept at 10% and 2% of the total weight while the Dibutyl Tin Dilaurate catalyst was kept at 0.1% by weight of the mixture. A small amount of toluene was added to this mixture to lower its viscosity. A piece of porous Polyethylene sheet was soaked in measured quantities of this mixture and the solvent was allowed to evaporate at room temperature over a period of ~ 24 hours. The membrane was then allowed to cure at 60^0C for 4 days to ensure completion of crosslinking and cut to the required shape. Membranes were fabricated using 50%, 70% and 90% ACA functionalized PHMS and were given the nomenclature 50ACA, 70ACA and 90ACA respectively. The details of polymerization, polymer characterization and membrane fabrication are delineated in Chapter 4. The chemical structure of the membrane polymer is shown in Figure 7.1 (a).

2.2.2 Allylcyclohexylamine based methacrylate polymer and copolymers

A thiol-ene click chemistry adduct was synthesized by AIBN mediated addition of the allyl double bond of the ACA to the thiol bond of mercaptoethanol. The reaction was carried out in a pressure tube, in bulk, and in the presence of UV light at 60^0C. The pressure tube was degassed with dry argon in a schlenk line and the reactants kept under argon pressure. The click adduct was esterified using methacryloyl chloride and triethyl amine as the catalyst to form the methacrylate monomer. The click adduct was dissolved in dry toluene and a stoichiometric amount of methacryloyl chloride and triethylamine were added, and the mixture was refluxed at 70^0C for 12 hours. The toluene was evaporated from the system at 40^0C overnight. The resultant mixture of the methacrylate monomer and triethyamine hydrochloride was added to hexane. The triethyamine hydrochloride being hexane insoluble separated out, and the supernatant fluid containing the methacrylate monomer was filtered and the hexane evaporated overnight in a vacuum oven at 40^0C. AIBN initiated radical polymerization was carried out in dioxane solvent with the methacrylate monomer. The methacrylate monomer was also copolymerized with 5mol% BuA or 5mol% DVB. The resultant polymers are referred to below as P(Acryl), P(Acryl)_BuA and P(Acryl)_DVB, respectively. The polymerizations were carried out at 70^0C in a 250 ml two necked round bottom flask fitted with a reflux condenser with the system being constantly purged with nitrogen. Plug membranes were fabricated inside 0.65 cm inner diameter glass pipettes. The glass pipettes were weighed and stuffed with a known weight of dry cotton wool. A small, but known weight of dry cotton wool was soaked with the polymer solution and the solvent allowed to evaporate slowly at 40C over a period of 3-4 days. When the solvent had nearly all evaporated, the polymer solution soaked cotton wool

was lightly pressed with a flat surface to set the membrane on top of the cotton wool base inside the glass pipettes, and the weight of the plug noted. The solvent was allowed to further evaporate over a period of 1 week at room temperature till the plug attained a constant weight. The slow solvent evaporation was carried out to prevent the formation of pinholes and to allow the plug membrane to adhere to the inner wall of the glass pipettes. This process gave rise to a fiber supported membrane structure. The volume inside the glass pipette above the membrane was used to hold ~1.5-1.7 ml of pervaporation feed solution. The details of polymer synthesis, characterization, membrane fabrication and characterization are delineated in Chapter 5. The chemical structure of the membrane polymers is shown in Figure 7.1 (b).

2.2.3 Imidazolium alkylphosphate ionic liquid based methacrylate polymer and copolymer:

A thiol-ene click chemistry adduct was synthesized by AIBN mediated addition of the vinyl double bond of the VIM to the thiol bond of mercaptoethanol. The solventless reaction was carried out in a schlenk tube at 60^0C in the presence of UV and catalyzed by AIBN. The reactants were weighed out in stoichiometric amount. The click adduct was subsequently reacted with TBP at 140^0C. The dibutyl phosphate anion serves as the counter ion for the imidazolium cation in this ionic liquid. The remnant hydroxyl group from the mercaptoethanol moiety on the ionic liquid was subsequently esterified using methacryloyl chloride and triethyl amine as the catalyst as per the method detailed in the previous section. The methacrylate monomer was homopolymerized and copolymerized separately with

5mol% of BuA, and 5mol% of DVB using AIBN initiator. The nomenclatures for these polymers were PVIM, PVIM_BuA and PVIM_DVB for the homopolymer, butyl acrylate copolymer and divinylbenzene copolymer respectively. The details of polymer synthesis, characterization, membrane fabrication and characterization are delineated in Chapter 6. The chemical structure of the membrane polymer is shown in Figure 7.1 (c). Plug membranes were fabricated as per the method detailed in the previous section.

2.3 Feed Compositions:

The model broth feed compositions to the membranes were kept close to the compositions of the fermentation product streams obtained for steady states with CSTR runs reported in Chapter 2. The three membrane feed compositions were as follows and they represent the compositions obtained with fermentation product streams at dilution rates of $0.04h^{-}1$, $0.11h^{-1}$ and $0.19h^{-1}$ respectively:

Feed composition M1: 1,3 PD: 10 g/l, Glycerol :15 g/l, Acetic Acid: 1.5 g/l , Butyric acid: 2 g/l, Ethanol: 0.5 g/l

Feed composition M2: 1,3 PD: 6 g/l, Glycerol :25 g/l, Acetic Acid: 1 g/l , Butyric acid: 1.5 g/l, Ethanol: 0.2 g/l

Feed composition M3: 1,3 PD: 3 g/l, Glycerol :30 g/l, Acetic Acid: 0.5 g/l , Butyric acid: 0.5 g/l, Ethanol: 0.1 g/l

M1, M2, M3, represent membrane feed compositions corresponding to the fermentation product stream obtained from using fermentation feed composition optimized by the

Design of experiment (detailed in Chapter 2) at dilution rates of $0.04h^{-1}$, $0.1h^{-1}$ and $0.19\ h^{-1}$ respectively.

2.4 Analytical Methods:

The concentrations of individual components in the initial feed solutions and permeate samples from the pervaporation experiments were analyzed using 0.22μm syringe filtered aqueous samples by gas chromatography (GC) using a DB-FFAP capillary column and an MS detector and a 1μL injection volume. GC injector, detector and initial oven temperatures were kept at 240C, 270C, and 40C respectively. The GC was standardized with broth compositions of progressively increasing concentration of each component.

2.5 Partition Coefficient Measurement:

The partition coefficient of 1,3-PD, glycerol, ethanol, acetic acid and butyric acid between water and TBP and between water and ACA was determined at 30C. 1 ml of a 10g/l solution of the respective component was mixed with 1ml of TBP or ACA for 15 minutes and the layers allowed to separate. The concentration of each tested component in the aqueous phase was determined by GC before and after partitioning. The following equation was used to compute the coefficient of partition:

$$K_p = \frac{C_{organic\ phase}}{C_{water}} \quad \text{----------(1)}$$

2.6 Pervaporation experiments:

2.6.1 Continuous Pervaporation :

Continuous Pervaporation was carried out on Functionalized Siloxane membranes (50ACA, 70ACA and 90ACA). Pervaporation was carried out in a custom made membrane holder providing a pervaporation area of 43cm^2. It was fabricated at the Technical Services Facility at University of Connecticut [21]. The feed solutions consisting of 1,3-PD-water binary mixtures were maintained at various temperatures. The feed solutions were recirculated over the membrane on a perforated brass support in the membrane holder by a peristaltic pump, providing a range of controllable cross flow rates. The permeate was collected in two parallel cold traps, cooled in a dry ice – acetone bath. A vacuum pump was employed to maintain the permeate side pressure at less than 1 mm Hg. Permeate samples were collected at regular time intervals until steady state was reached. The permeate compositions were analyzed by gas chromatography. The pervaporation equipment used and its schematic are detailed in an earlier work by Li et al 2010 [21]. Pervaporation experiments were carried out at a constant cross flow rate of 32l/h and temperatures of 30^{0}C, 40^{0}C and 50^{0}C using the feed compositions detailed in the earlier section. The feed composition was also evaluated from time to time to verify the concentrations of the components. The key performance indicators of the pervaporation experiment were the component fluxes and the separation factor defined as:

$$\alpha = \frac{\frac{J_i}{J_j}}{\frac{x_i}{x_j}} \text{ ----------(2)}$$

Where J_i and J_j represent the fluxes of the i^{th} and j^{th} component and x_i and x_j represent the feed mass fractions of the i^{th} and j^{th} component, respectively.

2.6.2 Batch Pervaporation

Batch pervaporation was carried out on the Allylcyclohexylamine based methacrylate polymers [P(Acryl), P(Acryl)_BuA and (PAcryl)_DVB)] as well as the imidazolium dialkylphosphate based methacrylate polymers [PVIM, PVIM_BuA and PVIM_DVB] using plug membranes fabricated as described above. The plug structures were affixed in an upright position in a water bath at 30^0C. The plug membrane had a pervaporation area of 4.91 mm^2. Each batch pervaporation experiment was allowed to run for a period of 20 - 25 hours and the permeate collected in a small dry–ice cooled trap. A vacuum pump was employed to pull a vacuum of 1 – 3mmHg on the downstream side. The permeate collected was thawed, weighed, diluted and analyzed for 1,3-PD concentration by GC. Pervaporation was monitored by key performance indicators of permeate flux for each component and separation factor given by equation 2.

3.Results and Discussions:

3.1 Partition Coefficient:

The partition coefficients of 1,3-PD, Glycerol, Ethanol, Acetic acid and Butyric Acid in ACA and Tributyl Phosphate (TBP) over water are shown in Figure 7.2.

Allylcyclohexylamine is a hydrophobic solvent, with a Log P_{ow} (Octanol – water redistribution coefficient) ~ 2.2 – 2.4, in which 1,3-PD is miscible in all proportions.

TBP is a hydrophobic solvent, with a Log P_{ow} (Octanol – water redistribution coefficient) ~4 in which 1,3 propanediol is miscible in all proportions.

Both ACA and TBP show a fairly favorable partition coefficient in favor of 1,3-PD. However, since 1,3-PD is infinitely soluble in water, the partition coefficient of these and other solvents have not been found to be high enough for economically feasible solvent extraction processes [22]. The partition coefficient of glycerol and ethanol follow 1,3-PD for both the solvents. The partition coefficients of acetic acid and butyric acid are very low in both ACA and TBP, despite the fact that ACA being a secondary amine may be expected to show some basicity.

3.2 Individual Component Mass Uptakes:

The results of mass uptake experiments are shown in Figure 7.3. All three polymer systems are fairly hydrophobic with water mass uptakes <1% [21]. The functionalized siloxane polymers show the lowest water mass uptake amongst the three families of polymers.

The hydrophobic character of the Allylcyclohexylamine methacrylate polymer system and the Imidazolium Ionic liquid based methacrylate polymer system are comparable. With the latter, the homopolymer (PVIM) has the lowest water uptake. For the ACA Acrylate system, the water uptake was reduced by copolymerization with 5% BuA and DVB.

The mass uptakes of ethanol, acetic acid and butyric acid are comparable for the three polymer systems and lie within 0.3 – 1.8%.

The mass uptake of glycerol for the functionalized siloxane system hovers around 2-3% and shows no trend with increasing ACA functionalization of the siloxane. Interestingly,

the high molecular weight styrene – butylacrylate copolymer used to make the phase separated blend in the siloxane system was tested for pervaporative enrichment of one such model broth (data not shown) and was found to be selective in favor of glycerol while failing to enrich 1,3-PD. The mass uptake of glycerol for the ACA based methacrylate polymers [P(Acryl), P(Acryl)_BuA and P(Acryl)_DVB], is around 7 – 9 %. Similar glycerol mass uptake values are observed for PVIM, PVIM_Bua and PVIM_DVB.

The mass uptake of 1,3-PD for the functionalized siloxane system increases with increasing levels of functionalization and lies within 2 – 5%. The 1,3-PD mass uptake for the ACA based methacrylate polymer decreases with copolymerization with BuA and DVB and lies in the range of 17 – 20%. The same trend is noted with the imidazolium based methacrylate polymers and this system has the highest affinity for 1,3-PD with mass uptakes between 18 – 30%. The three systems, chronologically developed, can be seen as groups with progressively increasing 1,3-PD affinity over water and have been shown in earlier chapters to be progressively more efficient in enriching 1,3-PD from binary feeds. Additionally, after water, glycerol is the other component present in a significant concentration that 1,3-PD needs to be separated from. A comparison of the three polymer systems also reveals that the relative difference in affinity for 1,3-PD versus glycerol increases in favor of 1,3-PD with the siloxane being the lowest, followed by the ACA-methacrylate system. The imidazolium ionic liquid based polymers have the greatest difference between 1,3-PD and glycerol mass uptakes.

3.3 Pervaporation results on multicomponent feed mixtures

3.3.1 The difference between the three polymer systems:

A sample comparison of the pervaporation results for a temperature of 30^0C and feed composition M1 is shown in Figures 7.4(a) – (c).

The water flux for the functionalized siloxane system is the highest and lies between 15-20g/m2h. The water flux for the other two polymer systems lies between 2.5 – 5 g/m2h and is the lowest for the imidazolium ionic liquid based polymers. This is consistent with the mass uptake results. The imidazolium ionic liquid polymers had the highest 1,3-PD mass uptake. The difference in the water and 1,3-PD mass uptakes was the highest in the imidazolium ionic liquid polymers. The 1,3-PD flux for the functionalized siloxane membranes was found to increase with the extent of functionalization and was observed to be within 1.3 – 2 g/m^{2}h. For the ACA based methacrylate polymers, the 1,3-PD flux lay between 2.75 – 3 g/m^{2}h and there was insignificant difference between the 1,3-PD flux for the homopolymer and copolymers. The 1,3-PD flux for the imidazolium ionic liquid based polymers was between 2.7 and 3 g/m^{2}h. While the homopolymer for this system exhibited the highest 1,3-PD flux, there was little difference in the performance between the BuA and DVB copolymers.

Contrary to the 1,3-PD flux observations, the glycerol flux for the functionalized siloxanes was higher than that obtained with the other two systems. The glycerol flux also increased with increase in functionalization levels of the siloxane and lay between 2.2 to 2.75 g/m^{2}h. The ACA based methacrylate polymers exhibited glycerol flux between 1.5 – 2 g/m^{2}h with

slightly higher fluxes being obtained with the homopolymer than with the copolymers. The glycerol flux for the imidazolium based polymers were significantly lower than those of the other two systems and were observed to be between 0.8 – 1 g/m^2h. The difference between the hompolymer and copolymer was insignificant.

The fluxes of ethanol, acetic acid and butyric acid were significantly higher for the siloxane polymer compared to the other two systems.

The Separation factor of each permeating component with respect to water is shown in Figure 7.4b. The Separation factor of 1,3-PD for the siloxane polymers was observed to be in the range of 7 – 15. Those for the ACA based methacrylate polymers was seen to lie between 60 – 72, while the imidazolium ionic liquid based polymers showed the highest efficiency with separation factors in the range of 90 – 117.

The separation factor for glycerol with respect to water was between 9 and 11 for the siloxane system. The enrichment of glycerol for the ACA based methacrylate polymer system and the imidazolium based methacrylate polymers was similar with separation factor between 25 and 30.

Ethanol concentration enrichment for the siloxane polymers was higher than that with the other two polymeric systems with separation factors between 10 and 12. The ACA_methacrylate polymer system showed ethanol separation factors between 4 and 8 with a slightly higher enrichment seen with the copolymers. The imidazolium_methacrylate polymers showed ethanol separation factors between 4 and 6. The separation factor of acetic acid for the siloxane polymers was between 3 and 4. This

was closely followed by the imidazolium_methacrylate polymers with separation factors between 2 and 3 and the ACA_methacrylate polymers with separation factors between 1 and 1.5. There was a significant disparity between the enrichment of butyric acid by the siloxane polymers in comparison to the other two systems. While the separation factor of butyric acid for the siloxanes was between 3 and 5, that for the other two systems was as low as 0.8 to 1.1.

The separation factor of 1,3-PD over the other broth components was also computed from equation 2 and the results are shown in Figure 7.4c. The siloxanes enriched both 1,3-PD and glycerol but failed to enrich 1,3-PD in favor of glycerol with the $\alpha_{1,3-PD/gly}$ values lying between 0.7 and 0.9. The ACA_methacrylate polymers, on the other hand preferentially enriched 1,3-PD over glycerol with $\alpha_{1,3-PD/gly}$ between 2.4 and 2.7. The imidazolium_methacrylate polymers were the most efficient in preferential enrichment of 1,3-PD over glycerol with $\alpha_{1,3-PD/gly}$ between 4.3 and 4.6. Similar observations were made with the preferential enrichment of 1,3-PD over other components. While 1,3-PD was preferentially enriched over ethanol, acetic acid and butyric acid by the siloxane polymer, the performance of the other two systems was significantly superior. This is underscored by the mass uptake results.

Thus, the overall permeability of 1,3-PD is higher with the sioxanes, but the separation efficacy is superior with the other two polymer families. It is common for membrane separation systems to show a trade off between the permeability and separation efficacy and this forms the basis for defining a performance upper bound [23].

3.3.2 Pervaporation results: The effect of temperature

Pervaporation was carried out with all the polymer systems at temperatures of 30, 40 and 50°C. The results are shown in Fig 7.5a – c.

The separation factor of 1,3-PD over water (Fig 7.5a) was seen to decrease for all systems. For the siloxanes, the effect was sharp with an increase in temperature from 30 – 40 ˚C, but tapered off with further increase in temperature. Increase in temperature causes an increase in diffusivity of all components and hence a reduction in selectivity. A similar trend was seen for pervaporation with binary feed systems in an earlier work with the siloxane polymer membranes.

The same trend was seen for all ACA_methacrylate polymers, wherein the separation factor decreased from ~70 to 57 for the homopolymer as well as copolymers. Similarly for the imidazolium_methacrylate polymers where the separation factors decreased from values as high as ~117 to 75 upon increasing the temperatures from 30 to 50°C. In addition to an increase in diffusivity, the polymers may be thought to increasingly swell due to the permeating components with increased temperature and that aids the diffusion through of water causing a reduction in separation efficiency.

Interestingly, the separation factor of 1,3-PD over glycerol ($\alpha_{1,3-PD/gly}$), shown in Fig 7.5b. was not significantly altered with increase in temperature, and this observation was seen for all three families of polymers. Increase in temperature reduces the separation factor of glycerol with respect to water ($\alpha_{gly/water}$). While increase in temperature increases the flux of all components, the increase in glycerol and 1,3-PD diffusivity is expected to be lower

than that of water owing simply to their molecular sizes compared to water. It is likely that the concomitant increase in flux of glycerol and 1,3-PD with temperature may have balanced out resulting in no significant trend in $\alpha_{1,3-PD/gly}$.

The flux of 1,3-PD with temperature is shown in Figure 7.5c. Barring two anomalous data points with 90ACA and P(Acryl), the flux of 1,3-PD increased with temperature.

3.3.3 Pervaporation results: The Effect of Feed Glycerol Concentration

Pervaporation with different feed compositions was carried out using the 90ACA (Siloxane system), P(Acryl) (ACA_methacrylate system) and PVIM (Imidazolium_methacrylate system) polymers only (Fig.7.6). Feed compositions M1, M2 and M3 were employed at a temperature of 30°C. While the feed compositions M1, M2 and M3 vary the concentrations of other broth components, the results were chosen to be plotted against glycerol concentration due to the fact that glycerol is present in a much higher concentration and is more likely to affect the transport properties and swell the membrane than ethanol, acetic acid and butyric acid. Additionally, from the mass uptake results, it is obvious that the membranes have a much higher affinity for glycerol compared to ethanol, acetic acid and butyric acid and thus glycerol is more likely to be absorbed and the activity of glycerol inside the membrane is likely to be higher with a correspondingly greater effect on the transport of 1,3-PD and water.

The separation factor of 1,3-PD over water ($\alpha_{1,3PD/water}$) was seen to decrease with increasing glycerol concentration in the feed. This is shown in Figure 7.6a. The most likely reason for this was the swelling of the membrane in the presence of glycerol which causes

higher diffusion of all components and a decrease in selectivity. Also, glycerol may be responsible for coupled water transport and may act as a carrier for water additionally causing a reduction in separation factors.

The separation factor of 1,3-PD over glycerol ($\alpha_{1,3PD/gly}$) undergoes a sharp decrease with increasing glycerol concentration and this is shown in Fig 7.6b. Figure 7.6c. shows the 1,3-PD flux versus glycerol feed concentration. It is interesting to note that 1,3-PD flux decreases with increasing glycerol feed concentration indicating that glycerol competes with 1,3-PD for permeation through the membrane. Additionally, the formation of hydrogen bonded molecular associations in the feed between 1,3-PD and glycerol is not unlikely [24]. Such loose associations at both ionic and molecular level for salts and polar organic molecules are known to exist which become increasingly diffuse with dilution and vanish near infinite dilution [25]. Such an "associated" entity may depress the diffusivity of 1,3-PD and hence its permeability on the pretext of its "larger" size.

3.3.4 Pervaporation results: Coupling Effect Vs Temperature

The pervaporative performance of all membranes with binary 1,3-PD–water feed solutions were compared with model broth solutions. While binary solutions consisted of only 1,3-PD and water in varying concentrations, the model solutions had varying concentrations of other metabolites. A quantitative estimation of the coupling effect was studied by comparing the overall mass transfer coefficients obtained in binary feed experiments vis-à-vis those obtained with model broth feeds under corresponding and comparable experimental conditions. As mentioned earlier, the compositions of the model broth solutions M1, M2 and M3 were chosen to replicate the steady state compositions obtained

with the CSTR fermentation. The transport behavior of 1,3-PD with binary feeds has been modeled in accordance to the solution-diffusion mechanism in an earlier work [21] and earlier chapter. The transport behavior of for pervaporative separation with model broth solutions is also expected to follow the same solution diffusion mechanism, which forms the basis for the computation of the overall mass transfer coefficients of 1,3-PD [26].

Pervaporation mass transport in nonporous dense membranes is often described by the solution diffusion mechanism where the diffusion is typically described by Fick's first law [27, 28] The driving force is the difference in activity or fugacity of the i^{th} species given by the following equation .

$$f_i = x_i^* \gamma_i P_i^{sat} \text{-------(3)}$$

where f is the fugacity, x_i^* is the mole fraction of the i^{th} component in the feed at the interface, γ_i is the activity coefficient, P_i^{sat} is the saturation pressure. The flux of the solute (i^{th} species) across the pervaporation membrane may be expressed as follows:

$$Ji = \frac{P_i}{l}(x_i^* \ \gamma_i \ P_i^{sat} - y_i^* P_p) \text{-------(4)}$$

Where J_i and P_i are the flux and membrane permeability of the i^{th} species, l is membrane thickness, y is mole fraction of the vapor and P_p is the total pressure at the permeate side. The steady state flux can be expressed alternatively, as per the following equation in terms of concentration in bulk solution [21, 29].

$$J_i = \frac{p_{i,ov}}{l}\ (x_i\ \gamma_i\ p_i^{sat} - \ y_i P_p) \text{ --------(5)}$$

where $P_{i,ov}$ is the overall permeability. The partial pressure on the permeate side, $y_i P_p$, upon application of vacuum, is neglected and thus the equation above becomes:

$$J_i = \frac{p_{i,ov}}{l} x_i \gamma_i p_i^{sat} = K_{i,ov} C_i \text{ ------(6)}$$

where $K_{i,ov}$ is the overall mass coefficient of solute *i and* C_i is the molar concentration in kg mole/m^3. $K_{i,ov}$ can be expressed as $P_{i,ov} \cdot \gamma_i \cdot \frac{P_i^{sat}}{l \cdot C^T}$ where C^T is the total molar concentration of the feed solution, and $C_i = x_i \cdot C^T$ relates the species flux to the concentration of the respective species in the feed. Thus the component flux could be used to compute the overall mass transfer coefficient and overall permeability of 1,3-PD. Activity coefficients of the feed concentrations were computed by the Wilson equation and saturation vapor pressure by the Antoine equation [27, 28].

The driving force of pervaporation is the chemical potential which is affected by the presence of other compounds in the model feed compositions M1, M2 and M3. This is a major factor behind the coupling phenomenon in multicomponent pervaporation set up where the impact of the coupling effect on the transport behavior of the target compound (1,3-PD) could be positive, negative or negligible [26].

Coupling effect has been studied for a wide variety of systems [30-34]. The addition of salts to a model broth was found to increase the pervaporative flux of 1-propanol through a PDMS composite membrane [30]. In pervaporative dehydration of binary and ternary mixtures of methanol and ethanol, alcohol fluxes during dehydration of ternary solutions decreased compared to the binary feed solutions [31]. The coupling effect here was attributed to a decrease in preferential dissolution into the hydrophilic membrane as the

alcohol tended to stay in the solutions containing a second alcohol because the presence of the alcohol decreased solution polarity. Butanol pervaporation has also been studied with respect to coupling effects [32-34].

The coupling effect was estimated quantitatively by the following equation [26]:

$$CE(\%) = \left(\frac{K_{PD}^{''} - K_{PD}^{'}}{K_{PD}^{'}}\right) \times 100 \text{ ---------- (7)}$$

Where CE (%) is the coupling effect, $K_{PD}^{''}$ and $K_{PD}^{'}$ are the overall mass transfer coefficients of 1,3-PD for the separation from the binary feed solutions versus model broth compositions, respectively. It is to be noted here that the mass transfer coefficients for binary and model solutions used for comparison pertained to comparable experimental conditions [26]. For example, membrane system, the feed temperature, feed 1,3-PD concentration and cross flow rate, wherever applicable, were the same for the data sets used for computation.

The computed coupling effects versus temperature are graphically shown in Figure 7.7 (a) – (c) for the membrane systems. All polymers show a negative coupling effect, which means the presence of glycerol and other components in the feed mixture adversely affects the 1,3-PD flux, a fact that is seen in the slight reduction in separation factors compared to binary feeds.

The coupling effect is distinctly higher for the siloxane polymers with multicomponent feed pervaporation versus binary feeds. The coupling effect appears to be greater for lower levels of functionalization than at 30C. As the temperature increases to 50C, the coupling

effect levels out for all siloxane polymers studied. For the 50 ACA polymer the coupling effect decreases with temperature while for the 90ACA polymer the opposite effect is seen.

Both the P(Acryl) and the P(VIM) homopolyers showed a small increase in the coupling effect with increase in temperature, perhaps due to enhanced glycerol dissolution in the membrane with temperature which adversely affected both the 1,3-PD flux as well as enrich over water and glycerol. No particular trend with temperature could be ascertained for the butyl acrylate copolymer for both the systems. There was a minimal temperature effect on the CE% with the P(Acryl)_DVB copolymer.

3.4 Robeson's Upper Bound

While membrane separation processes have a high initial investment cost, they offer the advantage of low energy in running the process [23]. Thus membrane processes are being considered as viable options to conventional separation processes. The key parameters for determining the membrane performance are permeability and the separation factor. The concept of an upper bound of separation performance, which defines a permeability – separation trade off is a well-studied aspect in gas separations [23]. The permeability and separation factor are considered as "trade-off" parameters as one generally increases at the cost of the other and this trade off is related to an "upper bound" relationship [35, 36]. In gas separations, the log of permeability versus the log of separation factor of the gas with higher permeability is seen to yield a performance limit for high separation – high permeability combination [23, 35, 36]. The relationship is expressed as

$P_i = k\alpha_{ij}^n$ ----------(8)

Where Pi is the permeability, α_{ij} is the separation factor of the ith component over jth component and n is the slope of the log- log graph and k is the pre-factor for the upper bound relationship.

For gas separations, 1/n was shown to have a linear relationship with the difference in the kinetic diameters of the permeating gas molecules. For gases, diffusion is the primary factor responsible for the separation. The value of the exponent n, was also predicted by activation energy theories for gas separations as was also shown y this theory to be dependent on the kinetic diameters of the permeating molecules. The front factor, k, on the other hand, has been shown to be related to the solubility of gases in the membrane matrix [23].

The upper bound relationship is based on homogenous polymer membrane matrices. For many established upper bound relationships, surface modifications or the use of mixed matrices with sieving structures incorporated into a homogenous polymer matrix have been seen to break the established upper bound limits for given systems [37 – 40].

In this paper the existence of a possible upper bound was explored with data collated from the experiments reported here and in earlier studies with binary feed mixtures. The separation factor of 1,3-PD with respect to water only was considered for the corresponding experiment. The collated data is presented in Figure 7.8.

The figure shows the three distinct polymer families labeled as Siloxanes, ACA methacrylates and Imidazolium IL methacrylates. An upper bound for the pervaporative

purification of 1,3-PD from aqueous mixtures using homogenous polymeric membranes could be envisaged. The exponent n and the front factor k were approximated at ~-0.217 and ~ 10^{13} respectively

A caveat on the estimation of the Robeson's upper bound parameters must be offered here. The data deals with a limited number of data points which may not be enough to define an upper bound for a process.

The phenomenon of concentration polarization which affects systems especially with high intrinsic enrichment is automatically covered by the upper bound definition in bringing forth the limitation in enrichment achievable for a target compound. However that said, Robesons upper bound may be exceeded with multilayer systems that mitigate such limitations.

3.5 Hansen Solubility Parameters

In pervaporation, a component is preferentially removed by virtue of its high solubility in the membrane phase or its higher diffusivity or both [19]. Pervaporation has found applications for removal of water in solvent dehydration, volatile organic removal from water or in aroma recovery. Amongst all applications, the dehydration of solvents is the best developed due to the fact that the use of hydrophilic membranes ensures in a solubility – diffusivity synergistic effect in favor of water selectivity [19]. Water, due to its smaller molecular size diffuses faster and the use of hydrophilic membranes also ensures a higher solubility [20]. However, for the separation of organic molecules from water, the solubility selectivity into the membrane material in favor of the organic molecule must be higher than

that of water. The membrane material must be significantly hydrophobic and must have substantial affinity for the organic permeant. This is one way a membrane may reject water and cause selective enrichment of the organic permeant. The solubility is proportional to the affinity of a given component for the membrane material. The affinity is described by the Hansen solubility parameters comprising of hydrogen bonding interaction (δ_H), polar interaction (δ_P) and dispersion interaction (δ_D). The large differences in Hansen parameters, especially the hydrogen bonding interaction δ_H, determine the feasibility of organic solvent dehydration [41, 42]. The proximity of 1,3-PD with water in terms of these parameters makes the pervaporative separation of 1,3-PD a difficult task.

Permeation may be defined as $P = D.S$ where D is the diffusion coefficient and S is the solubility for components into the membrane from the feed. The relative enrichment of components in a pervaporation feed occurs by virtue of their higher affinity for the membrane material or greater diffusivity or both [41, 42]. The membrane- component affinity is described by the Hansen solubility parameter comprising hydrogen bonding interaction (δ_H), polar interaction (δ_P) and dispersion interaction (δ_D) [19, 41]. For a binary system, the Hansen's solubility parameter distance Ra is a measure of the dissimilarity between two components [41].

$$R_a = \sqrt{4(\delta_{d1} - \delta_{d2})^2 + (\delta_{p1} - \delta_{p2})^2 + (\delta_{H1} - \delta_{H2})^2} \text{ ----------(9)}$$

The chemistry of the membrane and its interaction with permeating components affects Ra and the separation performance [20, 43]. Water has the highest δ_P, closely followed by glycols, such as 1,3-PD [19]. Water also possesses the highest δ_H also closely followed by

glycols [19]. Large differences between δ_H for water and organic solvents makes their pervaporative dehydration feasible and efficient [19, 43]. Additionally, the diffusive efficacy of components through a membrane depends upon their kinetic diameter (d_k) which considers the molecular size and shape [19, 20]. Given that the d_k of water is significantly lower than that of 1,3-PD, it diffuses faster [20]. Hence the onus of pervaporative enrichment in favor of 1,3-PD lies on preferential sorption of 1,3-PD into the membrane and the concomitant rejection of water [19]. The proximity of the solubility parameters of water and 1,3-PD compounds the difficulty of separation using conventional membrane materials such as PDMS and hence calls for its functionalization. The chemistry of functionalization, while enhancing the affinity for 1,3-PD must also make the membrane more hydrophobic and this is reflected in the partial solubility parameters.

The partial solubility parameters of water, 1,3-PD and TBP were obtained from literature [43-45]. The δ_H for PDMS were obtained from literature while δ_P and δ_D computed from the refractive index and dipole moments respectively [44-46]. Those of ACA were computed using a group contribution method [47], employing two kinds of characteristic groups: first-order groups that describe the basic molecular structure of compounds and second-order groups based on the conjugation theory to improve the accuracy of predictions. The contribution towards δ_H, δ_P and δ_D were computed from literature values provided for the participating groups and identifiable conjugates in ACA[47]. In the absence of the availability of reliable δ_H, δ_P and δ_D group contribution for Si-O, Si-H and Si-CH_3 the partial solubility parameters for the ACA modified siloxane materials could not be computed. Additionally, the solubility parameters for the imidazolium ionic liquid based

monomeric and polymeric structure could not be computed due to the absence of adequate data on group contributions pertinent to ionic liquid like structures.

The 3-parameter Hansen system is easily represented in a simple planar triangular graph using a set of fractional parameters derived from the three individual Hansen parameters. Such a graph is called a TEAS graph. TEAS parameters or fractional parameters, were computed from the partial interaction parameters and indicate a fractional contribution of each partial parameter to the whole solubility parameter. They are defined as $f_D = \frac{\delta D}{\delta D+\delta H+\delta P}$, $f_H = \frac{\delta H}{\delta D+\delta H+\delta P}$ and $f_P = \frac{\delta P}{\delta D+\delta H+\delta P}$. The Hansen's solubility parameter distance in the form of a TEAS graph is shown in Figure 7.9.

The distance of separation between 1,3-PD and water is similar to that between 1,3-PD and ACA or TBP. Thus 1,3-PD can be only partly partitioned into ACA or TBP, while the hydrophobic character of ACA and TBP is underscored by its large separation distance from water, due primarily to the disparities in δ_H and δ_P. While two materials may end up with the same solubility parameters, computed arithmetically, the individual contributions that make up this value may be different with ramifications on their mutual affinity.

3.6 Price Performance Trade Off:

A brief comparison of the prices for the materials developed in this work versus that used for the cyanoborate SLM [18] was carried out with retail price data from Sigma Alridch (http://www.sigmaaldrich.com), Oakwood Chemicals Inc (http://www.oakwoodchemical.com/). and Fluorochem Ltd. (http://www.fluorochem.co.uk). The computation was based on molecular structures and

prices of the individual chemicals making up the compound. A Price/performance trade off estimate was generated using the experimental results detailed here with model feed solutions and those reported in the work on the cyanoborate SLM. However the work on the cyanoborate SLM reported results with binary 1,3-PD –water feed compositions, which has been used here for comparison. A rough estimation was made of the total volume of membrane material required to reach a final 1,3-PD concentration of >90%, from a starting composition of 1% 1,3-PD for a feed flow of 100 g/h. The separation factors and 1,3-PD fluxes considered here for the computation were those obtained at 30^0C for a feed 1,3-PD concentration of 10g/l. The computation assumes that separation factor and flux of 1,3-PD remained constant after each enrichment stage. This assumption was made because separation factor and flux data for high 1,3-PD feed concentrations were not available. For the cyanoborate ionic liquid membrane stabilized in a nanoporous ceramic module, the thickness of the module reported – 3mm(with a 7mm inner diameter and 10 mm outer diameter) was used for computation. The nano-porous module reported in their work has a porosity of 30% [18, 48].

The tetrapropyl ammonium cyanoborate ionic liquid costs $36,004/mole, while the ACA based methacrylate monomer costs $1326/mol. The Imidazolium ionic liquid based methacrylate monomer costs $168.5/mol. The ACA functionalized siloxanes cost $1133/mol, $892/mol and $655/mol for the 90%, 70% and 50% functionalized materials, respectively.

The cost per unit weight of the tetrapropyl ammonium cyanoborate ionic liquid is $120/g, while that of the ACA based methacrylate monomer is $4.65/g. The cost of the

imidazolium ionic liquid based methacrylate monomer is $0.33/g. The ACA functionalized siloxanes cost $6/g, $5.6/g and $4.9/g for 90%, 70% and 50%, functionalized materials respectively.

The price performance estimates indicate that while the cost required to achieve the aforesaid levels of enrichment for the cyanoborate ionic liquid SLM is ~$50,000, the same enrichment can be achieved with the functionalized siloxanes at a cost of ~ $1714, $1638 and $1537, respectively, for the 50%, 70% and 90% functionalized materials.

The same performance can be achieved with the ACA based methacrylate homopolymer at a cost of ~$1200 and the imidazolium ionic liquid based methacrylate homopolymer at a cost of ~$100.

The development and study of such novel materials pave a way for establishment of commercially viable and energy efficient alternatives to conventional purification processes presenting a possibility of membrane module fabrication for continuous pervaporation.

4.Conclusion:

The pervaporative performance of three novel polymer systems developed in earlier works is examined with model feed compositions in continuous and batch pervaporation set ups. The separation factors of 1,3-PD and its enrichment over other components was studied with respect several experimental parameters. Coupling effect and its variation with temperature was studied The permeability and separation factors were collated from the

experiments in this work and from earlier binary pervaporation studies to arrive at Robeson's upper bound parameters for pervaportive enrichment of 1,3-PD using homogenous polymeric membranes.

5.References

1. A.J. Ragauskas, C.K. Williams, B.H. Davison, G. Britovsek, J. Cairney, C.A. Eckert, W.J. Frederick Jr., J.P. Hallett, D.J. Leak, C.L. Liotta, J.R. Mielenz, R. Murphy, R. Templer, T. Tschaplinski, The path forward for biofuels and biomaterial, Science. 311 (2010) 484–489.
2. Z.L. Xiu, A.P.Zeng, Present state and perspective of downstream processing of biologically produced 1,3-propanediol and 2,3-butanediol, Appl Microbiol Biotechnol. 78 (2008) 917–926.
3. R.K. Saxena, P. Anand, S. Saran, J. Isar, Microbial production of 1,3-propanediol: Recent developments and emerging opportunities, Biotechnology Advances. 27 (2009) 895–913.
4. A.P. Zeng, H. Biebl, Bulk chemicals from biotechnology: the case of 1,3-propanediol production and the new trends, in: T. Scheper, K. Schugerl, A.P. Zeng (Eds.), Advances in biochemical engineering and biotechnology, Vol. 74, Springer-Verlag, Berlin, Heidelberg, New York, 2002, pp239–59.
5. A. Triguero, R. Blanco, H. Machado, M. Rodríguez, Evaluation of liquid extraction potentials for downstream separation of 1,3-propanediol, Biotechnology Techniques. 13 (1999) 127–130.

6. T.T. Ames, Process for the isolation of 1,3-propanediol from fermentation broth. US Patent 6361983 B1 (2002).
7. Y. Gong, Y. Tong, X.L. Wang, D.H. Liu, The possibility of the desalination of actual 1,3-propanediol fermentation broth by electrodialysis, Desalination. 161 (2004) 169–178.
8. J. Hao, D.H. Liu, Desalination of fermented broth containing 1,3-propanediol by electrodialysis, Chinese J Proc Eng. 5 (2005) 36–39.
9. Z. Li, B. Jiang, D. Zhang, Z. Xiu, Aqueous two-phase extraction of 1,3-propanediol from glycerol-based fermentation broths, Separation and Purification Technology. 66 (2009) 472–478.
10. A. Baiada, A. Vitner, R.P. Jansen, A.M. Baniel, Process for producing 1, 3-propanediol. US Patent 7056439 B2 (2006).
11. A.K. Hilaly, T.P. Binder, Method of recovering 1,3-propanediol from fermentation broth. US Patent 6479716 B2 (2002)
12. M.H. Cho, S.I. Joen, S.H. Pyo, S. Mun, J.H. Kim, A novel separation and purification process for 1,3-propanediol, Process Biochem. 41 (2006) 739–744.
13. P. Anand, R.K. Saxena, R.G. Marwah, A novel downstream process for 1,3-propanediol from glycerol-based fermentation, Appl. Microbiol. Biotechnol. 90 (2011) 1267–1276.
14. J. Hao, F. Xu, H. Liu, D. Liu, Downstream processing of 1,3-propanediol fermentation broth, Journal of Chemical Technology and Biotechnology.81(2006) 102–108.

15. J.J. Malinowski, Reactive Extraction for Downstream Separation of 1,3-Propanediol, Biotechnology Progress. 16 (2000) 76–79.
16. S. Li, V.A. Tuan, J.L. Falconer, R.D, Noble, Separation of 1,3- propanediol from glycerol and glucose using a ZSM-5 zeolite membrane, J. Membr Sci. 191 (2001a) 53–59.
17. S. Li, V.A. Tuan, J.L. Falconer, R.D. Noble, Separation of 1,3- propanediol from aqueous solutions using pervaporation through an X-type zeolite membrane, Ind Eng Chem Res 40 (2001b) 1952– 1959.
18. P.Izák, M. Köckerling, U. Kragl, Stability and selectivity of a multiphase membrane, consisting of dimethylpolysiloxane on an ionic liquid, used in the separation of solutes from aqueous mixtures by pervaporation, Green Chem. 8 (2006) 947–948.
19. P. Shao, R.Y.M. Huang, Polymeric membrane pervaporation, Journal of Membrane Science. 287 (2007) 162-179
20. W.J.Koros, Membranes: Learning a lesson from nature, Chem Eng. Prog. 91 (1995) 68–81
21. S. Li, R. Srivastava, R.S. Parnas, Separation of 1-butanol by pervaporation using a novel tri-layer PDMS composite membrane, J. Membr. Sci. 363 (2010) 287–294.
22. J.J. Malinowski, Evaluation of liquid extraction potentials for downstream separation of1,3-propanediol, Biotechnology Techniques 13: 127–130, 1999.
23. L.M. Robeson, The upper bound revisited, J. Membr. Sci. 320 (2008) 390 – 400.
24. J.L. Dashnau, N.V. Nucci, K. A. Sharp, J. M. Vanderkooi, Hydrogen Bonding and the Cryoprotective Properties of Glycerol/Water Mixtures, *J. Phys. Chem. B* 110 (2006) 13670–13677.

25. H. Chakrabarti, B. Kanjilal, Measurement of the Diffusivity of Cesium Ion in Aqueous Rubidium Chloride Solution , Journal of Solution Chemistry 39 (2010) 409-416.

26. S.Y. Li, R. Srivastava, R.S. Parnas, Study of in situ 1-Butanol Pervaporation from A-B-E Fermentation Using a PDMS Composite Membrane: Validity of Solution-Diffusion Model for Pervaporative A-B-E Fermentation, Biotechnol. Prog. 27 (2011) 111–120.
27. J.G. Wijmans, R.W.Baker, The solution Diffusion model: a review, J. Membr.Sci. 107 (1995) 1–21.
28. S.J. Lue, W.W. Chen, S.Y. Wu, L.D. Wang, Vapor permeation modeling of multicomponent systems using a poly(dimethylsiloxane) membrane, J. Membr. Sci. 311 (2008) 380–389.
29. P. Wu, B.J. Brisdon, R. England, R.W. Field, Preparation of modified difunctional PDMS membranes and a comparative evaluation of their performance for the pervaporative recovery of p-cresol from aqueous solution, J. Membr. Sci. 206 (2002) 265–275.
30. Lipnizki F, Hausmanns S, Field RW. Influence of impermeable components on the permeation of aqueous 1-propanol mixtures in hydrophobic pervaporation. J Membr Sci. 2004;228:129–138. 32.
31. Van Baelen D, Reyniers A, Van der Bruggen B, Vandecasteele C, Degreve J. Pervaporation of Binary and Ternary Mixtures of Water with Methanol and/or Ethanol. Sep Sci Technol. 2005; 39:563. 33.

32. Favre E, Nguyen QT, Bruneau S. Extraction of 1-butanol from aqueous solutions by pervaporation. J Chem Technol Biotech- nol. 1996;65:221–228. 34.
33. Liu F, Liu L, Feng X. Separation of acetone–butanol–ethanol (ABE) from dilute aqueous solutions by pervaporation. Sep Purif Technol. 2005;42:273–282. 35.
34. Garcıa V, Pongra ´cz E, Muurinen E, Keiski RL. Recovery of n-butanol from salt containing solutions by pervaporation. Desalination 2009;241:201–211
35. L.M. Robeson, Correlation of separation factors versus permeability for polymeric membranes, J. Membr. Sci. 62 (1991) 165
36. L.M. Robeson, W.F. Burgoyne, M. Langsam, A.C. Savoca, C. F. Tien, High performance polymers for membrane separations Plymer 25 (1994) 4970
37. C.M. Zimmerman, A. Singh, W.J. Koros, Tailoring mixed matrix composite membranes for gas separations, J. Membr. Sci. 137 (1997) 145
38. S. Husain, W.J. Koros, Mixed matrix hollow fiber membranes made with modified HSSZ-13 zeolite in polyetherimide polymer matrix for gas separations, J. Membr. Sci. 288 (2007) 195
39. T.S. Chung, L.Y. Liang, Y.Li, S. Kulprathiraja, Mixed matrix membranes (MMMs) comprising of organic polymers with dispersed inorganic fillers or gas separations, Prog. Polym. Sci. 32 (2007) 483
40. D. Sen, H. Kalipcilar, L. Yilmaz, Development of polycarbonate based zeolite 4A mixed matrix gas separation membranes, J. Membr. Sci. 303 (2007) 194
41. M. Mulder, T. Franken, C.A. Smolders, Preferential sorption versus preferential permeability in pervaporation, J. Membr. Sci. 22 (1985) 155–173.

42. D.J. Benedict, S.J. Parulekar, S.P. Tsai, Pervaporation assisted esterification of lactic and succinic acids with downstream ester recovery, J. Membr. Sci. 281 (2006) 435–445.
43. C.M. Hansen, Hansen solubility parameter: A users handbook, second ed., CRC press Taylor and Francis group, Boca Raton, London, New York, 2007.
44. M. Alizadeh, F. Abbassi, M. Farahi, K. Jalili, Silicone based hydrogels prepared by interpenetrating polymeric network synthesis: Swelling properties and confinements effects on the formation kinetics, J appl Poly Sci. 124 (2012) 985–992.
45. J.N. Lee, C. Park, G.M. Whitesides, Solvent Compatibility of Poly(dimethylsiloxane)-Based Microfluidic Devices, Anal Chem. 75 (2003) 6544–6554.
46. N.A.Diachun, A.H. Marcus, D.M. Hussey, M.D.Fayer, Dynamics in Polydimethylsiloxane: The Effect of Solute Polarity, JACS. 116 (1994) 1027–1032.
47. E. Stefanis. C. Panayiotou, Prediction of Hansen Solubility Parameters with a New Group-Contribution Method, Int J. Thermophys. 29 (2008) 568–585.
48. P. Izak, M. Köckerling, U. Kragl, Mehrphasen–Membran. German Patent DE102006024397 B3 (2007).

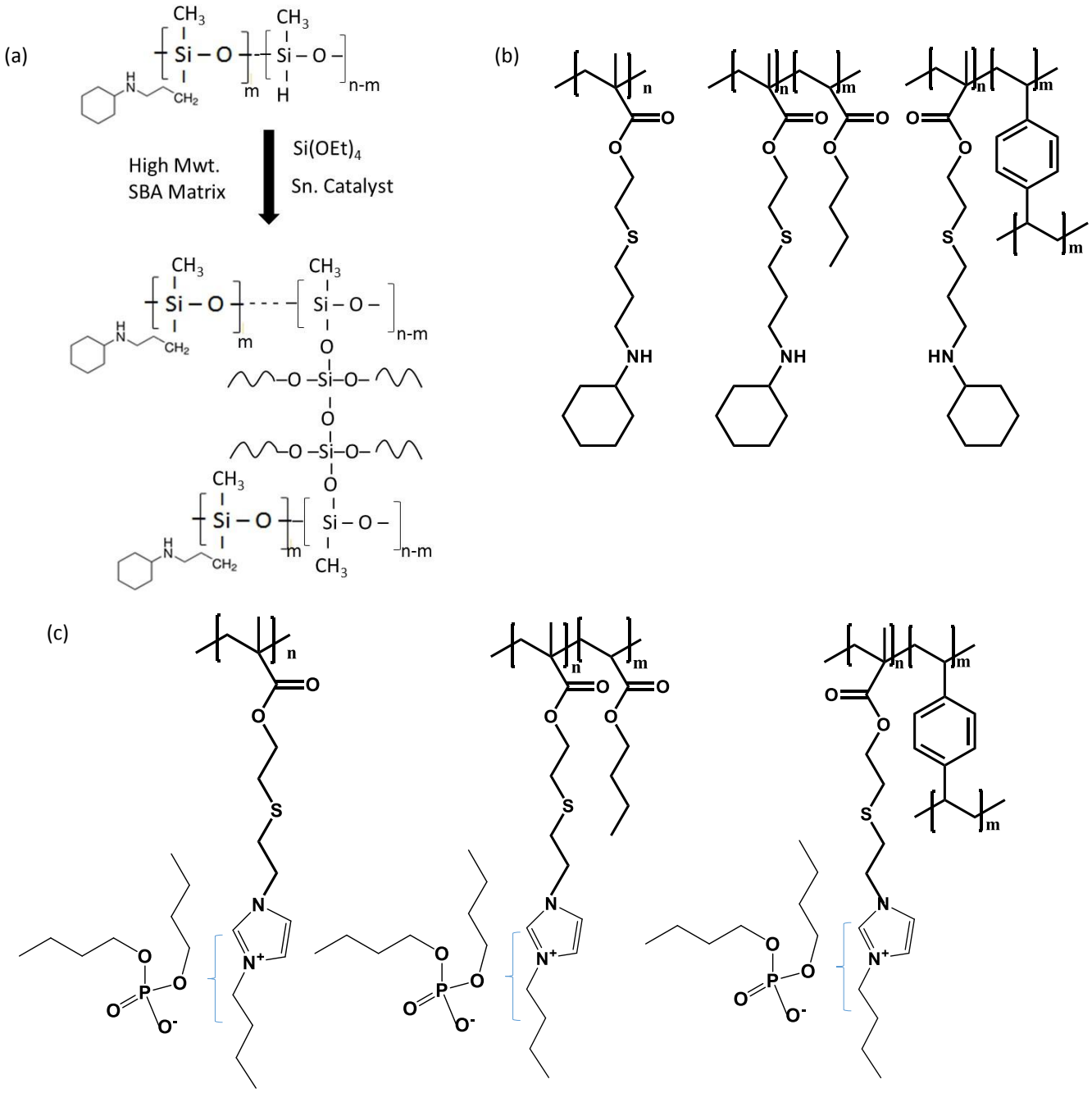

Figure 7.1 : Polymer structures (a) Functionalized Siloxanes (b) ACA based methacrylate polymers (c) Imidazolium alkylphosphate ionic liquid based methacrylate polymers

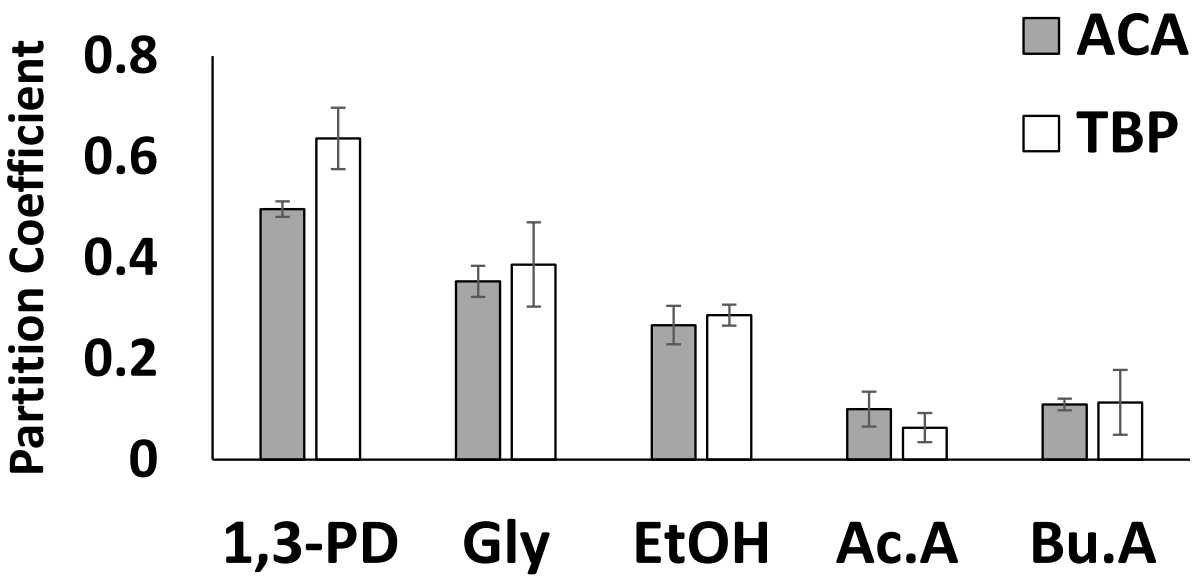

Figure 7.2 : Partition coefficient

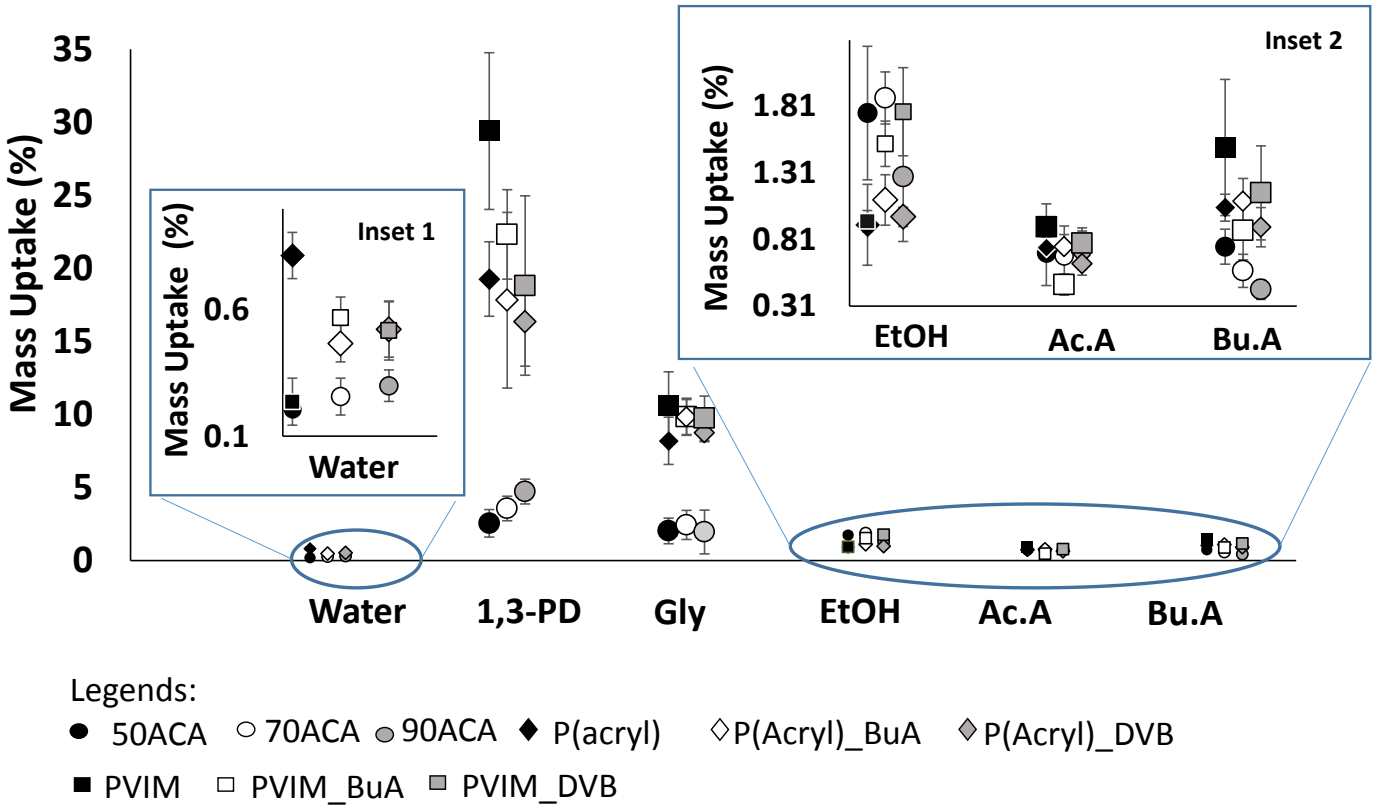

Figure 7.3: Component mass uptakes by membrane materials

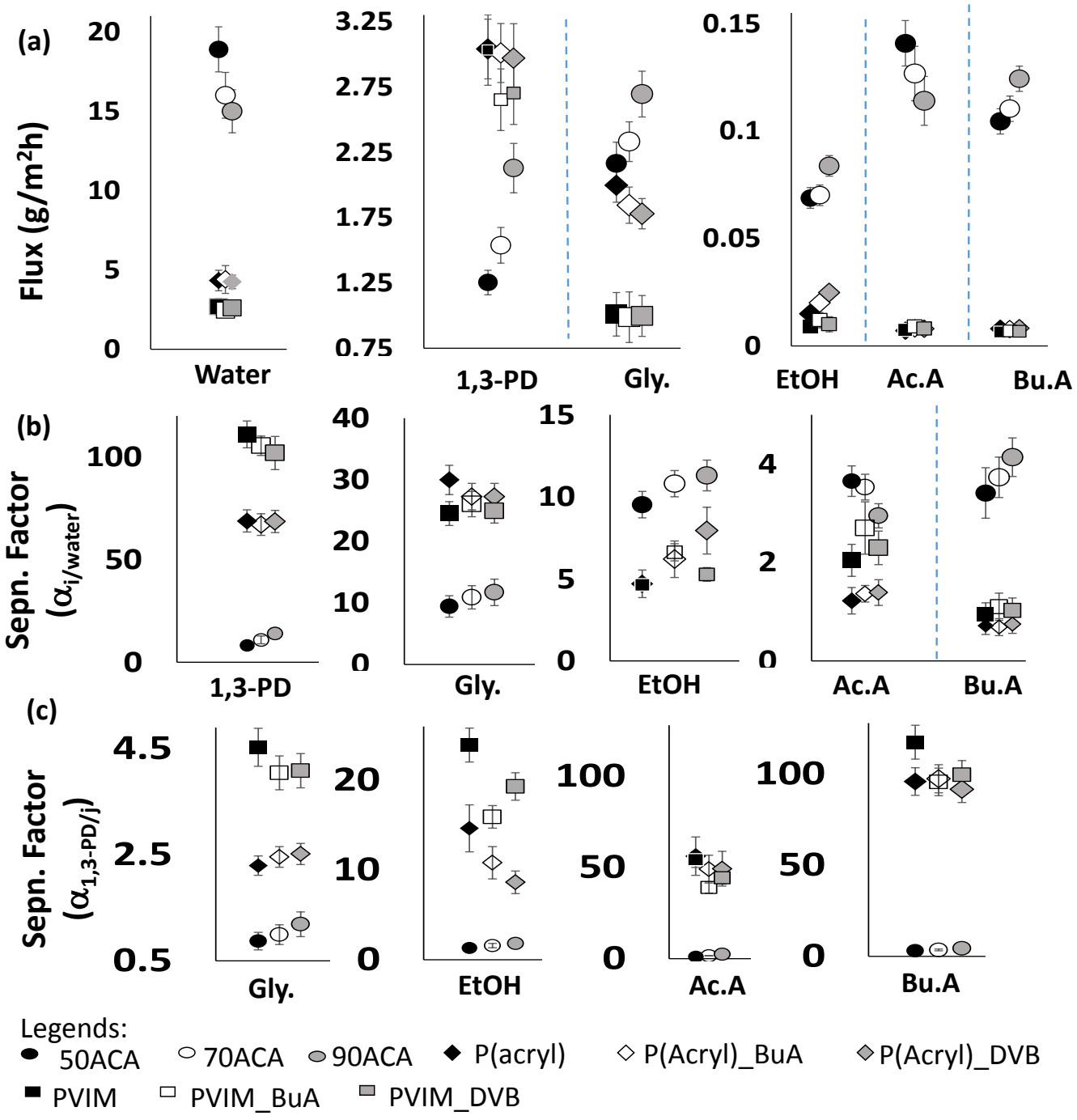

Figure 7.4: Flux and Separation factors for Feed composition M1, Temperature 30^0C

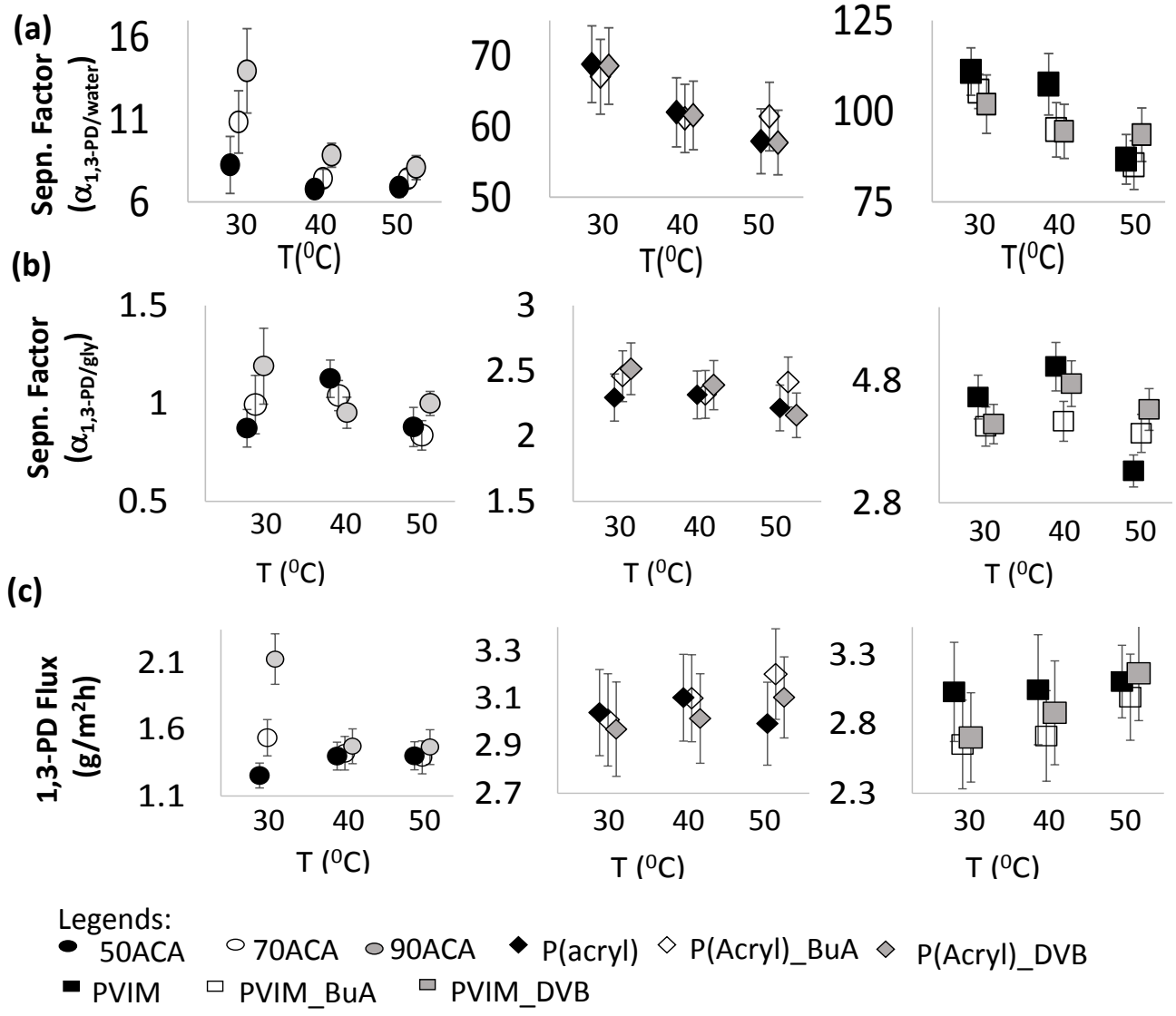

Figure7.5 : (a) Variation of 1,3-PD Separation factor with temperature (b) Variation of 1,3-PD enrichment over glycerol with temperature (c) Variation of 1,3PD flux with temperature

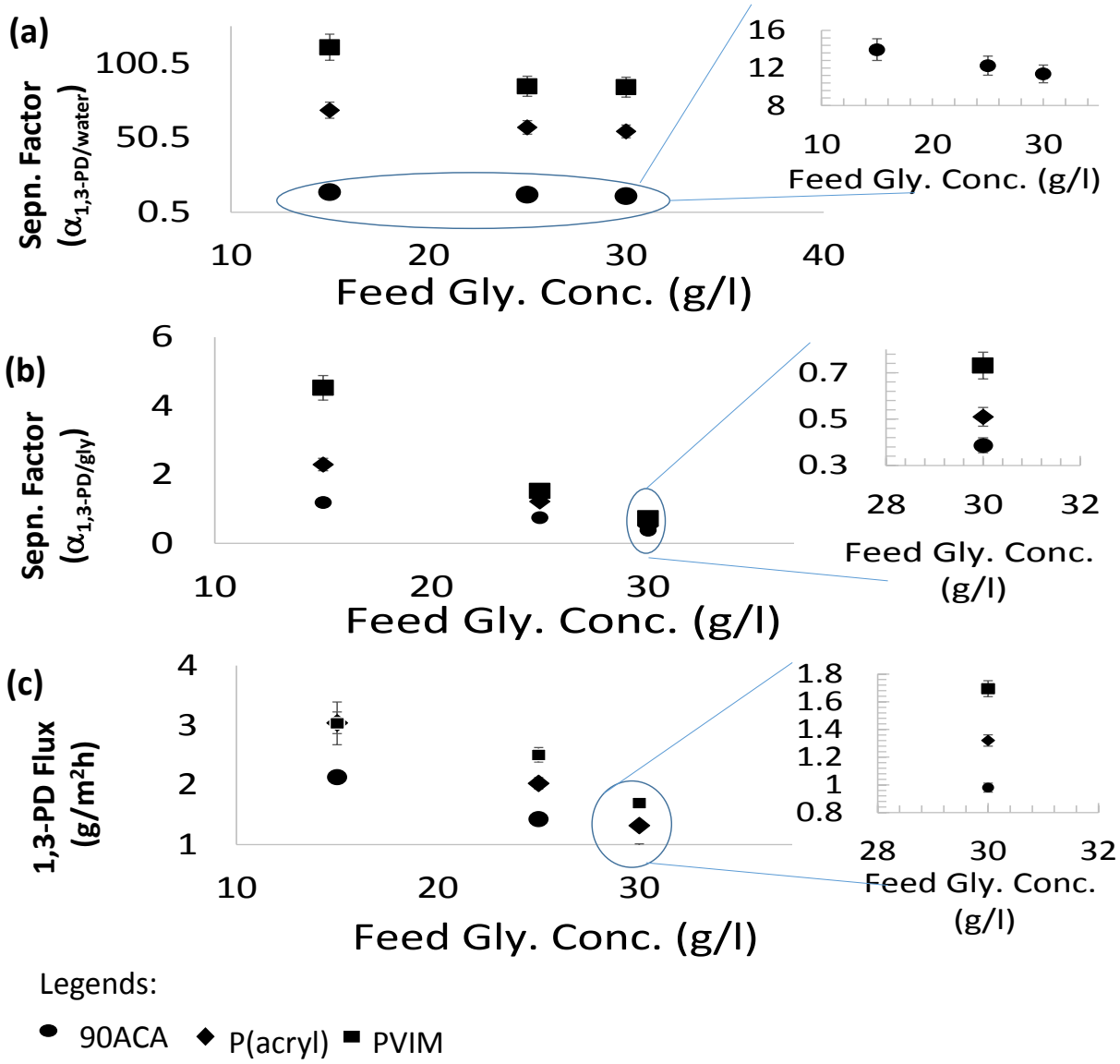

Figure 7.6 (a) Variation of 1,3-PD Separation factor with feed glycerol concentration (b) Variation of 1,3-PD separation factor with feed glycerol concentration (c) Variation of 1,3-PD flux with feed glycerol concentration

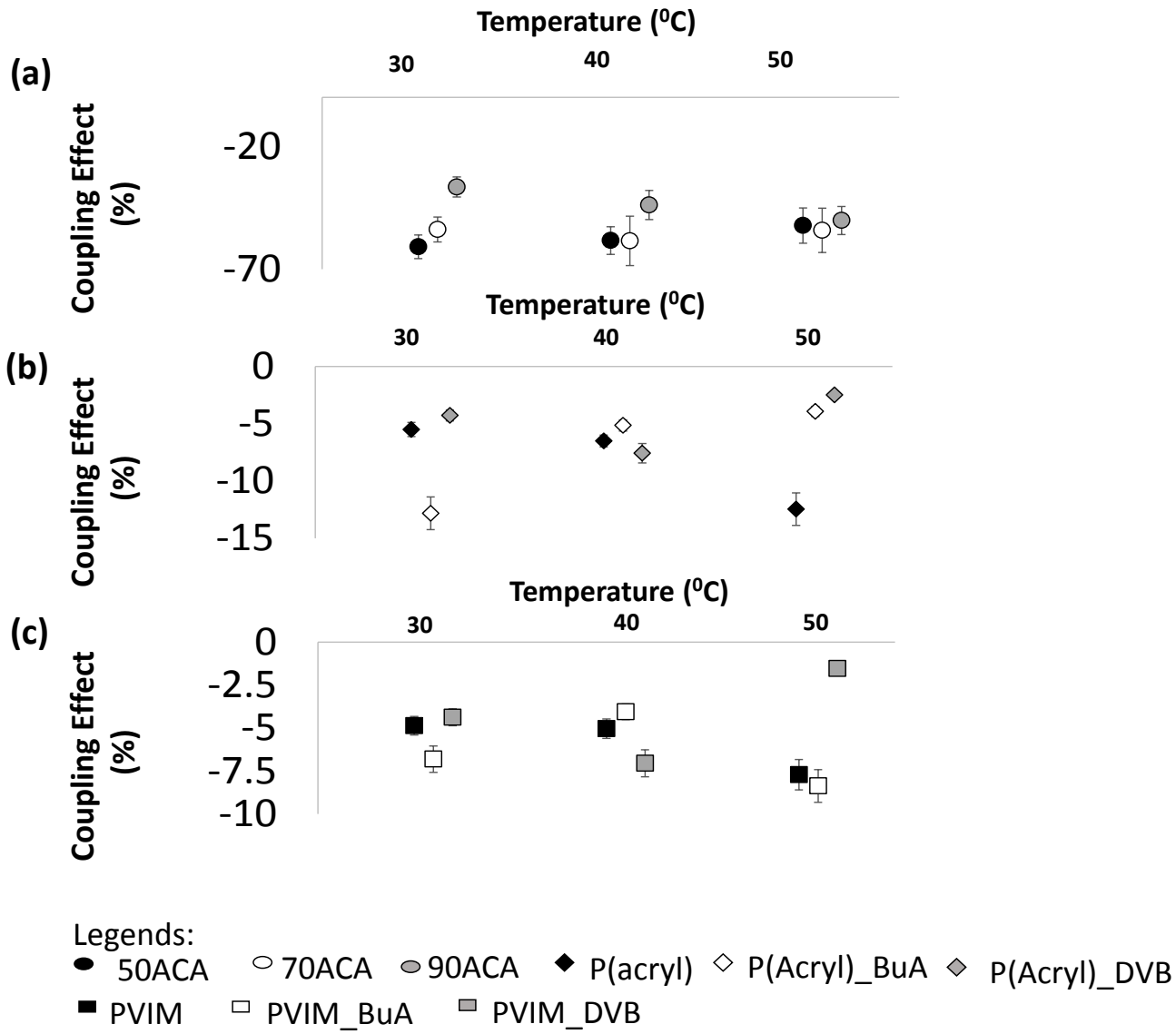

Figure 7.7: Variation of coupling effect with temperature (a) Functionalized Siloxanes (b) ACA based methacrylate polymers (c) Imidazolium alkylphosphate ionic liquid based methacrylate polymers

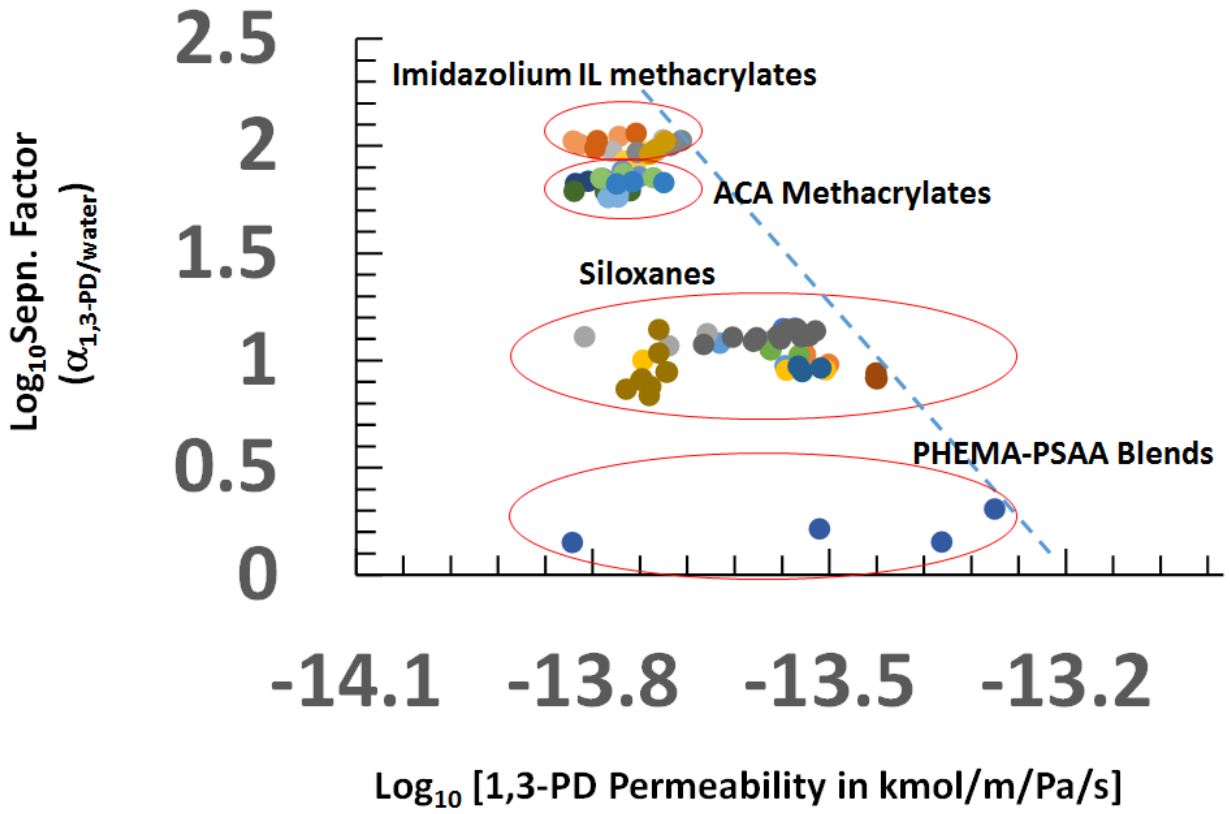

Figure 7.8: Log-Log plot of 1,3-PD permeability versus separation factor to arrive at a Robeson's upper bound

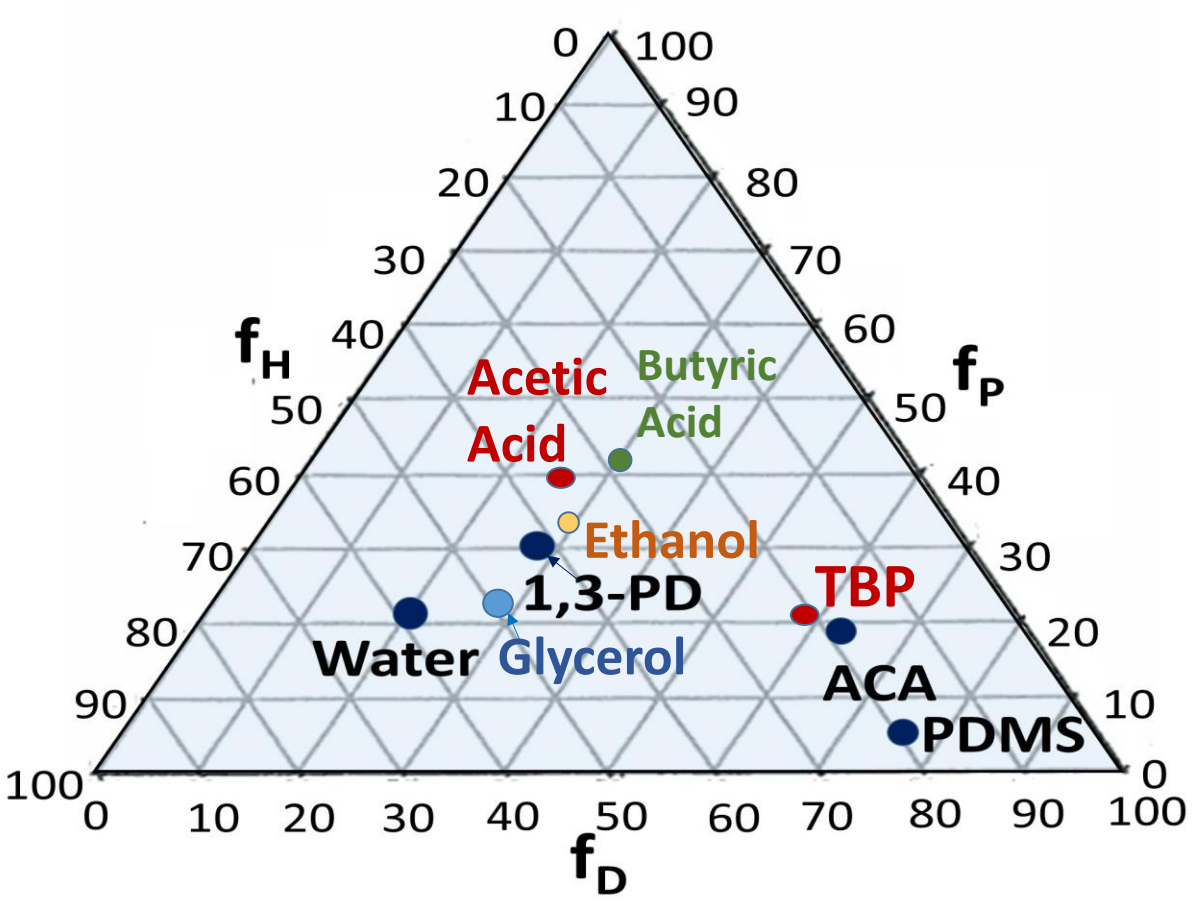

Figure7.9 : TEAS graph of the percentage contribution by the partial solubility parameters for each component.

Chapter 8. Thesis Summary and Way Forward

This research thesis put forward, in two parts, the production and concentration enrichment of 1,3-propanediol from waste industrial glycerol. The batch production was scaled up to 10 liter capacity at the Dave C. Swalm School of Chemical Engineering Mississippi State University in November 2013, with results closely matching those shown in Chapter 2. This demonstrates a possible feasibility of taking the results up for scaled up trials forming a blueprint for a continuous process for converting glycerol to 1,3-propanediol by fermentation. However, as mentioned before, purification and concentration enrichment accounts for the bulk of the process cost and thus warrants the development of an energy efficient process such as pervaporation for the work. This thesis concentrated on the development of materials and their evaluation in simple laboratory set ups. These materials could be developed into membrane modules or multilayer structures to optimize performance prior to scale up. Of the three materials developed, the imidazolium ionic liquid based methacrlyate polymers showed the most promise with respect to separation factors as well as cost – performance trade off. While the separation factor is indeed of greater importance given that 1,3-PD needs to be enriched from a very dilute concentration, the role of flux cannot be ignored. In this respect, the siloxane materials, which showed fair separations but better flux and superior mechanical properties, may be considered as a support layer in a multilayer matrix. Yet another aspect of possible research is the possible development of hollow fiber pervaporation modules based on these novel materials. The thermodynamic aspect of transport across these materials also provides for an interesting future research topic.